

E-ISSN: 2148-6247



# Turkish Journal of PHARMACEUTICAL SCIENCES

An Official Journal of the Turkish Pharmacists' Association, Academy of Pharmacy

Volume: **21** Issue: **6** December **2024**



[www.turkjps.org](http://www.turkjps.org)



PubMed  
Central

PubMed

Scopus

TRDIZIN

galenos  
Publishing House



# Turkish Journal of PHARMACEUTICAL SCIENCES

## OWNER

Arman ÜNEY on behalf of the Turkish Pharmacists' Association

## Editor-in-Chief

**Prof. Mesut Sancar, MSc, Ph.D.**

ORCID: orcid.org/0000-0002-7445-3235

Marmara University Faculty of Pharmacy, Department of Clinical Pharmacy, İstanbul, Türkiye  
E-mail: sancarmesut@yahoo.com

## Associate Editors

**Prof. Bensu Karahalil, Ph.D.**

ORCID: orcid.org/0000-0003-1625-6337

Gazi University Faculty of Pharmacy, Department of Pharmaceutical Toxicology, Ankara, Türkiye  
E-mail: bensu@gazi.edu.tr

**Prof. Betül Okuyan, MSc, Ph.D.**

ORCID: orcid.org/0000-0002-4023-2565

Marmara University Faculty of Pharmacy, Department of Clinical Pharmacy, İstanbul, Türkiye  
E-mail: betulokuyan@gmail.com

**Prof. İ. İrem Tatlı Çankaya, MSc, Ph.D.**

ORCID: orcid.org/0000-0001-8531-9130

Hacettepe University Faculty of Pharmacy, Department of Pharmaceutical Botany, Ankara, Türkiye  
E-mail: itatli@hacettepe.edu.tr

## Editorial Board

**Prof. Afonso Miguel Cavaco, Ph.D.**

ORCID: orcid.org/0000-0001-8466-0484

Lisbon University Faculty of Pharmacy, Department of Pharmacy, Pharmacology and Health Technologies, Lisboa, Portugal  
acavaco@campus.ul.pt

**Prof. Bezhan Chankvetadze, Ph.D.**

ORCID: orcid.org/0000-0003-2379-9815

Ivane Javakishvili Tbilisi State University, Institute of Physical and Analytical Chemistry, Tbilisi, Georgia  
jpba\_bezhan@yahoo.com

**Prof. Blanca Laffon, P.D.**

ORCID: orcid.org/0000-0001-7649-2599

DICOMOSA group, Advanced Scientific Research Center (CICA), University of A Coruña, Department of Psychology, Area Psychobiology, Central Services of Research Building (ESCI), Campus Elviña s/n, A Coruña, Spain  
blanca.laffon@udc.es

**Prof. Christine Lafforgue, Ph.D.**

ORCID: orcid.org/0000-0001-7798-2565

Paris Saclay University Faculty of Pharmacy, Department of Dermopharmacology and Cosmetology, Paris, France  
christine.lafforgue@universite-paris-saclay.fr

**Prof. Dietmar Fuchs, Ph.D.**

ORCID: orcid.org/0000-0003-1627-9563

Innsbruck Medical University, Center for Chemistry and Biomedicine, Institute of Biological Chemistry, Biocenter, Innsbruck, Austria  
dietmar.fuchs@i-med.ac.at

**Prof. Francesco Epifano, Ph.D.**

ORCID: 0000-0002-0381-7812

Università degli Studi G. d'Annunzio Chieti e Pescara, Chieti CH, Italy  
francesco.epifano@unich.it

**Prof. Fernanda Borges, Ph.D.**

ORCID: orcid.org/0000-0003-1050-2402

Porto University Faculty of Sciences, Department of Chemistry and Biochemistry, Porto, Portugal  
fborges@fc.up.pt

**Prof. Göksel Şener, Ph.D.**

ORCID: orcid.org/0000-0001-7444-6193

Fenerbahçe University Faculty of Pharmacy, Department of Pharmacology, İstanbul, Türkiye  
gşener@marmara.edu.tr

**Prof. Gülbin Özçelikay, Ph.D.**

ORCID: orcid.org/0000-0002-1580-5050

Ankara University Faculty of Pharmacy, Department of Pharmacy Management, Ankara, Türkiye  
gozcelikay@ankara.edu.tr

**Prof. Hermann Bolt, Ph.D.**

ORCID: orcid.org/0000-0002-5271-5871

Dortmund University, Leibniz Research Centre, Institute of Occupational Physiology, Dortmund, Germany  
bolt@ifado.de

**Prof. Hildebert Wagner, Ph.D.**

Ludwig-Maximilians University, Center for Pharmaceutical Research, Institute of Pharmacy, Munich, Germany  
h.wagner@cup.uni-muenchen.de

**Prof. K. Arzum Erdem Gürsan, Ph.D.**

ORCID: orcid.org/0000-0002-4375-8386

Ege University Faculty of Pharmacy, Department of Analytical Chemistry, İzmir, Türkiye  
arzum.erdem@ege.edu.tr

**Prof. Bambang Kuswandi, Ph.D.**

ORCID: orcid.org/0000-0002-1983-6110

Chemo and Biosensors Group, Faculty of Pharmacy University of Jember, East Java, Indonesia  
b\_kuswandi.farmasi@unej.ac.id

**Prof. Luciano Saso, Ph.D.**

ORCID: orcid.org/0000-0003-4530-8706

Sapienze University Faculty of Pharmacy and Medicine, Department of Physiology and Pharmacology "Vittorio Erspamer", Rome, Italy  
luciano.saso@uniroma1.it

**Prof. Maarten J. Postma, Ph.D.**

ORCID: orcid.org/0000-0002-6306-3653

University of Groningen (Netherlands), Department of Pharmacy, Unit of Pharmacoepidemiology and Pharmacoconomics, Groningen, Holland  
m.j.postma@rug.nl

**Prof. Meriç Köksal Akkoç, Ph.D.**

ORCID: orcid.org/0000-0001-7662-9364

Yeditepe University Faculty of Pharmacy, Department of Pharmaceutical Chemistry, İstanbul, Türkiye  
merickoksal@yeditepe.edu.tr

**Assoc. Prof. Nadja Cristhina de Souza Pinto, Ph.D.**

ORCID: orcid.org/0000-0003-4206-964X

University of São Paulo, Institute of Chemistry, São Paulo, Brazil  
nadja@iq.usp.br

**Assoc. Prof. Neslihan Ayygün Kocabaş, Ph.D. E.R.T**

ORCID: orcid.org/0000-0000-0000-0000

Total Research and Technology Feluy Zone Industrielle Feluy, Refining and Chemicals, Strategy-Development-Research, Toxicology Manager, Seneffe, Belgium  
neslihan.aygun.kocabas@total.com

**Prof. Rob Verpoorte, Ph.D.**

ORCID: orcid.org/0000-0001-6180-1424

Leiden University, Natural Products Laboratory, Leiden, Netherlands  
verpoort@chem.leidenuniv.nl



# Turkish Journal of PHARMACEUTICAL SCIENCES

**Prof. Robert Rapoport, Ph.D.**

ORCID: orcid.org/0000-0001-8554-1014  
Cincinnati University Faculty of Pharmacy,  
Department of Pharmacology and Cell Biophysics,  
Cincinnati, USA  
robertrapoport@gmail.com

**Prof. Tayfun Uzbay, Ph.D.**

ORCID: orcid.org/0000-0002-9784-5637  
Üsküdar University Faculty of Medicine,  
Department of Medical Pharmacology, İstanbul,  
Türkiye  
tayfun.uzbay@uskudar.edu.tr

**Prof. Wolfgang Sadee, Ph.D.**

ORCID: orcid.org/0000-0003-1894-6374  
Ohio State University, Center for  
Pharmacogenomics, Ohio, USA  
wolfgang.sadee@osumc.edu

## Advisory Board

**Prof. Yusuf ÖZTÜRK, Ph.D.**

Anadolu University, Faculty of Pharmacy,  
Department of Pharmacology, Eskişehir, TÜRKİYE  
ORCID: 0000-0002-9488-0891

**Prof. Tayfun UZBAY, Ph.D.**

Üsküdar University, Faculty of Medicine,  
Department of Medical Pharmacology, İstanbul,  
TÜRKİYE  
ORCID: orcid.org/0000-0002-9784-5637

**Prof. K. Hüsnü Can BAŞER, Ph.D.**

Anadolu University, Faculty of Pharmacy,  
Department of Pharmacognosy, Eskişehir, TÜRKİYE  
ORCID: 0000-0003-2710-0231

**Prof. Erdem YEŞİLADA, Ph.D.**

Yeditepe University, Faculty of Pharmacy,  
Department of Pharmacognosy, İstanbul, TÜRKİYE  
ORCID: 0000-0002-1348-6033

**Prof. Yılmaz ÇAPAN, Ph.D.**

Hacettepe University, Faculty of Pharmacy,  
Department of Pharmaceutical Technology, Ankara,  
TÜRKİYE  
ORCID: 0000-0003-1234-9018

**Prof. Sibel A. ÖZKAN, Ph.D.**

Ankara University, Faculty of Pharmacy,  
Department of Analytical Chemistry, Ankara,  
TÜRKİYE  
ORCID: 0000-0001-7494-3077

**Prof. Ekrem SEZİK, Ph.D.**

İstanbul Health and Technology University, Faculty  
of Pharmacy, Department of Pharmacognosy,  
İstanbul, TÜRKİYE  
ORCID: 0000-0002-8284-0948

**Prof. Gönül ŞAHİN, Ph.D.**

Eastern Mediterranean University, Faculty of  
Pharmacy, Department of Pharmaceutical  
Toxicology, Famagusta, CYPRUS  
ORCID: 0000-0003-3742-6841

**Prof. Sevda ŞENEL, Ph.D.**

Hacettepe University, Faculty of Pharmacy,  
Department of Pharmaceutical Technology, Ankara,  
TÜRKİYE  
ORCID: 0000-0002-1467-3471

**Prof. Sevim ROLLAS, Ph.D.**

Marmara University, Faculty of Pharmacy,  
Department of Pharmaceutical Chemistry, İstanbul,  
TÜRKİYE  
ORCID: 0000-0002-4144-6952

**Prof. Göksel ŞENER, Ph.D.**

Fenerbahçe University, Faculty of Pharmacy,  
Department of Pharmacology, İstanbul, TÜRKİYE  
ORCID: 0000-0001-7444-6193

**Prof. Erdal BEDİR, Ph.D.**

İzmir Institute of Technology, Department of  
Bioengineering, İzmir, TÜRKİYE  
ORCID: 0000-0003-1262-063X

**Prof. Nurşen BAŞARAN, Ph.D.**

Hacettepe University, Faculty of Pharmacy,  
Department of Pharmaceutical Toxicology, Ankara,  
TÜRKİYE  
ORCID: 0000-0001-8581-8933

**Prof. Bensu KARAHALİL, Ph.D.**

Gazi University, Faculty of Pharmacy, Department  
of Pharmaceutical Toxicology, Ankara, TÜRKİYE  
ORCID: 0000-0003-1625-6337

**Prof. Betül DEMİRCİ, Ph.D.**

Anadolu University, Faculty of Pharmacy,  
Department of Pharmacognosy, Eskişehir, TÜRKİYE  
ORCID: 0000-0003-2343-746X

**Prof. Bengi USLU, Ph.D.**

Ankara University, Faculty of Pharmacy,  
Department of Analytical Chemistry, Ankara,  
TÜRKİYE  
ORCID: 0000-0002-7327-4913

**Prof. Ahmet AYDIN, Ph.D.**

Yeditepe University, Faculty of Pharmacy,  
Department of Pharmaceutical Toxicology, İstanbul,  
TÜRKİYE  
ORCID: 0000-0003-3499-6435

**Prof. İlkey ERDOĞAN ORHAN, Ph.D.**

Gazi University, Faculty of Pharmacy, Department  
of Pharmacognosy, Ankara, TÜRKİYE  
ORCID: 0000-0002-7379-5436

**Prof. Ş. Güniz KÜÇÜKGÜZEL, Ph.D.**

Fenerbahçe University Faculty of Pharmacy,  
Department of Pharmaceutical Chemistry, İstanbul,  
TÜRKİYE  
ORCID: 0000-0001-9405-8905

**Prof. Engin Umur AKKAYA, Ph.D.**

Dalian University of Technology, Department of  
Chemistry, Dalian, CHINA  
ORCID: 0000-0003-4720-7554

**Prof. Esra AKKOL, Ph.D.**

Gazi University, Faculty of Pharmacy, Department  
of Pharmacognosy, Ankara, TÜRKİYE  
ORCID: 0000-0002-5829-7869

**Prof. Erem BİLENSOY, Ph.D.**

Hacettepe University, Faculty of Pharmacy,  
Department of Pharmaceutical Technology, Ankara,  
TÜRKİYE  
ORCID: 0000-0003-3911-6388

**Prof. Uğur TAMER, Ph.D.**

Gazi University, Faculty of Pharmacy, Department  
of Analytical Chemistry, Ankara, TÜRKİYE  
ORCID: 0000-0001-9989-6123

**Prof. Gülaçtı TOPÇU, Ph.D.**

Bezmialem Vakıf University, Faculty of Pharmacy,  
Department of Pharmacognosy, İstanbul, TÜRKİYE  
ORCID: 0000-0002-7946-6545

**Prof. Hasan KIRMIZİBEKMEZ, Ph.D.**

Yeditepe University, Faculty of Pharmacy,  
Department of Pharmacognosy, İstanbul, TÜRKİYE  
ORCID: 0000-0002-6118-8225

**Douglas Siqueira de Almeida Chaves,  
Ph.D.**

Federal Rural University of Rio de Janeiro,  
Department of Pharmaceutical Sciences, Rio de  
Janeiro, BRAZIL  
ORCID: 0000-0002-0571-9538

*\*Members of the Advisory Board consist of the scientists  
who received Science Award presented by TEB Academy  
of Pharmacy in chronological order.*



# Turkish Journal of PHARMACEUTICAL SCIENCES

---

Please refer to the journal's webpage (<https://www.turkjps.org/>) for "Editorial Policy" and "Instructions to Authors".

---

The editorial and publication process of the **Turkish Journal of Pharmaceutical Sciences** are shaped in accordance with the guidelines of ICMJE, WAME, CSE, COPE, EASE, and NISO. The Turkish Journal of Pharmaceutical Sciences is indexed in **PubMed, PubMed Central, Thomson Reuters / Emerging Sources Citation Index, Scopus, ULAKBİM, Türkiye Atıf Dizini, Embase, EBSCO Host, Türk Medline, Cabi, CNKI**.

The journal is published online.

**Owner:** Turkish Pharmacists' Association, Academy of Pharmacy

**Responsible Manager:** Mesut Sancar

---



**Publisher Contact**

**Address:** Molla Gürani Mah. Kaçamak Sk. No: 21/1

34093 İstanbul, Türkiye

**Phone:** +90 (530) 177 30 97

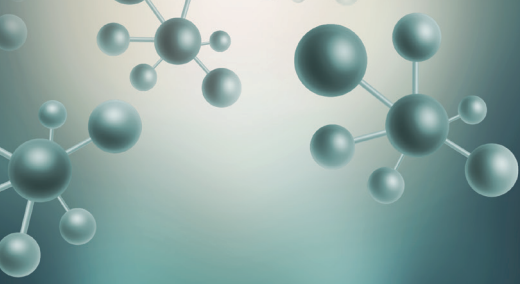
**E-mail:** [info@galenos.com.tr](mailto:info@galenos.com.tr) / [yayin@galenos.com.tr](mailto:yayin@galenos.com.tr)

**Web:** [www.galenos.com.tr](http://www.galenos.com.tr) | **Publisher Certificate Number:** 14521

**Publication Date:** December 2024

**E-ISSN:** 2148-6247

International scientific journal published bimonthly.



# Turkish Journal of PHARMACEUTICAL SCIENCES

## CONTENTS

### Original Articles

- 489** Initial Empirical Antibiotic Treatment in Patients with COVID-19 is Associated with Excess Adverse Drug Reactions without Clinical Benefit  
Pinar BAKIR EKİNCİ, Emre KARA, Gülçin TELLİ DİZMAN, Meliha Çağla SÖNMEZER, Ahmet Çağkan İNKAYA, Kutay DEMİRKAN, Serhat ÜNAL, Ömrüm UZUN
- 499** *In silico* and *in vitro* Evaluation of the Cytotoxic Potential of Hinokitiol against Osteosarcoma by Targeting Glycogen Synthase Kinase 3 $\beta$   
Binoy Varghese CHERIYAN, Punithavel SRINIVASAN, Georgepush JAYARAJ, Karthik Kadhiri KARUNAKAR, Prasanna Bharathi SAINATH, Anandakumar SHANMUGAM, Anitha ROY, Karthikeyan ELUMALAI
- 506** General Public Knowledge, Attitudes, and Practices Regarding Hair Dye Usage and Its Adverse Effects in the Northern Emirates of the United Arab Emirates  
Javedh SHAREEF, Sathvik Belagodu SRIDHAR, Safeera SHERIN, Sumanjebin ABDUL NAZAT
- 513** Impact of Simulated Gastrointestinal Fluid: Viscosity, Surface Tension, and pH on the Dissolution and Rheology Assessment of Viscosity of Two Commercial Candesartan Cilexetil Products  
Samah ATA, Rana SEJARE, Ola TARAWNEH, Rania HAMED, Mohammad AL-SABI, Samar BISHTAWI, Hadeel Abu MAHFOUZ, Sameer ALKOUZ
- 520** Insecticidal and Bactericidal Activities of *Cassia nigricans* Vahl and Molecular Docking Analysis of Insect Acetylcholinesterase  
Abdourahman FADIMATOU, Faiza BOUKLI HACENE, Meriem GHALEM, Guy Bertrand NOUMI, Jean MOMENI, Le-Ndiman MBAIDANEM, Said GHALEM
- 528** Effect of Combined Treatment with Levofloxacin and Metformin on Diabetes-the Diabetes Related Behavioral and Biochemical Alterations  
Poonam SINGH, Vaibhav WALIA, Prabhakar Kumar VERMA
- 536** Protective Effects of Rosmarinic Acid and Epigallocatechin Gallate Against Doxorubicin-Induced Cytotoxicity and Genotoxicity in CHO-K1 Cells  
Sinem HELVACIOĞLU, Muhammed HAMİTOĞLU, Ecem YILDIRIM, Şenay VURAL KORKUT, Aylin YABA, Ahmet AYDIN
- 544** Isolation of the Major Compounds and Determination of Biological Activities in the Underground Parts of *Trachystemon orientalis* D.Don  
Ayşe Nur KOZ, Tuğba SUBAŞ, Merve BADEM, Şeyda KANBOLAT, Ufuk ÖZGEN, Sıla Özlem ŞENER, Adem DEMİR, İhsan ÇALIŞ
- 551** Influence of Formulation Composition on the Characteristic Properties of 5-fluorouracil-loaded Liposomes  
Tahir Emre YALÇIN, Ceren YETGİN
- 557** Preparation and Characterization of the Release Behavior of PVA: Na-Alg Microsphere Containing Fampridine  
Serenay AKYOL ÖZDEMİR, Fatoş YÜKSEL GÜVENİLİR
- 566** *In silico* Evaluation of H1-Antihistamine as Potential Inhibitors of SARS-CoV-2 RNA-dependent RNA Polymerase: Repurposing Study of COVID-19 Therapy  
Mazin HAMDAN, Necla KULABAŞ, İlkay KÜÇÜKGÜZEL
- 577** Lactulose Versus Naloxone for Opioid-Induced Constipation in Intensive Care  
Mitra RAHIMI, Maral RAMEZANI, Shahin SHADNIA, Babak MOSTAFAZADEH, Mahnaz Dahdahsti AZANDARYANI, Mohammad Hosein ALIJANZADEH, Latif GACHKAR, Peyman Erfan Talab EVINI

### Index

- 2024 Author Index
- 2024 Subject Index
- 2024 Referee Index



# Initial Empirical Antibiotic Treatment in Patients with COVID-19 is Associated with Excess Adverse Drug Reactions without Clinical Benefit

Pınar BAKIR EKİNCİ<sup>1\*</sup>, Emre KARA<sup>1</sup>, Gülçin TELLİ DİZMAN<sup>2</sup>, Meliha Çağla SÖNMEZER<sup>2</sup>, Ahmet Çağkan İNKAYA<sup>2</sup>,  
 Kutay DEMİRKAN<sup>1</sup>, Serhat ÜNAL<sup>2</sup>, Ömrüm UZUN<sup>2</sup>

<sup>1</sup>Hacettepe University Faculty of Pharmacy, Department of Clinical Pharmacy, Ankara, Türkiye

<sup>2</sup>Hacettepe University Faculty of Medicine, Department of Infectious Diseases and Clinical Microbiology, Ankara, Türkiye

## ABSTRACT

**Objectives:** Empirical antibiotic use is common among hospitalized patients with coronavirus disease-2019 (COVID-19) pneumonia because it is difficult to differentiate it from concurrent bacterial pneumonia. The aim of this study was to determine risk factors for concurrent bacterial community-acquired pneumonia (b-CAP) and the need for initial empirical antibiotic coverage in patients with pulmonary involvement caused by Severe acute respiratory syndrome-Coronavirus-2 (SARS-CoV-2) infection.

**Materials and Methods:** This prospective observational study was conducted at a tertiary university hospital between March 2020 and April 2021. Patients aged over 18 years who were hospitalized due to COVID-19 were included. Risk factors and outcomes were compared between patients who initially received empirical antibiotics and those who did not.

**Results:** The presence of respiratory viral pathogens other than SARS-CoV-2 was investigated *via* respiratory panel multiplex polymerase chain reaction in 295 patients and potential bacterial respiratory pathogens in 306 patients admitted to the hospital. The co-infection rate was low (17.4%) and half of the patients (205/409, 50.1%) were administered initial empirical antibiotics for suspected concurrent b-CAP. Antibiotic use was higher in patients with multiple comorbidities, severe to critical pneumonia, and patients older than 65 years ( $p < 0.001$ ). The overall 30-day mortality rate was significantly higher (26.3% and 2.0%,  $p < 0.001$ ), and the duration of hospital stay was longer (median 13.0 and 5.5 days,  $p < 0.001$ ) in patients who received empirical antibacterial agents compared to those who did not.

**Conclusion:** Initial empirical antibiotic treatment is common among patients infected with SARS-CoV-2, although the coinfection rate is low. Empirical antibiotic(s) did not improve the clinical course in COVID-19 patients.

**Keywords:** SARS-CoV-2, COVID-19, antimicrobial, empirical therapy, co-infections, community-acquired pneumonia

## INTRODUCTION

Differential diagnosis of bacterial co-infections may be challenging in patients with severe to critical coronavirus disease-2019 (COVID-19) on hospital admission because the clinical presentation of COVID-19 may mimic atypical bacterial pneumonia, and pulmonary consolidation develops later during the disease.<sup>1</sup> In addition, physicians overwhelmed by pandemic conditions might tend to cover all potential causes of community-acquired pneumonia (CAP) and leave no button unturned.<sup>2,3</sup>

The World Health Organization guidelines recommend empirical antibiotic therapy based on local epidemiology for bacterial pneumonia in patients with severe COVID-19, older patients, and long-term nursing home residents,<sup>4</sup> but a few studies have shown that the rate of antibiotic usage is high despite low microbiological evidence. In most of these studies, empirical antibacterial treatment of suspected hospital-acquired and ventilator-associated pneumonia was investigated.<sup>5,6</sup> A meta-analysis emphasized that the incidence of co-infection was low (8%) at hospital admission, yet empirical antibacterial

\*Correspondence: pinar.bakir55@gmail.com, ORCID-ID: orcid.org/0000-0003-0694-6078

Received: 17.08.2023, Accepted: 19.12.2023



therapy was started in 48.6% to 72% of these patients.<sup>7</sup> During the COVID-19 pandemic in Türkiye, antibacterial drug sales decreased by 24.30% in 2020 compared with 2019, which was probably associated with the quarantine.<sup>8</sup> However, a study conducted on Severe acute respiratory syndrome-Coronavirus-2 (SARS-CoV-2)-infected patients in Türkiye showed that 71.2% of the patients were prescribed inappropriate antibiotics.<sup>9</sup>

Antibiotic misuse/abuse is well known to have a negative impact, such as increased antimicrobial resistance and adverse events related to the medication.<sup>10</sup> Therefore, the aim of this study was to determine the risk factors for concomitant bacterial CAP (b-CAP) and the need for initial empirical antibiotic coverage in patients with SARS-Cov-2 infection.

## MATERIALS AND METHODS

This prospective, observational, and single-center study was conducted at a tertiary university hospital between March 20, 2020, and April 15, 2021. This study was conducted by the Declaration of Helsinki, and the study protocol was reviewed and approved by the Hacettepe University Non-Interventional Clinical Research Ethics Committee and the Ministry of Health (approval number: GO 22/520, date: 31.05.2022). All participants provided informed consent.

In this hospital, authorization to use carbapenems, ceftazidime, cefepime, piperacillin-tazobactam, polymyxins, quinolones (except oral forms), glycopeptide antibiotics (vancomycin and teicoplanin), daptomycin, and linezolid as well as more than three days of treatment with the 3<sup>rd</sup> generation cephalosporins and intravenous fluoroquinolones requires infectious diseases (ID) approval because of reimbursement rules by the Social Security Institution. There is a close collaboration between the department of ID and other clinical departments in the management of patients with suspicious infections. Routine clinical practice includes daily clinical rounds of patients treated with an antimicrobial agent by an ID specialist, residents, and a clinical pharmacist during antimicrobial treatment.

### *Study population*

Patients aged over 18 years who tested positive by SARS-CoV-2 polymerase chain reaction (PCR) were included. Those with negative PCR test results but diagnosed presumptively based on characteristic findings on chest computed tomography (CT) and/or positive anti-SARS-CoV-2 immunoglobulin M (IgM) antibodies were also included in the analysis.<sup>11,12</sup> Chest imaging and respiratory panel multiplex PCR test (Seegene, South Korea<sup>6</sup>) were used to diagnose concurrent b-CAP (Supplement 1). Patients younger than 18 years, those with nosocomial pneumonia (pneumonia that developed 72 hours or more after hospital admission), or those without pulmonary involvement were excluded.

### *Data collection*

Data on patient characteristics, diagnostic and clinical parameters, such as changes in oxygen requirement and

fever, and antimicrobial therapy were collected. Patients were followed until the discontinuation of antimicrobial agents, discharge from the hospital, or death.

CURB-65 scores and pneumonia severity index (PSI) were used to predict mortality and determine severity of CAP. The CURB-65 and PSI scores at hospital admission were calculated. The severity of COVID-19 was classified according to the World Health Organization-China Joint Mission definitions.<sup>13</sup> Patients with tachypnea, oxygen saturation  $\leq 93\%$  or PaO<sub>2</sub>/FiO<sub>2</sub> ratio  $< 300$  mmHg, respiratory failure requiring mechanical ventilation, and septic shock were defined as severe to critical COVID-19 pneumonia. Patients with mild pneumonia were classified as mild to moderate COVID-19 patients.

Fever was defined as body temperature  $\geq 38$  °C, whereas oxygen demand was defined as SaO<sub>2</sub>  $< 90\%$  and/or the need for oxygen supplementation. Changes in the fever pattern and oxygen demand were recorded. A leukocyte count of less than  $4.1 \times 10^3/\mu\text{L}$  was defined as leukopenia, whereas a leukocyte count of more than  $11.2 \times 10^3/\mu\text{L}$  was defined as leukocytosis. C-reactive protein (CRP) values greater than 0.8 mg/dL and a procalcitonin (PCT) value greater than 0.1 ng/mL were considered abnormal/high.

The Kidney Disease: Improving Global Outcomes (KDIGO) criteria were used to define drug-related nephrotoxicity. To summarize, nephrotoxicity was defined as an increase in serum creatinine (SCr) by  $\geq 0.3$  mg/dL within 48 hours or an increase in SCr by  $\geq 1.5$  times the baseline within seven days after the initiation of the antibacterial agent. According to KDIGO guidelines, an increase in SCr to 1.5-1.9 times the baseline or an increase in SCr of  $> 0.3$  mg/dL was considered stage 1, and an increase in SCr to 2.0-2.9 times the baseline was considered stage 2, and an increase in SCr to  $\geq 3.0$  times the baseline or  $> 4.0$  mg/dL or the initiation of renal replacement therapy was considered stage 3.<sup>14</sup> The Cancer Therapy Evaluation Program of the National Cancer Institute of the National Institutes of Health, which has been accepted as the common toxicity criteria for adverse events, was used to determine drug-induced hepatotoxicity.<sup>15</sup> The Sanford Guide to Antimicrobial Therapy recommendations were used to determine the appropriateness of antimicrobial doses.<sup>16</sup> "Drugs.com Drug Interactions Checker" ([https://www.drugs.com/drug\\_interactions.html](https://www.drugs.com/drug_interactions.html)) database was used to detect potential drug-drug interactions (pDDIs) among antibacterial agents, and pDDIs were classified as "minor", "moderate" and "major" interactions.

### *Statistical analysis*

Statistical analysis was performed using IBM SPSS Statistics 23.0 for patients who were given empirical antibiotic treatment for b-CAP within 72 hours of admission and those who were not. In addition, SARS-CoV-2 PCR-positive patients were compared with those who tested negative but had highly suggestive CT findings or were SARS-CoV-2 IgM antibody-positive. The Shapiro-Wilk goodness-of-fit test will test whether the distributions related to the numerical variables match the normal distribution. Descriptive statistics, such as mean, standard deviation, median [IQR], minimum, and maximum, were used for

numerical variables that conformed to the normal distribution. For categorical variables, percentage values and frequency tables are given. Categorical variables were compared with the  $\chi^2$  tests. Mann-Whitney U non-parametric test was used to compare two independent groups. Univariate and multivariate logistic regression models were used to identify risk factors associated with antibiotic treatment. The logistic regression models included independent variables found to be significant predictors ( $p < 0.05$ ).

## RESULTS

A total of 262 patients (262/409, 64.1%) with positive PCR for COVID-19 and 147 (147/409, 35.9%) PCR-negative but diagnosed with COVID-19 according to clinical and CT imaging findings were evaluated. The median age of the patients was 62 years [IQR: 48-75 years], and 58.7% were males. The most common comorbidity was hypertension, followed by diabetes mellitus and coronary artery disease (Table 1).

Four hundred and five patients received antiviral treatment in accordance with the recommendations of the Turkish Ministry of Health at the time of diagnosis: favipiravir (76.8%,  $n= 311$ ), redeliver (3.2%,  $n= 13$ ), and hydroxychloroquine (20%,  $n= 81$ ). Antiviral therapy was not prescribed to four patients because of severe liver failure. Oseltamivir was added in 14 (6.8%) patients empirically.

Pulmonary co-infection was detected in 71 (17.4%) patients. Among the coinfecting agents, 83.1% ( $n= 59$ ) were bacteria and 16.9% ( $n= 12$ ) were respiratory viruses. The most common bacterial pathogen was *Haemophilus influenzae* ( $n= 36$ , 60.0%), followed by *Streptococcus pneumoniae* ( $n= 20$ , 33.3%) (Table 2). Urinary *Legionella* antigen was positive in one patient despite a negative respiratory multiplex PCR.

In total, 205 (50.1%) patients received initial empirical antibiotics for suspected b-CAP (Table 2). Antibacterial treatment with atypical coverage was given in 178 patients (86.8%). Chest CT did not suggest concurrent bacterial pneumonia in 66.8%

**Table 1. Demographic and clinical characteristics of patients with COVID-19 pneumonia**

	Total (n= 409)	Initial antibiotic therapy (n=205)	Not initially receiving antibiotic therapy (n= 204)	p value
<b>Age</b>				
Age (years), median (IQR)	62 (48-75)	70 (57.5-80.0)	54 (40.5-67.0)	< 0.001
> 65 years, n (%)	184 (45.0)	126 (61.5)	58 (28.4)	< 0.001
<b>Sex, n (%)</b>				
Male	240 (58.7)	134 (65.4)	106 (52.0)	0.006
<b>Vaccination rate, n (%)</b>				
Influenza vaccine	17 (4.2)	9 (4.4)	8 (3.9)	0.085
Pneumococcal vaccine	9 (2.2)	7 (3.4)	2 (0.98)	0.692
<b>Comorbidities, n (%)</b>				
Hypertension	166 (40.6)	103 (50.2)	63 (30.9)	< 0.001
Diabetes mellitus	111 (27.1)	73 (35.6)	38 (18.6)	< 0.001
Coronary artery disease	106 (25.9)	66 (32.2)	40 (19.6)	0.004
Malignancy	63 (15.4)	48 (23.4)	15 (7.4)	< 0.001
Neurological disease	56 (13.7)	48 (23.4)	8 (3.9)	< 0.001
COPD	44 (10.8)	38 (18.5)	6 (2.9)	< 0.001
Congestive heart failure	37 (9.0)	29 (14.1)	8 (3.9)	< 0.001
Benign prostatic hyperplasia	30 (7.3)	19 (9.3)	11 (5.4)	0.133
Chronic kidney disease	25 (6.1)	19 (9.3)	6 (2.9)	0.008
Asthma	25 (6.1)	8 (3.9)	17 (8.3)	0.061
Atrial fibrillation	23 (5.6)	20 (9.8)	3 (1.5)	< 0.001
Rheumatological diseases	19 (4.6)	8 (3.9)	11 (5.4)	0.474
Liver failure	7 (1.7)	4 (2.0)	3 (1.5)	1.000
Presence of comorbidity	308 (75.3)	189 (92.2)	119 (58.3)	< 0.001
Number of comorbidities, median (IQR)	2 (1-3)	3.0 (1.0-4.0)	1.0 (0.0-2.0)	< 0.001

Table 1. Continued

	Total (n= 409)	Initial antibiotic therapy (n=205)	Not initially receiving antibiotic therapy (n= 204)	p value
<b>Severity of COVID-19, n (%)</b>				
Severe-to-critical patient	168 (41.1)	129 (62.9)	39 (19.1)	< 0.001
Mild-moderate patient	241 (58.9)	76 (37.1)	165 (80.8)	
<b>Corticosteroid therapy, n (%)</b>				
Yes	158 (38.6)	125 (61.0)	33 (16.2)	< 0.001
No	251 (61.4)	80 (39.0)	171 (83.8)	
<b>Risk factors for CAP, n (%)</b>				
Risk factors	239 (58.4)	167 (81.5)	72 (35.3)	< 0.001
<b>Number of patients monitored for biochemical markers, n (%)</b>				
PCT	348 (85.1)	191 (93.2)	157 (77.0)	< 0.001
CRP	383 (93.6)	195 (95.1)	188 (92.2)	0.219
Erythrocyte sedimentation rate	302 (73.8)	157 (76.6)	145 (71.1)	0.205
<b>Development of nosocomial infections during hospitalization, n (%)</b>				
Presence of nosocomial infections	103 (25.2)	80 (39.0)	23 (11.3)	< 0.001
<b>Hospital stay [median (IQR)]</b>				
Duration of hospital stay: day	9.0 (5.0-17.0)	13.0 (8.0-27.5)	5.5 (4.0-10.0)	< 0.001
<b>Criteria for evaluating the severity of the disease, [median (IQR)]</b>				
CURB-65 score	2.0 (0.0-2.0)	2.0 (1.0-3.0)	0.0 (0.0-1.0)	< 0.001
PSI	94 (51.0-139.0)	132 (104.5-164.0)	54 (39.25-88.0)	< 0.001
<b>Adverse events</b>				
Acute kidney injury	46 (11.2)	37 (18.0)	9 (4.4)	< 0.001
ALT elevation	203 (49.6)	108 (52.7)	95 (46.6)	0.236
AST elevation	214 (52.3)	119 (58.0)	95 (46.6)	0.023
<b>Mortality, n (%)</b>				
30-day mortality	58 (14.2)	54 (26.3)	4 (2.0)	< 0.001
Mortality (in hospital)	79 (19.3)	70 (34.1)	9 (4.4)	< 0.001

ALT: Alanine aminotransferase, AST: Aspartate aminotransferase, CAP: Community-acquired pneumonia, PCT: Procalcitonin, CRP: C-reactive protein, IQR: Interquartile range, COPD: Chronic obstructive pulmonary disease, COVID-19: Coronavirus disease-2019, PSI: Pneumonia severity index

(n= 138) of the patients. Patients with high PCT and CRP levels, leukocytosis, oxygen demand, and fever were more likely to receive initial empirical antibiotic therapy (Table 3). Corticosteroid use was also significantly more common in patients who received antibiotic treatment (61%, n= 125) compared to those who did not (16.2%, n= 33,  $p < 0.001$ ). Anti-inflammatory treatment was given to 3 patients due to cytokine storm (tocilizumab in 2 patients, pulse corticosteroid in one). All three patients also received empirical antibiotics at admission to the hospital. Initial empirical antibiotic coverage was 5.338 (95% CI: 2.130-13.379) times more frequent in patients with chronic obstructive pulmonary disease (COPD), 4.457 (95% CI: 1.220-16.276) times with atrial fibrillation (AF), and 1.784 (95% CI: 1.060-3.004) times with diabetes mellitus. The PSI was higher in patients who received antibiotic treatment than

in those who did not [132 (range: 104.5-164.0) versus 54 (range: 39.25-88.0);  $p < 0.001$ ]. However, discontinuation of oxygen supplementation, clinical improvement, and defervescence were similar between patients who received antibiotics and those who did not (Table 3). Thirty-day mortality was significantly higher in patients who received initial antibiotics (26.3%) than in those who did not (2.0%) ( $p < 0.001$ ) (Table 1). The mortality rate increased with older age (1.028-fold), severe to critical patients (3.411-fold), antibiotic therapy (5.726-fold), and nosocomial infection (3.557-fold) (Table 4).

Administration of antibiotics was comparable between SARS-CoV-2 PCR-positive (131/262, 50.0%) and PCR-negative patients (74/147, 50.3%) ( $p = 0.947$ ). In the severe to critical disease subgroup, empirical antibiotics were administered more frequently in patients with positive PCR than in those with

**Table 2. Initial empirical antibiotic treatment for CAP in patients with COVID-19 confirmed *via* PCR positive for SARS-CoV-2 and those with suggestive clinical and radiological findings**

Parameters	Total (n= 409)	COVID-19 patients with positive PCR (n= 262)	COVID-19 patients with suggestive CT imaging & negative PCR (n= 147)	p value
<b>Antibiotic use, n (%)</b>				
Rate of antibiotic use	205 (50.1)	131 (50.0)	74 (50.3)	0.947
Coverage of atypical pathogens during treatment	178 (86.8)	112 (85.5)	66 (89.2)	0.453
Antibacterial treatment duration (day), median (IQR)	7 (6-10)	7.5 (6.0-10.0)	7 (6.75-10.0)	0.999
<b>Preference of antibiotics for the treatment of CAP, n (%)</b>				
Cefuroxime	5 (2.4)	2 (1.5)	3 (4.1)	0.354
Ceftriaxone	73 (35.6)	48 (36.6)	25 (33.8)	0.682
Amoxicillin-clavulanic acid	10 (4.9)	5 (3.8)	5 (6.8)	0.501
Ampicillin-sulbactam	45 (22.0)	26 (19.8)	19 (25.7)	0.333
Piperacillin-tazobactam	81 (39.5)	50 (38.2)	31 (41.9)	0.600
Meropenem	51 (24.9)	37 (28.2)	14 (18.9)	0.138
Fluoroquinolones	9 (4.4)	5 (3.8)	4 (5.4)	0.725
Macrolides	23 (11.2)	15 (11.5)	8 (10.8)	0.889
Doxycycline	147 (71.7)	92 (70.2)	55 (74.3)	0.532
<b>Respiratory multiplex PCR at admission, n (%)</b>				
Bacteria (n= 295)	59 (20.0)	33 (18.0)	26 (23.2)	0.280
Detected pathogens (n= 60)				
<i>Haemophilus influenzae</i>	36 (60.0)	18 (52.9)	18 (69.2)	
<i>Streptococcus pneumoniae</i>	20 (33.3)	14 (41.2)	6 (23.1)	
Dual pathogen <sup>†</sup>	4 (6.7)	2 (5.9)	2 (7.7)	
Virus (n= 306)	12 (3.9)	8 (4.2)	4 (3.5)	1.000
Detected viruses (n= 12)				
Human rhinovirus	3 (25.0)	1 (12.5)	2 (50.0)	
Influenza A	2 (16.7)	2 (25.0)	0 (0.0)	
Influenza B	2 (16.7)	1 (12.5)	1 (25.0)	
Bocavirus	2 (16.7)	1 (12.5)	1 (25.0)	
Adenovirus	2 (16.7)	2 (25.0)	0 (0.0)	
Dual pathogen <sup>‡</sup>	1 (8.3)	1 (12.5)	0 (0.0)	
<b>COVID-19 severity, n (%)</b>				
Severe-to-critical	168 (41.1)	112 (42.7)	56 (38.1)	0.359
Mild-moderate	241 (58.9)	150 (57.3)	91 (61.9)	
<b>Nosocomial infections during hospitalization, n (%)</b>				
Presence of nosocomial infections	103 (25.2)	76 (29.0)	27 (18.4)	<b>0.017</b>
<b>Mortality, n (%)</b>				
30-day mortality	58 (14.2)	41 (15.6)	17 (11.6)	0.256
Mortality (in hospital)	79 (19.3)	58 (22.1)	21 (14.3)	0.054

<sup>†</sup>Dual pathogens in bacterial respiratory, PCR: *Haemophilus influenzae* and *Streptococcus pneumoniae*, <sup>‡</sup>Dual pathogens in viral respiratory PCR: Human rhinovirus and Influenza B, COVID-19: Coronavirus disease 2019, CT: Computed tomography, PCR: Polymerase chain reaction, IQR: Interquartile range, CAP: Community-acquired pneumonia, SARS-CoV-2: Severe acute respiratory syndrome-Coronavirus-2

**Table 3. Antibiotic treatment and clinical, biochemical, and microbiological parameters**

		Total	Initial antibiotic therapy	Not receiving initial antibiotic therapy	<i>p</i> value
<b>Baseline inflammatory marker levels, n (%)</b>					
PCT (n= 397)	≥ 0.1 ng/mL	167 (42.1)	133 (65.5)	34 (17.5)	< 0.001
	< 0.1 ng/mL	230 (57.9)	70 (34.5)	160 (82.5)	
CRP (n= 405)	≥ 0.8 mg/dL	345 (85.2)	197 (97.0)	148 (73.3)	< 0.001
	< 0.8 mg/dL	60 (14.8)	6 (3.0)	54 (26.7)	
Leukocyte count (n= 409)	< 4.1 x 10 <sup>3</sup> /μL	53 (13.0)	20 (9.8)	33 (16.2)	< 0.001
	4.1-11.2 x 10 <sup>3</sup> /μL	269 (65.8)	114 (55.6)	155 (76.0)	
	> 11.2 x 10 <sup>3</sup> /μL	87 (21.3)	71 (34.6)	16 (7.8)	
<b>Inflammatory markers at antibiotic discontinuation, n (%)</b>					
PCT (n= 147)	No change	47 (32.0)	34 (28.3)	13 (48.1)	0.046
	Improved	100 (68.0)	86 (71.7)	14 (51.9)	
CRP (n= 321)	No change	97 (30.2)	42 (22.8)	55 (40.1)	0.001
	Improved	224 (69.8)	142 (77.2)	82 (59.9)	
Leukocyte (n= 136)	No change	61 (44.9)	36 (39.6)	25 (55.6)	0.078
	Improved	75 (55.1)	55 (60.4)	20 (44.4)	
<b>Baseline clinical parameters, n (%)</b>					
Oxygen saturation (n= 409)	SaO <sub>2</sub> ≥ 90 mmHg	200 (48.9)	35 (17.1)	165 (80.9)	< 0.001
	SaO <sub>2</sub> < 90 mmHg	209 (51.1)	170 (82.9)	39 (19.1)	
Fever (n= 409)	< 38 °C	130 (31.8)	48 (23.4)	82 (40.2)	0.001
	≥ 38 °C	279 (68.2)	157 (76.6)	122 (59.8)	
<b>Clinical parameters at antibiotic discontinuation, n (%)</b>					
Oxygen saturation (n= 209)	No change	96 (45.9)	77 (45.3)	19 (48.7)	0.699
	Improved	113 (54.1)	93 (54.7)	20 (51.3)	
Fever (n= 279)	No change	95 (34.1)	48 (30.6)	47 (38.5)	0.164
	Improved	184 (65.9)	109 (69.4)	75 (61.5)	
<b>Respiratory PCR monitoring, n (%)</b>					
Bacterial multiplex PCR (n= 295)	Positive	59 (20.0)	28 (17.9)	31 (22.3)	0.351
	Negative	236 (80.0)	128 (82.1)	108 (77.7)	
Viral multiplex PCR (n= 306)	Positive	12 (3.9)	8 (5.0)	4 (2.8)	0.320
	Negative	294 (96.1)	153 (95.0)	141 (97.2)	
<b>Bacterial culture within 72 hours of hospitalization, n (%)</b>					
Growth of the sputum culture (n= 52)	Yes	9 (17.3)	8 (17.8)	1 (14.3)	1.000
	No	43 (82.7)	37 (82.2)	6 (85.7)	
Growth of the blood culture (n= 272)	Yes	11 (4.0)	10 (6.0)	1 (1.0)	0.055
	No	261 (96.0)	157 (94.0)	104 (99.0)	

PCT: Procalcitonin, CRP: C-reactive protein, PCR: Polymerase chain reaction

**Table 4. Factors influencing mortality in logistic regression analysis**

	Univariable analysis		Multivariable analysis	
	Odds ratio (95% CI)	<i>p</i> value	Odds ratio (95% CI)	<i>p</i> value
Male	2.485 (1.314-4.701)	<b>0.005</b>	1.997 (0.963-4.142)	0.063
Age	1.057 (1.034-1.079)	<b>&lt; 0.001</b>	1.028 (1.003-1.053)	<b>0.030</b>
Comorbidities	7.101 (2.171-23.231)	<b>0.001</b>	1.366 (0.276-6.768)	0.702
Presence of risk factors for CAP	6.317 (2.789-14.305)	<b>&lt; 0.001</b>	1.653 (0.533-5.126)	0.384
Severe-to-critical patient	10.614 (5.042-22.344)	<b>&lt; 0.001</b>	3.411 (1.506-7.724)	<b>0.003</b>
Initial antibiotic therapy	17.881 (6.337-50.456)	<b>&lt; 0.001</b>	5.726 (1.866-17.569)	<b>0.002</b>
Nosocomial infection	6.936 (3.832-12.556)	<b>&lt; 0.001</b>	3.557 (1.826-6.930)	<b>&lt; 0.001</b>

CAP: Community-acquired pneumonia, CI: Confidence interval

negative PCR (64.9% versus 59.5%,  $p < 0.001$ ). Corticosteroid use (dexamethasone or methylprednisolone) was more frequent in SARS-CoV-2 PCR-positive patients (43.1% versus 30.6%,  $p = 0.013$ ). Nosocomial infections were more common in the SARS-CoV-2 PCR-positive group than in the PCR-negative group (29.0% versus 18.4%, respectively,  $p = 0.017$ ), and in those who received corticosteroids compared with those who did not (59.2% versus 40.8%, respectively,  $p < 0.001$ ). The median duration of antibiotic treatment did not differ between PCR-positive and PCR-negative patients ( $p = 0.999$ ) (Table 2). Antibiotic treatment did not improve the clinical course of patients with positive SARS-CoV-2 PCR and negative results (data not shown).

#### Adverse events and pDDIs during follow-up

Acute kidney injury occurred in 11.2% of patients. Thirty-seven patients who received antibiotic treatment experienced nephrotoxicity (52.8% for stage 1; 36.1% for stage 2; and 11.1% for stage 3). Nephrotoxicity was significantly higher in patients treated with antibiotics than in patients not treated with antibiotics (18.0% versus 4.4%;  $p < 0.001$ ). Patients treated with piperacillin-tazobactam experienced more nephrotoxicity than those treated with other antibiotics (31.3% versus 9.6%,  $p < 0.001$ ).

Elevated aminotransferase levels occurred in 60.9% ( $n = 249$ ) of the patients. Elevated aspartate aminotransferase levels were observed more frequently in patients receiving antibiotic treatment than in those who were not receiving antibiotic treatment [58.0% ( $n = 119$ ) versus 46.6% ( $n = 95$ ),  $p = 0.023$ ]. Alanine aminotransferase elevation was similar between patients who did and did not receive antibiotic(s) [52.7% ( $n = 108$ ) versus 46.6% ( $n = 95$ ),  $p = 0.236$ ].

Antibiotic-related pDDIs were detected in 77.1% of the patients treated with antibiotics (the rate of minor pDDIs was 30.7%, the rate of moderate pDDIs was 68.3%, and the rate of major pDDIs was 15.1%) (Supplement 2). The median number of pDDIs detected with antibiotics was 2 (1-3). The 30-day mortality was similar between patients with and without antibiotic-related pDDIs (25.3% versus 29.8%,  $p = 0.541$ ).

## DISCUSSION

Our results emphasize that initial empirical antibiotic treatment is mostly unnecessary in patients with COVID-19. We observed that empirical antibiotics did not affect mortality regardless of comorbidities and severity of pneumonia. In contrast, they lead to drug-related problems, such as nephrotoxicity and pDDIs. Although inflammatory markers were improved, clinical parameters remained similar between patients who did and did not receive antibiotics.

Several studies reported an incidence of 2.0-17.2% bacterial co-infection in patients with COVID-19. However, antibiotic therapy was administered to 48.6-100% of patients.<sup>2,17-22</sup> In our study ( $n = 409$ ) antibiotics were used in 50.1% of the COVID-19 patients for presumptive b-CAP. A cross-sectional study from our center found that respiratory bacterial co-infection was present in 26 (13.1%) of 198 outpatients with COVID-19, with only 10.6% received.<sup>23</sup> This could be explained by the preference of the physician for antibiotic administration to patients who require hospitalization for pulmonary infection.

Whether the patient was positive by PCR for SARS-CoV-2 or diagnosed presumptively based on clinical and imaging findings did not affect the clinical decision-making of the physicians to start antibiotics. Antibiotic treatment rates and antibiotic preferences were similar between patients with and without SARS-CoV-2 PCR ( $p = 0.947$ ). In a study by Beović et al.,<sup>24</sup> clinical presentation was the most common indication for antibiotic therapy in patients with COVID-19. It was also emphasized that laboratory markers and radiological evaluation were effective in the antibiotic therapy decision.<sup>24</sup> Similarly, in our study, antibiotic use was related to supplemental oxygen therapy, fever, and elevated acute-phase reactants.

The role of inflammatory markers in determining the efficacy of antibiotic therapy is limited. In our study, significant improvement was achieved in these parameters but not in the clinical course. The use of anti-inflammatory agents (corticosteroids or tocilizumab) and the rate of concomitant nosocomial infection are confounding factors in determining the impact of antibiotic treatment on serum levels of inflammatory markers. In our study, more patients who received empirical

antibiotics were also treated with corticosteroids (61.0% versus 16.2%;  $p < 0.001$ ). This finding could explain the improvement in inflammatory marker levels observed in the antibiotic-treated group, despite no clinical improvement.

Empirical antibacterial therapy may have undesirable consequences. Contrary to other studies,<sup>18,19,21</sup> we found that the nosocomial infection rate was significantly higher in patients treated with antibiotics for CAP (39.0% versus 11.3%, respectively,  $p < 0.001$ ). In addition, hospital stay was longer among patients treated with antibiotics ( $p < 0.001$ ). This could also be related to a more severe initial clinical presentation, the presence of certain comorbidities, such as COPD and diabetes mellitus, which are known to have a negative effect on the hospital stay of patients with COVID-19, and the more frequent use of corticosteroids in this patient population.

Pettit et al.<sup>2</sup> reported that the mortality rate of patients with COVID-19 receiving empirical antibiotic therapy for CAP was 13.8%.<sup>2</sup> A retrospective study by Ng et al.<sup>25</sup> On patients with COVID-19 showed that mortality was higher in patients receiving antibiotic treatment (13.3% versus 0.5%,  $p < 0.001$ ). Furthermore, their study did not associate antibiotic therapy with lower mortality [adjusted odds ratio 14,492, (95% CI 0.533-393.875)].<sup>25</sup> We found that initial empirical antibacterial treatment was an independent risk factor for mortality (Table 4).

#### Study limitations

This was a single-center, observational study; thus, the results may not be applicable to other centers. In some patients with positive CT imaging but negative PCR results, the absence of antibody test results makes the definitive diagnosis of COVID-19 unclear. We did our best to rule out other viral/bacterial infections and non-infectious causes, such as congestive heart failure, leaving us with a COVID-19 diagnosis during the pandemic.

## CONCLUSION

Attending physicians tend to prescribe antimicrobials to prevent adverse outcomes in high-risk COVID-19 patients, *i.e.*, patients with older age, severe disease, comorbidities such as COPD, AF, and diabetes mellitus, high inflammatory marker levels, fever, and the necessity for oxygen supplementation even when there is no evidence of co-infection. Irrational use of antibiotics may cause drug-related problems and negative effects by disrupting the gastrointestinal microbiota in patients with COVID-19, including altered metabolic activity and increased antibiotic resistance. This study provides further evidence for antimicrobial stewardship efforts and recommends discontinuing empirical antibiotics, even if they are not started.

#### Acknowledgment

This study was presented at the 16<sup>th</sup> World Intensive and Critical Care Congress (WICC), İstanbul, Türkiye, on 26-30 August 2023.

#### Ethics

**Ethics Committee Approval:** This study was conducted in accordance with the Declaration of Helsinki, and the study

protocol was reviewed and approved by the Hacettepe University Non-Interventional Clinical Research Ethics Committee (approval number: GO 22/520, date: 31.05.2022).

**Informed Consent:** All participants provided informed consent.

#### Authorship Contributions

Surgical and Medical Practices: P.B.E., E.K., G.T.D., M.Ç.S., Concept: P.B.E., E.K., A.Ç.İ., K.D., S.Ü., Ö.U., Design: P.B.E., G.T.D., M.Ç.S., A.C.I., K.D., S.Ü., Ö.U., Data Collection or Processing: P.B.E., E.K., G.T.D., M.Ç.S., Analysis or Interpretation: P.B.E., E.K., A.Ç.İ., Literature Search: P.B.E., A.Ç.İ., K.D., S.Ü., Ö.U., Writing: P.B.E., E.K.

**Conflict of Interest:** The authors have no conflicts of interest to declare.

**Financial Disclosure:** The authors declared that this study received no financial support.

## REFERENCES

- Sieswerda E, de Boer MGJ, Bonten MMJ, Boersma WG, Jonkers RE, Aleva RM, Kullberg BJ, Schouten JA, van de Garde EMW, Verheij TJ, van der Eerden MM, Prins JM, Wiersinga WJ. Recommendations for antibacterial therapy in adults with COVID-19-an evidence based guideline. *Clin Microbiol Infect.* 2021;27:61-66.
- Pettit NN, Nguyen CT, Lew AK, Bhagat PH, Nelson A, Olson G, Ridgway JP, Pho MT, Pagkas-Bather J. Reducing the use of empiric antibiotic therapy in COVID-19 on hospital admission. *BMC Infect Dis.* 2021;21:516.
- Young BE, Ong SWX, Kalimuddin S, Low JG, Tan SY, Loh J, Ng OT, Marimuthu K, Ang LW, Mak TM, Lau SK, Anderson DE, Chan KS, Tan TY, Ng TY, Cui L, Said Z, Kurupatham L, Chen MI, Chan M, Vasoo S, Wang LF, Tan BH, Lin RTP, Lee VJM, Leo YS, Lye DC; Singapore 2019 Novel Coronavirus Outbreak Research Team. Epidemiologic features and clinical course of patients infected with SARS-CoV-2 in Singapore. *JAMA.* 2020;323:1488-1494.
- World Health Organization (WHO) Living Guidance for Clinical Management of COVID-19: Living Guidance. Nov 23, 2021. [Accessed on 23 July 2022]. Available: <https://www.who.int/publications/i/item/WHO-2019-nCoV-clinical-2021-2>
- Evans TJ, Davidson HC, Low JM, Basarab M, Arnold A. Antibiotic usage and stewardship in patients with COVID-19: too much antibiotic in uncharted waters? *J Infect Prev.* 2021;22:119-125.
- Çalık Başaran N, Uyaroğlu OA, Telli Dizman G, Özışık L, Şahin TK, Taş Z, İnkaya AÇ, Karahan S, Alp Ş, Alp A, Metan G, Zarakol P, Sain Güven G, Öz ŞG, Topeli A, Uzun Ö, Akova M, Ünal S. Outcome of noncritical COVID-19 patients with early hospitalization and early antiviral treatment outside the ICU. *Turk J Med Sci.* 2021;51:411-420.
- Rawson TM, Moore LSP, Zhu N, Ranganathan N, Skolimowska K, Gilchrist M, Satta G, Cooke G, Holmes A. Bacterial and fungal coinfection in individuals with Coronavirus: a rapid review to support COVID-19 antimicrobial prescribing. *Clin Infect Dis.* 2020;71:2459-2468.
- İlaç Endüstrisi İşverenler Sendikası (İEİS)-Temel Göstergeler/Türkiye İlaç Pazarı: - n.d. [Accessed on May 26, 2023]. Available: <http://ieis.org.tr/ieis/tr/indicators/33/turkiye-ilac-pazari>
- Şencan İ, Çağ Y, Karabay O, Kurtaran B, Güçlü E, Öğütlü A, Demirbaş Z, Bulut D, Karlıdağ GE, Sefa Sayar M, Şibar EG, Eren Kutsoylu OÖ, Kul G, Erol S, Bektaş B, Ünver Ulusoy T, Kuzi S, Tasbakan M, Yiğit Ö, Ceran N, İnal AS, Ergen P, Yamazhan T, Uzar H, Ağalar C. Antibiotic

- use and Influencing factors among hospitalized patients with COVID-19: A multicenter point-prevalence study from Turkey. *Balkan Med J.* 2022;39:209-217.
10. Llor C, Bjerrum L. Antimicrobial resistance: risk associated with antibiotic overuse and initiatives to reduce the problem. *Ther Adv Drug Saf.* 2014;5:229-241.
  11. Kipritci Z, Keskin AU, Ciragil P, Topkaya AE. Evaluation of a Visually-Read Rapid Antigen Test Kit (SGA V-Chek) for detection of SARS-CoV-2 virus. *Mikrobiyol Bul.* 2021;55:461-464.
  12. Beavis KG, Matushek SM, Abeleda APF, Bethel C, Hunt C, Gillen S, Moran A, Tesic V. Evaluation of the EUROIMMUN Anti-SARS-CoV-2 ELISA Assay for detection of IgA and IgG antibodies. *J Clin Virol.* 2020;129:104468.
  13. Gomes C. Report of the World Health Organization (WHO)-China joint mission on Coronavirus Disease 2019 (COVID-19). *Braz J Implantol Health Sci.* 2020;2.
  14. Kellum JA, Lameire N; KDIGO AKI Guideline Work Group. Diagnosis, evaluation, and management of acute kidney injury: a KDIGO summary (Part 1). *Crit Care.* 2013;17:204.
  15. LiverTox: Clinical and research information on drug-induced liver injury [Internet]. Bethesda (MD): National Institute of Diabetes and Digestive and Kidney Diseases; 2012. Severity grading in drug induced liver injury. May 4, 2019. [Accessed on 25 November 2023]. Available online: <https://www.ncbi.nlm.nih.gov/books/NBK548241/>
  16. Gilbert DN, Robert C, Moellering JMD, Eliopoulos GM, Sande MA. The Sanford guide to antimicrobial therapy: Antimicrobial therapy. 2011;40:48-51.
  17. Wu C, Chen X, Cai Y, Xia J, Zhou X, Xu S, Huang H, Zhang L, Zhou X, Du C, Zhang Y, Song J, Wang S, Chao Y, Yang Z, Xu J, Zhou X, Chen D, Xiong W, Xu L, Zhou F, Jiang J, Bai C, Zheng J, Song Y. Risk factors associated with acute respiratory distress syndrome and death in patients with Coronavirus Disease 2019 Pneumonia in Wuhan, China. *JAMA Intern Med.* 2020;180:934-943.
  18. Huang C, Wang Y, Li X, Ren L, Zhao J, Hu Y, Zhang L, Fan G, Xu J, Gu X, Cheng Z, Yu T, Xia J, Wei Y, Wu W, Xie X, Yin W, Li H, Liu M, Xiao Y, Gao H, Guo L, Xie J, Wang G, Jiang R, Gao Z, Jin Q, Wang J, Cao B. Clinical features of patients infected with 2019 novel coronavirus in Wuhan, China. *Lancet.* 2020;395:497-506.
  19. Chen N, Zhou M, Dong X, Qu J, Gong F, Han Y, Qiu Y, Wang J, Liu Y, Wei Y, Xia J, Yu T, Zhang X, Zhang L. Epidemiological and clinical characteristics of 99 cases of 2019 novel coronavirus pneumonia in Wuhan, China: a descriptive study. *Lancet.* 2020;395:507-513.
  20. Wang Z, Yang B, Li Q, Wen L, Zhang R. Clinical features of 69 cases with Coronavirus Disease 2019 in Wuhan, China. *Clin Infect Dis.* 2020;71:769-777.
  21. Zhou F, Yu T, Du R, Fan G, Liu Y, Liu Z, Xiang J, Wang Y, Song B, Gu X, Guan L, Wei Y, Li H, Wu X, Xu J, Tu S, Zhang Y, Chen H, Cao B. Clinical course and risk factors for mortality of adult inpatients with COVID-19 in Wuhan, China: a retrospective cohort study. *Lancet.* 2020;395:1054-1062.
  22. Lehmann CJ, Pho MT, Pitrak D, Ridgway JP, Pettit NN. Community-acquired coinfection in Coronavirus Disease 2019: A retrospective observational experience. *Clin Infect Dis.* 2021;72:1450-1452.
  23. Telli Dizman G, Metan G, Ayaz Ceylan ÇM, Altunay H, Uzun M, Gürsoy G, Taş Z, Karahan G, Ahmadova F, Sarıcaoğlu T, Çalışkan ZC, Alp A, Sönmezler M, İnkaya A, Özyavuz Alp Ş, Uyaroğlu O, Er A, Özyavuz Alp Ş, Uyaroğlu O, Durusu Tanrıöver M, Çalık Başaran N, Durhan G, Demirkazık F. A COVID-19 first evaluation clinic at a university hospital in Turkey. *Turk J Med Sci.* 2022;52:1-10.
  24. Beović B, Doušak M, Ferreira-Coimbra J, Nadrah K, Rubulotta F, Belliato M, Berger-Estilita J, Ayoade F, Rello J, Erdem H. Antibiotic use in patients with COVID-19: a 'snapshot' Infectious Diseases International Research Initiative (ID-IRI) survey. *J Antimicrob Chemother.* 2020;75:3386-3390.
  25. Ng TM, Ong SWX, Loo AYY, Tan SH, Tay HL, Yap MY, Lye DC, Lee TH, Young BE. Antibiotic therapy in the treatment of COVID-19 Pneumonia: Who and when? *Antibiotics.* 2022;11:184.

**Supplement 1. Respiratory pathogens were tested using respiratory panel multiplex PCR (Seegene, South Korea)**

Viral pathogens	Bacterial pathogens
Adenovirus	<i>Streptococcus pneumoniae</i>
Bocavirus	<i>Haemophilus influenzae</i>
Enterovirus	<i>Mycoplasma</i> spp.
Human rhinovirus	<i>Legionella</i> spp.
Influenza A	
Influenza B	
Metapneumovirus	
Coronavirus OC43	
Coronavirus HKU1	
Coronavirus 229E	
Coronavirus NL63	
Parainfluenza 1	
Parainfluenza 2	
Parainfluenza 3	
Parainfluenza 4	
RSV A	
RSV B	
Microbiological culture (deep tracheal aspirate or sputum)	
-	Meticillin-sensitive <i>Staphylococcus aureus</i> <i>Streptococcus parasanguinis</i> <i>Haemophilus influenzae</i> <i>Klebsiella pneumoniae</i> <i>Klebsiella aerogenes</i>

PCR: Polymerase chain reaction, RSV: Respiratory Syncytial Virus

**Supplement 2. Classification of antibiotic-drug interactions**

Major antibiotic-drug interactions (n= 42)*		Moderate antibiotic-drug interactions (n= 221)*	
Clarithromycin and atorvastatin	14.3%	Doxycyclin-piperacillin	21.7%
Clarithromycin-methylprednisolone	9.5%	Doxycycline-calcium carbonate	20.8%
Moxifloxacin-dexamethasone	9.5%	Doxycycline-insulin	16.3%
Clarithromycin, fentanyl	7.1%	Doxycycline-ampicillin	10.4%
Clarithromycin/haloperidol	4.8%	Clarithromycin and dexamethasone	6.3%
Clarithromycin and quetiapine	4.8%	Ceftriaxone-furosemide	5.9%
Clarithromycin and tamsulosin	4.8%	Clarithromycin-lactulose	2.3%
Clarithromycin and midazolam	4.8%	Doxycycline-digoxin	1.8%
Clarithromycin and amiodarone	4.8%	Clarithromycin-amlodipine	1.8%
Clarithromycin and silodosin	4.8%	Clarithromycin, lansoprazole	1.4%
Meropenem and tramadol	4.8%	Doxycycline (warfarin)	0.9%
Clarithromycin and warfarin	2.4%	Doxycycline-rocuronium	0.9%
Clarithromycin-colchicine	2.4%	Clarithromycin-insulin	0.9%
Clarithromycin and escitalopram	2.4%	Clarithromycin and propofol	0.9%
Clarithromycin-hydroxychloroquine	2.4%	Levofloxacin, quetiapine	0.9%
Levofloxacin-methylprednisolone	2.4%	Levofloxacin-lactulose	0.9%
Levofloxacin-dexamethasone	2.4%	Ceftriaxone (warfarin)	0.5%
Levofloxacin/haloperidol	2.4%	Cefuroxime-pantoprazole	0.5%
Levofloxacin-insulin	2.4%	Piperacillin and warfarin	0.5%
Moxifloxacin (granisetron)	2.4%	Moxifloxacin, aspirin (low strength)	0.5%
Moxifloxacin-insulin	2.4%	Moxifloxacin/famotidine	0.5%
Meropenem-valproic acid	2.4%	Moxifloxacin/ibuprofen	0.5%
		Levofloxacin, aspirin (low strength)	0.5%
		Levofloxacin, mirtazapine	0.5%
		Doxycycline-sucralfate	0.5%
		Doxycycline (primidone)	0.5%
		Doxycycline, carbamazepine	0.5%
		Clarithromycin, clopidogrel	0.5%
		Clarithromycin-sertraline	0.5%

\*Indicates the total number of interactions



# *In silico* and *in vitro* Evaluation of the Cytotoxic Potential of Hinokitiol against Osteosarcoma by Targeting Glycogen Synthase Kinase 3 $\beta$

Binoy Varghese CHERIYAN<sup>1\*</sup>, Punithavel SRINIVASAN<sup>1</sup>, Georgepush JAYARAJ<sup>1</sup>, Karthik Kadhiri KARUNAKAR<sup>2</sup>,  
 Prasanna Bharathi SAINATH<sup>2</sup>, Anandakumar SHANMUGAM<sup>3</sup>, Anitha ROY<sup>4</sup>, Karthikeyan ELUMALAI<sup>1</sup>

<sup>1</sup>Saveetha University, Saveetha Institute of Medical and Technical Sciences, Saveetha College of Pharmacy, Department of Pharmaceutical Chemistry, Tamil Nadu, India

<sup>2</sup>Saveetha University, Saveetha Institute of Medical and Technical Sciences, Saveetha College of Pharmacy, Department of Pharmacology, Tamil Nadu, India

<sup>3</sup>University of Madras, Dr. ALM Post Graduate Institute of Basic Medical Science, Department of Microbiology, Tamil Nadu, India

<sup>4</sup>Saveetha University, Saveetha Institute of Medical and Technical Sciences, Saveetha Dental College and Hospitals, Department of Pharmacology, Tamil Nadu, India

## ABSTRACT

**Objectives:** The present study aimed to assess the antiproliferative and pro-apoptotic effects of hinokitiol in osteosarcoma cells *via in vitro* and *in silico* targeting of glycogen synthase kinase 3 $\beta$  (GSK3 $\beta$ ).

**Materials and Methods:** The (3-(4,5-dimethylthiazol-2-yl)-2,5-diphenyltetrazolium bromide) assay was used to evaluate the cytotoxic potential of hinokitiol in osteosarcoma cells. Various concentrations of hinokitiol (5, 10, 20, 40, 60, and 80  $\mu$ g/mL) were tested, and the half-maximal inhibitory concentration (IC<sub>50</sub>) was calculated. Cell morphology, migration (scratch assay), and gene expression analysis using real-time polymerase chain reaction for pro-apoptotic studies were conducted, with the IC<sub>50</sub> dose of hinokitiol utilized in all these experiments. Additionally the anti-proliferative effect of hinokitiol on GSK3 $\beta$  was also examined using *in silico* and gene expression methods.

**Results:** Hinokitiol significantly ( $p < 0.05$ ) and dose-dependently decreased the viability of MG-63 cells, with an IC<sub>50</sub> value of 40  $\mu$ g/mL. Cell morphology study revealed cellular shrinkage and reduced cell density. The scratch assay revealed anti-migratory activity, while gene expression studies indicated pro-apoptotic effects, including significant ( $p < 0.05$ ) upregulation of BAX and down-regulation of BCL-2 and GSK3 $\beta$ . Bonding interactions were also observed with GSK3 $\beta$  and atomic contact energy of -5.69 kcal/mol.

**Conclusion:** According to the current study findings, hinokitiol prevented Morphological study of the effects of hinokitiol on osteosarcoma cells from proliferating, migrating, and induced apoptosis by upregulating BAX (a pro-apoptotic signal) expression and downregulating BCL-2 (anti-apoptotic signal) expression in osteosarcoma cells. *In silico* findings of hinokitiol showed a significant bonding interaction with GSK3 $\beta$  and its downregulated gene expression probably prevented cancer cell survival.

**Keywords:** Hinokitiol, osteosarcoma, MTT assay, *in silico*, glycogen synthase kinase 3 $\beta$

## INTRODUCTION

Osteosarcoma is a rare malignant condition and is the most prevalent bone cancer. Osteosarcoma primarily affects youths and adolescents.<sup>1</sup> The treatment of osteosarcoma has advanced significantly in the modern era. The treatment

includes radiation, chemotherapy, and even surgery. Currently, individuals with osteosarcoma have a 5-year survival rate of approximately 60-70%. Ifosfamide and methotrexate are some of the chemotherapy drugs used. Various combinations and other cytotoxic substances like etoposide have also been

\*Correspondence: lallybinoy@gmail.com, ORCID-ID: orcid.org/0000-0003-0830-6816

Received: 10.06.2023, Accepted: 23.12.2023



proposed in the literature.<sup>2</sup> However, taking these medications can cause several difficulties and adverse effects, such as neutropenia, mouth fissures, exhaustion, severe diarrhea, nausea, and emesis. The most notorious culprit may be anthracyclines, which cause acute reactions such as chest pain and dyspnea, underscoring a significant drawback of chemotherapy.<sup>3</sup> Chemoresistance is another issue posed by contemporary therapies. These therapeutic limitations have inspired researchers to explore new avenues, such as finding new targets and understanding their mechanisms, to identify cutting-edge treatments for a variety of cancers, including osteosarcoma. The most popular cell lines for osteosarcoma are MG-63 cells, which were generated from young Caucasian patients and were derived from their fibroblastic or epithelial origins. MG-63 cells have a highly proliferative phenotype.<sup>4</sup> The intent of using this specific cell line was to improve its affordability and accessibility as well as be beneficial for experimental research.

Glycogen synthase kinase 3 $\beta$  (GSK3 $\beta$ ) is an important protein kinase that regulates metabolism, apoptosis, inflammation, and cell differentiation.<sup>5-7</sup> Aberrant activation of GSK3 $\beta$  has been observed in neurodegenerative diseases, cardiovascular diseases, and some oncological conditions.<sup>8,9</sup> Osteosarcomas express more GSK3 $\beta$  than normal cells and tissues. According to several recent studies down-regulated GSK3 $\beta$  may inhibit cancer cell growth and trigger apoptosis in human osteosarcoma cells.<sup>10,11</sup> The enhancement of Wnt signaling and catenin signaling through the inhibition of GSK3 $\beta$  is also believed to limit osteosarcoma cancer cell survival and proliferation. Based on these findings, increased expression of GSK3 $\beta$  in cancer is a potential therapeutic target.

Hinokitiol, chemically known as 2-hydroxy-4-isopropylcyclohepta-2,4,6-trien-1-one, (Figure 1), belongs to the monoterpenoid class and has a range of medicinal properties, including neuroprotective,<sup>12</sup> anti-tyrosinase,<sup>13</sup> anti-inflammatory<sup>14</sup> and anti-proliferative.<sup>15</sup> Hinokitiol has been demonstrated in recent studies to be effective against lung adenocarcinoma,<sup>16</sup> melanoma,<sup>17</sup> and breast cancer<sup>18</sup> cell lines. It also interferes with signaling pathways and explains how protein expression stops cancer cells from proliferating, migrating, and metastasizing. The effectiveness of hinokitiol against various cancers has been studied *in vitro*, and its benefits for bone loss have been evaluated; however, its potential against bone cancer remains unexplored. In this study, its efficacy against osteosarcoma was evaluated to assess the anti-proliferative and pro-apoptotic

effects of hinokitiol in osteosarcoma cells *via in vitro* and *in silico* targeting of GSK3 $\beta$ .

## MATERIALS AND METHODS

Hinokitiol was purchased from the Tokyo Chemical Industry to ensure material purity. The melting point of 51 °C and  $\lambda_{\text{max}}$  (238, 320) were assessed using a melting point apparatus and ultraviolet absorption spectroscopy (Shimadzu 160 A) and found the same.

### Cell line maintenance

From NCCS in Pune, MG-63 cells were purchased. The cells were grown in T25 culture flasks containing 10% fetal bovine serum (FBS) and 1% anti-biotics in Dulbecco's modified Eagle medium. Cells were housed in a humidified atmosphere with 5% CO<sub>2</sub> at 37 °C. Once confluence was reached, the cells were trypsinized and passaged.

### Cell viability [(3-(4,5-dimethylthiazol-2-yl)-2,5-diphenyltetrazolium bromide (MTT)] assay

Cytotoxicity (loss of viable cells) was assessed using the MTT assay.<sup>19</sup> This assay relies on the metabolic conversion of the soluble MTT salt, 3-(4, 5-dimethylthiazol-2-yl)-2,5-diphenyltetrazolium bromide, which symbolizes the normal function of mitochondrial dehydrogenase activity and cell viability, into an insoluble colored formazan product, which was estimated spectrophotometrically. The number of viable cells can be directly and proportionally estimated from the activity of mitochondria in living cells. MG-63 cells of 5X10<sup>3</sup> density per well were coated on 96-well plates, and to this medium FBS was added and kept for 24 h in an incubator. The cells were then exposed to various doses of hinokitiol in triplicate (5, 10, 20, 40, 60, 80  $\mu\text{g}/\text{mL}$ ) at 5% CO<sub>2</sub> at 37 °C for 24 h. Subsequently, cells were added with MTT reagent and incubated for 4 h (Sigma, MO, USA). The same amount of time was also spent incubating untreated [dimethyl sulfoxide (DMSO)] cells. MTT solubilization solution (Sigma) was used to dissolve the formazan crystals after the incubation period; the formed formazan crystals were then made into a solution in DMSO (100  $\mu\text{l}$ ) and incubated in the dark for an hour. A 96-well image reader was used to detect absorbance at 570 nm. The percentage of viable cells was defined as the percentage of control cells established in a serum-free medium. The control medium without treatment was considered 100% viable. The cell viability was calculated using the following formula: % cell viability = [A570 nm of treated cells/A570 nm of control cells] x 100.

### Cell morphology analysis

Based on the results of the MTT experiment, we selected the optimum dose (IC<sub>50</sub> 40  $\mu\text{g}/\text{mL}$ ) for further research. Using a phase-contrast microscope, changes in cell morphology were analyzed. In a 6-well plate, MG63 cells were seeded at a density of 2 x 10<sup>5</sup> and were kept overnight. The cells were treated with an optimal dose of hinokitiol (40  $\mu\text{g}/\text{mL}$ ) for 24 h, and untreated cells served as the negative control. When the incubation period ceased, the medium was removed, and the cells were washed with phosphate buffer saline (pH 7.4) and examined under a phase-contrast microscope.

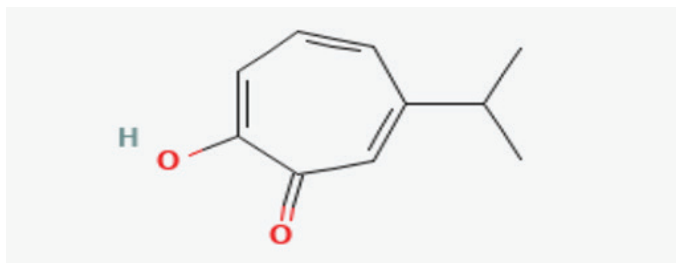


Figure 1. Structure of hinokitiol

### Cell migration was analyzed using the scratch-wound healing assay

MG63 cell line was planted onto a six-well culture plate at a density of  $2 \times 10^5$  and was kept overnight. The incubated cells were then washed with Dulbecco's phosphate-buffered saline (DPBS), and a sterile micropipette tip of 200  $\mu$ l, was used to make a scratch.<sup>20</sup> The detached cells and other cellular debris were washed with DPBS. The cells were then treated with an optimal dose of hinokitiol (40  $\mu$ g/mL) for 24 h, and untreated cells served as the negative control. After incubation, the wells were washed and fixed in 4% paraformaldehyde. Photographs were taken using an inverted microscope (Euromex, The Netherlands).

### RNA extraction and gene expression by real-time polymerase chain reaction (RT-PCR)

Using RT-PCR, the gene expression of pro-apoptotic and anti-apoptotic cells was examined, and Trizol Reagent (Sigma) was used to separate the total RNA. Briefly, 1-2  $\mu$ g of total RNA was transformed to cDNA using, PrimeScript, 1<sup>st</sup> strand cDNA synthesis kit (Takara, Japan) by the manufacturer's instructions.<sup>21</sup> Primers were designed to specifically amplify targeted genes. The primer sequences BAX-Forward: 5'gctggacattggacttctc3'; reverse: 5'ctcagcccatcttctccag3'; BCL-2- forward: 5'gctggacattggacttctc3'; reverse: 5'ctcagcccatcttctccag3'. GAPDH- Forward: 5'cgaccactttgcaagctca3'; reverse: 5' ccctcttcaaggggtctac3'. GSK3 $\beta$ - Forward: 5'ccgactaacaccactggaagct3' Reverse: 5'aggatgtagccagaggtggat3'. PCR was performed using iTaq Universal SYBR Green Supermix (Bio-Rad, USA), which contains SYBR green dye and all PCR components.<sup>22</sup> Stratagene's MX3000p PCR machine was used to perform real-time PCR. The results were analyzed using the comparative computed tomography method and  $2^{-\Delta\Delta C_T}$  and the Schmittgen and Livak 2CT method was utilized to calculate fold changes.

### Molecular docking

#### Structure preparation

The crystal structure of GSK3 $\beta$  was downloaded from the Protein Data Bank (PDB) at (PDB\_http://www.pdb.org/pdb/home/home CODE: 2O5K). The 3D structure of hinokitiol was downloaded from the Pubchem database for docking.

#### Molecular docking

Auto Dock 4.2 was used to perform docking calculations. Auto Dock Tools (ADT) were used to create grid boxes and .pdbqt files to generate proteins and ligands. ADT was used to modify the native GSK3 $\beta$  structure by adding polar hydrogens, unified Kollman charges, solvation parameters, and fragmental volumes. The Auto Grid was used to construct grid maps representing proteins throughout the docking process. The dimensions of the x, y, and z axes were set to 100, 100, and 100, respectively, and the grid spacing was set to 0.403. The 100 docking conformers were performed using the Lamarckian Genetic Algorithm (LGA), and the Auto Dock application was run with the following parameters; Maximum number of energy evaluations allowed is 250000; GA crossover mode

is two points; GA population size is 150. Out of 100 LGA conformers, the conformer with the lowest binding energy was chosen for further analysis. We measured the binding energy and determined both particular and non-specific interaction residues of the entire molecule coupled to GSK3 $\beta$ . The software packages Pymol and Discovery Studio were used to visualize the docked conformations.

### Statistical analysis

Data obtained from the study (Cell Viability and Gene expression) were analyzed by One-Way analysis of variance followed by Student's *t*-test using SPSS version 20 and represented as mean  $\pm$  standard deviation for triplicate analyses. Statistical significance was determined at a level of  $p < 0.05$ .

## RESULTS

### Hinokitiol significantly reduces MG-63 cell viability

Cellular survival following exposure to hinokitiol at various concentrations (5, 10, 20, 40, 60, and 80  $\mu$ g/mL) was determined using absorbance readings obtained from the MTT assay. Results were compared with the corresponding negative controls (untreated cells) after 24 h of incubation and expressed as percentages of viability. Hinokitiol significantly ( $p < 0.05$ ) decreased MG-63 cell viability in a dose-dependent manner, with a half-maximal inhibitory concentration (IC<sub>50</sub>) of 40  $\mu$ g/mL (Figure 2)

### Morphological study of the effects of hinokitiol on osteosarcoma (MG63) cells

A decrease in the cell population was observed following hinokitiol incubation. As depicted in (Figure 3) treatment with the IC<sub>50</sub> dose of 40  $\mu$ g/mL hinokitiol led to noticeable cellular shrinkage and a reduction in cell density, causing overall morphological alterations. MG-63 cells were treated with the test compound hinokitiol (IC<sub>50</sub> 40  $\mu$ g/mL) along with the control group for 24 h. The images were obtained at a magnification (x 10) using an inverted phase-contrast microscope.

### Hinokitiol decreases wound closure in MG-63 cells

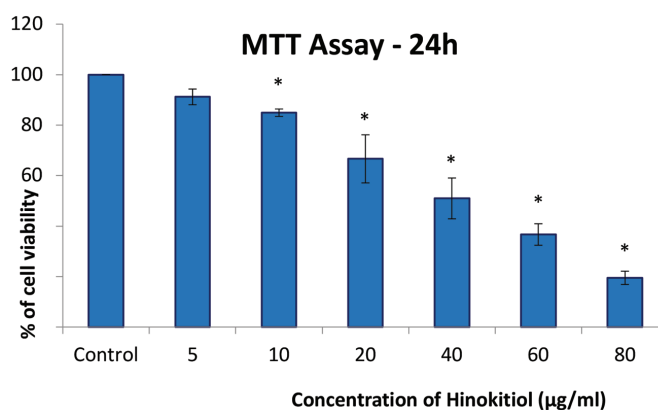


**Figure 2.** Cytotoxic effect of Hinokitiol on osteosarcoma cancer cells by MTT assay method. Data are shown as means  $\pm$  SD (n= 3). \*Compared with the control blank group,  $p < 0.05$

SD: Standard deviation

At an  $IC_{50}$  of 40  $\mu$ g/ml, hinokitiol greatly reduced MG-63 cell motility in the wound-healing experiment, a common method for assessing cell migration and cell-cell contact. Hinokitiol virtually completely prevented MG63 cell migration after 24 hours of incubation (Figure 4).

#### Gene expression profiles of hinokitiol-induced genes

Hinokitiol treatment modulates apoptosis marker gene expression in MG-63 cells. To identify the mechanism of apoptosis caused by treatment with hinokitiol in osteosarcoma cell lines (MG-63), an messenger ribonucleic acid (mRNA) expression study of three genes mainly considered for their involvement in apoptotic pathway regulation, such as BAX, BCL-2, and GSK3 $\beta$  were studied. Hinokitiol treatment significantly ( $p < 0.05$ ) decreased the expression of BCL-2, an apoptosis inhibitor in cells, and GSK3 $\beta$ , a kinase, compared with untreated cells. Additionally, a significant ( $p < 0.05$ ) up regulation of BAX gene expression and downregulation of BCL-2 and GSK3 $\beta$  were observed in the hinokitiol-treated group compared to the control group (Figures 5, 6).

#### Docking study

Molecular modeling is an application in which molecular docking techniques are used to study how receptors interact with ligands. The Autodock 4.2 suite was used to visualize the binding affinities of the hinokitiol against target protein GSK3 $\beta$  (PDB CODE: 2O5K) based on binding energy to elucidate the probable mechanisms of the compounds. The best docking complex was obtained from 100 different conformers for further research based on the extent of hydrogen bonding, maximal occupancy of the binding pocket with the lowest binding energy, and other potential non-covalent interactions. The lowest binding energy (-5.69 kcal/mol) was observed among 100 conformers.

The amino acids of isoleucine 62, alanine 83, aspartic acid (ASP) 133, tyrosine (TYR) 134, valine (VAL) 135, proline (PRO) 136, TYR 140, arginine (ARG) 141, Glycine 185, asparagine ASN 186, LEU 188, ASP 200, and ARG 220 were noted as active site residues in the binding cavities of GSK3 $\beta$  via discovery studio visualizer. Interestingly, the current docking

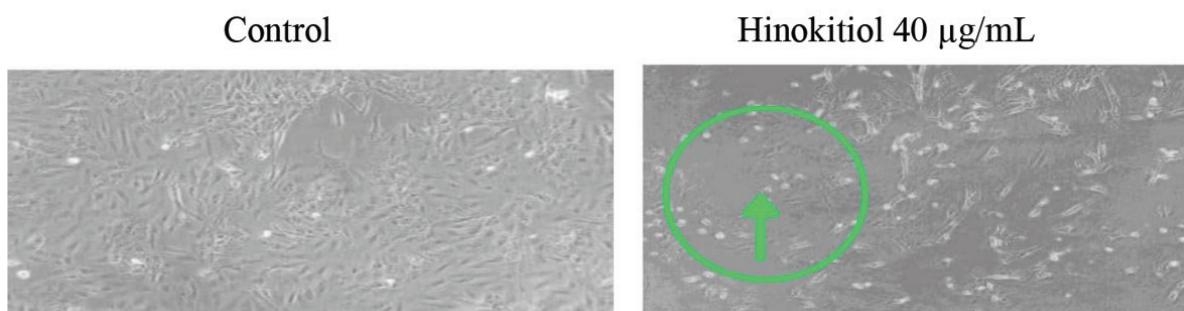


Figure 3. Morphological study of hinokitiol on osteosarcoma (MG63) cell line

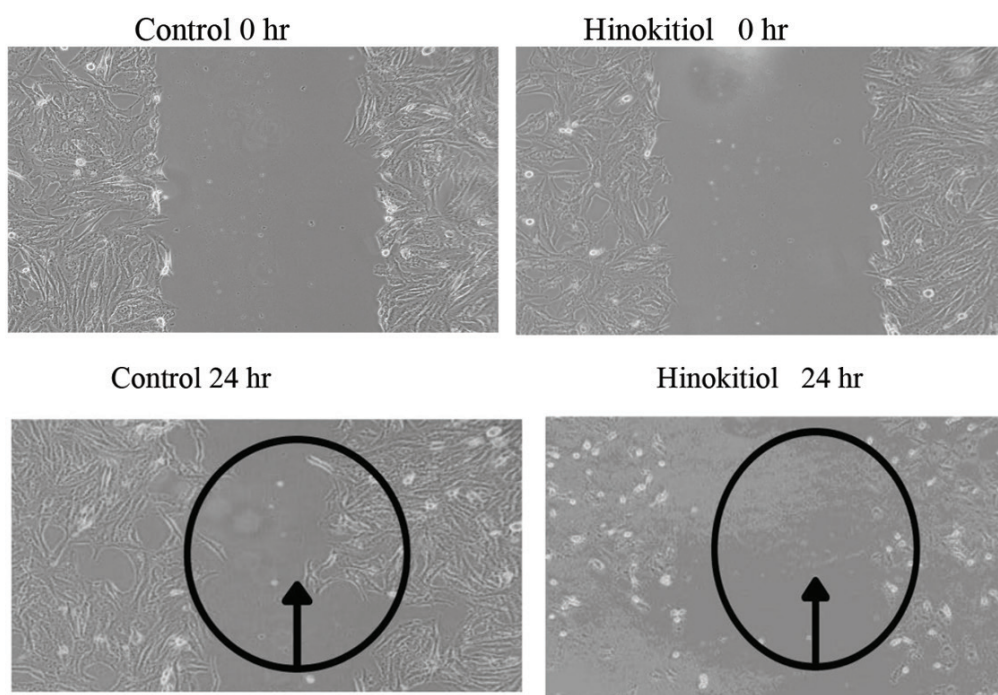
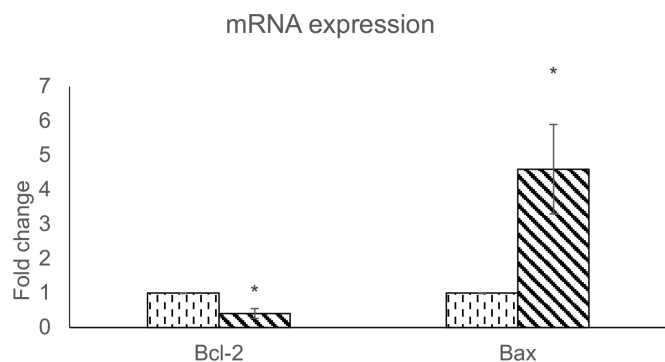
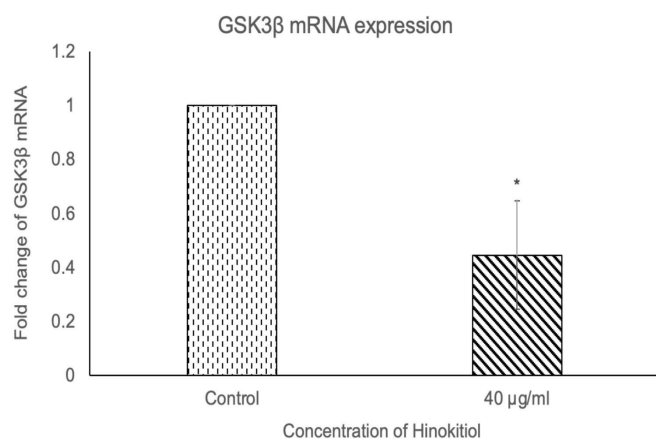


Figure 4. Cell Migration study of hinokitiol on osteosarcoma (MG63) cell line by scratch assay



**Figure 5.** mRNA levels of target genes were analyzed by RT-PCR using GAPDH as a reference. Data are mean  $\pm$  SEM of three independent tests with triplicate reactions. \* $p < 0.05$  vs. control

RT-PCR: Real time-polymerase chain reaction, SEM: Standard error of mean  
mRNA: Messenger ribonucleic acid



**Figure 6.** *GSK3 $\beta$*  gene expression is normalized to GAPDH mRNA expression and the results are expressed as fold change from control. Each bar represents mean  $\pm$  SEM of three independent observations. “\*” represents statistical significance between control versus drug treatment groups at  $p < 0.05$  level

SEM: Standard error of mean, mRNA: Messenger ribonucleic acid

investigation demonstrated that hinokitiol interacts with the amino acids ARG 113, TYR 134, LEU 81, VAL 135, and LYS 197 *via* hydrogen bonds and hydrophobic interactions within the binding cavity. Hinokitiol formed three strong hydrogen bonds between the hydroxyl and carbonyl groups of the ligand with the side chains of ARG 113, TYR 134, and LEU 81 (Figure 7B). The bond distances of 2.9 Å, 2.1 Å, and 1.7 Å were noted respectively. The one carbon-hydrogen bond was found in ASP 133. It was also observed to involve three alkyl hydrophobic interactions within the amino acids of VAL 135 and LYS 197. Furthermore, the following amino acids were involved in the van der Waals interactions: PRO 136, ASP 190, VAL 82, and GLU 80 (Figure 7).

## DISCUSSION

In this investigation, we examined the anticarcinogenic effects of hinokitiol on human osteosarcoma MG-63 cells, which were not previously reported. Due to their well-known lack of functioning p53 (p53 null status), MG-63 cells are excellent models for the development of innovative therapeutic therapies for patients with osteosarcoma.<sup>23</sup>

The MTT assay relies on living cells converting MTT into formazan crystals to detect mitochondrial activity, which is a typical method for assessing the metabolic activity of viable cells.<sup>19</sup> This method is universally used to assess the *in vitro* cytotoxic nature of drugs and chemicals in cell lines because the overall mitochondrial activity of the majority of cell populations is correlated with the ratio of viable cells.<sup>19</sup> In the study, we found a dose-dependent decrease in the percentage of viable MG-63 cells as we increased the concentration of hinokitiol; however, we have selected a hinokitiol ( $IC_{50}$ ) dose of 40  $\mu$ M for further research. Morphological analysis of the MG-63 cells was done following exposure to the hinokitiol in the osteosarcoma cell line using an inverted phase-contrast microscope. The findings demonstrated that compared with untreated cells, hinokitiol-treated cells underwent considerable morphological alterations characterized by decreased cell density and cell shrinkage, which is a common feature of apoptotic cells. The scratch-wound healing assay examines the capability of cells to drift and consequently heal the wound created in a confluent plate of cells. Cell migration can be easily measured using the scratch test because the metastatic process is a major contributor to cancer patient deaths.<sup>24</sup> Cancer cells propagate and proliferate throughout the body. They traverse through the extracellular matrix, enter the circulation, attach to an unrelated location, and then extravasate to produce far-off foci.<sup>24</sup> Hinokitiol 40  $\mu$ M treatment significantly reduced cell movement in the osteosarcoma migration assay. The results of our study were consistent with tomentosin-induced toxicity on MG-63 cell lines.<sup>23</sup> The efficacy of cancer medication therapy depends on its capacity to cause cancer cells to undergo programmed cell death. According to previous studies, there are two primary apoptotic pathways: intrinsic or mitochondrial pathway and extrinsic pathway.<sup>25</sup> Most cancer drugs follow the mitochondrial pathway, and in the current study of cell viability, we observed that hinokitiol reduced mitochondrial activity. In the mitochondrial pathway, the process of apoptosis starts with the generation of intracellular impulses that eventually result in the opening of the inner membranes of mitochondria and the gradual release of pro-apoptotic proteins into the cytoplasm.<sup>25</sup> Changes in mitochondria are controlled by B-cell lymphoma protein 2 (BCL-2) and (BAX) proteins. BAX protein promotes apoptosis by releasing cytochrome C from the mitochondria. This facilitates subsequent activation of caspases, which eventually results in cell death.<sup>25</sup> According to theory, BCL-2 limits the activation of the apoptotic machinery downstream by preventing BAX from releasing cytochrome C. Consequently, cells survive, although BCL-2 is also engaged in relocating proliferating cells back to the resting phase of the cell cycle.<sup>26</sup> Thus, the impact of hinokitiol on the apoptosis-related genes

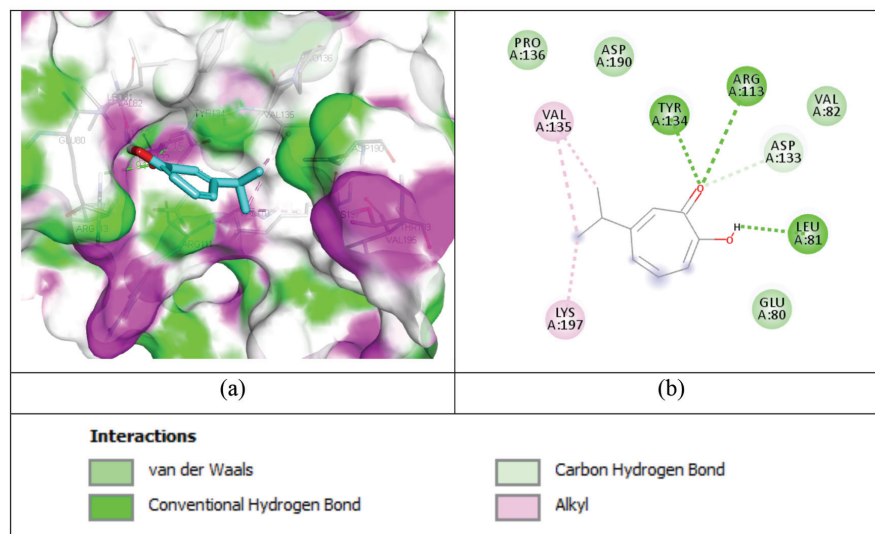


**Figure 7.** Three-dimensional (3D) and two-dimensional (2D) binding interactions poses of hinokitiol in the binding pocket of GSK3 $\beta$  (PDB CODE: 205K). Hydrophobic interactions and hydrogen bond and are indicated by pink and green dashed lines

*BAX* and *BCL-2* was evaluated. *BAX* genes are crucial for controlling apoptosis. In the present study, hinokitiol treatment reduced the expression of *BCL-2*, an apoptosis inhibitor. Significantly higher *BAX* gene (proapoptotic) expression was observed in the hinokitiol-treated group.

GSK3 $\beta$  is a protein that is highly relevant in different cancers because it plays a significant role in cell growth, proliferation, and migration.<sup>5-7</sup> The serine/threonine protein kinase GSK3 $\beta$  has emerged as a crucial enzyme in controlling several crucial cellular signaling pathways by phosphorylating its substrates. Phosphorylating many oncogene proteins, such as  $\beta$ -catenin, carcinogenic transcription factors, and c-Myc, causes their ubiquitin degradation and inactivation.<sup>27</sup> GSK3 $\beta$  adversely affects cell survival and proliferation in normal physiological settings. GSK3 $\beta$  is therefore commonly thought of as a “tumor-suppressor gene”. According to Tang et al.,<sup>11</sup> osteosarcoma cells that overexpress GSK3 $\beta$  have a considerable positive impact on colony growth and tumor growth. Importantly, the findings showed that osteosarcoma tumors were aided in growth by the aberrant activation of GSK3 $\beta$ . According to Cai et al.,<sup>28</sup> therapy with a GSK3 $\beta$  inhibitor reduces cell survival and proliferation rates, suggesting that GSK3 $\beta$  may be linked to the development of osteosarcoma. In the current study, we evaluated the role of hinokitiol on GSK3 $\beta$  by *in silico* models, and the results revealed a significant binding interaction. The GSK3 $\beta$  gene expression analysis also showed hinokitiol’s potential to negatively regulate its function, thereby promoting cell death and mitigating cell survival. A downregulated GSK3 $\beta$  in osteosarcoma has reduced tumor cell viability and triggered apoptosis, according to recent researches. The results of our study were further substantiated by earlier findings that hinokitiol has an apoptotic and anti-hepatofibrotic impact on hepatic stellate cells *via* activating GSK3 $\beta$  and inhibiting the Wnt/-catenin pathway.<sup>29</sup>

## CONCLUSION

We used a potent bioactive agent known to have anti-proliferative activity in various cell lines. In the current study, we evaluated the anti-proliferative activity of hinokitiol against the osteosarcoma cell line showed significant cytotoxic activity. A deep examination of the cell line after treatment with hinokitiol revealed morphological changes such as cell shrinkage and reduced cell density. *In vitro* evaluation of the wound healing assay revealed anti-migratory effects, which are characteristic properties of anti-cancer drugs. The study also analyzed *mRNA* gene expression by RT-PCR in the MG-63 cell line, and the pro-apoptotic *BAX* gene was upregulated and the anti-apoptotic gene *BCL-2* and GSK3 $\beta$  was downregulated. The study also used *in silico* models to assess the binding energy of the biomarker enzyme GSK3 $\beta$  regulated on numerous signaling pathways for cancer progression hinokitiol, and showed effective interactions at various binding sites of GSK3 $\beta$ . Because the present study was carried out only in the osteosarcoma MG-63 cell line, further research on other osteosarcoma cell lines will substantiate the claim of hinokitiol as a strong candidate drug for ameliorating bone cancer.

### Acknowledgement

We, authors, are deeply grateful to Saveetha College of Pharmacy, SIMATS, for providing test facilities to carry out the study.

### Ethics

**Ethics Committee Approval:** There is no ethical problem related to the study.

**Informed Consent:** This study does not involve human participants or animal subjects requiring consent.

### Authorship Contributions

Concept: B.V.C., Design: B.V.C., Data Collection or Processing: P.S, G.J., Analysis or Interpretation: K.K.K, P.B.S, Literature Search: A.K.S, A.R., Writing: P.S., G.J., K.E.

**Conflict of Interest:** The authors have no conflicts of interest to declare.

**Financial Disclosure:** The authors declared that this study received no financial support.

## REFERENCES

- Isakoff MS, Bielack SS, Meltzer P, Gorlick R. Osteosarcoma: current treatment and a collaborative pathway to success. *J Clin Oncol*. 2015;33:3029-3035.
- Kansara M, Teng MW, Smyth MJ, Thomas DM. Translational biology of osteosarcoma. *Nat Rev Cancer*. 2014;14:722-735.
- Broder H, Gottlieb RA, Lepor NE. Chemotherapy and cardiotoxicity. *Rev Cardiovasc Med*. 2008;9:75-83.
- Czekanska EM, Stoddart MJ, Richards RG, Hayes JS. In search of an osteoblast cell model for *in vitro* research. *Eur Cells Mater*. 2012;24:1-17.
- Embi N, Rylatt DB, Cohen P. Glycogen synthase kinase-3 from rabbit skeletal muscle. Separation from cyclic-AMP-dependent protein kinase and phosphorylase kinase. *Eur J Biochem*. 2005;107:519-527.
- Tejeda-Muñoz N, Robles-Flores M. Glycogen synthase kinase 3 in Wnt signaling pathway and cancer. *IUBMB Life*. 2015;67:914-922.
- Holmes T, O'Brien TA, Knight R, Lindeman R, Symonds G, Dolnikov A. The role of glycogen synthase kinase-3 $\beta$  in normal hematopoiesis, angiogenesis and leukaemia. *Curr Med Chem*. 2008;15:1493-1499.
- Luo J. Glycogen synthase kinase 3 $\beta$  (GSK3 $\beta$ ) in tumorigenesis and cancer chemotherapy. *Cancer Lett*. 2009;273:194-200.
- Domoto T, Pyko IV, Furuta T, Miyashita K, Uehara M, Shimasaki T, Nakada M, Minamoto T. Glycogen synthase kinase-3 $\beta$  is a pivotal mediator of cancer invasion and resistance to therapy. *Cancer Sci*. 2016;107:1363-1372.
- Mai W, Miyashita K, Shakoori A, Zhang B, Yu ZW, Takahashi Y, Motoo Y, Kawakami K, Minamoto T. Detection of active fraction of glycogen synthase kinase 3 $\beta$  in cancer cells by nonradioisotopic *in vitro* kinase assay. *Oncology*. 2006;71:297-305.
- Tang QL, Xie XB, Wang J, Chen Q, Han AJ, Zou CY, Yin JQ, Liu DW, Liang Y, Zhao ZQ, Yong BC, Zhang RH, Feng QS, Deng WG, Zhu XF, Zhou BP, Zeng YX, Shen JN, Kang T. Glycogen synthase kinase-3 $\beta$ , NF- $\kappa$ B signaling, and tumorigenesis of human osteosarcoma. *J Natl Cancer Inst*. 2012;104:749-763.
- Koufaki M, Theodorou E, Alexi X, Nikoloudaki F, Alexis MN. Synthesis of tropolone derivatives and evaluation of their *in vitro* neuroprotective activity. *Eur J Med Chem*. 2010;45:1107-1112.
- Yoshimori A, Oyama T, Takahashi S, Abe H, Kamiya T, Abe T, Tanuma S. Structure-activity relationships of the thujaplicins for inhibition of human tyrosinase. *Bioorg Med Chem*. 2014;22:6193-6200.
- Chiu KC, Shih YH, Wang TH, Lan WC, Li PJ, Jhuang HS, Hsia SM, Shen YW, Yuan-Chien Chen M, Shieh TM. *In vitro* antimicrobial and anti-inflammatory potential of honokiol and magnolol against oral pathogens and macrophages. *J Formos Med Assoc*. 2021;120:827-837.
- Zhang G, He J, Ye X, Zhu J, Hu X, Shen M, Ma Y, Mao Z, Song H, Chen F.  $\beta$ -Thujaplicin induces autophagic cell death, apoptosis, and cell cycle arrest through ROS-mediated Akt and p38/ERK MAPK signaling in human hepatocellular carcinoma. *Cell Death Dis*. 2019;10:255.
- Li LH, Wu P, Lee JY, Li PR, Hsieh WY, Ho CC, Ho CL, Chen WJ, Wang CC, Yen MY, Yang SM, Chen HW. Hinokitiol induces DNA damage and autophagy followed by cell cycle arrest and senescence in gefitinib-resistant lung adenocarcinoma cells. *PLoS One*. 2014;9:e104203.
- Huang CH, Lu SH, Chang CC, Thomas PA, Jayakumar T, Sheu JR. Hinokitiol, a tropolone derivative, inhibits mouse melanoma (B16-F10) cell migration and *in vivo* tumor formation. *Eur J Pharmacol*. 2015;746:148-157.
- Wang WK, Lin ST, Chang WW, Liu LW, Li TY, Kuo CY, Hsieh JL, Lee CH. Hinokitiol induces autophagy in murine breast and colorectal cancer cells. *Environ Toxicol*. 2016;31:77-84.
- van Meerloo J, Kaspers GJ, Cloos J. Cell sensitivity assays: the MTT assay. *Methods Mol Biol*. 2011;731:237-245.
- Felice F, Zambito Y, Belardinelli E, Fabiano A, Santoni T, Di Stefano R. Effect of different chitosan derivatives on *in vitro* scratch wound assay: a comparative study. *Int J Biol Macromol*. 2015;76:236-241.
- Huang KJ, Kuo CH, Chen SH, Lin CY, Lee YR. Honokiol inhibits *in vitro* and *in vivo* growth of oral squamous cell carcinoma through induction of apoptosis, cell cycle arrest and autophagy. *J Cell Mol Med*. 2018;22:1894-1908.
- Morrison TB, Weis JJ, Wittwer CT. Quantification of low-copy transcripts by continuous SYBR Green I monitoring during amplification. *Biotechniques*. 1998;24:954-958.
- Lee CM, Lee J, Nam MJ, Choi YS, Park SH. Tomentosin displays anti-carcinogenic effect in human osteosarcoma MG-63 cells *via* the induction of intracellular reactive oxygen species. *Int J Mol Sci*. 2019;20:1508.
- Sundaram GM, Quah S, Sampath P. Cancer: the dark side of wound healing. *FEBS J*. 2018;285:4516-4534.
- Jürgensmeier JM, Xie Z, Deveraux Q, Ellerby L, Bredesen D, Reed JC. Bax directly induces release of cytochrome c from isolated mitochondria. *Proc Natl Acad Sci U S A*. 1998;95:4997-5002.
- Hardwick JM, Soane L. Multiple functions of BCL-2 family proteins. *Cold Spring Harb Perspect Biol*. 2013;5:a008722.
- Dang CV. MYC on the path to cancer. *Cell*. 2012;149:22-35.
- Cai X, Li M, Vrana J, Schaller MD. Glycogen synthase kinase 3- and extracellular signal-regulated kinase-dependent phosphorylation of paxillin regulates cytoskeletal rearrangement. *Mol Cell Biol*. 2006;26:2857-2868.
- Lee IH, Im E, Lee HJ, Sim DY, Lee JH, Jung JH, Park JE, Shim BS, Kim SH. Apoptotic and antihepatofibrotic effect of honokiol *via* activation of GSK3 $\beta$  and suppression of Wnt/ $\beta$ -catenin pathway in hepatic stellate cells. *Phytother Res*. 2021;35:452-462.



# General Public Knowledge, Attitudes, and Practices Regarding Hair Dye Usage and Its Adverse Effects in the Northern Emirates of the United Arab Emirates

Javedh SHAREEF\*, Sathvik Belagodu SRIDHAR, Safeera SHERIN, Sumanjebin ABDUL NAZAT

Ras Al Khaimah Medical and Health Sciences University, RAK College of Pharmacy, Department of Clinical Pharmacy and Pharmacology, Ras Al Khaimah, United Arab Emirates

## ABSTRACT

**Objectives:** This study aimed to assess the general population's knowledge, attitudes, and practices regarding hair dye (HD) usage and its adverse effects in the Northern Emirates of the United Arab Emirates.

**Materials and Methods:** A cross-sectional study was conducted over 3 months in the general population of Ras Al Khaimah. Information was collected by administering a pre-validated self-administered questionnaire related to HDs. Data collected were analyzed using descriptive statistics and binary logistic regression to correlate HD use with various sociodemographic variables. Results with a  $p$ -value less than 0.05 were considered statistically significant.

**Results:** In total, 333 of the 405 distributed questionnaires completed the study, with a response rate of 82.20%. Most (52.85%) participants used natural HDs, and most (30.59%) admitted that their motivation to use HD was to remove gray hair. Of the total sample, nearly 75% agreed that they had never performed an allergic test before using the HD, and almost 70% believed that providing advice regarding the HD would be beneficial. Sex ( $p < 0.0001$ ), age (in years) ( $p = 0.032$ ), and occupation ( $p = 0.042$ ) were associated with the frequency of HD use, which was statistically significant.

**Conclusion:** In the present study, HD was common among students, employees, and middle-aged students. Approaches such as educational awareness programs with special attention to the safe and effective use of HDs may help individuals select appropriate HDs and avoid preventable adverse effects.

**Keywords:** Hair dye, health knowledge, adverse effects, surveys and questionnaires

## INTRODUCTION

Healthy and beautiful hair enhances personality, physical appearance, and beauty. Maintaining good, healthy, and stylish hair has gained much importance presently and significantly among adolescents, exerting a profound effect on their outlook.<sup>1</sup> In today's modern world, the use of hair dye (HD) products is widely accepted, irrespective of gender, age, educational status, or social status to conceal gray hairs or just for changing fashion trends.<sup>2</sup>

Temporary, semi-permanent, and permanent HDs are the different types of HDs used to modify hair color to achieve a beautiful and youthful appearance. HDs consisting of natural and synthetic agents provide hair with good shape, attractive and elegant appearance, and long-lasting color. The periodic use of HDs or coloring products has become routine for many individuals, devoting considerable time and financial expenditure to achieving soft, silky, and shiny hair.<sup>1,3</sup>

\*Correspondence: javedh@rakmhsu.ac.ae, ORCID-ID: orcid.org/0000-0002-5892-5909

Received: 23.10.2023, Accepted: 04.01.2024



Copyright© 2024 The Author. Published by Galenos Publishing House on behalf of Turkish Pharmacists' Association. This is an open access article under the Creative Commons Attribution-NonCommercial-NoDerivatives 4.0 (CC BY-NC-ND) International License.

The assumption that HDs are safe and will not cause damage to human health, and the increase in hair coloring trend have raised concerns about their safety, as some synthetic agents contain toxic substances known to be detrimental to their well-being.<sup>4</sup> Studies have reported that cosmetics, including hair products, are associated with various known and unknown adverse reactions ranging from mild local reactions to more severe systemic life-threatening reactions jeopardizing a person's life in danger.<sup>3-6</sup> Keeping in view the numerous health hazards associated with HD, adequate knowledge and accurate information about HD composition, its use, and adverse effects are important in reducing the prevalence of HD-associated complications among users.

It has been reported that the use of paraphenylenediamine (PPD), a synthetic aromatic amine, is the leading cause of contact dermatitis among HD users. In addition, hyperpigmentation, leukoderma, hair loss, chemical burns, skin malignancy, and systemic diseases are some of the adverse effects of HD preparations.<sup>2,4</sup>

However, there is a paucity of studies describing the adverse effects of HDs among HD users. To the best of our knowledge, no previous study has attempted to assess the level of knowledge, attitudes, and practices regarding HD use among users in the Northern Emirates of the United Arab Emirates. Considering this, the present study aimed to assess knowledge, attitudes, and practices regarding HD and its adverse effects among HD users.

## MATERIALS AND METHODS

### *Study design and settings*

This cross-sectional, self-administered questionnaire-based study was conducted in the Emirate of Ras Al Khaimah from February 2022 to July 2022. Ethical approval was obtained from the institutional research ethics committee and from the Ras Al Khaimah Research Ethics Committee before the initiation of the study (approval number: MOHAP/REC/2022/7-2022-UG-P, date: 21.02.2022). Subjects of either gender aged 18 years and above who had used HD (natural/synthetic) at least once in their lifetime were included after obtaining informed consent.

### *Study procedure*

The sample size was calculated using the Rao soft calculator.<sup>7</sup> Assuming that the estimated urban population of Ras Al Khaimah is nearly one lakh, and the prevalence rate of HDs used in the Gulf Cooperation Council based on earlier studies is 30%. The minimum sample size is 330 respondents with a 5% margin of error, 95% confidence interval, and 50% response distribution. A convenient sampling technique was used to enroll participants in the study. Information was collected from the general population and employees of our university through a questionnaire developed by the researcher *via* Google Forms provided through emails. In addition, subjects who visited the hair and beauty salons were contacted, and information was collected by providing a hard copy of the questionnaire. For the questions sent through the Google survey form, the informed

consent form page will be opened, and only after consenting to answer the questions by marking a voluntary checkbox will the respondents be directed to the main survey instrument.

Participants were informed that the study was voluntary, and we assured them of the anonymity and confidentiality of their responses. Sufficient time (approximately one week) and an email reminder were provided to each participant to complete and submit the questionnaire. The investigator re-checked every submitted response to ensure the collected data's quality and to avoid any incomplete information in the questionnaire. Questions that could reveal the personal identity of the study subject were not included in the tool.

### *Questionnaire development and scoring*

A self-administered or interviewer-assisted survey on knowledge, attitude, and practice related to HD use was prepared by referring to previous literature and similar studies and modified as per study requirements.<sup>5,6,8,9</sup> The questionnaire's content validity was evaluated by three experts in the field, who assessed the relevance, clarity, and comprehensiveness of the items to ensure accurate representation of key aspects of knowledge, attitudes, and practices concerning HD use. The questionnaire was improved as a result of their input, proving its pre-validity. A convenience sample of ten people was used for a pilot test to evaluate the instrument's reliability. Cronbach's alpha was used to determine internal consistency, and a value of > 0.7 indicated satisfactory reliability. We acknowledge the significance of concept and criterion validity and recommend that they be investigated in future research using methods like factor analysis or correlations with existing measures, even though formal tests for these validities were not carried out in this study. Multiple-choice items were evaluated according to the total number of correct answers chosen, and the questionnaire was scored using a binary approach (1 for correct/positive responses, 0 for incorrect/negative ones). The questionnaire's reliability and clarity for the intended audience were validated by the pilot study.

There are two sections and sixteen questions in the survey instrument. The demographic data of the respondents, such as age, gender, nationality, marital status, and employment, is gathered in the first part. Questions about the type of HD, usage frequency, side effects, and motivations for using HDs are included in the second section. These questions were answered with the following responses: "yes", "no", and "I do not know". When appropriate, several questions were made to let respondents choose more than one answer. Descriptive analysis of the information gathered from these answers was done to find patterns in HD use-related knowledge, attitudes, and behaviours.

### *Statistical analysis*

Participants' responses to the questions were coded, entered into an Excel spreadsheet, and analyzed using SPSS version 27 (IBM Corp., Armonk, NY, USA). Descriptive statistics were employed to assess the mean and standard deviation for continuous variables and the percentages and frequencies

for categorical variables to narrate demographic factors. The chi-square test was used to test the association between the frequency of HD use and demographic variables. Binary logistic regression was used to relate HD use to various sociodemographic variables. A value of  $p < 0.05$  was considered statistically significant.

## RESULTS

The questionnaire was distributed among 405 participants. In total, 333 subjects (82.20%) fully completed and returned the questionnaire. Among the remaining 72 participants, 57 did not respond to the e-mails, and 15 responses were partially completed and not considered for the analysis. Among the 333 participants who completed the study, 99 completed the questionnaire *via* Google Forms, and the remaining 234 completed face-to-face interviews.

### Sociodemographic characteristics of the study participants

Of the total study population, female (68.5%) predominance was noted over males, and the study population's median age was 30.0 (in years). Most of the study participants were in the age group 21-40 years. The majority of the study participants were non-Arab (74.2%), and nearly half of the study subjects were unmarried (48.9%) and none were classified as "divorced". More than one-third of the participants were working employees (39.9%), and almost half were students (47.4%) (Table 1). An analysis of the responses to the questions related to knowledge, attitude, and practice among the HD users revealed that only 8.4% responded that they had experienced allergic reactions related to HD preparations. When asked about performing an allergic test before using HD, 72.97% answered that they had never previously performed an allergic test before using HD.

Regarding the ingredients in HD, only one-third (34.53%) of the participants read the list. Among the total participants, only 45.64% agreed that they seek advice or suggestions before buying HD. Almost 70% of users indicated that providing educational advice regarding HD would benefit them. Less than 10% of the study participants stated that available HD preparations in the market are safe and can be used in all age groups. Most of the study participants acknowledged that they were unaware of the hazardous chemicals/toxic ingredients of HDs, did not get enough information when buying HD products, and neither consulted nor received pharmacist advice (Table 2).

Concerning the types of HD preferred by the study participants, more than half (52.85%) preferred the use of natural dye,

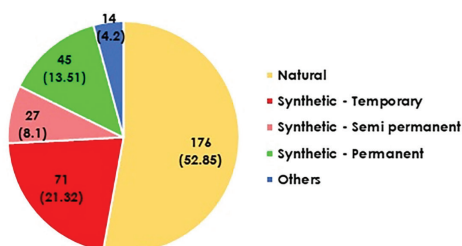


Figure 1. Different types of hair dyes used by the study participants (n= 333)

while 42.93 preferred synthetic dyes of different types, and the remaining 4.20% answered others consisting of egg, hibiscus, and other natural substances (Figure 1).

### Adverse effects of HDs

Fewer adverse effects such as fizzy hair (n= 6; 11.53%), rashes over the face and forehead (n= 14; 26.92%), headache (n= 10; 19.23%), hair fall (n= 6; 11.53%), and itching (n=16; 32%) associated with HDs use were reported among the study participants (Figure 2).

The reason for HD use varied considerably among the participants. Most respondents (30.59%) reported that HD helped them get rid of gray hair, while 18.76% believed it made them look more beautiful (Figure 3).

Regarding the source of information about HDs, most (30%) of the study subjects reported using the Internet, whereas 26.19% chose advertisement as the major source of information related to HD (Figure 4).

Table 1. Sociodemographic characteristics of the study populations (n= 333)

Variables	Frequency	Percentage
<b>Sex</b>		
Female	228	68.5
Male	105	31.5
Median age	30.0 (range: 17-76) (in years)	
<b>Age group (in years)</b>		
< 20	26	7.8
21-40	179	53.8
41-60	84	25.2
> 61	44	13.2
<b>Nationality</b>		
Arabs	86	25.8
Non-Arabs	247	74.2
<b>Marital status</b>		
Married	146	43.8
Unmarried	163	48.9
Divorced	24	7.2
<b>Education</b>		
School level	37	11.1
Graduate level	136	40.8
Postgraduate and above	160	48.0
<b>Occupation</b>		
Working	133	39.9
Not working	28	8.4
Student	158	47.4
Home maker	14	4.2

*Associations between sociodemographic variables and HD ing practices*

Participants with female ( $p < 0.0001$ ), aged between 21 and 40 years ( $p = 0.032$ ) and employees ( $p = 0.042$ ) are inclined to use HD more frequently than other age groups, which was found to be statistically significant (Table 3). The frequency of HD use was higher among highly educated participants, the difference was not statistically significant ( $p = 0.052$ ).

The correlation between sociodemographic characteristics and frequency of HD use using binary logistic regression analysis after adjusting for all other variables showed that sex [odds ratio (OR) = 0.068, 95% confidence interval (CI) (0.024 – 1.199),  $p < 0.0001$ ], marital status [odds ratio (OR) = 0.242, 95% confidence interval (CI) (0.098 – 0.602),  $p = 0.002$ ], and employment [odds ratio (OR) = 1.737, 95% confidence interval (CI) (1.058 – 2.851),  $p = 0.029$ ] were significantly associated with HD use. In the adjusted model, age (in years), nationality, and education were not significantly associated with the frequency of HD use.

**DISCUSSION**

Hair care has gained considerable importance, and HD use has increased globally to enhance youth and beauty. Additionally, significant growth and rapid development in the cosmetic industry and the limited evidence on safety profiles related to

HDs influence guidance on the safe and effective use of HD preparations.<sup>5,6</sup> The present study assesses the knowledge, attitude, and practice regarding HDs and their adverse effects among HD users.

The study results point out that more than half of the study participants were female, indicating their predominance in using HDs at least once to have a smart and young look in the work field. The increased percentage is insignificant considering that the prevalence of HD use among females in earlier studies ranged from 60% to 90%.<sup>10-12</sup> A previous study conducted in Riyadh, Saudi Arabia reported that 82.6% of their female participants had used HD at some point.<sup>13</sup> In the present study, the median age at first use of HD was 29.5 years, expressing HD is common among teenagers and young adults, echoing previous studies, which reported that the median age at first HD ing ranged between 22-36 years, respectively.<sup>12-14</sup>

Concerning the different types of HDs used by the study participants, > 50% preferred natural (henna) dye, indicating its popularity in the community. It must be noted that henna dye is traditional in Islamic countries and has religious and social significance. The growing popularity that natural dyes provide the best normal results without any chemical ingredients and the increased concern that synthetic dyes are likely to cause

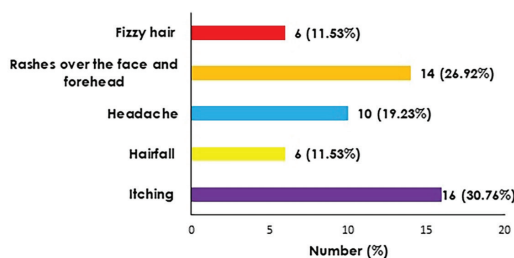


**Figure 2.** Adverse effects reported by the study participants associated with hair dyes (n= 52)

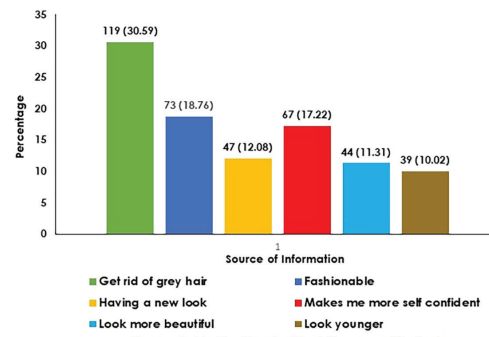


**Figure 3.** Motivation behind the use of hair dyes

**Table 2. Results of a questionnaire on HD-related knowledge, attitude, and practice**

Sl no.	Questions	n= 333 (%)		
		Yes (%)	No (%)	I don't know (%)
1	Have you ever experienced any allergic reactions with the use of any HD?	28 (8.40)	237 (71.17)	68 (20.42)
2	Have you ever performed an allergy test before using a HD?	51 (15.31)	243 (72.97)	39 (11.71)
3	Do you usually read/check the list of ingredients present in HDs?	115 (34.53)	124 (37.23)	94 (28.22)
4	Do you seek any advice or suggestions before buying your HD?	152 (45.64)	43 (12.91)	138 (41.44)
5	Do you think educational advice on HD would be beneficial for you?	233 (69.96)	30 (9.0)	70 (21.02)
6	Do you think that all the available HDs in the market are safe?	29 (8.70)	139 (41.74)	165 (49.54)
7	Is it safe to use all available HDs in all age groups?	20 (6.0)	240 (72.07)	73 (21.92)
8	Are you aware of any hazardous chemicals and toxins present in HDs?	99 (29.72)	207 (62.16)	27 (8.10)
9	Did you ever consult or receive pharmacist advice when buying your HD?	91 (27.32)	148 (44.44)	94 (28.22)
10	Do you think you get enough information when buying a product?	71 (21.32)	145 (43.54)	117 (35.13)

Sl no.: Serial number, HD: Hair dye

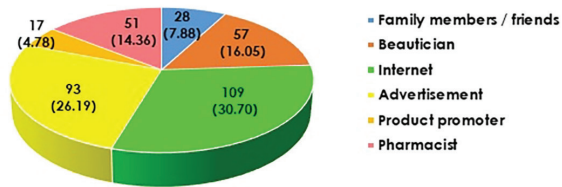


Figure 4. Source of information about hair dyes

Table 3. Association between frequency of HD use and sociodemographic characteristics

Characteristics	Frequency of HD use (per year)			p value
	Once	2-5 times	> 5 times	
<b>Gender</b>				
Female	142	68	18	0.0001*
Male	55	19	31	
<b>Age group (in years)</b>				
< 20	12	6	8	0.032*
21-40	108	51	20	
41-60	55	14	15	
> 61	22	16	6	
<b>Nationality</b>				
Non-Arabs	142	66	39	0.526
Arabs	55	21	10	
<b>Marital status</b>				
Married	76	40	30	0.075
Unmarried	105	41	17	
Divorced	16	6	2	
<b>Education</b>				
School level	19	11	01	0.052
Graduate	76	32	28	
Postgraduate and above	102	44	14	
<b>Occupation</b>				
Working	75	35	23	0.042 <sup>e</sup>
Not working	2	6	0	
Student	88	44	26	
Home maker	12	2	0	

\*p value < 0.05 is statistically significant, \*Chi-square test, <sup>e</sup>Fischer's exact test

serious adverse effects could also be why we prefer natural dyes. Regarding safety, fewer adverse effects related to HDs were reported, shadowing the previous study results.<sup>12,15</sup> This emphasizes the need for performing an allergy test before using any HD products to improve safety and prevent possible side

effects in the future. The most common reason for using HDs was to cover gray hair, which enhanced their self-confidence. In the modern world, the desire to be youthful is most common, and people prefer to conceal their gray hair at an early age, which is supported by the study responses and their desire to be more beautiful, fashionable, and stand out as young people. The above findings correlate with those of earlier studies, which reported that HD's principal purpose was to cover the gray hair and have a youthful appearance.<sup>9,13,14</sup>

Regarding the source of information about HDs, most of the study participants expressed that the internet, social media, and newspaper advertisements were the primary sources of information for understanding HD preparation. This section discusses fast-growing online information technology, including the internet and media, which has opened the way for consumers to reach out quickly and can be an effective platform for consumers to learn more about HD products. However, sometimes, making sense of overwhelming information from an online platform becomes difficult, which can be misleading or lead to negative health outcomes.<sup>11,13,14</sup>

Nearly two-thirds of the study sample reported that they never experienced any adverse effects associated with HD use, and almost the same revealed that they never performed an allergy test before using HD. Appropriate advice must be reinforced in HD users as sometimes mild-moderate adverse effects are underreported because of self-diagnosis and self-medication, which are more common in cosmetics products.<sup>6,16</sup> It is important to highlight that severe reactions can sometimes cause permanent disability or life-threatening. Only less than half of the study sample declared that they usually read or checked the ingredients before using HD or sought advice while buying HD. A study in Saudi Arabia reported that more than half of the women who developed adverse effects from cosmetics did not seek medical advice or consult a pharmacist.<sup>5</sup>

More than 60% of the study population reported that they were unaware of the hazardous chemicals/toxic ingredients present in HD. Understanding the ingredients in HDs, adhering to the instructions for proper use, and seeking medical advice from healthcare professionals will help ensure the safe and effective use of HDs. Misuse or overuse of HDs is likely to damage hair. Furthermore, few published studies have documented conflicting findings that some compositions in permanent HDs are linked with the development of certain malignancies, but the evidence was weak and could not prove causality.<sup>10,17,18</sup>

Additional studies on the carcinogenic potential of HDs should be conducted to resolve public concerns. Many participants expressed that HDs available in the market are unsafe and not recommended for use in all age groups. This is particularly important in pregnancy and young children. Concerns regarding safety during pregnancy have been raised, which is a matter of active debate. Studies evaluating the association between HD use in pregnancy and neonatal outcomes have concluded that the strength of evidence is limited to moving the needle on recommendations for the safety of HDs during pregnancy and might cause neonatal health problems.<sup>19,20</sup>

The presence of toxic ingredients such as PPD, the most potent and key ingredient in HD formulations, raises an important public health concern. Exposure to these products can induce local and systemic toxic effects when applied topically and/or ingested orally, and the outcome depends mainly on the dose taken. Acute (short-term) exposure to high levels of p-phenylenediamine may cause angioedema leading to dysphasia and respiratory distress, rhabdomyolysis, intravascular hemolysis, acute renal failure, and hepatic necrosis, whereas chronic (long-term) exposure in humans results in Eczematous contact dermatitis. Studies have demonstrated that children are susceptible to PPD allergy, and their use might increase the risk of carcinoma and infertility problems in the future.<sup>21-23</sup>

The different types of HD use and motivation justify the increased frequency of HD use observed in the present study. Participants aged between 21 and 40 years and employed individuals tended to use HDs more frequently, which was statistically significant. This observation highlights that individuals aged between 21 and 40 years are either job seekers or employees who would like to continue to maintain a fresh look, believe that it will add shine and dimension to hair, make it more beautiful, and perceive it as an integral part of self-expression and fashion.

#### Study limitations

First, the study relied on self-reporting information provided by HD users through survey questionnaires in which the data obtained reflected the respondents' personal opinions. However, self-reporting is a common and practical method of collecting data. The information provided may not mirror real-life practice because some respondents may be unwilling to reveal practice deficiencies. The possibility of recall bias cannot be excluded entirely. Secondly, We recognise that only individuals from the northern emirates of the United Arab Emirates were included in the study sample, which could limit the results' applicability to the whole population of the United Arab Emirates. Future research with a sample that is more geographically diverse would improve the findings' representativeness.

## CONCLUSIONS

The present study highlights the extensive use of HDs by individuals aged 21-40 years, emphasizing the importance given to their esthetic value. The focus should be on providing appropriate information to HD users regarding the safe use and chemical ingredients of HD products. Performing a patch test before HD use and adhering to usage instructions may help choose safer HD products and avoid possible adverse reactions. The conflicting results regarding the safe use of HDs in pregnancy warrant further investigation with more accurate data on neonatal health issues in the future.

#### Ethics

**Ethics Committee Approval:** Ethical approval was obtained from the institutional research ethics committee and from the Ras Al Khaimah Research Ethics Committee before the initiation of the study (approval number: MOHAP/REC/2022/7-2022-UG-P, date: 21.02.2022).

**Informed Consent:** Subjects of either gender aged 18 years and above who had used HD (natural/synthetic) at least once in their lifetime were included after obtaining informed consent.

#### Authorship Contributions

Concept: J.S., S.B.S., Design: J.S., S.B.S., S.S., Data Collection or Processing: S.S., S.A., Analysis or Interpretation: J.S., S.B.S., Literature Search: J.S., S.B.S., S.S., Writing: J.S., S.B.S., S.A.

**Conflict of Interest:** The authors have no conflicts of interest to declare.

**Financial Disclosure:** The authors declared that this study received no financial support.

## REFERENCES

- Lunge SB, Doshi BR, Pande S, Vyshak BM. Comparative study of knowledge, attitude, and practices of hair care among the final year MBBS students versus final year engineering students. *Int J Trichology*. 2020;12:43-47.
- Kusagur MS, Asifa N, SugaReddy. Trends in hair care and cleansing: a knowledge, attitude, and practice study. *Clin Dermatol Rev*. 2017;1:56-60.
- Jayaganesh S, Sudhir S, Jainendra M, Bachan SR, Asif Ali M. Mechanism of hair dyeing and their safety aspects: a review. *Asian J Appl Sci*. 2017;10:190-196.
- Palaniappan V, Karthikeyan K, Anusuya S. Dermatological adverse effects of hair dye use: A narrative review. *Indian J Dermatol Venereol Leprol*. 2023:1-17.
- Kotby FA, Beayari SMF, Abdulrhman Alsalmi K, Sulaimani AA, Bakheet Alharbi A, Samir A Al-Abdrabbuh D. Knowledge and practice of women toward the adverse effects of cosmetics in Saudi Arabia. *IJMDC*. 2020;4:113-117.
- Dehvari M, Ghaneian MT, Morowatisharifabad MA, Karimi M, Jasemizad T. Knowledge, attitudes and practice of women about adverse effects of cosmetics in Yazd city, Iran. *Health Scope*. 2018;7:e68257.
- Raosoftware® calculator. <http://www.raosoftware.com/samplesize.html> [accessed: 17<sup>th</sup> Jan 2022].
- Shawana A, Afzal M, Hussain M. Knowledge, attitude and practices university BSN nursing students about undesirable effects of cosmetics in Lahore city. *Glob Sci J*. 2020;8:1331-1338.
- Joshi MV, Nilkanth JV, Rasane SR. Knowledge, practice and adverse reactions amongst Hair dye users-a cross-sectional study. *Int J Ayurvedic Med*. 2021;12:645-648.
- Zhang Y, Birmann BM, Han J, Rosner BA, Tamimi RM, Wang Y, Eliassen AH. Personal use of permanent hair dyes and cancer risk and mortality in US women: prospective cohort study. *BMJ*. 2020;370:m2942.
- Heikkinen S, Pitkaniemi J, Sarkeala T, Malila N, Koskenvuo M. Does hair dye use increase the risk of breast cancer? A population-based case-control study of Finnish women. *PLoS One*. 2015;10:e0135190.
- Dhafiri MA, Al Furaikh B, Aljasir A, Alowfi A, Alquraishi A, Alhussain N, Alotaibi A, Alanazi A. Practice and impact of hair dyeing; a local study. *Int J Innov Res Med Sci*. 2022;7:764-770.
- AlGhamdi KM, Moussa NA. Knowledge and practices of, and attitudes towards, the use of hair dyes among females visiting a teaching hospital in Riyadh, Saudi Arabia. *Ann Saudi Med*. 2011;31:613-619.

14. Patel D, Narayana S, Krishnaswamy B. Trends in use of hair dye: a cross-sectional study. *Int J Trichology*. 2013;5:140-143.
15. Jyrwa S, Sebastian J, Shastry V. Cosmetovigilance in a tertiary care hospital: A prospective observational study. *J Cosmet Dermatol*. 2021;20:804-811.
16. He L, Michailidou F, Gahlon HL, Zeng W. Hair dye ingredients and potential health risks from exposure to hair dyeing. *Chem Res Toxicol*. 2022;35:901-915.
17. Eberle CE, Sandler DP, Taylor KW, White AJ. Hair dye and chemical straightener use and breast cancer risk in a large U.S. population of black and white women. *Int J Cancer*. 2019.
18. Cancer. Do hair dyes increase cancer risk? Harvard Health Publishing. <https://www.health.harvard.edu/blog/do-hair-dyes-increase-cancer-risk-2021012021767>
19. Shishavan MK, Sayyah-Melli MR, Rashidi MR, Gharabaghi PM, Ghojazadeh M, Rahmani V. The association of hair coloring during pregnancy with pregnancy and neonatal outcomes: a cross-sectional study. *IJWHR*. 2021;9:130-135.
20. Gupta M. A study of knowledge, attitude, and practices regarding hair dye use among the general population. *Our Dermatol Online*. 2017;9:15-18.
21. Jayanthi CR, Divyashree RN, Vijayalakshmi, Dharani S, Soumya R. A cross-sectional study of hair dye use among doctors and nurses working at a tertiary care centre. *Int J Res Pharmacol Pharmacother*. 2021;7:85-96.
22. Salami M, Pourahmad J, Zarei MH. Toxicity of para-phenylenediamine (PPD;1, 4 diaminobenzene) on isolated human lymphocytes: The key role of intracellular calcium enhancement in PPD-induced apoptosis. *Toxicol Ind Health*. 2023;39:388-397.
23. Banerjee P, Ulker OC. Combinative *ex vivo* studies and *in silico* models ProTox-II for investigating the toxicity of chemicals used mainly in cosmetic products. *Toxicol Mech Methods*. 2022;32:542-548.



# Impact of Simulated Gastrointestinal Fluid: Viscosity, Surface Tension, and pH on the Dissolution and Rheology Assessment of Viscosity of Two Commercial Candesartan Cilexetil Products

Samah ATA<sup>1</sup>, Rana SEJARE<sup>1</sup>, Ola TARAWNEH<sup>1\*</sup>, Rania HAMED<sup>1</sup>, Mohammad AL-SABI<sup>2,3</sup>, Samar BISHTAWI<sup>1</sup>,  
 Hadeel Abu MAHFOUZ<sup>1</sup>, Sameer ALKOUZ<sup>1</sup>

<sup>1</sup>Al-Zaytoonah University of Jordan Faculty of Pharmacy, Department of Pharmacy, Amman, Jordan

<sup>2</sup>King Faisal University, College of Veterinary Medicine, Department of Microbiology, Al-Ahsa, Saudi Arabia

<sup>3</sup>Jordan University of Science and Technology, Department of Basic Medical Veterinary Sciences, Irbid, Jordan

## ABSTRACT

**Objectives:** The aim of this study was to investigate the effect of simulated gastrointestinal viscosity, surface tension, and pH on the dissolution rate of two commercial candesartan cilexetil (CC) products.

**Materials and Methods:** *In vitro* dissolution of two commercial CC products and immediate release of 16 mg of CC were applied under two conditions: (1) the requirements of the United States Pharmacopeia (USP) and (2) conditions physiologically related to the gastrointestinal tract mimicking viscous food intake. The solubility of CC in different simulation fluids was also measured. The dissolution media's viscosity, surface tension, and pH were also measured. The viscosity of the gel layer was measured during CC dissolution.

**Results:** The CC dissolution rate was highest in the USP medium. It was found that the media type affected CC dissolution. The non-USP media exhibited a slower dissolution rate than the USP specification. The highest viscosity media lowered the dissolution rate in one of the CC products. Acidic pH showed a significant decrease in dissolution for both CC products. The solubility of CC was affected by solvent type (p value < 0.001).

**Conclusion:** Higher viscosity media slow the dissolution rate of a product, where a gel layer forms on the tablet surface. The results show variation in the dissolution media. This may reveal differences in the dissolution rates of the same drug in different products and media. Considering, viscosity's effect on dissolution might improve patient outcomes when treated with different products.

**Keywords:** Immediate release, dissolution, viscosity, simulated gastrointestinal fluid, gel

## INTRODUCTION

The dissolution test is a tool that is conducted for measuring the *in vitro* performance of solid oral dosage forms and is performed during the design and optimization of tablet formulations as a comparative tool.<sup>1</sup> The data obtained from *in vitro* dissolution can be highly correlated with *in vivo* biopharmaceutical specifications.<sup>2</sup> Consequently, the generated data are used to predict the *in vivo* performance of oral drug products.<sup>3</sup> Therefore, the media used in *in vitro* dissolution studies

should simulate the anticipated *in vivo* dissolution conditions, which sequentially mimic the physiological conditions in the gastrointestinal tract (GIT).<sup>4</sup>

Viscosity, surface tension, pH, and ionic strength of dissolution media are crucial conditions that affect drug dissolution.<sup>5</sup> In addition, several previous studies documented the effects of various dissolution conditions on the dissolution of poorly soluble drugs.<sup>6,7</sup>

\*Correspondence: ola.tarawneh@zuj.edu.jo, ORCID-ID: orcid.org/0000-0001-5876-6939

Received: 07.08.2023, Accepted: 12.01.2024



Solubility along with the dissolution of class II drugs can be affected by the complex luminal environment throughout GIT, including pH, buffer capacity, ionic strength, surface tension, osmolality, food intake, viscosity, GI motility, and volume available for drug dissolution.<sup>8</sup> When selecting a proper test method in a well-controlled environment, the dissolution test remains sensitive and affected by the finished product composition, material properties (including material source), and manufacturing process of the tested drug.<sup>9</sup> Hence, the choice of an appropriate medium for the evaluation of the dissolution of BCS class II drugs, which simulates the physiological conditions of GI fluids, is crucial for better predicting *in vivo* oral performance and differences in bioavailability among different formulations.<sup>10,11</sup>

The limited dissolution of highly permeable/low-soluble drugs, classified as class II drugs according to BCS, makes them less likely to be absorbed in the oral cavity.<sup>7</sup> Moreover, the physiological conditions of GIT may influence the speed of drug dissolution; for example, increasing the viscosity and surface tension of the dissolution medium may affect drug liberation from its pharmaceutical dosage form.<sup>8</sup> Therefore, testing the effects of these conditions on the dissolution of BCS class II drugs is important.

Candesartan cilexetil (CC) is an angiotensin II receptor blocker of BCS class II drugs.<sup>12</sup> CC is commonly used for the treatment of heart failure, hypertension, diabetic nephropathy, and myocardial infarction.<sup>13</sup> CC was previously used as a model drug for class II drugs due to its low solubility in water (lower than  $8 \times 10^{-8}$  M) and low bioavailability.<sup>14</sup> Therefore, the aim of this study was to investigate the effects of different parameters including viscosity, surface tension, and pH, on the dissolution of two CC tablets.

## MATERIALS AND METHODS

### Materials

CC powder was obtained from Dar Al Dawa Pharmaceuticals (Amman, Jordan). Two commercial 16 mg CC immediate-release tablets were collected from the Jordanian market; CC product 1 (AstraZeneca Company, UK, batch number: GTIN 07321839721397, production date: 01-2019) and CC product 2 (United Pharmaceuticals Manufacturing Co., Amman, Jordan, batch number: M073 JPD, production date: 01-2018). Table 1 presents the excipients and pharmaceutical uses of the two CC products.

Tween<sup>®</sup> 20 was purchased from Tedia Company (OH, USA), sodium lauryl sulfate (SLS, 94%) from Laboratory Rasayan (Gujarat, India), hydroxypropyl methylcellulose (HPMC; M = 69.49) from AZ Chem for Lab Chemicals (Pretoria, South Africa), and acetonitrile (CH<sub>3</sub>CN, 99.9%) from Sigma-Aldrich (Germany). Sodium acetate anhydrous (CH<sub>3</sub>COONa, 99%, Guangdong Guangzhou Sci-Tech Co., Ltd, Guangzhou, China), sodium hydroxide (NaOH, 99%, EMD Millipore Corporation, Fairburn, Georgia), glacial acetic acid (CH<sub>3</sub>CO<sub>2</sub>H, 99.8%, Scharlab, Barcelona, Spain), hydrochloric acid (HCl, 37% w/w, Fisher, Shanghai, China), ethanol (EOH, Fisher, Shanghai,

China), sodium tri-phosphate (Na<sub>3</sub>PO<sub>4</sub>, 98%, Fisher, Shanghai, China), and potassium dihydrogen phosphate (KH<sub>2</sub>PO<sub>4</sub>, 99.9%, Fisher, Shanghai, China). All chemical reagents used in the preparation of dissolution media were analytical grades.

### Dissolution media

The contents of the compendial United States Pharmacopeia (USP) medium buffer and the four non-compendial dissolution media were prepared to investigate the effects of low pH (0.1N HCl), low surface tension (0.4% w/v SLS), and high viscosity (0.1 and 0.2% w/v HPMC).

### Preparation of the CC calibration curve

Calibration curves for CC in the CC-USP, HCl, SLS, 0.1% HPMC, and 0.2% HPMC media were prepared according to previously documented procedures,<sup>15</sup> which were briefly described as follows: 100 mg of CC was weighed into a 100 mL volumetric flask, 10 mL of acetonitrile was added, and the flask was sonicated for 10 min. An additional volume of acetonitrile was added to the mixture to reach a final volume of 100 mL. The resulting standard stock solution (1 mg/mL) was used to prepare the final standard concentrations of 2, 5, 6, 10, 20, and 35 µg/mL by diluting the stock solution in plain USP medium (CC-USP) as well as in the other investigated media, including HCl, SLS, 0.1% HPMC, and 0.2% HPMC. The calibration curves were prepared three times, and the mean of the resulting curves was obtained.

The concentration of the dissolved drug in the media was measured using an ultraviolet (UV)-Vis spectrophotometer-1800 (SHIMADZU) scanned over a range of 200-400 nm to detect the maximum wavelength absorbance ( $\lambda_{max}$ ). The absorbance

**Table 1. Excipients of two commercially available CC tablets as issued on a leaflet by the manufacturers. product 1 (AstraZeneca Company, UK, batch number: GTIN 07321839721397, production date: 01-2019) and product 2 (United Pharmaceuticals Manufacturing Co., Amman, Jordan, batch number: M073 JPD, production date: 01-2018)**

Pharmaceutical function	Product 1	Product 2
Disintegration enhancer Thickening agent	Carmellose sodium	
Disintegration enhancer Compression molding Adhesion agent		Microcrystalline cellulose*
Flow enhancer Direct-compression excipient	Lactose monohydrate	Lactose monohydrate
Dissolution enhancer	HPMC	HPMC
Direct-compression excipient Disintegration enhancer Diluent	Maize starch	Maize starch
Wetting agent Penetration enhancer	Macrogol	Polyethylene glycol
Colorant Ultraviolet absorber	Iron oxide (E127)	Ferric iron oxides

UV: Ultraviolet, CC: Candesartan cilexetil

was measured against 1 mL of acetonitrile in 100 mL of each prepared medium. The measured absorbance was plotted against drug concentrations to determine absorptivity using the Beer-Lambert equation.<sup>16</sup>

#### Hardness testing

Randomly selected tablets of CC products 1 and 2 ( $n=10$ ) were tested for hardness using an automated hardness tester (electrolab, India). The mean and standard deviation (SD) of the force were recorded in Newton (N).

#### In vitro dissolution testing

Dissolution testing was conducted in 900 mL of the investigated media to which the tablets were added. In all experiments, the temperature was fixed at  $37\text{ }^{\circ}\text{C} \pm 0.5$  using USP apparatus II (paddles) rotating at 50 rpm. Samples were withdrawn from the media at specific time intervals (15, 30, 45, 60, 75, 90, 105, and 120 min). Samples (3 mL) were first passed through a  $0.22\text{ }\mu\text{m}$  syringe filter, and the amount of dissolved CC in the media was analyzed using a UV-Vis spectrophotometer at  $\lambda_{\text{max}} 254$  nm. According to USP requirements, immediate-release dosage forms require the release of not less than 80% of the claimed amount after 45 min.<sup>17</sup> The dissolution rate of CC (expressed as dissolution percentage; %) was calculated by establishing calibration curves for each medium, with Milli-Q water used as a control. The applied tests were repeated six times for each product, and the raw material was dissolved in the investigated media. The same control and number of replicates were used in the solubility study, surface tension measurement, viscosity measurements, pH measurements, and ionic strength measurements.

#### Solubility of CC

The solubility of CC in the investigated media was measured as previously described (Hassan et al.,<sup>15</sup>). Briefly, CC was added in excess of 15 mL of each medium. The mixtures were kept at  $37\text{ }^{\circ}\text{C}$  for 24 h and then filtered through a  $0.2\text{ }\mu\text{m}$  syringe filter. The filtrates were collected, and UV absorbance was measured using a UV-Vis spectrophotometer at  $\lambda_{\text{max}} 254$  nm.<sup>18</sup>

#### Surface tension measurements

The surface tension of dissolution media containing drugs was measured using a micro-roughened platinum plate tensiometer (Tensiometer Attension®, Biolion Scientific, Sweden). The measurements were performed on the surface of Platinum plates immersed in 40 mL of the investigated media, which were placed in a round vessel made of Pyrex (with 50 mm diameter) and then incubated in a water bath for three minutes at  $37\text{ }^{\circ}\text{C}$ .

#### Viscosity testing of the dissolution media and gel layer formed on the tablet surface

The viscosities of dissolution media and the gel layer formed on the surface of the tablets undergoing dissolution were measured at  $37\text{ }^{\circ}\text{C}$  using Rheometer DVT3 (Brookfield, USA), coupled with a 4-mm diameter cone and plate geometry of  $1^{\circ}$ . Tablets were first placed in dissolution vessels containing dissolution media. After 15 min, the formed gel layer on the tablets was

carefully removed using a spatula. Viscosity measurements were performed at a shear rate of  $75\text{ s}^{-1}$ , speed of 10 rpm, and strain stress of 0.01-10%.

#### pH and ionic strength testing

The pH of the media was measured using a pH meter (Mettler Toledo, USA) calibrated before each measurement. The ionic strength of the media was calculated using the following equation:

$$I = \frac{1}{2} \sum_1^n c_i z_i^2 \quad (1)$$

Where  $I$  is the ionic strength,  $n$  is the number of species in the solution,  $c_i$  is the molar concentration of ion  $i$ ,  $z_i$  is the charge number of ions, and  $\Sigma$  refers to the summation symbol (the sum of overall ions in the solution).<sup>7</sup>

#### Statistical analysis

Data analysis was conducted using GraphPad Prism version 7. One-Way analysis of variance and Two-Way analysis of variance followed by the Tukey test were used to differentiate and compare the dissolution profiles of CC products 1 and 2 in the tested media. Data were presented as mean  $\pm$  SD. A  $p$  value lower than 0.05 ( $p$  value  $<$ ) was deemed statistically significant.

## RESULTS

#### CC calibration curves

The calibration curves of raw CC were obtained in all dissolution media with  $\lambda_{\text{max}}$  of 254 nm. The plotted curve was linear for all three replicates in a concentration range of 2 to 35  $\mu\text{g/mL}$ . Results: Mean correlation factor  $R^2 = 0.9997$  and mean slope ( $\epsilon$ ) of  $27.5\text{ mg}^{-1} \cdot 0.1\text{L}^{-1} \cdot \text{cm}$ .

#### CC hardness test

Products 1 and 2 had a significantly higher index of hardness ( $92.0 \pm 3.7\text{ N}$ ;  $p$  value  $< 0.01$ ) compared to products 2 ( $56.6 \pm 4.9\text{ N}$ ).

#### Solubility, surface tension, viscosity, and ionic strength of raw CC in dissolution media

Table 3 presents the solubility of raw CC in different dissolution media and its physicochemical properties. The highest solubility was observed in CC-USP medium ( $20.9 \pm 0.5\text{ }\mu\text{g/mL}$ ), followed by SLS ( $14.7 \pm 0.3\text{ }\mu\text{g/mL}$ ) and 0.1% HPMC ( $13.9 \pm 0.4\text{ }\mu\text{g/mL}$ ) media. Lower solubility was observed in 0.2% HPMC ( $5.6 \pm 0.3\text{ }\mu\text{g/mL}$ ) and HCl ( $3.7 \pm 0.2\text{ }\mu\text{g/mL}$ ) media.

The highest surface tension was achieved using Milli-Q® water ( $72.0 \pm 0.0\text{ mN/m}$ ). The surface tension of the CC-dissolved media was comparable between the investigated media, ranging from 34.8 and 34.7 mN/m in HCl CC-USP media, respectively, followed by 33.2 mN/m in 0.1% and 0.2% HPMC, and then 30.20 mN/m in SLS media.

The highest viscosity was observed in the 0.2% HPMC medium, which was ten times higher than the viscosity of the Milli-Q® water, which was used as a control ( $8.0 \pm 0.8$  vs.  $0.8 \pm 0.1$  cP 0.2% HPMC, Milli-Q® water respectively). The viscosity

decreased as the HPMC concentration decreased to 0.1% ( $5.5 \pm 0.3$  cP). The CC-USP, HCl, and SLS media exhibited similar viscosities ( $1.2 \pm 0.1$ ,  $1.2 \pm 0.1$ ,  $1.2 \pm 0.1$  cP, respectively), which were approximately eight times lower than that of the 0.2% HPMC medium.

The ionic strength of the HCl media was the highest (0.1 mM), whereas the other media, except Milli-Q® water, had relatively similar ionic strengths of 0.06–0.07 mM. The results are presented in Table 2.

#### *In vitro* dissolution of Product 1

Figure 1 shows the dissolution profiles of product 1 tablets in the investigated media. CC dissolution was significantly affected by the dissolution media employed. While using the CC-USP medium, product 1 met the recommended USP release rate at 45 min post-dissolution of  $106.9 \pm 6.2\%$ , whereas the USP requirements were not observed in the other dissolution media. As an example, low dissolution was observed in the SLS medium ( $51.80 \pm 4.72\%$  after 45 min), followed by that observed in the HCl medium ( $30.6 \pm 8.96\%$  after 45 min). Almost no release was detected when HPMC was used as a viscosity enhancer at a 0.2% w/v concentration. However, the rate of CC release was slightly increased to  $12.16 \pm 7.79\%$  after 120 min when the concentration of HPMC was reduced to 0.1% w/v.

The differences in CC release rate using different dissolution media were marked immediately after 15 min post-dissolution. The CC-USP medium achieved a dissolution of  $65.86 \pm 13.77\%$  in 15 min, followed by the SLS medium ( $24.1 \pm 6.61\%$ ;  $p$  value  $< 0.001$ ). Compared with the CC-USP medium, the rate of release was slower ( $p$  value  $< 0.001$ ) in HCl medium with a release rate of  $21.77 \pm 6.48\%$  after 15 min.

#### *In vitro* dissolution of product 2

Figure 2 illustrates the dissolution profiles of product 2 tablets in the investigated media. The dissolution profiles were significantly affected by the media employed. At 45 min, the highest CC dissolution was recorded in the CC-USP medium ( $100.5 \pm 6.19\%$ ), followed by the 0.1% HPMC medium ( $97.36 \pm 6.77\%$ ). However, dissolution was significantly lower in SLS ( $56.0 \pm 1.8\%$ ), 0.2% HPMC ( $32.3 \pm 9.2\%$ ,  $p$  value  $< 0.001$ ), and HCl media ( $24.0 \pm 1.7\%$ ,  $p$  value  $< 0.001$ ).

#### Viscosity of the gel layer temporarily formed on dissolved tablets

A clear gel layer was formed on the surface of the tablets containing product 1 but not those containing product 2. The viscosity of the gel layer (Figure 3) was highest when using Milli-Q® water ( $5.15 \pm 0.31$  CP). The viscosity of the gel layer decreased to  $4.25 \pm 0.16$  CP, and  $3.66 \pm 0.14$  CP when using 0.2% HPMC and 0.1% HPMC media, respectively. The viscosities of the gel layers formed in the CC-USP medium ( $1.53 \pm 0.16$  CP) and the HCl medium ( $1.66 \pm 0.46$  CP) media were comparatively similar and low.

## DISCUSSION

CC is a BCS class II drug that is typically characterized by low solubility and high permeability, which limit its oral bioavailability.<sup>13,14</sup> Therefore, the *in vitro* dissolution testing of CC is important for predicting its *in vivo* absorption and bioavailability. Consequently, optimization of the experimental parameters of the *in vitro* dissolution testing when compared to *in-vivo* conditions was needed. Comparing the two commercial CC products is not the primary aim of this study; on the contrary, it aims to identify new validated methods that are not usually applied in QC analysis to determine the physicochemical properties of the products.<sup>19,20</sup>

Dissolving the investigated commercial CC tablets in USP medium met the USP compendial requirements. However,

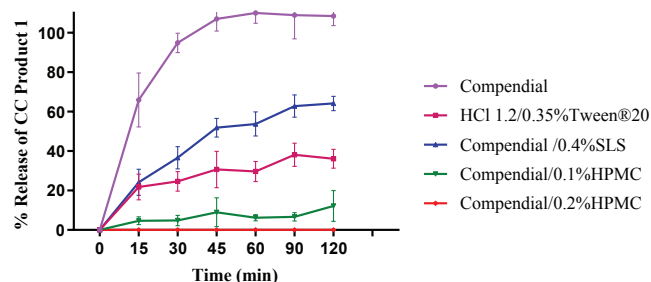


**Figure 1.** Dissolution profiles of candesartan cilexetil CC-product 1 (AstraZeneca Company, UK, batch number: GTIN 07321839721397, production date: 01-2019) were obtained at a rotation speed of 50 rpm and 37 °C, ( $n = 6$ ). Dissolution was performed using CC-USP, HCl, SLS, 0.1% HPMC, and 0.2% HPMC media

CC: Candesartan cilexetil, USP: United States Pharmacopeia, HCl: Hydrochloric acid, SLS: Sodium lauryl sulfate, HPMC: Hydroxypropyl methylcellulose

**Table 2.** Composition of the media (components per 100 mL) used for dissolving candesartan and cilexetil

Media	pH	Phosphate buffer at pH 6.5		Tween® 20 (g)	HCl (mL)	SLS (g)	HPMC (g)
		Na <sub>2</sub> HPO <sub>4</sub> ·7H <sub>2</sub> O (g)	NaH <sub>2</sub> PO <sub>4</sub> ·H <sub>2</sub> O (g)				
CC-USP	6.5	0.96	0.88	0.35			
HCl	1.2			0.35	8.3		
SLS 0.4% w/v	6.5	0.96	0.88	0.35		0.4	
0.1% HPMC	6.5	0.96	0.88	0.35			0.1
0.2% HPMC	6.5	0.96	0.88	0.35		0.2	

CC: Candesartan cilexetil, USP: United States Pharmacopeia, HCl: Hydrochloric acid, SLS: Sodium lauryl sulfate, HPMC: Hydroxypropyl methylcellulose

changes in the dissolution media conditions such as the viscosity and the surface tension were not responded in the same pattern when using different types of investigated media. Surfactants are usually used in the preparation of dissolution

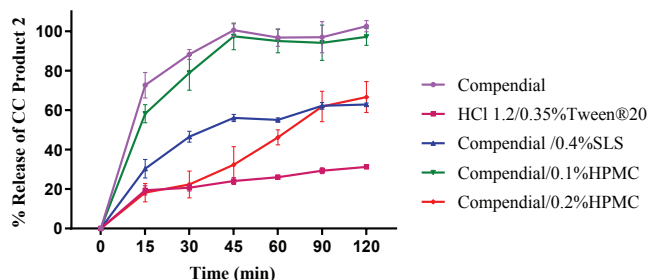


**Figure 2.** Dissolution profiles of candesartan cilexetil (CC-product 2: United Pharmaceuticals Manufacturing Co., Amman, Jordan, batch number: M073 JPD, production date: 01-2018) were obtained at a rotation speed of 50 rpm and 37 °C (n= 6). Dissolution was performed using CC-USP, HCl, SLS, 0.1% HPMC, and 0.2% HPMC media

CC: Candesartan cilexetil, USP: United States Pharmacopeia, HCl: Hydrochloric acid, SLS: Sodium lauryl sulfate, HPMC: Hydroxypropyl methylcellulose

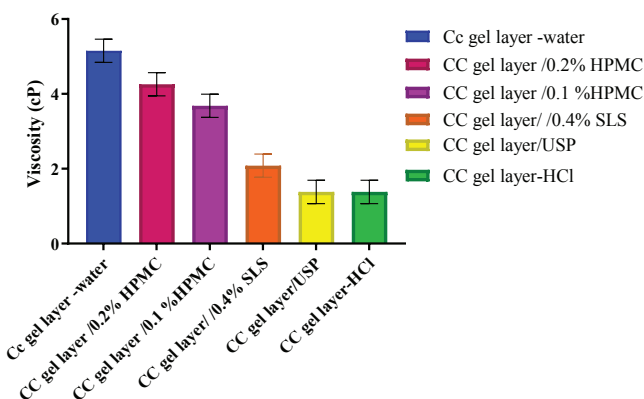


**Figure 3.** The viscosity of the gel layer formed on the surface of commercially available tablets of candesartan cilexetil (product 1: AstraZeneca Company, UK, batch number: GTIN 07321839721397, production date: 01-2019) after 15 min dissolution in various media at 37 °C and 50 rpm.

CC: Candesartan cilexetil, USP: United States Pharmacopeia, HCl: Hydrochloric acid, SLS: Sodium lauryl sulfate, HPMC: Hydroxypropyl methylcellulose

media to enhance the drug wetting and dissolution process.<sup>21</sup> When the surfactant concentration was increased, micelles were formed, and their stability was generally related to the critical micelle concentration (CMC).<sup>22</sup> The rationale for selecting specific surfactants for *in vitro* testing is essential to understand their interaction with drug molecules and other ingredients in dissolution media and excipients.<sup>23,24</sup> A 0.5 w/w% tween® 20 sample had a surface tension of 3.7 mN/m,<sup>22</sup> whereas the surface tension of SLS was 39.4 mN/m at an estimated CMC of 0.58 w/v%.<sup>25</sup> Differences in surface tension and CMC between the two surfactants used to explain the rheological behavior and wetting of dissolved drugs.<sup>25</sup> The USP medium includes tween® 20, which may enhance the dissolution of CC. The addition of 0.4% SLS to the USP medium was performed to further reduce surface tension and simulate gastric fluid conditions, which were approximately 30 mN/m.<sup>26,27</sup> However, the addition of SLS did not increase the rate of CC dissolution in the tablet products. This result can be attributed to the interaction between the anionic SLS and the cations present in the buffer, which may result in the formation of insoluble material that lowers the effect of SLS.<sup>28</sup> Moreover, the addition of more components may disrupt the water structure, reducing the cohesive dielectric constant and cohesive energy, leading to lowering solvent polarity<sup>28</sup> and, as a result, causing a reduction in drug dissolution. Generally, the viscosity of the dissolution media plays an essential role in the dissolution of drugs.<sup>5</sup> It was found that CC tablets and the raw material used in this study exhibited different dissolution patterns. The dissolution of CC in product 2 was comparable to that of raw CC in the CC-USP medium. On the other hand, the dissolution of CC in product 1 was comparable to that of raw CC in the CC-USP and 0.1% HPMC media but was slower in 0.2% HPMC, which has a higher viscosity level. The recorded viscosity of raw CC in the 0.2% HPMC medium was approximately eight times higher than that of the CC-USP medium, which may explain the slow dissolution of raw CC in the 0.2% HPMC medium. High viscosity can inhibit drug dissolution by reducing the dissolution rates.<sup>29</sup> Therefore, the passage of the drug through the surrounding medium is impeded, increasing the resistance to drug diffusion.<sup>30</sup> Viscosity may vary according to food content and the different parts of the GIT, which affects the diffusion of the drug into the surrounding media.<sup>31</sup> The variation between commercial drugs

**Table 3.** Solubility, surface tension, viscosity, and ionic strength of raw CC in different media at 37 °C. Data are presented as mean ± SD. Milli-Q water was used as a control. The tests were repeated six times for each product, and the raw material was dissolved in the investigated media

Dissolution media	pH	Solubility (µg/mL)	Surface tension mN/m	Viscosity (CP)	Ionic strength (mM)
Milli-Q® water	6.99	1.7 ± 0.6	72.0 ± 0.0	0.8 ± 0.1	0.00
CC-USP	6.5	20.9 ± 0.5	34.7 ± 0.0	1.2 ± 0.1	0.06
HCl	1.2	3.7 ± 0.2	34.8 ± 0.8	1.2 ± 0.1	0.10
SLS	6.5	14.7 ± 0.3	30.20 ± 0.1	1.2 ± 0.1	0.07
0.1% HPMC	6.5	13.9 ± 0.4	33.2 ± 0.9	5.5 ± 0.3	0.06
0.2% HPMC	6.5	5.6 ± 0.3	33.2 ± 0.3	8.0 ± 0.8	0.06

CC: Candesartan cilexetil, USP: United States Pharmacopeia, HCl: Hydrochloric acid, SLS: Sodium lauryl sulfate, HPMC: Hydroxypropyl methylcellulose

and non-compendial requirements could be related to different compositions and sources of raw materials.<sup>20</sup> Therefore, an explanation of the food breeds that may reduce the availability of drugs should be noticed in the product leaflets.

Typically, the first step in drug dissolution is wetting followed by gelling the tablet.<sup>4</sup> The formed gelling layer is stagnant and is expected to dissolve to enhance the release of drugs from the tablet.<sup>26</sup> In this study, gel layers were formed in the tablets containing product 1 after 15 min of dissolution. Tablets of product 2 disintegrated quickly, probably as a result of the existence of microcrystalline cellulose. In addition, a harder tablet may increase the probability of dissolution failure.<sup>32</sup> On the other hand, higher compression forces are employed to attain tablet hardness, which results from an increase in interparticle bonding.<sup>33</sup> Hardness can be affected by processing techniques such as direct compaction, hot melt extrusion, or fused melting deposition, as well as by affecting intermolecular interactions, causing an increase in the tablet's hardness.<sup>34</sup> Furthermore, disintegration can be somehow related to tablet hardness. A harder tablet may increase the probability of dissolution failure; therefore, it takes longer for the tablet to interact with the medium to form the presumed gel layer.<sup>35</sup> In addition, the ionic strength of the media affects the formation and viscosity of gel layers formed on the surface of tablets.<sup>9</sup> High ionic strength increases the electrolyte concentration, thus increasing the spaces between water molecules as a result of the salting-out effect, which decreases gelation.<sup>36</sup> This will support the current findings that lower viscosity of the formed gel layers was observed in media of higher ionic strength (HCl and SLS) compared to the viscosity of gels formed in media of lower ionic strength (Milli-Q water, 0.1 and 0.2% HPMC).

The pH of the dissolution media plays an important role in drug ionization throughout the GIT.<sup>37</sup> In fasting conditions, the pH of the stomach can reach 1.2 or lower.<sup>11</sup>

When CC ( $pK_a = 4.66$ ) is taken under fasting conditions with a low stomach pH, CC will be expected to exist in its unionized form, and thereby, it will precipitate. This was obvious in the current study, as the observed solubility of CC in the HCl medium was five to six times lower than that in the CC-USP medium, which affected the dissolution results for both products. It is worth mentioning that the leaflets of CC products lack instructions for avoiding the intake of tablets in the fasted stomach. This could be revised in the future to enhance the effects of CC.

## CONCLUSIONS

The *in vitro* dissolution of two commercial products of immediate-release tablets containing CC in USP and non-USP media with various physiological properties was studied. Both products were consistent with the compendial requirement for immediate release according to USP, whereby more than 85% of the claimed amount was released after 45 min. However, the dissolution of tablets varied when using different media conditions. A higher-viscosity media slowed the dissolution rate of one CC product. It was found that a gel layer could form

on tablets, thereby reducing the dissolution rate. The present results showed that variations in the pharmacopeia requirements of dissolution media may not only exhibit differences in the dissolution of the same drug in different products but can also show different dissolution profiles between these products in the investigated media. The findings of this study should be taken into consideration when revising the instructions in the published leaflets of the investigated CC tablets.

## Ethics

**Ethics Committee Approval:** Not required.

**Informed Consent:** Not required.

## Authorship Contributions

Concept: A.F., F.B.H., M.G., G.B.N., J.M., L.-N.M., S.G., Design: A.F., F.B.H., M.G., G.B.N., J.M., L.-N.M., S.G., Data Collection or Processing: A.F., F.B.H., G.B.N., L.-N.M., Analysis or Interpretation: A.F., M.G., J.M., L.-N.M., Literature Search: A.F., F.B.H., M.G., G.B.N., J.M., L.-N.M., S.G., Writing: A.F., F.B.H., G.B.N., L.-N.M.

**Conflict of Interest:** The authors have no conflicts of interest to declare.

**Financial Disclosure:** This project was financially supported by the Deanship of Academic Research and Graduate Studies at Al-Zaytoonah University of Jordan (grant number: 27/12/2019-2020).

## REFERENCES

- Qiu Y, Chen Y, Zhang GG, Yu L, Mantri RV. In vitro/in vivo correlations: fundamentals, development considerations, and application. *Developing Solid Oral Dosage Forms: Pharmaceutical Theory and Practice*. 2nd ed. London: Elsevier; 2017. p. 415-447.
- Siddique S, Abdul MIM, Rahman SAU, Khan IU, Hussain T, Mahmood T, Nawaz Y. Development and execution of a novel strategic statistical tool to determine in-vitro in-vivo correlation for sustained release capsules of metoprolol tartrate in humans. *Sci Res Essays*. 2019;14:1-8.
- Cristofolletti R, Dressman JB. Dissolution methods to increasing discriminatory power of in vitro dissolution testing for ibuprofen free acid and its salts. *J Pharm Sci*. 2017;106:92-99.
- Hamed R, Al-Baraghtli T, Sunoqrot S. Correlation between the viscoelastic properties of the gel layer of swollen HPMC matrix tablets and their in vitro drug release. *Pharm Dev Technol*. 2018;23:838-848.
- Shahzad Y, Ibrar N, Hussain T, Yousaf AM, Khan IU, Rizvi SAA. Relevancy of Nizatidine's release from floating tablets with viscosity of various cellulose ethers. *Sci*. 2021;3:22.
- Mudie DM, Samiei N, Marshall DJ, Amidon GE, Bergström CA. Selection of in vivo predictive dissolution media using drug substance and physiological properties. *AAPS journal*. 2020;22:1-13.
- Hamed R, Awadallah A, Sunoqrot S, Al-Jaafreh N, Hasan M. pH-dependent solubility and dissolution behavior of carvedilol-case example of a weakly basic BCS class II drug. *AAPS PharmSciTech*. 2016;17:418-426.
- Hamed R, AlJanabi R, Sunoqrot S, Abbas A. The effect of pH, buffer capacity and ionic strength on quetiapine fumarate release from matrix tablets prepared using two different polymeric blends. *Drug Dev Ind Pharm*. 2017;43:1330-1342.

9. Damian F, Harati M, Schwartzenhauer J, Van Cauwenberghe O, Wettig SD. Challenges of dissolution methods development for soft gelatin capsules. *Pharmaceutics*. 2021;13:214.
10. Butler J, Hens B, Vertzoni M, Reppas C, Dressman JB, Koziolok M, Holmstock N, Berben P, Duchateau G, Jorga K, Augustijns P, Wilson CG, Kuentz M. In vitro models for the prediction of in vivo performance of oral dosage forms: Recent progress from partnership through the IMI OrBiTo collaboration. *Eur J Pharm Biopharm*. 2019;136:70-83.
11. Wakamatsu J, Sato K, Uryu K, Maru I. Clinical demonstrations of controlled-release tablets constructed by the combined usage of shellac and hydroxypropyl methylcellulose. *Future Pharmacology*. 2021;1:48-59.
12. Amer AM, Allam AN, Abdallah OY. Preparation, characterization and ex vivo-in vivo assessment of candesartan cilexetil nanocrystals via solid dispersion technique using an alkaline esterase activator carrier. *Drug Dev Ind Pharm*. 2019;45:1140-1148.
13. Figueroa-Campos A, Sánchez-Dengra B, Merino V, López-Rubio A, Lagaron JM. Candesartan cilexetil in vitro-in vivo correlation: predictive dissolution as a development tool. *Pharmaceutics*. 2020;12:633.
14. Mady OY, Abulmeaty MMA, Donia AA, El-Mahdy MM, Abulmeaty MMA, Amer MM. Formulation and bioavailability of novel mucoadhesive buccal films for candesartan cilexetil in rats. *Membranes (Basel)*. 2021;11:659.
15. Hassan HA, Charoo NA, Ali AA, Alkhatem SS. Establishment of a bioequivalence-indicating dissolution specification for candesartan cilexetil tablets using a convolution model. *Dissolution Technol*. 2015;22:36-43.
16. Mortensen N, Toews P, Bates J. Crosslinking-dependent drug kinetics in hydrogels for ophthalmic delivery. *Polymers (Basel)*. 2022;14:248.
17. Poudel S, Kim DW. Developing pH-modulated spray dried amorphous solid dispersion of candesartan cilexetil with enhanced in vitro and in vivo performance. *Pharmaceutics*. 2021;13:497.
18. Hoppe K, Sznitowska M. The effect of polysorbate 20 on solubility and stability of candesartan cilexetil in dissolution media. *AAPS PharmSciTech*. 2014;15:1116-1125.
19. Alkather Z, Hailat M, Al-Shdefat R, Abu Dayyih W. Development and Validation of HPLC method for five gliptins in pharmaceutical dosage forms in finished marketed products. *Curr Pharm Anal*. 2021;17:1263-1271.
20. Tarawneh OA, Madi AM, Hamed R, Alnadi SH, Sunoqrot S. In vitro characterization and evaluation of commercialized paracetamol products in Jordan. *Dissolution Technol*. 2019;26:36-44.
21. van der Merwe J, Steenekamp J, Steyn D, Hamman J. The role of functional excipients in solid oral dosage forms to overcome poor drug dissolution and bioavailability. *Pharmaceutics*. 2020;12:393.
22. Al-Soufi W, Novo M. A Surfactant concentration model for the systematic determination of the critical micellar concentration and the transition width. *Molecules*. 2021;26:5339.
23. Mah PT, Peltonen L, Novakovic D, Rades T, Strachan CJ, Laaksonen T. The effect of surfactants on the dissolution behavior of amorphous formulations. *Eur J Pharm Biopharm*. 2016;103:13-22.
24. Liu T, Hao J, Yang B, Hu B, Cui Z, Li S. Contact angle measurements: an alternative approach towards understanding the mechanism of increased drug dissolution from ethylcellulose tablets containing surfactant and exploring the relationship between their contact angles and dissolution behaviors. *AAPS PharmSciTech*. 2018;19:1582-1591.
25. Guo Y, Wang C, Dun J, Du L, Hawley M, Sun CC. Mechanism for the reduced dissolution of ritonavir tablets by sodium lauryl sulfate. *J Pharm Sci*. 2019;108:516-524.
26. Yang B, Wei C, Qian F, Li S. Surface wettability modulated by surfactant and its effects on the drug release and absorption of fenofibrate solid dispersions. *AAPS PharmSciTech*. 2019;20:234.
27. Hamed R, Alnadi SH, Awadallah A. The effect of enzymes and sodium lauryl sulfate on the surface tension of dissolution media: toward understanding the solubility and dissolution of carvedilol. *AAPS PharmSciTech*. 2020;21:146.
28. Khan H, Seddon JM, Law RV, Seddon KR, Guiseppi-Elie A, Khan GM. Effect of glycerol with sodium chloride on the Krafft point of sodium dodecyl sulfate using surface tension. *J Colloid Interface Sci*. 2019;538:75-82.
29. Zaheer K, Langguth P. Designing robust immediate release tablet formulations avoiding food effects for BCS class 3 drugs. *Eur J Pharm Biopharm*. 2019;139:177-185.
30. Jin L, Qi H, Gu X, Huang J, Zhang X, Zhai X. Effect of sodium alginate type on drug release from chitosan-sodium alginate-based in situ film-forming tablets. *AAPS PharmSciTech*. 2020;21:55.
31. D'Arcy DM, Persoons T. Understanding the potential for dissolution simulation to explore the effects of medium viscosity on particulate dissolution. *AAPS PharmSciTech*. 2019;20:47.
32. Byrne B, McDermott O, Noonan J. Applying lean six sigma methodology to a pharmaceutical manufacturing facility: a case study. *Processes*. 2021;9:550.
33. Dular Vovko A, Hodžić B, Brec T, Hudovornik G, Vrečer F. Influence of formulation factors, process parameters, and selected quality attributes on carvedilol release from roller-compacted hypromellose-based matrix tablets. *Pharmaceutics*. 2022;14:876.
34. Nashed N, Lam M, Ghafourian T, Pausas L, Jiri M, Majumder M, Nokhodchi A. An insight into the impact of thermal process on dissolution profile and physical characteristics of theophylline tablets made through 3D printing compared to conventional methods. *Biomedicines*. 2022;10:1335.
35. Mostafa M, Gardouh AR, Abogresha NM, Gad S. Factorial design, formulation, in vitro and in vivo evaluation of rapid orally disintegrating tablets prepared by sublimation technique using captopril as a model drug. *J Drug Delivery Sci Technol*. 2020;57:101635.
36. Heng W, Wei Y, Zhou S, Zhang R, Zhao X, Luo C. Effects of temperature and ionic strength of dissolution medium on the gelation of amorphous lurasidone hydrochloride. *Pharm Res*. 2019;36:72.
37. Sheng JJ, Kasim NA, Chandrasekharan R, Amidon GL. Solubilization and dissolution of insoluble weak acid, ketoprofen: effects of pH combined with surfactant. *Eur J Pharm Sci*. 2006;29:306-314.



# Insecticidal and Bactericidal Activities of *Cassia nigricans* Vahl and Molecular Docking Analysis of Insect Acetylcholinesterase

Abdourahman FADIMATOU<sup>1\*</sup>, Faiza BOUKLI HACENE<sup>2</sup>, Meriem GHALEM<sup>2</sup>, Guy Bertrand NOUMI<sup>1</sup>, Jean MOMENI<sup>1</sup>,  
 Le-Ndiman MBAIDANEM<sup>1</sup>, Said GHALEM<sup>2</sup>

<sup>1</sup>University of Ngaoundere, Faculty of Science, Department of Chemistry, Ngaoundere, Cameroon

<sup>2</sup>University of Tlemcen, Faculty of Science, Department of Chemistry, Laboratory of Natural and Bioactive Substances, Tlemcen, Algeria

## ABSTRACT

**Objectives:** This study focused on the phytochemical, insecticidal, and bactericidal activities of *Cassia nigricans* Vahl, as well as molecular docking analysis of an acetylcholinesterase (AChE) inhibitor as a promising natural insecticide.

**Materials and Methods:** The leaves of *C. nigricans* were successively extracted with n-hexane, acetone, and methanol. Silica gel column chromatography of the methanol extract yielded compound 1. The insecticidal properties of the extracts and compound 1 were evaluated in terms of contact toxicity against *Sitophilus zeamais*. Bactericidal activity was achieved by photodynamic inactivation of fecal coliforms (FCs) and enterococci in water using extracts and compound one as natural photosensitizers. Compound 1 was analyzed for physicochemical and pharmacokinetic parameters and molecular docking against the AChE protein (6XYU).

**Results:** Compound 1 was characterized as emodin (1,3,8-trihydroxy-6-methylanthracene-9,10-dione) using 1D-2D-<sup>1</sup>H-<sup>13</sup>C nuclear magnetic resonance and mass spectrometry. Insecticidal properties showed that emodin exhibited the highest toxicity with a lethal concentration 50 (LC<sub>50</sub>) = 5.00 mg/mL compared with all extracts. The n-hexane extract showed the highest insecticidal activity (LC<sub>50</sub> = 177.48 mg/mL) compared with the methanol (LC<sub>50</sub> = 195.08 mg/mL) and acetone (LC<sub>50</sub> = 374.14 mg/mL) extracts. Complete inhibition of fecal enterococci by photosensitization was observed after 60 min of light exposure to emodin-treated water at all concentrations (1-5 mg/mL) and 120 minutes for FCs under the same conditions. Based on the docking score, the binding energy of emodin (-6.38 kcal/mol) was close to that of the marketed insecticide pirimiphos-methyl (-6.25 kcal/mol).

**Conclusion:** In addition, emodin was subjected to insecticide probability prediction and absorption, distribution, metabolism, excretion, and toxicity analysis and was found to be satisfactory as a natural insecticide. Emodin is a promising candidate for insecticidal pest control.

**Keywords:** *Cassia nigricans*, insecticidal, bactericidal, molecular docking

## INTRODUCTION

Several methods are used to control stored grain insect pests: smoking, heating, and synthetic chemicals.<sup>1</sup> Synthetic insecticides have drawbacks, and their high cost limits their accessibility to farmers. To minimize post-harvest losses, plants containing alkaloids, terpenoids, and anthraquinones are used as natural insecticides and are of purely ecological interest as they are not harmful to the environment.<sup>2</sup> Some compounds

can act as insecticides by inhibiting insect acetylcholinesterase (AChE) and preventing the breakdown of acetylcholine, the accumulation of which causes insect death. Many compounds such as the organophosphates used as insecticides for pest control exert their effects as AChE inhibitors (AChEI).<sup>3</sup> Numerous models are used for AChEI as part of the study of the insecticidal effect, such as the molecular docking analysis against insect AChE.<sup>4</sup>

\*Correspondence: fadimatouabdourahman02@gmail.com, ORCID-ID: orcid.org/0009-0007-6970-8313

Received: 24.07.2023, Accepted: 12.01.2024



Copyright© 2024 The Author. Published by Galenos Publishing House on behalf of Turkish Pharmacists' Association. This is an open access article under the Creative Commons Attribution-NonCommercial-NoDerivatives 4.0 (CC BY-NC-ND) International License.

Some natural compounds used to protect stored foodstuffs can have a bactericidal effect.<sup>5</sup> The bactericidal effect may be due to the photodynamic inactivation of microorganisms by the photosensitizing effect of plants or compounds in the presence of light.<sup>6</sup> This photosensitizing effect is directly linked to the presence of substances that generate singlet oxygen, which can damage microorganisms present in the environment.<sup>7</sup> The alkaloids, coumarins, and anthraquinones present in plants are responsible for photosensitizing and bactericidal activities.<sup>8</sup>

*Cassia nigricans* Vahl (Caesalpinaceae) was previously studied for its antimicrobial, insecticidal, analgesic, anti-inflammatory, and antiplasmodial activities.<sup>9</sup>

This work presents for the first time the insecticidal activity by contact toxicity against *Sitophilus zeamais*, the photosensitized inactivation of fecal coliforms (FC) and fecal enterococci (FE) by the leaves of *C. nigricans*, the molecular docking of the isolated anthraquinone against *Drosophila melanogaster* AChE (DmAChE) and the analysis of its absorption, distribution, metabolism, excretion, and toxicity (ADMET) properties.

## MATERIALS AND METHODS

### Plant material

The leaves of *C. nigricans* were collected in Dobem, Chad, in September 2021. The plant was identified at the National Herbarium of Cameroon, Yaounde, Cameroon where a Voucher Specimen 26339 SFR/Cam was deposited.

### Extraction and isolation

Dried and ground *C. nigricans* leaves (1 kg) were extracted with 4 L of *n*-hexane for 48 hours and concentrated to produce the *n*-hexane extract (HE). The residues were successively extracted with acetone and methanol following the same procedure used previously to obtain the acetone extract (AE) and the methanol extract (ME).

Column chromatography (CC) of ME (40 g) on silica gel (60-120 Mesh) using a gradient of increasing polarity of *n*-hexane/EtOAc (1-100% EtOAc) yielded 83 fractions. Fractions 39-54, eluted with the Hexane/EtOAc (3/1) system formed a precipitate that was purified by recrystallization with 5% methanol/EtOAc yielding compound 1 (1 g). <sup>1</sup>H and <sup>13</sup>C NMR spectra were recorded at 400 and 100 MHz using tetramethylsilane as reference (spectrometer Bruker AM-400 Darmstadt, Germany Company). Analytical thin layer chromatography (TLC) plates on silica gel 60 F254 TLC (Merck, Germany) were used for TLC analysis.

### Obtaining and rearing insects

*S. zeamais* strains were collected from infested maize grains from Booster Soumian Entreprise, an agropastoral and quality control company in Chad. Mass rearing was performed with adult insects collected from already-infested maize grains at the Booster Soumian Entreprise rearing site. The insects were reared in the dark on white maize grains in a chamber (temperature 28 ± 2 °C, relative humidity 65 ± 5%).<sup>10</sup>

### Contact toxicity tests

Contact toxicity tests were performed using Ndomo et al.<sup>10</sup> Five concentrations of crude extracts (25, 50, 100, 200, and 400

mg/mL) and compound 1 (5, 12.5, 25, 50, and 100 mg/mL) were prepared. One mL of each dose was added to 40 g of clean and undamaged maize grains. After evaporation of the solvent, each insect was infested with a batch of 20 two-day-old unsexed adult insects. The marketed insecticide pirimiphos-methyl was used as a positive control. The number of dead insects was estimated daily for 3 days. Abbott's (1925) formula was used to calculate the corrected insect mortality rate.<sup>11</sup>

% Mortality = (Number of dead insects / Total number of insects) x 100

Mc (%) = (Mt - Mo) / (100 - Mo)

Mc: Corrected mortality (%); Mt: Mortality in treated batches (%); Mo: Mortality in untreated controls (%)

LC<sub>50</sub> values were determined by Probit analysis.<sup>12</sup>

### Microorganisms

The microorganisms used for the photosensitization tests were FC and FE from an open well for consumption by the population of Dobem, Chad. This water contained 25.10<sup>2</sup> colony-forming units (CFU) FC/100 mL and 15.10<sup>2</sup> CFU FE/100 mL.

### Photosensitized inactivation of bacteria

Five concentrations of 1, 2, 3, 4, and 5 mg/mL of ME and compound 1 were used for photosensitization experiments according to the method of Sunda et al.<sup>13</sup> A batch of treated water samples (with ME and compound 1) and another batch of untreated water samples (blank) were exposed to light (ultraviolet lamp, brand B-100 AP, emitting between 320 and 400 nm, with a maximum at 365 nm). The lamp was placed 15 cm from the water samples for 0, 30, 45, 60, 120, and 180 min. A batch of treated and untreated samples was kept in the dark. For each dataset, the standard error was calculated (mean ± standard deviation).

### Bacteriological analysis

Bacteriological analysis was performed via culture in rapid *Escherichia coli* and Bile Esculin agar media for FC and FE. After the photosensitization experiments, 1 mL of water from the samples was inoculated into the culture medium, and the number of colonies formed after 24 h of incubation at 44.5 °C was counted.<sup>12</sup> The number of germs in CFU was determined in water samples before and after the application of the photosensitizer.

### Molecular docking and dynamics analysis

Molecular Operating Environment (MOE, 2013) software<sup>14</sup> was used to dock a DmAChE protein against compound 1 and two marketed insecticides into the protein's active site. The crystal structure of DmAChE (PID: 6XYU, resolution: 2.51 Å) was downloaded from the Protein Data Bank (<https://www.rcsb.org/>). The water molecules and heteroatoms in the proteins were removed. Compound 1 and two marketed insecticides: emodin (PubChem CID 3220), cypermethrin (PubChem CID 91691), and pirimiphos-methyl (PubChem CID 34526), were collected from the chemical database (<https://pubchem.ncbi.nlm.nih.gov/>), input into the MOE program, and subjected to 3D protonation and energy minimization. The MMFF94X force field

was used to minimize the number of ligands and the protein structure. After docking, the best and top conformations were determined based on the S-scores and the interacting residues.<sup>15</sup> The physicochemical, pharmacokinetic, and ADMET properties of compound 1 were predicted using the SwissADME web tool.<sup>16</sup>

### Statistical analysis

Experiments were performed in triplicate, and mean values were obtained. All statistical analyses were performed using SPSS version 21.0. Data on corrected mortality were subjected to analysis of variance using the Waller-Duncan test.

## RESULTS

### Phytochemical studies

Extraction of *C. nigricans* leaves with HE, AE, and ME gave yields of 28.6 g (2.9%), 36.5 g (3.9%), and 95.3 g (11.2%) of crude extracts respectively.

### Characterization of the isolated compound

Chromatographic fractionation of ME yielded compound 1, whose structure (Figure 1) was established by spectral data and by comparison with literature data.<sup>17</sup>

Compound 1: Orange needles; melting point 260-263 °C. Solubility in dimethyl sulfoxide (DMSO); HRESIMS at m/z 270.3 (calculated for C<sub>15</sub>H<sub>10</sub>O<sub>5</sub>). ESI-MS (70 ev): m/z (rel. Int.) 271.3 (5), 226.5 (10), 224.4 (15), and 222.6 (20). <sup>1</sup>H-NMR (500 MHz, DMSO-*d*<sub>6</sub>) and <sup>13</sup>C-NMR (125 MHz, DMSO-*d*<sub>6</sub>) (Table 1).

### Mortality of *S. zeamais*

A time- and concentration-dependent increase in the mortality rate of adult *S. zeamais* was observed for all extracts and emodin (Table 2). The highest dose (400 mg/mL) caused 95.7, 22.2, and 55.7% mortality in insects on the second day of exposure for HE, AE, and ME, respectively. The insecticidal activity of emodin was found to be higher than that of HE, which was the most active extract tested. Similarly, the activity of emodin (LC<sub>50</sub>, 5 mg/mL) was higher than that of the positive control, Pirimiphos-methyl (LC<sub>50</sub>, 1.25 mg/mL) (Table 3).

### Photosensitizer inactivation by bacteria

Results of the light exposure of water samples treated and untreated with ME and emodin showed complete inactivation of

FC after 3 h of exposure for ME treatment and 2 h for emodin treatment (Table 4). Complete inhibition of EF was observed after 2 h of light exposure in water treated with ME and after 1 h of treatment with emodin for all tested concentrations. No inactivation of FC et FE in the water was observed after 3 h of light exposure in the untreated water samples and all treated water samples exposed to darkness. The photo disinfection efficiency increased as a function of concentration and irradiation time (Figures 2, 3).

### Molecular docking

A molecular docking analysis of emodin was performed to study its binding to DmACHE and to compare it with marketed insecticides used to control pests in crops, fruit trees, and ornamental plants. The crystal structure of DmAChE was used as a model to study insecticidal potential due to the unavailability of DmAChE from *S. zeamais* in the PDB. The binding energy of emodin (-6.38 kcal/mol) was close to that of pirimiphos-methyl (-6.25 kcal/mol) and lower than that of cypermethrin (5.52 kcal/mol) (Table 5). Emodin has two types of interaction bonds (pi-pi) with residues TRP83 and TYR370, similar to those of tacrine-derived insecticides used as ligands.<sup>18</sup> Emodin and pirimiphos-methyl have a common amino acid TRP83 residue for binding to the 6XYU active site (Table 5).

**Table 1. Spectra of compound 1 in DMSO-d<sub>6</sub>**

N°	<sup>1</sup> δ <sub>c</sub> en ppm	DEPT-135	Published <sup>16</sup> δ <sub>c</sub> en ppm	<sup>1</sup> H-multiplicity (J in Hz)
1	166.0	C	166.03	
2	108.3	CH	108.39	1Hd (2.4)
3	161.8	C	161.87	
4	109.2	CH	109.43	1Hd (2.4)
5	120.8	CH	124.59	1Hs
6	148.6	C	148.71	
7	124.5	CH	120.93	1Hs
8	164.8	C	164.90	
9	190.0	C	190.19	
10	181.6	C	181.85	
4a	135.4	C	135.58	
8a	113.6	C	113.85	
9a	109.2	C	109.22	
10a	133.1	C	133.29	
Ar-CH <sub>3</sub>	21.9	CH <sub>3</sub>	21.96	3Hs
1-OH	-			1Hs
3-OH	-			1Hs
8-OH	-			1

DMSO: Dimethyl sulfoxide, DEPT: Distortionless enhancement by polarisation transfer

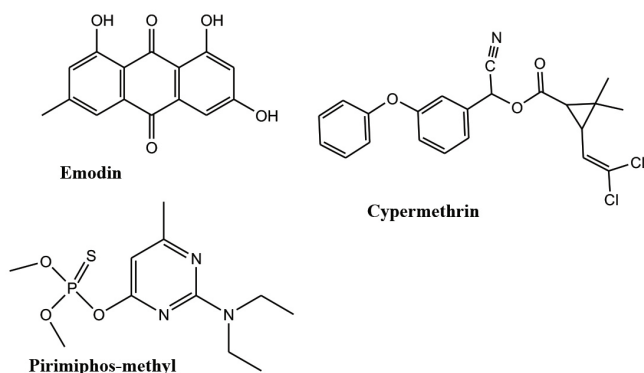


**Figure 1.** Structures of the isolated compounds and drugs

### ADMET analysis

Evaluation of the pharmacokinetic parameters of emodin and other marketed insecticides enabled us to assess insecticide-likeness as well as intestinal absorption and brain permeation, which are key toxicokinetic parameters that determine insecticide toxicity, including neurotoxicity. The insecticide-likeness of emodin was evaluated based on Tice's rule of five, which helps identify herbicides and insecticides.<sup>19</sup> The

pharmacokinetic properties (Table 6) show that all ligands have hydrogen bond donors  $\leq 2$  and hydrogen bond acceptors between 1 and 8. The molecular weights of these ligands ranged from 150 to 500 g/mol, and the ClogP values ranged from 0 to 5. The number of notable bonds for all ligands is  $<12$ . The same is true for the bioavailability radar of the predicted physicochemical and pharmacokinetic properties (Figure 4).

**Table 2. Effects of the extracts and emodin on the mortality of *S. zeamais***

Samples	Concentration (mg/mL)	Mean percentage mortality $\pm$ standard error at 24 to 72 h post-treatment		
		24 h	48 h	72 h
HE	25.0	0.0 $\pm$ 0.0 <sup>a</sup>	0.0 $\pm$ 0.0 <sup>a</sup>	0.0 $\pm$ 0.0 <sup>a</sup>
	50.0	0.0 $\pm$ 0.0 <sup>a</sup>	0.0 $\pm$ 0.0 <sup>a</sup>	0.0 $\pm$ 0.0 <sup>a</sup>
	100.0	0.0 $\pm$ 0.0 <sup>a</sup>	12.6 $\pm$ 0.4 <sup>b</sup>	17.4 $\pm$ 0.5 <sup>b</sup>
	200.0	12.3 $\pm$ 0.3 <sup>b</sup>	32.3 $\pm$ 0.3 <sup>c</sup>	50.3 $\pm$ 0.3 <sup>c</sup>
	400.0	95.7 $\pm$ 0.2 <sup>c</sup>	100.0 $\pm$ 0.0 <sup>d</sup>	100.0 $\pm$ 0.0 <sup>d</sup>
AE	25.0	0.0 $\pm$ 0.0 <sup>a</sup>	0.0 $\pm$ 0.0 <sup>a</sup>	0.0 $\pm$ 0.0 <sup>a</sup>
	50.0	0.0 $\pm$ 0.0 <sup>a</sup>	0.0 $\pm$ 0.0 <sup>a</sup>	0.0 $\pm$ 0.0 <sup>a</sup>
	100.0	0.0 $\pm$ 0.0 <sup>a</sup>	0.0 $\pm$ 0.0 <sup>a</sup>	0.0 $\pm$ 0.0 <sup>a</sup>
	200.0	0.0 $\pm$ 0.0 <sup>a</sup>	0.0 $\pm$ 0.0 <sup>a</sup>	0.0 $\pm$ 0.0 <sup>a</sup>
	400.0	22.2 $\pm$ 0.9 <sup>b</sup>	42.3 $\pm$ 0.2 <sup>b</sup>	58.3 $\pm$ 0.3 <sup>b</sup>
ME	25.0	0.0 $\pm$ 0.0 <sup>a</sup>	0.0 $\pm$ 0.0 <sup>a</sup>	0.0 $\pm$ 0.0 <sup>a</sup>
	50.0	0.0 $\pm$ 0.0 <sup>a</sup>	0.0 $\pm$ 0.0 <sup>a</sup>	0.0 $\pm$ 0.0 <sup>a</sup>
	100.0	0.0 $\pm$ 0.0 <sup>a</sup>	0.0 $\pm$ 0.0 <sup>a</sup>	13.6 $\pm$ 0.4 <sup>b</sup>
	200.0	0.0 $\pm$ 0.0 <sup>a</sup>	17.6 $\pm$ 0.6 <sup>b</sup>	32.6 $\pm$ 0.4 <sup>c</sup>
	400.0	55.7 $\pm$ 0.5 <sup>b</sup>	76.6 $\pm$ 0.3 <sup>c</sup>	100.0 $\pm$ 0.0 <sup>d</sup>
Emodin	5.0	18.0 $\pm$ 0.4 <sup>a</sup>	24.1 $\pm$ 0.6 <sup>a</sup>	58.3 $\pm$ 0.5 <sup>a</sup>
	12.5	24.6 $\pm$ 0.6 <sup>a</sup>	38.6 $\pm$ 0.8 <sup>a</sup>	63.5 $\pm$ 0.9 <sup>a</sup>
	25.0	38.6 $\pm$ 0.4 <sup>b</sup>	52.9 $\pm$ 0.7 <sup>b</sup>	73.0 $\pm$ 0.5 <sup>b</sup>
	50.0	70.7 $\pm$ 0.6 <sup>c</sup>	85.5 $\pm$ 0.4 <sup>c</sup>	100.0 $\pm$ 0.0 <sup>c</sup>
	100.0	100.0 $\pm$ 0.0 <sup>d</sup>	100.0 $\pm$ 0.0 <sup>d</sup>	100.0 $\pm$ 0.0 <sup>c</sup>
Control (untreated)	0.0	0.0 $\pm$ 0.0 <sup>a</sup>	0.0 $\pm$ 0.0 <sup>a</sup>	0.0 $\pm$ 0.0 <sup>a</sup>

Each value is the mean  $\pm$  standard error of three replicates. Means followed by the same letter within a column are not significantly different ( $p < 0.05$ ) from each other using the new Duncan multiple range test. HE: *n*-hexane extract, AE: Acetone extract, ME: Methanol extract

**Table 3. LC<sub>50</sub> values of the extracts and emodin at 72 h**

Extract	LC <sub>50</sub> (mg/mL)	95% CL <sup>a</sup> (mg/mL)	Pearson chi-square	Slope $\pm$ SE	Intercept $\pm$ SE
HE	177.48	(146.59-217.43)	2.23	5.12 $\pm$ 1.00	-11.52 $\pm$ 2.24
AE	374.14	(310.86-513.55)	0.71	6.77 $\pm$ 2.14	-17.43 $\pm$ 5.45
ME	195.08	(160.72-241.84)	5.18	4.88 $\pm$ 0.94	-11.19 $\pm$ 2.15
Emodin	5.00	(1.39-8.50)	5.25	1.55 $\pm$ 0.40	-1.08 $\pm$ 0.49

LC: Lethal concentration, CL: Confidence limit, SE: Standard error, HE: *n*-hexane extract, AE: Acetone extract, ME: Methanol extract, <sup>a</sup>Confidence limit

## DISCUSSION

The high yield of ME (11.2%) compared to HE (2.9%) and AE (3.9%) could be due to the presence of many more polar compounds in the leaves of *C. nigricans*. Terpenoids, flavonoids, anthraquinones, and quinones were detected in all extracts. However, coumarins, glycosides, alkaloids, and tannins were not detected in HE compared with AE and ME. These results are similar to those of previous studies on the plant.<sup>9</sup> Compound 1 was identified as emodin, a known compound, by MS and 1D and 2D NMR analyses, and its structure was confirmed by literature data.<sup>17</sup> The analytical TLCs performed on the three extracts: HE, AE, and ME) showed that only ME had a spot ( $R_f = 0.56$ ) corresponding to emodin. The yield of emodin obtained from ME was 1g (1.04%).

Insect mortality tests showed that HE, AE, and ME were active against *S. zeamais*, the most destructive insect pest of stored maize. Results are similar to those of previous studies on the insecticidal activity of *C. nigricans* extracts on mosquito larvae (*Anopheles gambiaea*) and whiteflies (*Bemisia tabaci*).<sup>20,21</sup> Emodin exhibited very high toxicity against *S. zeamais* compared to all

extracts. The lowest concentration (100 mg/mL) necessary to achieve 100% insect mortality on the first day of exposure using emodin was recorded. HE ( $LC_{50}$  of 177.48 mg/mL) was more active than ME ( $LC_{50} = 195.08$  mg/L) and AE ( $LC_{50} = 374.14$  mg/mL). The efficacy of HE and ME against *S. zeamais* could be due to the presence of terpenoids and phenolic compounds, which are highly toxic to insects.<sup>22</sup> Previous reports have shown that emodin inhibits AChE and Glutathione S-transferase activities in insects, resulting in their death.<sup>23</sup> Previous studies have shown that emodin may be useful as a new natural larviciding agent against mosquitoes.<sup>24</sup> Our study revealed for the first time the insecticidal activity of *C. nigricans* leaf extract and emodin against *S. zeamais*.

The minimum concentration of emodin resulting in complete inactivation was 4 mg/mL for FC and 3 mg/mL for FE for an irradiation time of 30 min (Table 4). Therefore, the FE (Gram+) is more sensitive to ME than FC (Gram-). These results are similar to those of previous studies showing that emodin under visible light was more likely to penetrate the

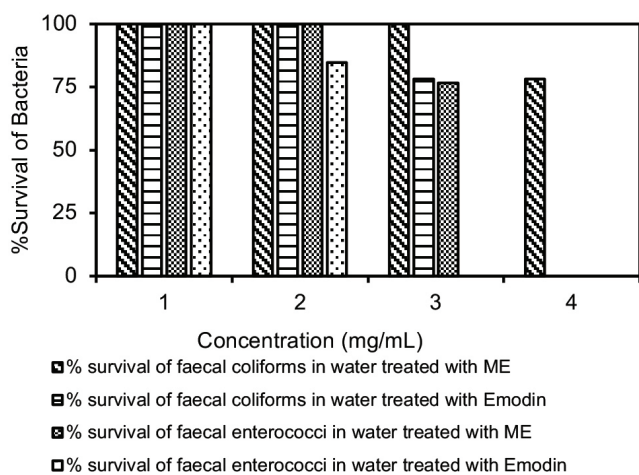


**Figure 2.** Bacterial survival (%) as a function of photosensitizer concentration. Irradiation time: 0.5 h  
ME: Methanol extract

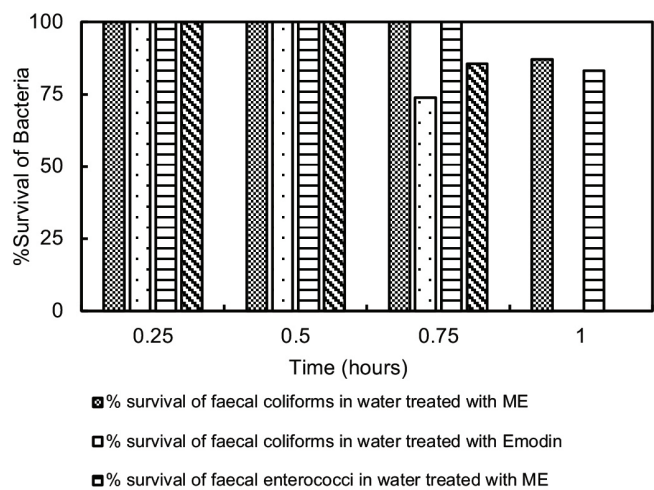


**Figure 3.** Bacterial survival (%) as a function of irradiation time. Sensitizer concentration: 1 mg/mL  
ME: Methanol extract

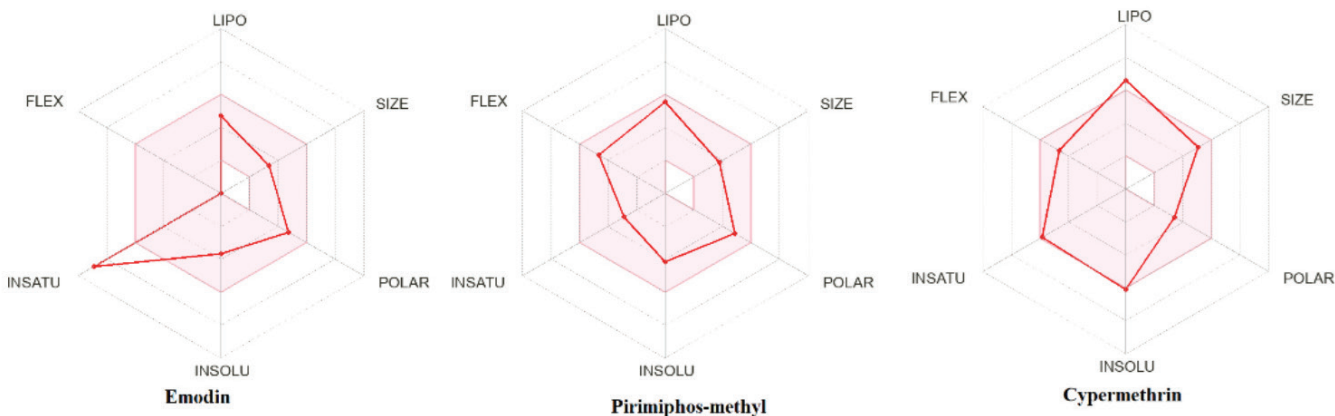


**Figure 4.** Bioavailability radar plots of the drugs and emodin

intracellular environment of Gram-positive bacteria permeable to bioactive compounds, thus enhancing the local killing effect on the bacteria. In contrast to Gram-positive bacteria, Gram-negative bacteria are more resistant to photodynamic effects because of the different surface structures of the bacterial cells.<sup>25,26</sup> The photosensitizing activity of ME may be due to a combination of several factors: photosensitizer, sunlight, and oxygen.<sup>6</sup> This photoreactivity is mainly due to the presence of photoactivatable molecules (anthraquinones and quinones), which are natural dyes capable of storing light energy that is then transferred to stable oxygen to generate singlet oxygen.<sup>9</sup> When emodin is exposed to light, visible light photons are excited and transfer energy to the oxygen molecules as they return to their ground state, generating reactive oxygen species with cytotoxic properties that cause irreversible damage to cell membranes, DNA, and proteins in bacterial cells.<sup>25</sup>

The energy score results showed that the lowest values were obtained with emodin and pirimiphos-methyl, which is an

insecticide used as AChEI. Results indicate that all ligands are non-violent and conform to the rules of Hao et al.,<sup>27</sup> and Clarke et al.<sup>28</sup> The ADMET evaluation showed that emodin and the selected insecticides predicted high intestinal absorption but were not expected to penetrate the brain (Figure 5). All ligands did not inhibit the human ether-a-go-go gene growth enzyme (Table 6). The acute oral toxicity of emodin (2.01 mol/kg) was higher than that of the marketed insecticides pirimiphos-methyl (3.10 mol/kg) and cypermethrin (3.19 mol/kg). The aqueous solubilities of emodin is -3.91, that of pirimiphos-methyl -3.16, and 6.24, respectively. MD results revealed that emodin created a high-affinity pi-pi bond with TRP83 in the DmAChE active site (distance: 3.63 Å) similar to that created by iodobenzyltacrine with TRP83.<sup>18</sup> Additionally, emodin established a pi-pi bond with the same TYR370 at a distance of 3.84 Å (Figure 6). *In silico* molecular docking studies provide more detailed information on the interactions between emodin and DmAChE (6XYU).

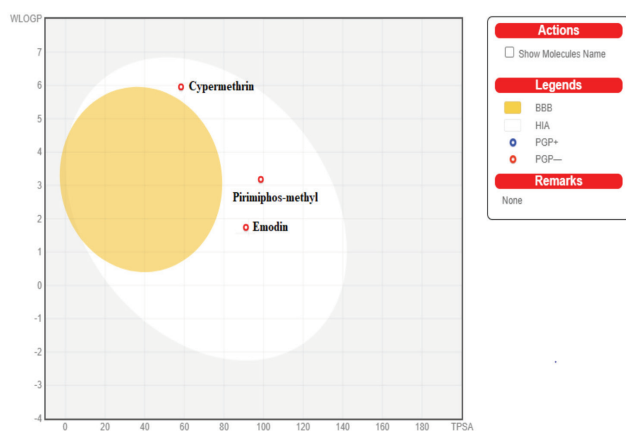


**Figure 5.** Egan BOILED-egg plot prediction model for intestinal and brain permeation. The white and yellow regions are the physicochemical spaces of compounds predicted to exhibit high intestinal absorption and permeation, respectively

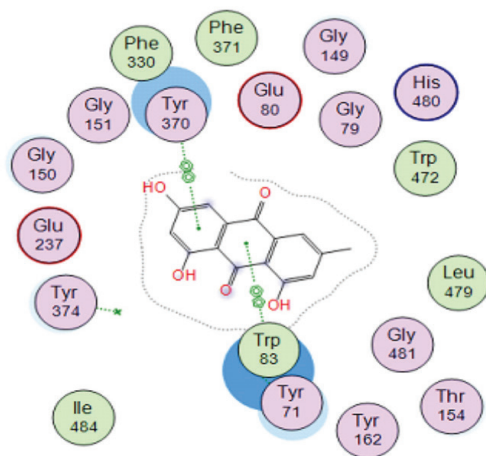


**Figure 6.** 2D visualization of the best pose of Emodin\_6XYU for docking with MOE  
MOE: Molecular Operating Environment

**Table 4.** Inhibitory concentrations of ME and emodin

Microorganisms	Irradiation time (minute)	Methanol concentration (mg/mL)					
		1.0	2.0	3.0	4.0	5.0	
ME	30	-	-	-	-	+	
	45	-	-	-	+	+	
	FC	60	-	-	+	+	+
		120	-	+	+	+	+
FE	180	+	+	+	+	+	
	30	-	-	-	+	+	
	45	-	-	+	+	+	
	60	-	+	+	+	+	
Emodin	120	+	+	+	+	+	
	180	+	+	+	+	+	
	30	-	-	+	+	+	
	45	-	+	+	+	+	
FC	60	+	+	+	+	+	
	120	+	+	+	+	+	
	FE	180	+	+	+	+	+
		30	-	-	+	+	+

-: No inhibition, +: Inhibition, ME: Methanol extract, FC: Fecal coliform, FE: Fecal enterococci

**Table 5. Results of docking score**

Ligand names	Role of receptor residues	Types of interaction bonds	Distance (Å)	Docking score (kcal/mol)
Emodin	TRP 83	Pi-pi	3.63	-6.3836
	TYR 370	Pi-pi	3.84	
Pirimiphos methyl	TYR 71	H-acceptor	2.78	-6.2595
	TYR 370	Pi-H	4.46	
cypermethrin	THR 154	H-donor	3.40	-5.5267
	GLY 155	H-acceptor	3.30	

TRP: Tryptophane, TYR: Tyrosine, THR: Threonine, GLY: Glycine

**Table 6. Druglikeness and pharmacokinetic parameters of the ligands**

	Emodin	Pirimiphos-methyl	Cypermethrin
Molecular weight g/mol	270.24	305.33	416.30
Number of heavy atoms	20	19	28
Number of aromatic heavy atoms	12	6	12
Fraction Cps3	0.07	0.64	0.27
Number of rotatable bonds	0	7	7
Number of H bond acceptors	5	5	4
Number of H bond donors	3	0	0
TPSA (Å <sup>2</sup> )	94.83	98.61	59.32
Log Po/w (XLogP3)	2.72	4.20	6.05
LogP		2.52732	6.17798
Refractivity molar	70.78	79.86	108.87
LogS (SILICOS-IT)	-3.91	-3.16	-6.24
Blood-brain barrier (log BB)	-0.948	0.049	0.147
Human intestinal absorption (%)	87.671	94.716	92.464
Human ether-a-go-go-related gene inhibition	No	No	No
Acute oral toxicity (LD <sub>50</sub> , mol/kg)	2.021	3.108	3.195
Oral rat chronic toxicity (LOAEL, log mg/kg_bw/day )	1.575	0.683	0.832

TPSA: Topological polar surface area, LD<sub>50</sub>: Lethal dose 50, LOAEL: Lowest-observed-adverse-effect level

The labeled insecticides pirimiphos-methyl and cypermethrin give the possibility of using emodin as a promising insecticide. The results clearly show that emodin is promising in terms of binding affinity and pharmacokinetic properties. These results are consistent with in vitro studies on the inhibition of human AChE, which showed the inhibitory activity of emodin at an IC<sub>50</sub> = 15.215.21 ± 3.52 µM.<sup>29</sup>

## CONCLUSION

Extracts of *C. nigricans* as well as emodin isolated from the ME of the leaves were toxic to *S. zeamais* and can be used as natural insecticides to protect stored products. Additionally, ME exhibited bactericidal activity due to the presence of photoactivatable molecules, including emodin, which is a photoreaction site that can lead to the inactivation of FC and

FE present in polluted waters. Molecular docking confirmed the binding positions of emodin in the active center of AChE. Emodin does not passively cross the BBB but is passively absorbed from the HIA, making it a promising natural insecticide for pest control.

### Acknowledgments

The authors thank the Laboratory of Natural and Bioactive Substances, Faculty of Science, University of Tlemcen for their material support.

### Ethics

**Ethics Committee Approval:** Our research project does not require ethical approval, as we have not conducted any animal or human experiments.

**Informed Consent:** Not required.

### Authorship Contributions

Concept: A.F., F.B.H., M.G., G.B.N., J.M., L-N.M., S.G., Design: A.F., F.B.H., M.G., G.B.N., J.M., L-N.M., S.G., Data Collection or Processing: A.F., F.B.H., G.B.N., L-N.M., Analysis or Interpretation: A.F., F.B.H., M.G., G.B.N., J.M., L-N.M., S.G., Literature Search: A.F., M.G., J.M., L-N.M., Writing: A.F., F.B.H., G.B.N., L-N.M.

**Conflict of Interest:** The authors have no conflicts of interest to declare.

**Financial Disclosure:** The authors declared that this study received no financial support.

### REFERENCES

- Nwosu LC, Adedire CO, Ogunwolu EO, Ashamo MO. Toxicological and histopathological effects of *Dennettia tripetala* seed used as grain protectant, food, and medicine. *Food Qual Saf.* 2017;1:211-219.
- Souto AL, Sylvestre M, Tölke ED, Tavares JF, Barbosa-Filho JM, Cebrián-Torrejón G. Plant-derived pesticides as an alternative to pest management and sustainable agricultural production: prospects, applications, and challenges. *Molecules.* 2021;26:4835.
- Georgiev B, Nikolova M, Aneva I, Dzhurmanski A, Sidjimova B, Berkov S. Plant products with acetylcholinesterase inhibitory activity for insect control. *BioRisk.* 2022;17:309-315.
- Johnson TO, Ojo OA, Ikiriko S, Ogunkua J, Akinyemi GO, Rotimi DE, Oche JR, Adegboyega AE. Biochemical evaluation and molecular docking assessment of *Cymbopogon citratus* as a natural source of acetylcholine esterase (AChE)-targeting insecticides. *Biochem Biophys Rep.* 2021;28:101175.
- Sadiki FZ, Boumajane A, Mohammed S, Channaoui S. Chemical profile, antibacterial, antioxidant and insecticidal properties of the essential oil from *Tetraclinis articulata* (Vahl) masters cones. *J Essent Oil Res.* 2022;34:383-393.
- Bartolomeu M, Reis S, Fontes M, Neves MGPMS, Faustino MAF, Almeida A. Photodynamic action against wastewater microorganisms and chemical pollutants: an effective approach with low environmental impact. *Water.* 2017;9:630.
- Abrahamse H, Hamblin MR. New photosensitizers for photodynamic therapy. *Biochem J.* 2016;473:347-364.
- Siewert B, Stuppner H. The photoactivity of natural products-An overlooked potential of phytomedicines? *Phytomedicine.* 2019;60:152985.
- Rashed K. Phytochemical properties and biological activities from *Cassia nigricans*: a review. *Int J Innov Pharm Sci Res.* 2021;9:8-13.
- Ndomo AF, Tapondjou AL, Tendonkeng F, Tchouanguep FM. Evaluation of the insecticidal effect of leaves from *Callistemon viminalis* (Myrtaceae) against a major bean pest: *Acanthoscelides obtectus* (Say) (Coleoptera: Bruchidae). *Tropicicultura.* 2009;27:137-143.
- Abbott WS. A method of computing the effectiveness of an insecticide. *J Econ Entomol.* 1925;18:265-267.
- Finney DJ. Probit analysis (3<sup>rd</sup> ed). Cambridge; Cambridge University Press; 1971.
- Sunda M, Taba KM, Rosillon F, Wathelet B. Contribution to the study of water disinfection by photosensitization with plant extracts. *C R Chim.* 2016;19:827-831.
- Molecular Operating Environment (MOE) 2013.08. Chemical Computing Group Inc., 1010 Sherbooke St. West, Suite #910, Montreal, QC, Canada, H3A 2R7, 2014. Available from: <https://www.chemcomp.com/en/Products.htm>
- Javaid A, Ashfaq UA, Zafar Z, Akmal A, Taj S, Khalid H. Phytochemical analysis and antidiabetic potential of *armoracia rusticana*: pharmacological and computational approach. *Comb Chem High Throughput Screen.* 2021;24:465-471.
- Daina A, Michielin O, Zoete V. SwissADME: a free web tool to evaluate pharmacokinetics, drug-likeness and medicinal chemistry friendliness of small molecules. *Sci Rep.* 2017;7:42717.
- Erdoğan MK, Ağca CA, Geçibesler İH. The antiproliferative potential of isolated emodin and aloe-emodin from *Rheum ribes* on different cancer cell lines. *Biyolojik Çeşitlilik ve Koruma.* 2020;13:160-168.
- Nachon F, Rosenberry TL, Silman I, Sussman JL. A second look at the crystal structures of drosophila melanogaster acetylcholinesterase in complex with tacrine derivatives provides insights concerning catalytic intermediates and the design of specific insecticides. *Molecules.* 2020;25:1198.
- Avram S, Funar-Timofei S, Borota A, Chennamaneni SR, Manchala AK, Muresan S. Quantitative estimation of pesticide-likeness for agrochemical discovery. *J Cheminform.* 2014;6:42.
- Georges K, Jayaprakasam B, Dalavoy SS, Nair MG. Pest-managing activities of plant extracts and anthraquinones from *Cassia nigricans* from Burkina Faso. *Bioresour Technol.* 2008;99:2037-2045.
- Ba NM, Sawadogo F, Dabire-Binso CL, Drabo I, Sanon A. Insecticidal activity of three plant extracts on the cowpea pod sucking bug, *Clavigralla tomentosicollis*, STAL (Hemiptera: Coreidae). *Pak J Biol Sci.* 2009;12:1320-1324.
- Tlak Gajger I, Dar SA. Plant allelochemicals as sources of insecticides. *Insects.* 2021;12:189.
- Nuthakki VK, Sharma A, Kumar A, Bharate SB. Identification of embelin, a 3-undecyl-1,4-benzoquinone from *Embelia ribes* as a multitargeted anti-Alzheimer agent. *Drug Dev Res.* 2019;80:655-665.
- Li P, Wen F, Yan H, Xu Q, Su W. Antimicrobial activity of Emodin in combination with visible light against *Escherichia coli* and *Staphylococcus aureus*: applications for food safety technology. *LWT.* 2023;114750.
- Jiang Q, E F, Tian J, Yang J, Zhang J, Cheng Y. Light-excited antibiotics for potentiating bacterial killing via reactive oxygen species generation. *ACS Appl Mater Interfaces.* 2020;12:16150-16158.
- Penha CB, Bonin E, da Silva AF, Hioka N. Photodynamic inactivation of foodborne and food spoilage bacteria by curcumin. *LWT-Food Sci Technol.* 2017;76:198-202.
- Hao G, Dong Q, Yang G. A comparative study on the constitutive properties of marketed pesticides. *Mol Inform.* 2011;30:614-622.
- Clarke ED. Beyond physical properties-application of Abraham descriptors and LFER analysis in agrochemical research. *Bioorg Med Chem.* 2009;17:4153-4159.
- Augustin N, Nuthakki VK, Abdullaha M, Hassan GP, Gandhi SG, Bharate SB. Discovery of helminthosporin, an anthraquinone isolated from *Rumex abyssinicus* Jacq as a dual cholinesterase inhibitor. *ACS Omega.* 2020;5:1616-1624.



# Effect of Combined Treatment with Levofloxacin and Metformin on Diabetes-the Diabetes Related Behavioral and Biochemical Alterations

✉ Poonam SINGH<sup>1</sup>, ✉ Vaibhav WALIA<sup>2</sup>, ✉ Prabhakar Kumar VERMA<sup>1\*</sup>

<sup>1</sup>Maharshi Dayanand University Faculty of Pharmaceutical Sciences, Haryana, India

<sup>2</sup>Shree Guru Gobind Singh Tricentenary University, SGT College of Pharmacy, Haryana, India

## ABSTRACT

**Objectives:** The current experiment was conducted to investigate the combined effect of levofloxacin (LVX) and metformin treatment on blood glucose levels, malondialdehyde (MDA), nitrite levels, and anxiety in streptozotocin (STZ)+ nicotine adenine dinucleotide (NAD)-induced diabetic rats.

**Materials and Methods:** In this study, Wistar rats have been used. After receiving a single dose of STZ + NAD (45 mg/kg, *i.p.*+ 50 mg/kg, *i.p.*), the rats developed diabetes. Glucose levels in diabetic rats exceeded 200 mg/dL (verified on the third day). Saline was administered to non-diabetic rats (controls). The diabetic rats were administered metformin (50 mg/kg, *p.o.*), LVX (30 mg/kg, *i.p.*), or metformin + LVX for 14 days. Blood samples were obtained after the 14<sup>th</sup> day of therapy, and the rats were given behavioral parameters to determine locomotor activity and anxiety level. Blood plasma samples were separately collected for the determination of nitrite and MDA levels.

**Results:** It was observed that the combined treatment of metformin and LVX significantly increased glucose levels in the blood of diabetic rats compared with diabetic control ( $p < 0.05$ ) and diabetic rats treated with metformin alone ( $p < 0.001$ ) at days 3 and 7. Further, combined treatment of metformin and LVX significantly reduced time spent at the center of the open field test ( $p < 0.001$ ), significantly reduced time spent and entry made in the light chamber of the light-dark test ( $p < 0.001$ ), significantly increased time spent in the open arm and reduced the time spent in the closed arm of the Elevated plus maze ( $p < 0.001$ ) compared with alone metformin-treated diabetic rats. Further, combined treatment with metformin and LVX significantly increased the nitrite level, ( $p < 0.001$ ) but reduced the MDA level in plasma compared with metformin alone-treated diabetic rats ( $p < 0.001$ ).

**Conclusion:** The present study suggests that combined treatments with levofloxacin and metformin may modulate glucose levels and anxiety-related activity.

**Keywords:** Diabetes, glucose, malondialdehyde, anxiety, levofloxacin

## INTRODUCTION

Diabetes is the most common disease worldwide, and there is also a rise in the incidence of morbidity and mortality due to this disorder.<sup>1</sup> Diabetics struggle to regulate their fluctuating blood glucose levels (BGL),<sup>2</sup> which can result in fatalities, permanent strokes, and heart attacks.<sup>3</sup> Fluoroquinolones (FQ) are crucial as secure, broad-spectrum antibiotics in the treatment of diseases that are resistant to other antibiotic classes, but they may also cause problems with BGL,<sup>4</sup> which could be challenging

to regulate, particularly for diabetic patients.<sup>5</sup> Type 2 diabetes (T2D) accounts for almost 85-95% cases of diabetes.<sup>6</sup> It has been reported that a hyperglycemic environment; lower production of interleukins; reduced immunity, and urinary dysmotility in diabetes are accompanied by the emergence of various infections.<sup>7</sup> FQ drugs are commonly used to treat various illnesses and have pharmacokinetic advantages, good penetration, and high oral bioavailability. However, FQs are associated with an increased incidence of tendon rupture, peripheral neuropathy, and FQ-associated aortic aneurysm and

\*Correspondence: vermapk422@rediffmail.com, ORCID-ID: orcid.org/0000-0001-7652-6082

Received: 02.09.2023, Accepted: 12.01.2024



Copyright© 2024 The Author. Published by Galenos Publishing House on behalf of Turkish Pharmacists' Association.  
This is an open access article under the Creative Commons Attribution-NonCommercial-NoDerivatives 4.0 (CC BY-NC-ND) International License.

aortic dissection.<sup>8</sup> Although blood sugar abnormalities caused by FQ are uncommon, they are a serious and potentially fatal consequence that is more likely to occur in the elderly, those suffering from diabetes, and kidney failure individuals.<sup>9</sup> In addition, FQ may have been associated with hypoglycemia by increasing pancreatic insulin.<sup>10</sup> Furthermore, the administration of levofloxacin (LVX) in diabetic rats revealed hypoglycemic effects.<sup>11</sup> Previous studies have suggested that high levels of hypoglycemia in patients with diabetes are associated with the use of levofloxacin.<sup>12</sup> FQs possess insulinotropic activity at clinically relevant concentrations and thus enhance glucose-induced insulin secretion.<sup>13</sup> Furthermore, the risk of a hypoglycemic emergency increases with the combination of levofloxacin with insulin or sulfonylurea.<sup>14</sup> A recent survey revealed hazardous interactions between sulfonylureas and antimicrobials when used together.<sup>15</sup> In the present study, we studied the combined effects of levofloxacin and metformin in rats with diabetes.

## MATERIALS AND METHODS

### Animal

Male, body weight. 150-200 g, Wistar rats were obtained from a disease-free animal house at the Lala Lajpat Rai University of Veterinary and Animal Sciences in Hisar and kept in the Central Animal House at the Maharshi Dayanand University in Haryana under controlled lighting and environmental conditions, with unrestricted access to nutritious food and water. The rats were given time to adjust to the laboratory conditions before the experiment, which was conducted between 9.00 and 17.00. The study protocols were approved by the Institutional Animal Ethics Committee, Maharshi Dayanand University, Haryana (approval number: 1767/RE/S/14/CPCSEA: 31.08.2017, dated: 14.12.2018). Animals were cared for properly according to the requirements of the Committee for the Purpose of Control and Supervision of Experiments on Animals (CPCSEA), Ministry of Environment, Forest and Climate Change, Government of India.

### Drugs and treatments

In the current study, streptozotocin (STZ) (Central Drug House, India); levofloxacin (Cipla Pvt. Ltd., India); metformin (Cipla Pvt. Ltd., India); nicotine adenine dinucleotide (NAD) (Central Drug House, India) were used. All treatments were administered in an unchanged volume (amount) of 5 mL/kg; *i.p.*, STZ solution was freshly prepared at pH 4.5 in 0.1 M citrate buffer.

### Induction of diabetes

Induction of diabetes by a single intraperitoneal dose of STZ + NAD (45 + 50 mg/kg. On days 1, 3, 7, and 14, BGL were monitored using a glucometer. Diabetic rats are characterized by BGL exceeding 200 mg/dL.<sup>16,17</sup>

### Loco-motor activity

Rats were placed alone in the center of an open field, and their behavioral activity was monitored using a camera (for video making) set up at a height of 100 cm. Over a 5-min period, an observer who was blind to the treatments counted the number

of squares crossed no. and time spent at corners and centers by rat.<sup>18,19</sup>

### Assessment of anxiety-related behavior

#### Light-dark test (LDT)

Every rat was placed singly in the exact center of the light chamber, and their behavior was recorded for 5 minutes by a viewer who was blind to treatments using a camera (for making video) held at a height of 100 cm. The time spent and entry in the light and dark chambers were recorded for each rat.<sup>20</sup>

#### Elevated plus maze (EPM)

Every rat was placed individually in a maze with its face on the open arm, and its behavior activity was captured or recorded using a camera (for video recording) held at 100 cm height for 5 minutes by a viewer who was blind to treatment. The time taken to enter and exit the open and closed arms were recorded for each rat.<sup>21</sup>

### Biochemical estimation

#### Plasma separation from blood

On day 14<sup>th</sup>, a blood sample was drawn, centrifuged at 2500 rpm for 10 min, and plasma was separated for biochemical testing.

#### Nitrite assay

An equal quantity of plasma was added with an equal quantity of Griess reagent (0.1% N-1-naphthyl ethylenediamine dihydrochloride; 1% sulfanilamide; and 2.5% *o*-phosphoric acid), a mixture of solution was incubating at the temp. of the room for 10 min, and absorbance at 540 nm was determined.<sup>22</sup>

#### Thiobarbituric acid reacting substances assay

To measure lipid peroxidation, 0.2 mL of blood plasma was added to 0.2 mL of sodium dodecyl sulfate; 1.5 mL of acetic acid; and 1.5 mL of thiobarbituric acid. Using water, the volume was increased to 4 mL. The mixture was further heated for sixty minutes in a 95 °C water bath before cooling to room temperature. 1 mL of H<sub>2</sub>O and 5 mL *n*-butanol/pyridine mixture were added after cooling. The resulting solution was forcefully agitated and centrifuged at 4000 rpm for 10 min. Layers of organic matter were isolated and utilized to calculate absorbance at 532 nm.<sup>23</sup>

### Experimental protocol

The current study used Wistar rats and the number of animals=10 in each group. Induction of diabetes via a single intraperitoneal injection of STZ + NAD (45 mg/kg + 50 mg/kg). Rats with diabetes levels >200 mg/dL were considered diabetic. BGL was measured on days 1, 3, 7, and fourteen. The non-diabetic group was given saline. Metformin (50 mg/kg, *p.o.* and LVX (30 mg/kg) on the first day, metformin administered 30 min before STZ-NAD administration, followed by every day for 14 days. After sixty minutes of treatments, blood was drawn from the tail vein on the 14<sup>th</sup> day, and the rats were then subjected to behavioral tests for levels of anxiety using the OFT, EPM, and LDT tests. Blood plasma was used to determine malondialdehyde (MDA) and nitrite levels.<sup>24</sup>

Animals: Wistar rats were used in the present study.  
n= 10 in each group.

- 1: Rats treated with vehicle (saline)
- 2: STZ + NAD-treated rats (45 mg/kg, *i.p.* + 50 mg/kg, (*i.p.*)
- 3: MET-treated rats (50 mg/kg, *p.o.*)
- 4: LVX-treated rats (30 mg/kg, *i.p.*)
- 6: MET + LVX-treated rats (50 mg/kg, *p.o.* + 30 mg/kg (*i.p.*)

#### Statistical analysis

Data were analyzed by "One-Way analysis of variance" (ANOVA) followed by Tukey's post hoc test, by using Graph-Pad Prism software (version 9.4.0).

Values are expressed as mean  $\pm$  standard error of mean  $p < 0.05$  was considered statistically significant.

## RESULTS

### Effects of different treatments on BGL of rats

"One-Way ANOVA" suggested the effects of different treatments on BGL at (A) day 1 ( $F_{4,45} = 8.909$ ,  $p < 0.001$ ) (B) day 3 ( $F_{4,45} = 21.19$ ,  $p < 0.001$ ), (C) day 7 ( $F_{4,45} = 17.41$ ,  $p < 0.001$ ) and (D) day 14 ( $F_{4,45} = 0.7248$ ,  $p = 0.5797$ ).

Tukey's post hoc test suggested that administration of STZ + NAD significantly increased glucose levels compared with non-diabetes (control) ( $p < 0.001$ ). Metformin and LVX significantly decreased the sugar level of diabetic rats on the 7<sup>th</sup> day ( $p < 0.01$ ,  $p < 0.05$ ). Further, combined treatment with metformin and LVX significantly increased the BGL of diabetic rats on the 3<sup>rd</sup> day compared with diabetic rats ( $p < 0.05$ ), and metformin alone treated diabetic rats ( $p < 0.001$ ) (shown in Figure 1).

### Effects of different treatments on the performance of rats in OFT

"One-Way ANOVA" suggested the effects of different treatments on no. of squares crossed in the OFT ( $F_{4,45} = 5.433$ ;  $p = 0.0012$ ); the time spent in the center of the rats in the OFT ( $F_{4,45} = 3.960$ ;  $p = 0.0077$ ), and time spent in the periphery of rats in the OFT ( $F_{4,45} = 3.766$ ;  $p = 0.0100$ ).

Tukey's post hoc test suggested that metformin and levofloxacin treatment significantly reduced the no. Of square crossed by diabetic rats ( $p < 0.05$ ,  $p < 0.01$ ). Furthermore, levofloxacin treatment significantly increased the time spent at the center ( $p < 0.05$ ) and significantly reduced the time spent at the periphery of the open field ( $p < 0.05$ ) as compared to its respective control group. Further, combined treatment with metformin and levofloxacin significantly decreased the time spent at the center compared with metformin alone-treated diabetic rats ( $p < 0.001$ ) (shown in Figure 2).

### Effects of different treatments on anxiety-related behavior in rats in the LDT and EPM test

"One-Way ANOVA" suggested the significant effects of different treatments on time spent in the light chamber ( $F_{4,45} = 21.33$ ;  $p < 0.0001$ ); time spent in the dark chamber ( $F_{4,45} = 21.94$ ;  $p < 0.001$ ), no. of entry in the light chamber ( $F_{4,45} = 27.54$ ;  $p < 0.001$ )

and no. of entry in the dark chamber in LDT ( $F_{4,45} = 22.47$ ;  $p < 0.001$ ).

Tukey's post hoc test suggested that diabetic rats spend significantly less time in the light chamber of LDT than control rats ( $p < 0.05$ ). Metformin treatment significantly increased the time spent in the light chamber ( $p < 0.001$ ), entries made in the light chamber ( $p < 0.01$ ), and dark chamber of LDT ( $p < 0.05$ ) as compared to its respective control. Levofloxacin alone and in combination with metformin significantly decreased the entry made in the light or dark chamber of LDT as compared to T2D rats ( $p < 0.001$ ;  $p < 0.001$ ;  $p < 0.001$ ;  $p < 0.001$ ). Further, combined treatments of metformin and levofloxacin significantly decreased the time spent in the light chamber and entry into the light and dark chambers compared with metformin alone treated diabetic rats ( $p < 0.001$ ) (shown in Figure 3).

"One-Way ANOVA" suggested a significant effect of different treatments on the time spent by the rats in the open arm ( $F_{4,45} = 43.94$ ;  $p < 0.001$ ), closed arm ( $F_{4,45} = 55.94$ ;  $p < 0.001$ ), and entries made in the open arm ( $F_{4,45} = 55.94$ ;  $p = 0.001$ ) and closed arm of EPM ( $F_{4,45} = 3.443$ ;  $p = 0.0154$ ).

Tukey's post hoc test suggested that T2D rats spend significantly less time on the open arm and significantly more time on the closed arm as compared to the control ( $p < 0.01$ ). Administration of levofloxacin significantly increased the time spent in the open arm and reduced the time spent in the closed arm of EPM compared with diabetic rats ( $p < 0.001$ ,  $p < 0.001$ ). Further, combined treatment with metformin and levofloxacin significantly increased the time spent in the open arm and reduced the time spent in the closed arm of EPM compared with metformin alone treated diabetic rats ( $p < 0.001$ ) (shown in Figure 4).

### Effects of different treatments on plasma nitrite and malondialdehyde levels in rats

"One-Way ANOVA" suggested significant effects of different treatments on nitrite levels in the plasma ( $F_{4,45} = 3.801$ ;  $p = 0.0096$ ) and plasma malondialdehyde levels ( $F_{4,45} = 7.198$ ;  $p < 0.001$ ) of rats.

Tukey's post hoc test suggested that the plasma nitrite level of T2D rats was significantly lower than that of the control ( $p < 0.05$ ). Levofloxacin treatment significantly reduced the MDA level of T2D rats ( $p < 0.05$ ). Furthermore, combined treatment with metformin and levofloxacin significantly increased the nitrite level ( $p < 0.001$ ) but reduced the MDA level compared with metformin alone in diabetic rats ( $p < 0.001$ ) (shown in Figure 5).

## DISCUSSION

Diabetes mellitus is a metabolic disorder characterized by persistent increases in BGL due to abnormalities in either insulin secretion or action or both.<sup>25</sup> STZ is commonly used to induce experimental diabetes in experimental rodents.<sup>26</sup> In the present study, the administration of a single dose of STZ-induced diabetes in rats. The diabetic rats did not show any significant alterations in OFT performance compared with the

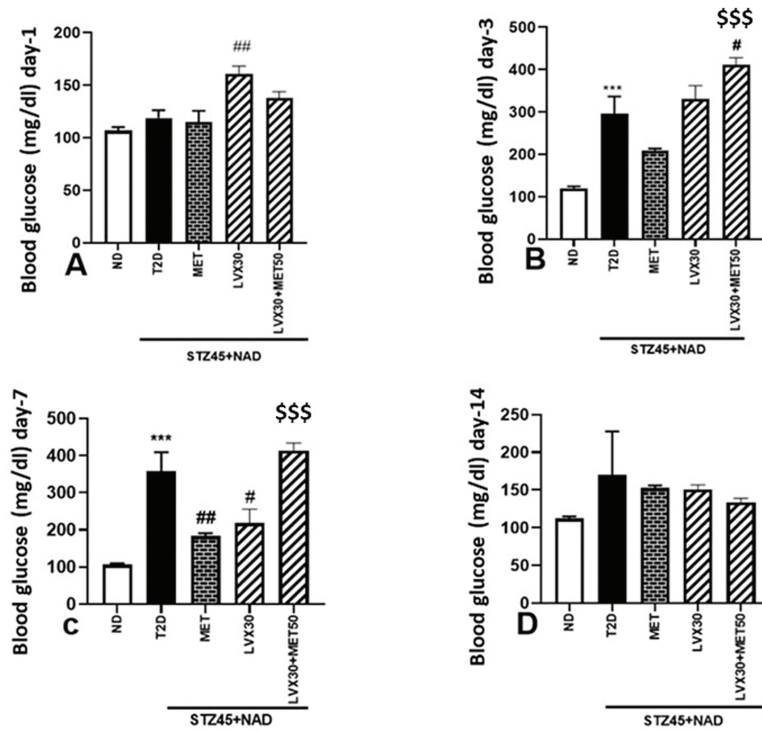


**Figure 1.** Effect of various treatments on the blood glucose level of rats. Values were expressed as mean  $\pm$  SEM,  $n=10$  in each group  $**p < 0.01$ ,  $***p < 0.001$  significant difference from the non-diabetic rat.  $\#p < 0.05$ ,  $##p < 0.01$  significant difference from the diabetic rat.  $$$$p < 0.001$  significant difference from the metformin-treated diabetic rat SEM: Standard error of mean

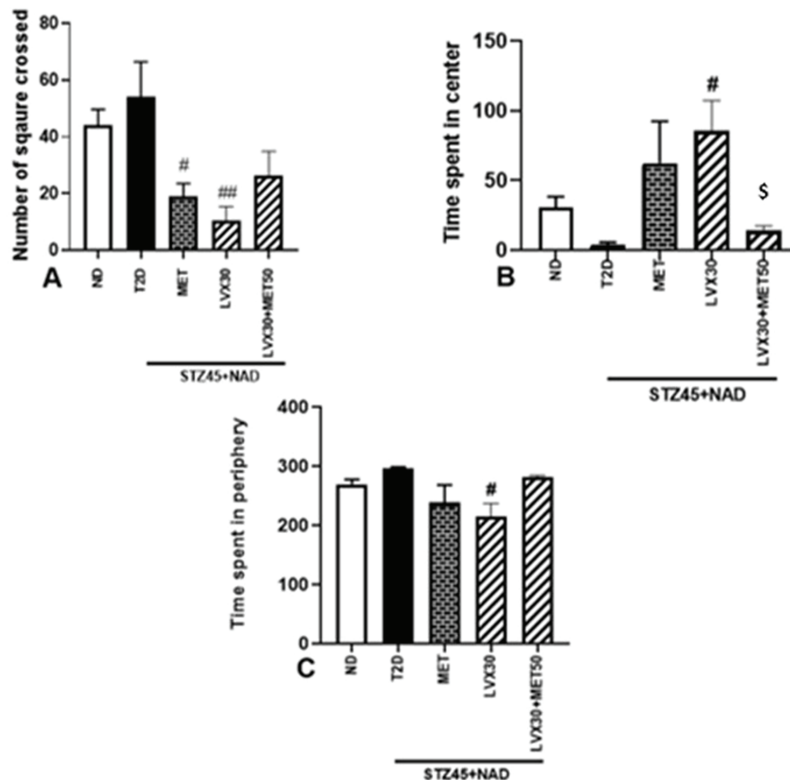


**Figure 2.** Effect of various treatments on the performance of diabetic rats in OFT. Values were expressed as mean  $\pm$  SEM,  $n=10$  in each group.  $\#p < 0.05$ ,  $##p < 0.01$  significant difference from the diabetic rat.  $\$p < 0.05$  significant difference from the metformin-treated diabetic rat SEM: Standard error of mean

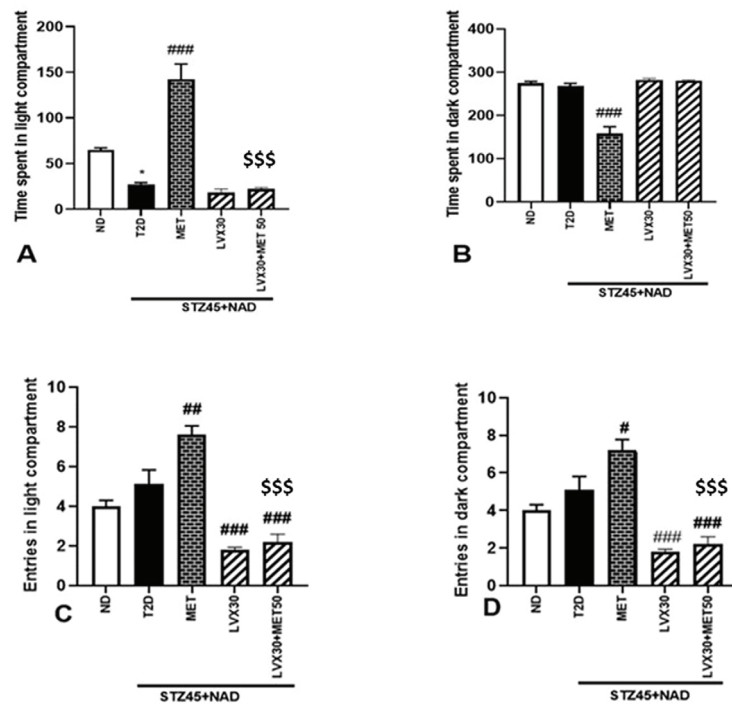


**Figure 3.** Effect of various treatments on the anxiety related behavior of rats in light-dark test. Values were expressed as mean  $\pm$  SEM, n=10 in each group. \* $p < 0.05$  significant difference from the non-diabetic rat. # $p < 0.05$ , ## $p < 0.01$ , ### $p < 0.001$  significant difference from the diabetic rat. \$\$\$ $p < 0.001$  significant difference from the metformin-treated diabetic rat

SEM: Standard error of mean

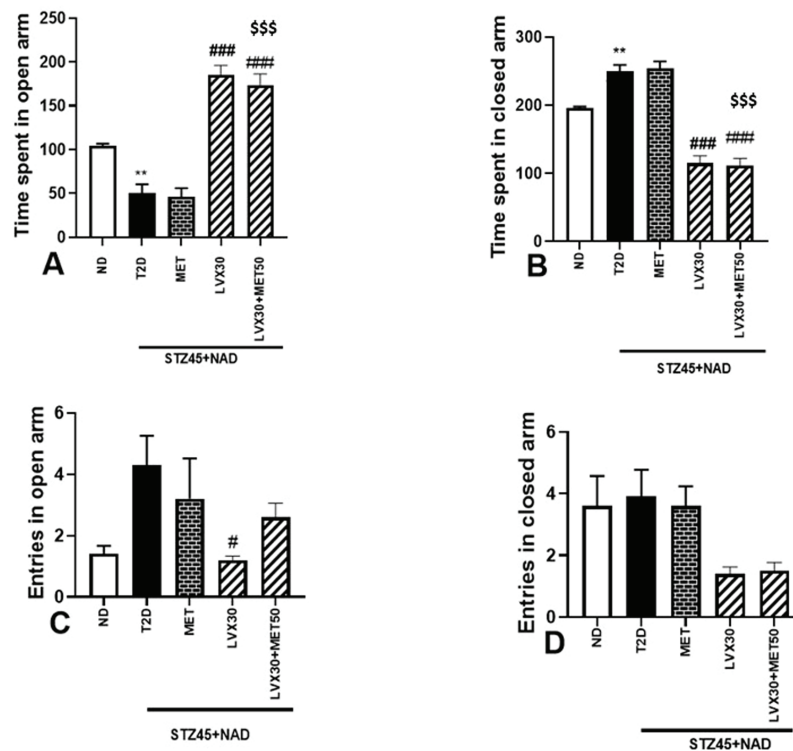


**Figure 4.** Effect of various treatments on the anxiety-related behavior of rats in EPM test. Values were expressed as mean  $\pm$  SEM, n=10 in each group. \*\* $p < 0.01$ , significant difference from the non-diabetic rat. # $p < 0.05$ , ### $p < 0.001$  significant difference from the diabetic rat. \$\$\$ $p < 0.001$  significant difference from the metformin-treated diabetic rat

SEM: Standard error of mean

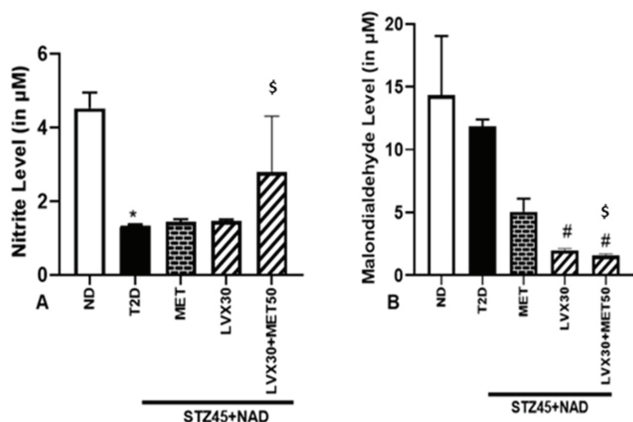


**Figure 5.** Effect of various treatments on the plasma nitrite and MDA level of rats. Values were expressed as mean  $\pm$  SEM, n=10 in each group. \* $p$  <0.05 significant difference from the non-diabetic rat. # $p$  <0.05 significant difference from the diabetic rat. § $p$  <0.05 significant difference from the metformin-treated diabetic rat

SEM: Standard error of mean

control group. However, diabetic rats displayed anxiety-related behavior parameters in the LDT or light and dark box and EPM tests, which were evident by reducing the time spent in the light chambers of LDT and the open arm of EPM. Prior studies have suggested that diabetic rats exhibit anxiety-related behavior.<sup>27</sup> In this current study, diabetes rats showed a significant increase in MDA level in blood plasma and a significant reduction in nitrite level in blood plasma compared with the control group. STZ treatment has been shown to influence glucose, nitric oxide (NO), and MDA levels.<sup>28-30</sup> However, several studies revealed different effects of STZ on nitrite levels; for example, one study suggested a rise in nitrite levels in blood plasma after STZ therapy, and other studies suggested a decrease in nitrite after STZ treatment. STZ therapy has been demonstrated to increase MDA levels in diabetic rats.<sup>31,32</sup>

In the present study, metformin treatment reduced the BGL of diabetic rats. Metformin is mainly used for T2D mellitus treatment. Metformin reduced BGL without increasing insulin secretion but by increasing the effects of insulin. Thus, metformin is referred to as “insulin sensitizer”. Metformin inhibits hepatic glucose synthesis by reducing the rate of gluconeogenesis and glycogenolysis. Metformin also increases peripheral glucose disposal by promoting glucose disposal in skeletal muscle. It normally does not cause low blood sugar levels, which makes it a unique anti-diabetic medicine.<sup>33</sup> In the open field test, metformin treatment significantly decreased the total no. of square crossed and reversed the anxiogenic effect of STZ in LDT only. Previous studies have suggested an anxiolytic-like effect of metformin treatment in diabetic rats.<sup>34,35</sup> It was established in a previous study that metformin treatment displayed a rapid anxiolytic effect without tolerance due to the upregulation of Gamma-aminobutyric acid (GABA)-A receptors.<sup>36</sup> In the present study, metformin treatment did not affect the nitrite and MDA levels of diabetic rats. A previous study suggested that the concentration of NO was significantly

increased following metformin therapy.<sup>37</sup> Reactive oxygen species production is directly related to the increase in lipid peroxidation, and insulin resistance is mainly associated with lipid peroxidation. Furthermore, metformin administration has been shown to decrease lipid peroxidation.<sup>38-40</sup>

In this study, the administration of levofloxacin increased the glucose level at day 1. Furthermore, levofloxacin significantly reduced the glucose level in diabetic rats for 7 days. It has been reported that FQs may cause severe low BGL by increasing insulin secretion.<sup>41</sup> Depending on the dosage, FQs raise insulin levels in the blood via an adenosine triphosphate-sensitive K<sup>+</sup> blockade pathway.<sup>42</sup> Further, the insulin-tropic effect of FQs developed as a result of the stimulatory effects of beta-cell nutrition rather than the initial production of insulin.<sup>43</sup> Srividhya et al.,<sup>44</sup> suggested that the administration of either gatifloxacin or levofloxacin was associated with hyperglycemia rather than hypoglycemia in elderly patients. Levofloxacin administration in diabetic rats significantly increased the time spent at the center and decreased the time spent at the periphery of an open field. Further, in the LDT, levofloxacin treatment significantly reduced the entry made by diabetic rats in the light and dark boxes of LDT, whereas in the EPM test, levofloxacin treatment significantly increased the time spent in the open arm and significantly reduced the time spent in the closed arm EPM. Levofloxacin treatment significantly decreased the entry made by diabetic rats in the open arm of EPM. Thus, levofloxacin treatment exerted anxiolysis in the EPM test. Previous studies reported that the administration of levofloxacin (10-20-40 mg/kg i.p.) did not induce a depression-like response in the forced swim test but displayed an anxiety-like response in the EPM test in rats with no change in locomotor activity.<sup>45,46</sup> It has been reported that quinolones prevent the binding of GABA and thus increase central nervous system stimulation.<sup>47</sup> Furthermore, quinolones activate N-methyl-D-aspartate receptors or adenosine receptors and exert anxiogenic effects.<sup>48-51</sup> Levofloxacin treatment did not affect the plasma nitrite level but significantly decreased the plasma MDA level of diabetic rats.

In the present study, it was observed or research findings that the combined treatment of levofloxacin and metformin increased the glucose level of diabetic rats at 3<sup>rd</sup>-day. Furthermore, the combination of levofloxacin and metformin treatment did not affect the OFT performance of diabetic rats. Combined treatment with levofloxacin and metformin significantly decreased the entry in LDT. Combined treatment with levofloxacin and metformin significantly increased the time spent in the open arms and significantly reduced the time spent in the closed arms of EPM. The combined treatment of levofloxacin and metformin did not affect the nitrite level but significantly reduced the MDA level in diabetic rats. We will determine blood glucose insulin sensitivity and lipid peroxidation to determine possible pathophysiological alterations.

## CONCLUSION

In conclusion, the current study showed that levofloxacin treatment had antihyperglycemic effects in diabetic rats. Thus,

levofloxacin might be repurposed for diabetes alleviation. Furthermore, combined treatment with levofloxacin and metformin may modulate glucose levels and anxiety-related behavior parameters. Thus, caution should be exercised while administering these drugs together.

### Ethics

**Ethics Committee Approval:** The study protocols were approved by the Institutional Animal Ethics Committee, Maharshi Dayanand University, Haryana (approval number: 1767/RE/S/14/CPCSEA: 31.08.2017, dated: 14.12.2018).

**Informed Consent:** Not required.

**Surgical and Medical Practices:** P.S., **Concept:** P.K.V., **Design:** V.W., **Data Collection or Processing:** P.S., **Analysis or Interpretation:** P.K.V., **Literature Search:** P.S., **Writing:** P.S.

**Conflict of Interest:** The authors have no conflicts of interest to declare.

**Financial Disclosure:** The authors declared that this study received no financial support.

## REFERENCES

- World Health Organization, Geneva. Global report on diabetes. 2016.
- Krassak M, Brehm A, Bernroider E, Brehm A. Alterations in postprandial hepatic glycogen metabolism in type 2 diabetes. *Diabetes*. 2004;53:3048-3056.
- Akirov A, Grossman A, Shochat T, Shimon I. Mortality among hospitalized patients with hypoglycemia: insulin related and non-insulin related. *J Clin Endocrinol Metab*. 2017;102:416-424.
- Aspinall SL, Good CB, Jiang R, McCarran M, Dong D, Cunningham FE. Severe dysglycemia with the fluoroquinolones: a class effect? *Clin Infect Dis*. 2009;49:402-408.
- Chou HW, Wang JL, Chang CH, Lee JJ, Shau WY, Lai MS. Risk of severe dysglycemia among diabetic patients receiving levofloxacin, ciprofloxacin, or moxifloxacin in Taiwan. *Clin Infect Dis*. 2013;57:971-980.
- Ishiwata Y, Itoga Y, Yasuhara M. Effect of levofloxacin on serum glucose concentration in rats. *Eur J Pharmacol*. 2006;551:168-174.
- Kelesidis T, Canseco E. Levofloxacin-induced hypoglycemia: a rare but life-threatening side effect of a widely used antibiotic. *Am J Med*. 2009;122:e3-e4.
- Althaqafi A, Ali M, Alzahrani Y, Ming LC, Hussain Z. How safe are fluoroquinolones for diabetic patients? A systematic review of dysglycemic and neuropathic effects of fluoroquinolones. *Ther Clin Risk Manag*. 2021;17:1083-1090.
- Amin KA, Awad EM, Nagy MA. Effects of Panax quinquefolium on streptozotocin-induced diabetic rats: role of C-peptide, nitric oxide and oxidative stress. *Int J Clin Exp Med*. 2011;4:136-147.
- Anderson VR, Perry CM. Levofloxacin: a review of its use as a high-dose, short-course treatment for bacterial infection. *Drugs*. 2008;68:535-565.
- Arokiyaraj S, Balamurugan R, Augustian P. Antihyperglycemic effect of *Hypericum perforatum* ethyl acetate extract on streptozotocin-induced diabetic rats. *Asian Pac J Trop Biomed*. 2011;1:386-390.
- Banday MZ, Sameer AS, Nissar S. Pathophysiology of diabetes: An overview. *Avicenna J Med*. 2020;10:174-188.
- Banik S, Hossain MS, Bhatta R, Akter M. Attenuation of lipid peroxidation and atherogenic factors in diabetic patients treated with gliclazide and metformin. *J Res Med Sci*. 2018;23:77.
- Casqueiro J, Casqueiro J, Alves C. Infections in patients with diabetes mellitus: A review of pathogenesis. *Indian J Endocrinol Metab*. 2012;16(Suppl 1):S27-36.
- Sunmonu TO, Afolayan AJ. Protective effect of *Artemisia afra* Jacq. on isoproterenol-induced myocardial injury in Wistar rats. *Food Chem Toxicol*. 2010;48:1969-1972.
- Dang A, Kamat R, Padmanabh RV. Ciprofloxacin induced nightmares in an adult patient. *Indian J Psychiatry*. 2008;50:305-306.
- Diniz Vilela D, Gomes Peixoto L, Teixeira RR, Freitas-Lima LC, Soares BA, Venâncio DP, Mattos MN, Leite RD, Espindola FS. The role of metformin in controlling oxidative stress in muscle of diabetic rats. *Oxid Med Cell Longev*. 2016;2016:6978625.
- Crawley J, Goodwin FK. Preliminary report of a simple animal behavior model for the anxiolytic effects of benzodiazepines. *Pharmacol Biochem Behav*. 1980;13:167-170.
- Pellow S, Chopin P, File SE, Briley M. Validation of open:closed arm entries in an elevated plus-maze as a measure of anxiety in the rat. *J Neurosci Methods*. 1985;14:149-167.
- Ohkawa H, Ohishi N, Yagi K. Assay for lipid peroxides in animal tissues by thiobarbituric acid reaction. *Anal Biochem*. 1979;95:351-358.
- Berton O, Ramos A, Chaouloff F, Mormde P. Behavioral reactivity to social and nonsocial stimulations: a multivariate analysis of six inbred rat strains. *Behav Genet*. 1997;27:155-166.
- Broadhurst PL. Psychogenetics of emotionality in the rat. *Ann N Y Acad Sci*. 1969;159:806-824.
- Erden BF, Ulak G, Yildiz F, Utkan T, Ozdemirci S, Gacar N. Antidepressant, anxiogenic, and antinociceptive properties of levofloxacin in rats and mice. *Pharmacol Biochem Behav*. 2001;68:435-441.
- Ghasemi A, Jeddi S. Streptozotocin as a tool for induction of rat models of diabetes: a practical guide. *EXCLI J*. 2023;22:274-294.
- Green LC, Wagner DA, Glogowski J, Skipper PL, Wishnok JS, Tannenbaum SR. Analysis of nitrate, nitrite, and [15N]nitrate in biological fluids. *Anal Biochem*. 1982;126:131-138.
- Jelić-Knezović N, Galijašević S, Lovrić M, Vasilj M, Selak S, Mikulić I. Levels of nitric oxide metabolites and myeloperoxidase in subjects with type 2 diabetes mellitus on metformin therapy. *Exp Clin Endocrinol Diabetes*. 2019;127:56-61.
- Fan J, Li D, Chen HS, Lu D, Zhu MY, Wei YQ, Wang H. Metformin produces anxiolytic-like effects in rats by facilitating GABAA receptor trafficking to membrane. *Br J Pharmacol*. 2019;176:297-316.
- Ghaly H, Kriete C, Sahin S, Berger I, Xu J, Salvatore C, Goebel I. The insulinotropic effect of fluoroquinolones. *Biochem Pharmacol*. 2009;77:1040-1052.
- Kandasamy A, Srinath D. Levofloxacin-induced acute anxiety and insomnia. *J Neurosci Rural Pract*. 2012;3:212-214.
- Lewis G, Juhasz A, Smith E. Environmental metabolites of fluoroquinolones: synthesis, fractionation and toxicological assessment of some biologically active metabolites of ciprofloxacin. *Environ Sci Pollut Res Int*. 2011;19:2697-2707.
- Li C, Mercurio NJ, Chapin RW, Gold HS, McCoy C. Fluoroquinolone prescribing for diabetic foot infections following an FDA drug safety

- communication for aortic aneurysm risk. *Antimicrob Agents Chemother.* 2021;65:e0070821.
32. Liao SH, Hu SY, How CK, Chou HL, Wu ZT, Chang YC, Huang HL. Risk for hypoglycemic emergency with levofloxacin use, a population-based propensity score matched nested case-control study. *Plos one.* 2022;4:17:e0266471.
33. Mandell L, Tillotson G. Safety of fluoroquinolones: An update. *Can J Infect Dis.* 2002;13:54-61.
34. Nasri H, Rafieian-Kopaei M. Metformin: Current knowledge. *J Res Med Sci.* 2014;19:658-664.
35. Obafemi TO, Jaiyesimi KF, Olomola AA, Adedokun O, Fatokun CO, Akinola AK, Awosika OE. Combined effect of metformin and gallic acid on inflammation, antioxidant status, endoplasmic reticulum (ER) stress and glucose metabolism in fructose-fed streptozotocin-induced diabetic rats. *Toxicol Rep.* 2021;8:1419-1427.
36. Olayinka ET, Ore A, Ola OS. Influence of different doses of levofloxacin on antioxidant defense systems and markers of renal and hepatic dysfunctions in rats. *Advances in Toxicology.* 2015;1:2015.
37. Pilla SJ, Pitts SI, Maruthur NM. High concurrent use of sulfonyleureas and antimicrobials with drug interactions causing hypoglycemia. *J Patient Saf.* 2022;18:e217-e224.
38. Pouzaud F, Bernard-Beaubois K, Thevenin M, Warnet JM, Hayem G, Rat P. In vitro discrimination of fluoroquinolones toxicity on tendon cells: involvement of oxidative stress. *J Pharmacol Exp Ther.* 2004;308:394-402.
39. Ramachandran A. Know the signs and symptoms of diabetes. *Indian J Med Res.* 2014;140:579-581.
40. Şahin TD, Göçmez SS, Eraldemir FC, Utkan T. Anxiolytic-like and antidepressant-like effects of resveratrol in streptozotocin-induced diabetic rats. *Noro Psikiyatrs Ars.* 2019;56:144-149.
41. Salama A, Asaad GF, Shaheen A. Chrysin ameliorates STZ-induced diabetes in rats: possible impact of modulation of TLR4/NF- $\kappa$ B pathway. *Res Pharm Sci.* 2021;17:1-11.
42. Singh P, Walia V, Verma PK. Hypoglycemia and anxiolysis mediated by levofloxacin treatment in diabetic rats. *J Diabetes Metab Disord.* 2023;22:1197-1209.
43. Saraya A, Yokokura M, Gono T, Seino S. Effects of fluoroquinolones on insulin secretion and beta-cell ATP-sensitive K<sup>+</sup> channels. *Eur J Pharmacol.* 2004;497:111-117.
44. Srividhya S, Ravichandran MK, Anuradha CV. Metformin attenuates blood lipid peroxidation and potentiates antioxidant defense in high fructose-fed rats. *J Biochem Mol Biol Biophys.* 2002;6:379-385.
45. Suryawanshi NP, Bhutey AK, Nagdeote AN, Jadhav AA, Manoorkar GS. Study of lipid peroxide and lipid profile in diabetes mellitus. *Indian J Clin Biochem.* 2006;21:126-130.
46. Tang ZJ, Zou W, Yuan J, Wang L, Chen J, Yu G, Liu X. Antidepressant-like and anxiolytic-like effects of hydrogen sulfide in streptozotocin-induced diabetic rats through inhibition of hippocampal oxidative stress. *Behav Pharmacol.* 2015;26:427-435.
47. Tillotson GS. Quinolones: structure-activity relationships and future predictions. *J Med Microbiol.* 1996;44:320-324.
48. Wang SH, Xie YC, Jiang B, Zhu J, Zhang XH, Chen X, Lu Y. Fluoroquinolone associated myasthenia gravis exacerbation: clinical analysis of 9 cases. *Zhonghua Yi Xue Za Zhi.* 2013;93:1283-1286.
49. Yegin SÇ, Yur F, Çetin S, Güder A. Effect of lycopene on serum nitrite-nitrate levels in diabetic rats. *Indian J Pharm Sci.* 2015;77:357-360.
50. Zemdegs J, Martin H, Pintana H, Bullich S, Manta S, Marques MA, Magalhães CL. Metformin promotes anxiolytic and antidepressant-like responses in insulin-resistant mice by decreasing circulating branched-chain amino acids. *J Neurosci.* 2019;39:5935-5948.
51. Zhang W, Zhao L, Zhang J, Li P, Lv Z. Metformin improves cognitive impairment in diabetic mice induced by a combination of streptozotocin and isoflurane anesthesia. *Bioengineered.* 2021;12:10982-10993.



# Protective Effects of Rosmarinic Acid and Epigallocatechin Gallate Against Doxorubicin-Induced Cytotoxicity and Genotoxicity in CHO-K1 Cells

Sinem HELVACIOĞLU<sup>1</sup>, Muhammed HAMİTOĞLU<sup>2\*</sup>, Ecem YILDIRIM<sup>3</sup>, Şenay VURAL KORKUT<sup>4</sup>, Aylin YABA<sup>3</sup>, Ahmet AYDIN<sup>2</sup>

<sup>1</sup>Istinye University Faculty of Pharmacy, Department of Pharmaceutical Toxicology, İstanbul, Türkiye

<sup>2</sup>Yeditepe University Faculty of Pharmacy, Department of Pharmaceutical Toxicology, İstanbul, Türkiye

<sup>3</sup>Yeditepe University Faculty of Medicine, Department of Histology and Embryology, İstanbul, Türkiye

<sup>4</sup>Yıldız Technical University Faculty of Arts and Science, Department of Molecular Biology and Genetics, İstanbul, Türkiye

## ABSTRACT

**Objectives:** The chemotherapeutic drug doxorubicin (DOX) affects not only cancer cells but also healthy cells in an undesirable manner. The purpose of this study was to investigate the protective roles of rosmarinic acid (RA) and Epigallocatechin gallate (EGCG) alone and in combination against DOX-induced oxidative stress, cytotoxicity, and genotoxicity in healthy cells. In addition, this study evaluated the expression of the mammalian target of rapamycin (mTOR) protein in the Chinese hamster ovary cell line (CHO-K1).

**Materials and Methods:** Cell viability was analyzed using the WST-1 cytotoxicity assay. mTOR expression in the CHO-K1 cell line was determined by western blotting. DNA damage was analyzed using a comet assay. Reactive oxygen species (ROS) levels were determined microscopically using the dihydroethidium staining method.

**Results:** RA demonstrated superior protective effects against DOX-induced cytotoxicity compared to EGCG. Epigallocatechin gallate and RA did not exert genotoxic effects, but DOX increased genotoxicity in CHO-K1. Neither RA nor EGCG exhibited genotoxic effects; however, DOX significantly increased genotoxicity in CHO-K1 cells. Both RA and EGCG markedly reduced DOX-induced genotoxicity, as confirmed by the comet assay. In the DOX-treated group, the expression of mTOR protein was notably suppressed. EGCG further reduced mTOR protein levels when administered alone or in combination with DOX, whereas RA did not exhibit a similar effect. RA decreased intracellular generation of ROS in CHO-K1 cells. However, at high concentrations, Epigallocatechin gallate did not protect against oxidative stress and cell damage due to its prooxidant properties.

**Conclusion:** Epigallocatechin gallate and RA are promising plant-derived active components. Another important point is the evaluation of the safety of herbal products. It should be considered that herbal products may increase the toxicity of chemotherapeutic agents.

**Keywords:** DNA damage, comet assay, Western blot, mTOR, WST-1 assay, oxidative stress

## INTRODUCTION

Doxorubicin (DOX) is a broad-spectrum anthracycline-based chemotherapeutic agent widely used as a first-line treatment for pediatric and adult patients. It is commonly employed for various cancer types, including breast stomach, and prostate cancer, as well as soft tissue and bone sarcomas. However, the cytotoxic and genotoxic effects of DOX are not limited to cancer

cells, as it also damages healthy cells. Consequently, secondary malignant tumors may arise during or after chemotherapy, distinguishing them from primary tumors.<sup>1</sup>

The genotoxicity of DOX, primarily resulting from free radicals generated during its metabolism, plays a central role in secondary tumor development. Phytochemicals effectively protect against free radical-induced oxidative damage. Studies

\*Correspondence: mohammad.saz@yeditepe.edu.tr, ORCID-ID: orcid.org/0000-0002-4545-0756

Received: 28.12.2023, Accepted: 20.02.2024



Copyright© 2024 The Author. Published by Galenos Publishing House on behalf of Turkish Pharmacists' Association. This is an open access article under the Creative Commons Attribution-NonCommercial-NoDerivatives 4.0 (CC BY-NC-ND) International License.

have demonstrated the potential of natural substances to protect against the adverse effects of chemical drugs without compromising their therapeutic efficacy because of their inherent antioxidant capacity.<sup>2</sup> Rosmarinic acid (RA), an ester derived from caffeic acid and 3,4-dihydroxyphenyllactic acid, is found in a variety of Lamiaceae family plants.<sup>3</sup> It demonstrates diverse biological activities, including antioxidative, anti-inflammatory, antimutagenic, antiangiogenic, antiapoptotic, and antifibrotic properties. In particular, it is a natural antioxidant that can compete with unsaturated fatty acids for binding to lipid peroxyl groups to terminate the chain reaction of lipid peroxidation and reduce the rate of lipid peroxidation. The ability of RA to scavenge radiation-induced reactive oxygen species (ROS).<sup>4</sup> Additionally, epigallocatechin gallate (EGCG), another plant-based compound, serves as a phenolic compound prevalent in a wide array of plants, notably green tea. Its capacity to inhibit cellular oxidation and protect cells from free radical-induced damage renders it a subject of research as a potential cancer chemopreventive agent, exhibiting robust antioxidative, anti-inflammatory, and anticarcinogenic attributes.<sup>5</sup> EGCG and RA are both phenolic compounds, whereas RA is a stilbenoid, whereas EGCG is a tannin with a flavan-3-ol structure that has been esterified with gallic acid. Compared with RA, EGCG contains more phenolic -OH groups (Figure 1).

mTOR participates in several signaling pathways involved in the regulation of cell division, apoptosis, and autophagy in the body. Studies have established a connection between the mTOR signaling pathway and various disorders, including cancer.<sup>6</sup> Research suggests that rapamycin can potentially augment the antitumor effects of DOX by downregulating mTOR signaling.<sup>7</sup> For instance, demonstrated that combining mTOR inhibitors with DOX resulted in an increased therapeutic response in patients with leiomyosarcoma compared with DOX alone.<sup>8</sup>

Hence, in this study, the protective effects of RA and EGCG were investigated alone and in combination against DOX-induced genotoxicity and oxidative stress in Chinese hamster ovary cell line (CHO-K1) cells. The effects of these substances on cell proliferation were evaluated according to the mTOR expression level.

## MATERIALS AND METHODS

### Sample preparation

DOX hydrochloride, RA, and (-) -EGCG (Sigma-Aldrich, USA) were dissolved in phosphate-buffered saline (PBS) (Gibco, USA) to prepare a master stock solution and stored in -20 °C

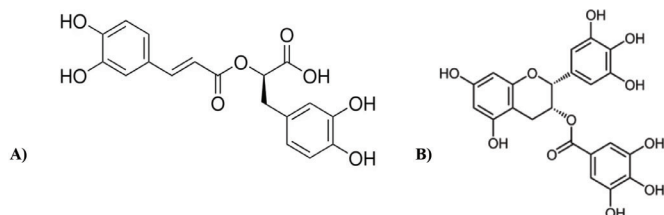


**Figure 1.** A) Chemical structure of RA, B) Chemical structure of EGCG  
RA: Rosmarinic acid, EGCG: Epigallocatechin gallate

before use. Then, the working solutions were prepared freshly at concentrations of 1, 2, and 400  $\mu\text{M}$  in complete Ham's F12 culture medium.

### Cell line and culture conditions

CHO-K1 cells were obtained from the Institute of Pharmacology and Toxicology, Würzburg, Germany. The samples were cultured in Ham's medium F12 supplemented with 10% (*v/v*) fetal bovine serum and 1% (*v/v*) antibiotics (10000 U/mL penicillin and 50 mg/mL streptomycin). Cell cultures were cultured in a humidified incubator at 37 °C with 5%  $\text{CO}_2$ . Twice a week, cells were passaged through a 0.25% trypsin solution. Reagents for cell culture were obtained from (Gibco, Carlsbad, CA).

### WST-1 cytotoxicity assay

Viability was measured using the WST-1 (Roche, Germany) colorimetric assay. Cells were seeded ( $5 \times 10^3$  cells in 100  $\mu\text{L}$  of culture medium) were seeded into 96-well plates and grown for 24 h. The cells were then exposed to 100  $\mu\text{L}$ /well of newly prepared medium containing the tested substance for 24, 48, or 72 h. After the end of the incubation period, the medium was withdrawn, and the cells were washed twice with PBS, then 100  $\mu\text{L}$  of WST-1 were added to each well. The wells were then incubated for 4 h at 37 °C. After 4 h, absorbance was measured at 450 nm using a microplate reader (Thermo Multiskan Ascent, USA) after 4 h. (a-c) / (b-c)  $\times$  100 was used to calculate the percentage of cytotoxicity, where a represents the absorbance of treated cells, b represents the absorbance of control cells, and c represents the absorbance of the blank. The half maximal inhibitory concentration ( $\text{IC}_{50}$ ) was assessed from the dose-response curves.<sup>9</sup>

### Alkaline comet assay

After seeding in a 6-well plate, the cells were treated for 4 h the next day with DOX, RA, EGCG, and their combinations. When the cells were harvested for the comet assay, a cell viability test was conducted. To achieve this, 15  $\mu\text{L}$  of the staining solution containing fluorescein diacetate (Serva Electrophoresis GmbH, Germany) and gel red (Biotium, USA) were combined with 35  $\mu\text{L}$  of the cell suspension. Cell viability was determined by counting 200 cells using an Eclipse 55i microscope fitted with a FITC filter (Nikon GmbH, Japan).<sup>10</sup> Twenty  $\mu\text{L}$  of the cell suspension and 180  $\mu\text{L}$  of pre-warmed low-melting-point agarose (Carl Roth, Germany) were mixed for the comet assay. Forty-five  $\mu\text{L}$  of cell agarose was loaded onto cold microscope slides previously coated with 1.5% high-melting-point agarose. Pre-cooled glass cuvettes containing the lysis solution (2.5 M NaCl, 100 mM  $\text{Na}_2\text{EDTA}$ , and 10 mM Tris adjusted to pH 10) combined with 10% dimethyl sulfoxide and 1% Triton X-100 (Sigma Aldrich; USA) were filled with the cells on the slides. The cells were then allowed to undergo lysis at 4 °C in the dark. Following lysis, the slides were incubated for 20 min at 4 °C in electrophoresis buffer (5 M NaOH and 0.2 M  $\text{Na}_2\text{EDTA}$ , pH 13). Next, electrophoresis was run at 25 V and 0.3 A for 20 min. After electrophoresis, the slides were fixed in frigid methanol for 5 min and neutralized with Tris buffer for 5 min. Following drying, 20  $\mu\text{L}$  of GelRed solution per slide was used to stain the

slides, which were examined using a 200-fold magnification fluorescence microscope (Labophot-2; Nikon GmbH, Germany) and Komet 6-software (Komet version 6, ANDOR™ Technology). The percentage of DNA in the tail region for a total of 100 cells (50 on each slide) was used to express the results.<sup>11</sup>

#### Microscopic analysis of ROS production

Dihydroethidium (DHE), (Merck Biosciences GmbH, Germany) was used to detect the superoxide anion concentration in the mitochondria of living cells. DHE is blue in the cytosol until it is oxidized, at which point it intercalates into the cell's DNA, resulting in a bright fluorescent red. After treatment, fresh medium containing 10  $\mu$ M DHE was added to the cells and incubated for 20 min in the dark at room temperature. Following the incubation period, the cells were washed twice with PBS. ImageJ software was used to measure the gray values of 200 cells in each treatment for quantification.<sup>12</sup>

#### Western blot analysis

Western blotting analysis was carried out as described previously.<sup>13</sup> Briefly, total protein from CHO-K1 cells was extracted using radioimmunoprecipitation lysis buffer (SantaCruz, Texas, USA) with phenylmethylsulfonylfluoride, protease inhibitor cocktail, and sodium orthovanadate. Then, each lane was filled with 20  $\mu$ g of the whole lysate, which was electrophoretically separated using a NuPAGE 4-12% Bis-Tris gel (Invitrogen™, USA) and electroblotted onto a nitrocellulose transfer membrane. (Advansta, San Jose, USA). The membrane was blocked for 1 h to reduce non-specific binding using 5% non-fat dry milk in TBS-T buffer (Tris-buffered saline with 0.1% tween-20). The membrane was placed with appropriate primary antibodies anti-mTOR (1:1000 dilution; Cell Signaling, Germany) overnight at 4 °C. After incubating the primary antibody, the membrane was washed three times with TBS-T for 10 min each time, incubated for 1 h at room temperature with the anti-mouse immunoglobulin G secondary antibody (1:2000 dilution, Cell Signaling), and finally rinsed with TBS-T. mTOR protein expression was detected using a chemiluminescent substrate (Thermo Scientific, USA), immunoblot images were taken, and bands were measured using Image Lab Software (BioRad, Germany). The ratio of each protein's expression level to that of  $\beta$ -Actin from the same samples, which served as the internal control, was used to calculate the expression of each protein.

#### Statistical Analysis

Data were expressed as the mean  $\pm$  standard error of mean and analyzed using GraphPad Prism 9 software (GraphPad, Boston, USA). The differences among the means were analyzed using analysis of variance followed by Dunnett's analysis. The treatment and control groups were compared. It was considered statistically significant when  $p < 0.05$ .

## RESULTS

#### WST-1 cell proliferation assay

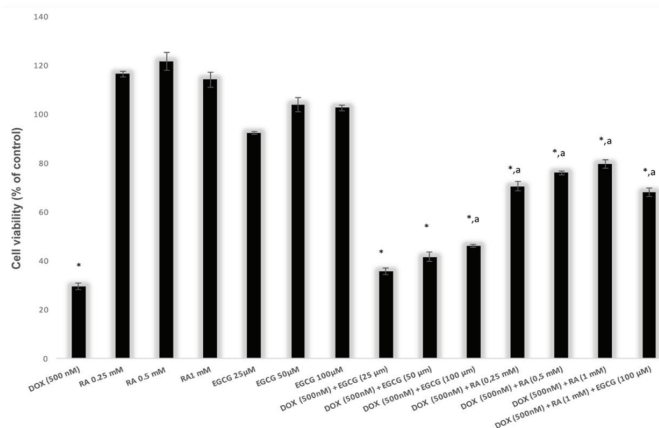
In cells treated with DOX and EGCG, relative cell proliferation consistently decreased in a dose- and time-dependent manner.

Table 1 presents the IC<sub>50</sub> values of cells treated with DOX and EGCG at 24, 48, and 72 h. However, treatment with RA at various concentrations (ranging from 0.0625 mM to 1 mM) for 24, 48, and 72 h did not reduce the viability of CHO-K1 cells. Consequently, the IC<sub>50</sub> value could not be calculated for the concentrations used in this study.

Furthermore, the possible protective effects of RA and EGCG, either alone or in combination, against DOX-induced cytotoxicity in CHO-K1 cells were examined using the WST-1 assay. To evaluate the protective effect, a DOX concentration of 500 nM, as determined by its IC<sub>50</sub> value, was chosen for the investigation. CHO-K1 cells were subjected to different dosages of EGCG, RA, and their combination for 24 h. The results exhibited a statistically significant protective effect of both EGCG and RA against DOX-induced cytotoxicity. Notably, a 1 mM RA concentration demonstrated the most pronounced protective effect against DOX-induced cytotoxicity (Figure 2).

#### Microscopic analysis of ROS formation

The generation of ROS due to DOX administration was quantified by analyzing DHE fluorescence, with an illustrative example provided in Figure 3A. DOX was tested at a concentration of 1000 nM over different time intervals of 0.5, 1, 2, and 4 h (Figure 3B). ROS production increased notably in cells treated with 1000 nM DOX for 0.5 h. This increase was statistically significant after 2-h treatment compared with the control group.



**Figure 2** Cells were treated with different concentrations of DOX, RA, EGCG, and their combinations for 24 h. Viability was quantitated by WST-1 assay. \* $p \leq 0.05$  vs. control group and  $ap \leq 0.05$  vs. DOX 500 nM group.

RA: Rosmarinic acid, EGCG: Epigallocatechin gallate, DOX: Doxorubicin

**Table 1.** IC<sub>50</sub>-values of CHO-K1 cells after 24, 48 and 72 hours of incubation with DOX and EGCG. Values are expressed as mean  $\pm$  SD of triplicate experiments

Compounds	IC <sub>50</sub>		
	24 hours	48 hours	72 hours
DOX (nM)	696.8 $\pm$ 1.4	467.2 $\pm$ 2.2	131 $\pm$ 2.7
EGCG ( $\mu$ M)	305 $\pm$ 0.4	277 $\pm$ 1.5	260.5 $\pm$ 3.3

CHO-K1: Chinese hamster ovary cell line, EGCG: Epigallocatechin gallate, DOX: Doxorubicin, SD: Standard deviation, IC<sub>50</sub>: Half maximal inhibitory concentration

Figure 4 illustrates the protective effect of RA against DOX-induced oxidative stress. Across all tested concentrations, RA alone did not induce a significant increase in ROS generation; instead, it exhibited a noteworthy decrease in ROS levels compared with the DOX group. In contrast, EGCG alone or in

combination with RA did not reduce ROS formation compared with the DOX-treated group (Figure 5). Notably, the application of 100  $\mu\text{M}$  EGCG resulted in an increase in ROS levels in CHO-K1 cells.

#### Alkaline comet assay

According to the cell viability assay results, no significant reduction in cell viability was observed in any of the evaluated groups in the comet test compared with the control group (data not shown). In DOX-treated cells, there was an evident dependence on dose increase in DNA damage (Figure 6A). This effect was statistically significant at concentrations of 1000, 2000, and 4000 nM compared with the negative control group. As illustrated in Figure 6B, RA administration led to a notable and dose-dependent decrease in cells exhibiting DNA damage. In contrast, EGCG alone or in combination with RA did not exert a protective effect against DOX-induced genotoxicity (Figures 6C and D).

#### mTOR protein expression in CHO-K1 cells

The protein levels of mTOR, which plays a significant role in oxidative stress, were assessed using western blotting. mTOR protein expression levels were decreased in the DOX group compared with the control group (Figure 7A). mTOR protein expression level was significantly higher in the group administered RA at a concentration of 1 mM with DOX than in the group administered DOX alone (Figure 7B). A significant decrease in mTOR expression was observed in the EGCG-treated group, alone or in combination with DOX, compared with the negative control group. However, these differences were not significant compared with the DOX-treated group (Figure 7C).

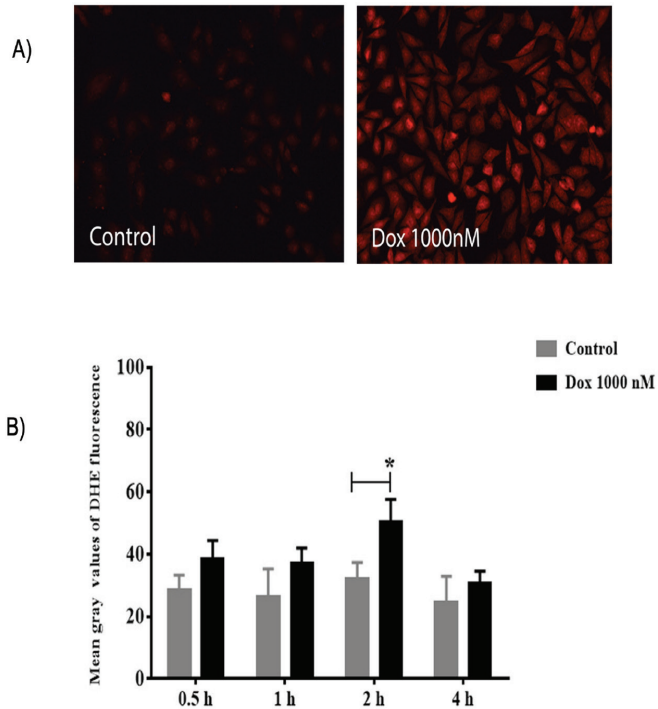


**Figure 3.** ROS formation in CHO-K1 cells treated with 1000 nM Dox for 0.5 to 2 hours using DHE assay. A) DHE fluorescence was quantified using image j software, which measured the mean grey value of 200 cells. B) Results are shown as mean  $\pm$  SEM of three separate tests. \* $p \leq 0.05$  vs. control group

RA: Rosmarinic acid, EGCG: Epigallocatechin gallate, DOX: Doxorubicin, CHO-K1: Chinese hamster ovary cell line, SEM: Standard error of mean

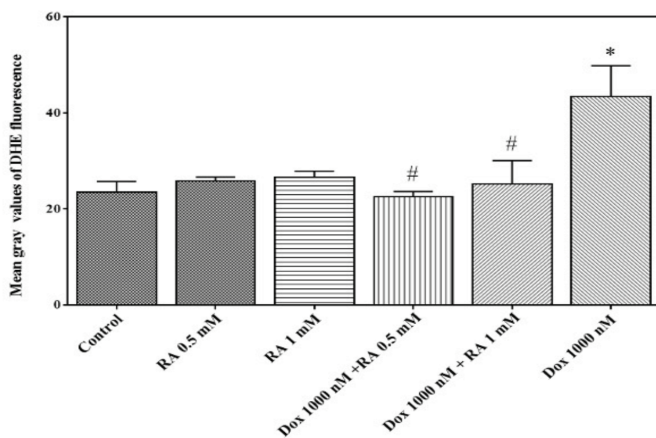


**Figure 4.** ROS production and its inhibition by RA in CHO-K1 cells. DHE fluorescence was quantified using image j software, which measured the mean grey value of 200 cells. Results are shown as mean  $\pm$  SEM of three independent tests. Kruskal-Wallis test was used for analysis, \* $p \leq 0.05$  vs. control and # $p \leq 0.05$  vs. DOX 1000 nM

RA: Rosmarinic acid, DOX: Doxorubicin, CHO-K1: Chinese hamster ovary cell line, SEM: Standard error of mean, DHE: Dihydroethidium

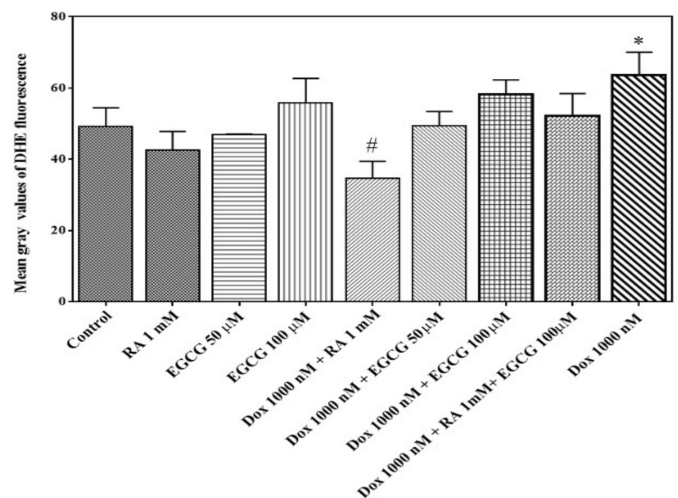


**Figure 5.** Intracellular ROS after treating the cells with RA 1mM and EGCG (50, 100  $\mu\text{M}$ ) for 2 h with and without the addition of DOX. DHE fluorescence was quantified using image j software, which measured the mean grey value of 200 cells. Results are shown as mean  $\pm$  SEM of three independent tests. \* $p \leq 0.05$  vs. control and # $p \leq 0.05$  vs. DOX 1000 nM

ROS: Reactive oxygen species, RA: Rosmarinic acid, EGCG: Epigallocatechin gallate, DOX: Doxorubicin, DHE: Dihydroethidium, SEM: Standard error of mean

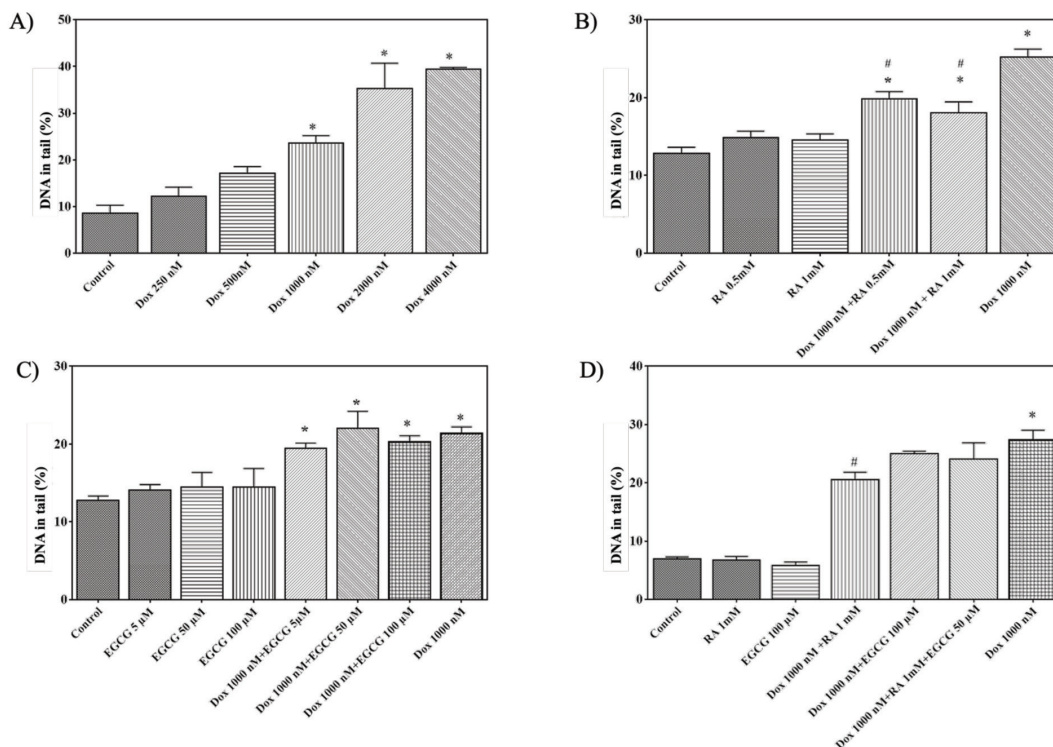


**Figure 6.** Alkaline comet assay results (tail intensity) obtained in CHO-K1 cells after treatment with different compounds. A) Concentration-dependent increase in DNA damage after 4 hours of DOX treatment in CHO-K1 cells.  $*p \leq 0.05$  vs. control group. B) DNA damage induction by DOX treatment with or without RA inhibition in CHO-K1 cells.  $*p \leq 0.05$  vs. control and  $\#p \leq 0.05$  vs. DOX 1000nM. C) DNA damage induction by DOX treatment with or without EGCG in CHO-K1 cells.  $*p \leq 0.05$  vs. control group. D) DNA damage induction by DOX treatment with or without RA and EGCG combination in CHO-K1 cells.  $*p \leq 0.05$  vs. control and  $\#p \leq 0.05$  vs. DOX 1000nM. In the evaluation of comet analysis results, each treatment group had 100 cells evaluated, with the findings represented as a percentage of DNA in the tail. The data are given as mean  $\pm$  SEM of 3 independent experiments

RA: Rosmarinic acid, EGCG: Epigallocatechin gallate, DOX: Doxorubicin, CHO-K1: Chinese hamster ovary cell line, SEM: Standard error of mean

## DISCUSSION

Genotoxicity is one of the most important mechanisms of adverse effects associated with DOX therapy as an anticancer drug. Various pharmacologic treatments, including hematopoietic cytokines, iron-chelating agents, and antioxidants, have been studied to mitigate the adverse effects of DOX.<sup>14,15</sup> In light of these findings, our hypothesis focused on the potential protective effects of phenolic compounds possessing antioxidant properties, such as RA and EGCG, against DOX-induced oxidative stress and DNA damage in healthy cell lines. To investigate this, a fluorescent dye-based detection method was employed to detect superoxide in CHO-K1 cells. Our findings revealed that RA significantly inhibited DOX-induced ROS formation, whereas EGCG did not exhibit protective effects in this context. Furthermore, when RA and EGCG were co-injected, no significant reduction in ROS formation was observed. Additionally, EGCG did not exert a protective effect against DOX-induced genotoxicity in the comet assay in CHO-K1 cells, whereas RA exerted a significant protective effect. Previous studies have revealed the dual nature of EGCG, which possesses both antioxidant and pro-oxidant properties.<sup>16</sup> Catechins, including EGCG, can undergo autooxidation and function as pro-oxidants under specific circumstances.<sup>17</sup> The reported anticancer activity of EGCG, including its ability

to induce apoptosis in cancer cells, is attributed to these prooxidant characteristics.<sup>18</sup> In several studies examining EGCG's ability to prevent various cell lines from oxidative DNA damage, researchers found that at low concentrations, EGCG reduced DNA damage while acting as a pro-oxidant at higher concentrations. Specifically, it was noted that a concentration of 200  $\mu$ M EGCG increased oxidative DNA damage in human lymphocyte DNA induced by  $H_2O_2$ .<sup>19</sup>

In the present study, 0.5 and 1 mM RA exerted protective effects against DOX-induced genotoxicity in CHO-K1 cells. These findings are consistent with earlier reports suggesting that concentrations of 0.28, 0.56, and 1.12 mM RA did not induce genotoxic effects and notably decreased DOX-induced DNA damage in V79 cells over a 3-h period.<sup>20</sup>

These findings suggest that protection against DNA damage induced by DOX is associated with a reduction in ROS levels. Given that the generation of free radicals constitutes one of the primary mechanisms underlying DOX's genotoxicity, a decrease in free radical formation would likely lead to a reduction in DNA damage.<sup>21</sup> In similar studies documented in the literature, it has been demonstrated that compounds possessing antioxidant properties can protect against ROS production and the genotoxic effects induced by DOX. For instance, in one study,

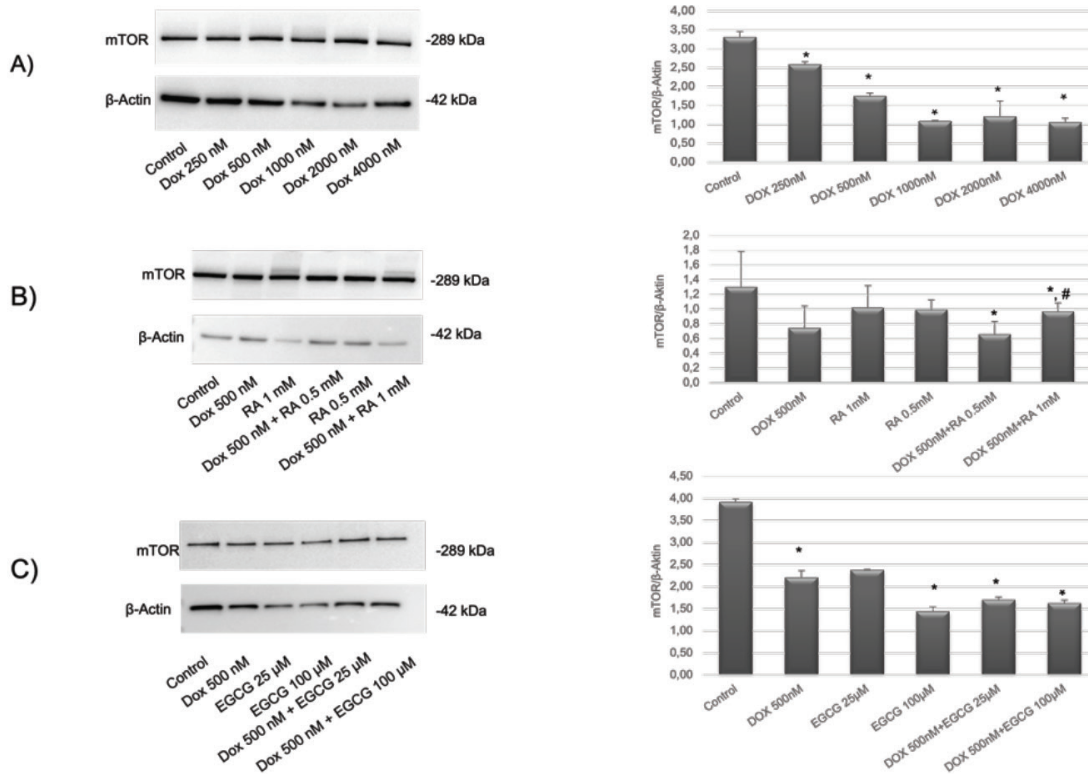


**Figure 7.** Western blot analysis A) mTOR protein level after 24 h of DOX treatment in CHO-K1 cells. \* $p \leq 0.05$  vs. control group. B) DOX treatment with or without RA in CHO-K1 cells. \* $p \leq 0.05$  vs. control and # $p \leq 0.05$  vs. DOX 500nM. C) DOX treatment with or without EGCG in CHO-K1 cells. \* $p \leq 0.05$  vs. control group. Protein levels were normalized to  $\beta$ -actin. Data are given as a mean of ( $n=3$ )  $\pm$  SEM  
mTOR: Mammalian target of rapamycin, RA: Rosmarinic acid, EGCG: Epigallocatechin gallate, DOX: Doxorubicin, CHO-K1: Chinese hamster ovary cell line, SEM: Standard error of mean

thymoquinone mitigated DNA damage and oxidative stress triggered by DOX in human leukocyte cells.<sup>22</sup>

Moreover, the administration of RA and EGCG, either alone or in combination, reduced DOX-induced cytotoxicity in non-cancerous cell lines. The existing literature has demonstrated the protective effects of polyphenolic compounds against DOX-induced cytotoxicity in normal cells. For example, in one study, quercetin significantly mitigated the cytotoxic effect of DOX.<sup>23</sup> Additionally, silymarin, a prominent flavonolignan found in *Silybum marianum* L., has been indicated to lessen DOX-induced cytotoxicity by shielding the cell membrane from damage caused by free radicals.<sup>24</sup> In another study, hydroxytyrosol, the primary phenolic compound found in olive oil, effectively prevented the cytotoxicity of DOX generated in cardiomyocytes by regulating the oxidative response and apoptotic processes mediated by the Bcl-2/Bax ratio.<sup>25</sup>

In response to a variety of extracellular stimuli, including growth hormones, nutrients availability, and stress, mTOR regulates cell proliferation and metabolism. Deregulation of the mTOR signaling system is intimately linked to aging, metabolic disorders, and malignancies.<sup>26,27</sup>

EGCG has exhibited inhibition of mTOR and PI3K expression in numerous cancer cell lines.<sup>28</sup> EGCG is an inhibitor of both

the PI3K and mTOR pathways.<sup>29</sup> Interestingly, mTOR expression levels decreased with increasing DOX doses compared with the control group. The observed reduction in mTOR levels was attributed to oxidative stress and the formation of free radicals triggered by exposure to DOX.

In the literature, it has been stated that oxidative stress regulates mTORC1 and that ROS inhibit the mTOR signaling pathway.<sup>30</sup> It has been stated that moderate stress levels can trigger stress responses by inducing stress-adaptation genes and partially suppressing mTOR activity, whereas high-intensity stress may suppress mTOR.<sup>31</sup> There are various reports that mTOR is inhibited or activated by oxidative stress. This difference is believed to vary depending on the cell line or the type of oxidant.<sup>32</sup> In this study, mTOR levels were decreased in the EGCG-administered groups. This observation may be due to the pro-oxidant properties of EGCG.<sup>33</sup> When RA was co-administered with DOX, it increased the level of mTOR compared with DOX-treated cells. Lou et al.<sup>34</sup> showed that RA stimulates liver regeneration via the mTOR pathway. Strong and persistent mTOR activation caused by RA treatment increased RA-mediated hepatocyte proliferation. However, the interaction between the mTOR pathway and RA has not been extensively characterized.

### Study limitations

Limited number of normal (healthy) cell lines were used in the study. Furthermore, different pathways should be studied to elucidate the protective mechanisms of phenolic compounds. *In vitro* and *in vivo* toxicity assays and clinical trials are required for the use of plant products.

### CONCLUSION

In conclusion, this study showed that RA can protect against DOX-induced toxicity using different methods. However, when the two phenolic compounds were applied in combination, the protective effect against DOX-induced DNA damage was not as much as we expected. Dual behavior was observed for EGCG, which exhibited both pro-oxidant and antioxidative properties. Identification of plants that protect against genotoxic agents and secondary cancers caused by chemotherapy may be used in the near future to reduce the side effects of chemotherapy.

### Ethics

**Ethics Committee Approval:** Not required.

**Informed Consent:** Not required.

### Authorship Contributions

Concept: S.H., M.H., Design: S.H., M.H., A.Y., Data Collection or Processing: S.H., E.Y., Analysis or Interpretation: S.H., Ş.V.K., A.A., Literature Search: S.H., E.Y., S.V.K., A.Y., Writing: S.H., M.H.

**Conflict of Interest:** The authors have no conflicts of interest to declare.

**Financial Disclosure:** The authors declared that this study received no financial support.

### REFERENCES

- Dong C, Chen L. Second malignancies after breast cancer: The impact of adjuvant therapy. *Mol Clin Oncol*. 2014;2:331-336.
- Venkatesh P, Shantala B, Jagetia GC, Rao KK, Baliga MS. Modulation of doxorubicin-induced genotoxicity by Aegle marmelos in mouse bone marrow: a micronucleus study. *Integr Cancer Ther*. 2007;6:42-53.
- Nunes S, Madureira AR, Campos D, Sarmiento B, Gomes AM, Pintado M, Reis F. Therapeutic and nutraceutical potential of rosmarinic acid-cytoprotective properties and pharmacokinetic profile. *Crit Rev Food Sci Nutr*. 2017;57:1799-1806.
- Peters GJ, van der Wilt CL, van Moorsel CJ, Kroep JR, Bergman AM, Ackland SP. Basis for effective combination cancer chemotherapy with antimetabolites. *Pharmacol Ther*. 2000;87:227-253.
- Thorn CF, Oshiro C, Marsh S, Hernandez-Boussard T, McLeod H, Klein TE, Altman RB. Doxorubicin pathways: pharmacodynamics and adverse effects. *Pharmacogenet Genomics*. 2011;21:440-446.
- Zou Z, Tao T, Li H, Zhu X. mTOR signaling pathway and mTOR inhibitors in cancer: progress and challenges. *Cell Biosci*. 2020;10:31.
- Li J, Liu W, Hao H, Wang Q, Xue L. Rapamycin enhanced the antitumor effects of doxorubicin in myelogenous leukemia K562 cells by downregulating the mTOR/p70S6K pathway. *Oncol Lett*. 2019;18:2694-2703.
- Babichev Y, Kabaroff L, Datti A, Uehling D, Isaac M, Al-Awar R, Prakesch M, Sun RX, Boutros PC, Venier R, Dickson BC, Gladly RA. PI3K/AKT/mTOR inhibition in combination with doxorubicin is an effective therapy for leiomyosarcoma. *J Transl Med*. 2016;14:67.
- Ngamwongsatit P, Banada PP, Panbangred W, Bhunia AK. WST-1-based cell cytotoxicity assay as a substitute for MTT-based assay for rapid detection of toxigenic *Bacillus* species using CHO cell line. *J Microbiol Methods*. 2008;73:211-215.
- Bankoglu EE, Schuele C, Stopper H. Cell survival after DNA damage in the comet assay. *Arch Toxicol*. 2021;95:3803-3813.
- Reimann H, Bankoglu EE, Stopper H, Hintzsche H. *In vitro* evaluation of chromosomal damage and DNA strand breaks after treatment with the poppy seed alkaloid thebaine. *Mutat Res Genet Toxicol Environ Mutagen*. 2021;870-871:503393.
- Queisser N, Oteiza PI, Stopper H, Oli RG, Schupp N. Aldosterone induces oxidative stress, oxidative DNA damage and NF-κB-activation in kidney tubule cells. *Mol Carcinog*. 2011;50:123-135.
- Yaba A, Demir N. The mechanism of mTOR (mammalian target of rapamycin) in a mouse model of polycystic ovary syndrome (PCOS). *J Ovarian Res*. 2012;5:38.
- Li L, Takemura G, Li Y, Miyata S, Esaki M, Okada H, Kanamori H, Khai NC, Maruyama R, Ogino A, Minatoguchi S, Fujiwara T, Fujiwara H. Preventive effect of erythropoietin on cardiac dysfunction in doxorubicin-induced cardiomyopathy. *Circulation*. 2006;113:535-543.
- Yeh YC, Lai HC, Ting CT, Lee WL, Wang LC, Wang KY, Lai HC, Liu TJ. Protection by doxycycline against doxorubicin-induced oxidative stress and apoptosis in mouse testes. *Biochem Pharmacol*. 2007;74:969-980.
- Kanadzu M, Lu Y, Morimoto K. Dual function of (-)-epigallocatechin gallate (EGCG) in healthy human lymphocytes. *Cancer Lett*. 2006;241:250-255.
- Valcic S, Burr JA, Timmermann BN, Liebler DC. Antioxidant chemistry of green tea catechins. New oxidation products of (-)-epigallocatechin gallate and (-)-epigallocatechin from their reactions with peroxy radicals. *Chem Res Toxicol*. 2000;13:801-810.
- Furukawa A, Oikawa S, Murata M, Hiraku Y, Kawanishi S. (-)-Epigallocatechin gallate causes oxidative damage to isolated and cellular DNA. *Biochem Pharmacol*. 2003;66:1769-1778.
- Sutherland BA, Rahman RM, Appleton I. Mechanisms of action of green tea catechins, with a focus on ischemia-induced neurodegeneration. *J Nutr Biochem*. 2006;17:291-306.
- Furtado RA, de Araújo FR, Resende FA, Cunha WR, Tavares DC. Protective effect of rosmarinic acid on V79 cells evaluated by the micronucleus and comet assays. *J Appl Toxicol*. 2010;30:254-259.
- Quiles JL, Huertas JR, Battino M, Mataix J, Ramirez-Tortosa MC. Antioxidant nutrients and adriamycin toxicity. *Toxicology*. 2002;180:79-95.
- Al-Shdefat RI, Abd-Elaziz MA, Al-Saikhan FI. Genoprotective and genotoxic effects of thymoquinone on doxorubicin-induced damage in isolated human leukocytes. *Trop J Pharm Res*. 2014;13:2015-2020.
- Ismail IH, Andrin C, McDonald D, Hendzel MJ. BMI1-mediated histone ubiquitylation promotes DNA double-strand break repair. *J Cell Biol*. 2010;191:45-60.
- Wellington K, Jarvis B. Silymarin: a review of its clinical properties in the management of hepatic disorders. *BioDrugs*. 2001;15:465-489.
- Sirangelo I, Liccardo M, Iannuzzi C. Hydroxytyrosol prevents doxorubicin-induced oxidative stress and apoptosis in cardiomyocytes. *Antioxidants (Basel)*. 2022;11:1087.

26. Laplante M, Sabatini DM. mTOR signaling in growth control and disease. *Cell*. 2012;149:274-293.
27. Dazert E, Hall MN. mTOR signaling in disease. *Curr Opin Cell Biol*. 2011;23:744-755.
28. Xiao J, Ho CT, Liong EC, Nanji AA, Leung TM, Lau TY, Fung ML, Tipoe GL. Epigallocatechin gallate attenuates fibrosis, oxidative stress, and inflammation in non-alcoholic fatty liver disease rat model through TGF/SMAD, PI3 K/Akt/FoxO1, and NF-kappa B pathways. *Eur J Nutr*. 2014;53:187-199.
29. Van Aller GS, Carson JD, Tang W, Peng H, Zhao L, Copeland RA, Tummino PJ, Luo L. Epigallocatechin gallate (EGCG), a major component of green tea, is a dual phosphoinositide-3-kinase/mTOR inhibitor. *Biochem Biophys Res Commun*. 2011;406:194-199.
30. Zhao D, Yang J, Yang L. Insights for Oxidative Stress and mTOR signaling in myocardial ischemia/reperfusion injury under diabetes. *Oxid Med Cell Longev*. 2017;2017:6437467.
31. Aramburu J, Ortells MC, Tejedor S, Buxadé M, López-Rodríguez C. Transcriptional regulation of the stress response by mTOR. *Sci Signal*. 2014;7:re2.
32. Oka SI, Hirata T, Suzuki W, Naito D, Chen Y, Chin A, Yaginuma H, Saito T, Nagarajan N, Zhai P, Bhat S, Schesing K, Shao D, Hirabayashi Y, Yodoi J, Sciarretta S, Sadoshima J. Thioredoxin-1 maintains mechanistic target of rapamycin (mTOR) function during oxidative stress in cardiomyocytes. *J Biol Chem*. 2017;292:18988-19000.
33. Azam S, Hadi N, Khan NU, Hadi SM. Prooxidant property of green tea polyphenols epicatechin and epigallocatechin-3-gallate: implications for anticancer properties. *Toxicol In Vitro*. 2004;18:555-561.
34. Lou K, Yang M, Duan E, Zhao J, Yu C, Zhang R, Zhang L, Zhang M, Xiao Z, Hu W, He Z. Rosmarinic acid stimulates liver regeneration through the mTOR pathway. *Phytomedicine*. 2016;23:1574-1582.



# Isolation of the Major Compounds and Determination of Biological Activities in the Underground Parts of *Trachystemon orientalis* D.Don

Ayşe Nur KOZ<sup>1</sup>, Tuğba SUBAŞI<sup>1\*</sup>, Merve BADEM<sup>2</sup>, Şeyda KANBOLAT<sup>2</sup>, Ufuk ÖZGEN<sup>1</sup>, Sıla Özlem ŞENER<sup>3</sup>, Adem DEMİR<sup>4</sup>,  
 İhsan ÇALIŞ<sup>5</sup>

<sup>1</sup>Karadeniz Technical University Faculty of Pharmacy, Department of Pharmacognosy, Trabzon, Türkiye

<sup>2</sup>Karadeniz Technical University Faculty of Pharmacy, Department of Biochemistry, Trabzon, Türkiye

<sup>3</sup>University of Health Sciences, Faculty of Pharmacy, Department of Pharmacognosy, Ankara, Türkiye

<sup>4</sup>Recep Tayyip Erdoğan University Faculty of Science, Department of Chemistry, Rize, Türkiye

<sup>5</sup>Near East University Faculty of Pharmacy, Department of Pharmacognosy, Nicosia, Turkish Republic of Northern Cyprus

## ABSTRACT

**Objectives:** *Trachystemon orientalis* D.Don, an edible plant, is widely used in folk medicine. This study aimed to investigate the antioxidant and lipase inhibitory activities of the extracts and isolated compounds from the underground parts of *T. orientalis* (TOU).

**Materials and Methods:** Isolation studies were carried out on the subextracts (the chloroform, ethyl acetate and remaining aqueous) prepared from the methanol extract of TOU using various chromatographic methods, and the structures of the purified compounds were determined by 1D-NMR, 2D-NMR, and mass spectroscopy techniques. To determine antioxidant activity, ferric-reducing antioxidant power (FRAP) and Cu(II) ion-reducing antioxidant capacity (CUPRAC) assays were performed. Lipase inhibitory activity was determined using an *in vitro* spectrophotometric method.

**Results:** In the isolation studies, rosmarinic acid (1) was isolated from the ethyl acetate subextract and danshensu (2), globoidnan B (3), and rabdosiin (4) were isolated from the remaining aqueous subextract. These compounds were isolated from TOU for the first time. The ethyl acetate subextract had higher activity than the other extracts in the FRAP and CUPRAC assays ( $794.818 \pm 8.999$ ,  $583.06 \pm 5.882$   $\mu$ M Trolox equivalents (TE)/g), respectively] and rosmarinic acid exhibited the highest activity [ $1260.273 \pm 4.499$ ,  $608.250 \pm 1.195$   $\mu$ M TE/g, respectively). Lipase enzyme inhibitory studies showed that the remaining aqueous and ethyl acetate subextracts had significant inhibitory activity [half maximal inhibitory concentration ( $IC_{50}$ ) =  $38.131 \pm 0.720$ ,  $38.841 \pm 1.359$   $\mu$ g/mL respectively]. All isolated compounds inhibited lipase, and rosmarinic acid was the most effective ( $IC_{50}$  =  $49.421 \pm 1.448$   $\mu$ g/mL).

**Conclusion:** According to the results of this study, *T. orientalis* and its isolated compounds may be a promising natural therapeutic agent for the treatment of obesity *via* its high antioxidant capacity and lipase inhibitory activity.

**Keywords:** Antioxidant, isolation, lipase inhibition, obesity, *Trachystemon orientalis*

## INTRODUCTION

Overweight and obesity are defined as excessive fat accumulation caused by an imbalance in lipid metabolism.<sup>1</sup> It has been reported that there were two billion overweight adults

in 2016, and 650 million were affected by obesity.<sup>2</sup> Obesity and hyperlipidemia are associated with oxidative stress and are risk factors for many metabolic disorders, such as atherosclerosis, diabetes, hypertension, and cardiovascular diseases.<sup>3,4</sup> Inhibition of lipid digestion and absorption in the gastrointestinal

\*Correspondence: tugbasubas08@gmail.com, ORCID-ID: orcid.org/0000-0002-0956-6567

Received: 26.10.2023, Accepted: 26.02.2024

\*This study was presented at the 9<sup>th</sup> International Mediterranean Symposium on Medicinal and Aromatic Plants (MESMAP-9). Ankara, Türkiye, 3-5 May 2023, pp. 60.



tract is an important option for the treatment or prevention of obesity. In this context, inhibition of the pancreatic lipase enzyme, the primary lipase that breaks down triacylglycerols into monoglycerides and fatty acids, is targeted.<sup>4,5</sup> Orlistat, the most widely used drug for treating obesity approved by the European Medicines Agency and Food and Drug Administration, inhibits pancreatic lipase.<sup>6</sup> However, due to side effects such as steatorrhea, diarrhea, abdominal pain, acute kidney injury, and increased risk of osteoporosis, the search for more effective compounds with fewer side-effect profiles continues.<sup>5,6</sup> Natural products are under investigation for the discovery of safer and more effective pancreatic lipase inhibitors.<sup>7</sup>

*Trachystemon orientalis* D. Don is the only species of *Trachystemon* D. Don genus of the Boraginaceae family.<sup>8</sup> It is a perennial and herbaceous plant with a black color and tuberous rhizome, reaching 30-40 cm in height.<sup>9</sup> The plant, known as "Hodan, Ispit, Kalirin, Kaldırayak, Tamara and Acı Hodan" in Türkiye, grows in the Black Sea Region, Caucasus, and Bulgaria.<sup>10</sup> The aerial parts of the plant are used as vegetables, and pickles are made from the petioles and roots.<sup>11,12</sup> In addition to its use as food, it is also used as a folk medicine in Türkiye.

It is used as a diuretic, antipyretic, sudorific, and antidepressant and for sore throats.<sup>13</sup> Its roots are used for anti-inflammatory, wound healing, and rheumatism, breast cancer, stomach pain, and swelling.<sup>14-16</sup> It has been shown to contain flavonoids, phenolic compounds, anthocyanins, tannins, essential oils, mucilage, saponin, resin, and fatty acids.<sup>10,17,18</sup> Studies have shown that it has antioxidant, allelopathic, herbicidal, antiviral, antifungal, antimutagenic, antidiabetic, and butyrylcholinesterase inhibitory activities.<sup>10,12,14,18-20</sup> In an *in vitro* study, it has been shown that rhizomes have anticancer effects on endometrial cancer cells.<sup>21</sup>

To the best of our knowledge, no study has been conducted on the isolation of major compounds from the underground parts (rhizomes and roots) of (TOU). This study aimed to investigate the antioxidant and lipase inhibitory activities of the extracts and isolated compounds from the underground parts of *T. orientalis* (TOU).

## MATERIALS AND METHODS

### *Chemicals and instrumentation*

Ethyl acetate and chloroform were purchased from Sigma-Aldrich (St. Louis, USA), methanol from Riedel-de Haën (France), and *n*-hexane from Isolab (Eschau, Germany). For antioxidant activity studies, 6-hydroxy-2,5,7,8-tetramethylchroman-2-carboxylic acid (Trolox) and 2,4,6-tripyridyl-s-triazine (TPTZ) were obtained from Fluka Chemie GmbH (Buchs, Switzerland); for lipase inhibition studies, *p*-nitrophenyl butyrate (*p*-NPB) and Tris-HCl were obtained from Sigma-Aldrich. For column chromatography (CC), Sephadex LH-20 (Sigma-Aldrich) and silica gel 60 [normal phase silica gel (Merck 9385, Merck 7734), and reverse-phase silica gel (Merck 9303)] were used. For thin layer chromatography (TLC), silica gel 60 F<sub>254</sub> 20 x 20 cm (Merck 5554) was used. TLC points were determined by sputtering 1% Vanillin/H<sub>2</sub>SO<sub>4</sub> using an ultraviolet lamp (Mineralight UVGL-58).

Nuclear magnetic resonance (NMR) spectra were obtained using a Bruker Ascend™ 400 MHz/54 mm ultra-low height. Mass spectroscopy (MS) analyses were performed using Thermo TSQ Quantum Access Max. In addition, a shaker (Heidolph Unimax 1010) was used for extraction, and a rotary evaporator (Heidolph Hei-VAP Precision) was used for solvent evaporation. All absorbance measurements were carried out using a BMG Labtech Spectrostar Nano spectrophotometer. A Starter 3000 OHARUS pH meter was used for all pH measurements.

### *Plant material*

*T. orientalis* was collected from Sümer Village (Fındıklı district, May 2019, Rize province, Türkiye) and authenticated by Prof. Dr. Ufuk ÖZGEN, one of the authors. The voucher specimen (KATO 15486) was deposited at the KATO Herbarium (in the Faculty of Forestry, Karadeniz Technical University), Trabzon, Türkiye.

### *Extraction and isolation*

Air-dried plant materials were cleaned and powdered, and then the powder (250 g) was extracted with methanol (two times, 1.5 L) at room temperature (25 °C). The combined and filtered extracts were evaporated at 40 °C. The methanolic extract (TOU-M, 6.3 g) was suspended in a mixture of water: methanol (9:1). The obtained suspension was partitioned with chloroform, and after evaporation, a chloroform subextract (TOU-C, 0.6 g) was acquired. To obtain an ethyl acetate subextract (TOU-E, 0.25 g), a water: methanol mixture (9:1) was partitioned with ethyl acetate, and the solvent was evaporated. After the remaining aqueous phase had evaporated to dryness, the remaining aqueous subextract (TOU-A, 5.5 g) was obtained.

TOU-E (0.2 g) was chromatographed over Sephadex LH-20 CC with MeOH as the eluent to yield 21 fractions. Fractions 13-17 were combined, and compound 1 (150 mg) was obtained.

TOU-A (5.3 g) was subjected to vacuum liquid chromatography followed by elution with water: methanol mixture gradiently (100:0 → 0:100). The 111 fractions (A) were gathered. After fractions (A) 5-6 (38 mg) were combined, they were applied to Sephadex LH-20 CC using MeOH to provide 30 fractions and fractions 22-26 gave compound 2 (13.3 mg). Fractions (A) 10-12 (25.2 mg) were combined and chromatographed over Sephadex LH-20 CC using MeOH as the eluent to yield 13 fractions, and fractions 5-8 were combined to yield compound 3 (10 mg). Fraction (A) 41 gave compound 4 (15 mg).

Each collected fraction was subjected to TLC to determine the compounds (mobile phase: EtOAc: MeOH: H<sub>2</sub>O 7:2:1, reagent: 1% Vanillin: H<sub>2</sub>SO<sub>4</sub>). The fractions were combined according to their *R<sub>f</sub>* values on a TLC plate and used for further analysis.

### *Structure identification*

The structure of the isolated compounds was identified with the help of 1D-NMR, 2D-NMR, and MS.

### *Ferric reducing antioxidant power (FRAP) assay*

The basis of the FRAP assay was to determine the ability of the samples to reduce Fe<sup>+3</sup> to Fe<sup>+2</sup>.<sup>22</sup> Ethanol solutions of five different concentrations (62.5-1000 µM) of Trolox were used

for calibration. Samples of TOU-M and subextracts (10 mg/mL) were prepared. Samples' solvents were used as blanks. FRAP reagent (1.5 mL) was added to the sample solutions (50  $\mu$ L). The tubes were incubated (at 25  $^{\circ}$ C, 20 min) after cortixin. Next, the absorbances of the samples were determined at 595 nm with the help of a spectrophotometer. The FRAP values of the samples were compared with those of Trolox (standard) and expressed as  $\mu$ M Trolox equivalent antioxidant capacity (TEAC) per g sample.

#### *Cu(II) ion reducing antioxidant capacity (CUPRAC) assay*

The principle of the CUPRAC assay is to measure the copper reduction capacity of the samples.<sup>23</sup> Methanol solutions with five different concentrations (62.5-1000  $\mu$ M) of Trolox were used for calibration. Samples of TOU-M and subextracts (10 mg/mL) were prepared. Samples' own solvents were used as blanks. Five hundred  $\mu$ L of each sample solution was taken 1000  $\mu$ L of  $\text{NH}_4\text{CH}_3\text{COO}^-$  and 1000  $\mu$ L of  $\text{CuCl}_2 \cdot 2\text{H}_2\text{O}$  was added. Then, 1000  $\mu$ L of Nc reagent was pipetted into the test solutions, while 1000  $\mu$ L of reagent solvent (methanol) for the sample blank was pipetted at 20 sec intervals. After cortixin the tubes, they were retained in the dark (at 25  $^{\circ}$ C, 30 min). The absorbance was then measured at 450 nm using a spectrophotometer. The activity of the samples was expressed as TEAC ( $\mu$ M) by comparing it with Trolox (standard).

#### *Lipase inhibition*

Lipase inhibition was evaluated using the method<sup>24</sup> and the substrate was *p*-nitrophenyl butyrate (*p*-NPB). The prepared extracts and orlistat (standard) were diluted with a buffer solution (0.1M Tris-HCl buffer, pH 8.0) at different concentrations (12.5-400 and 6.25-100  $\mu$ g/mL, respectively). The experimental microplate wells were prepared as follows: enzyme solution (ES) (90  $\mu$ L, 200 units/mL), substrate solution (SS) (5  $\mu$ L, 10 mM), buffer solution (BS) (5  $\mu$ L); B: ES (90  $\mu$ L, 200 units/mL), BS (10  $\mu$ L); C: ES (90  $\mu$ L, 200 units/mL), sample solution (5  $\mu$ L), SS (5  $\mu$ L, 10 mM); D: ES (90  $\mu$ L, 200 units/mL), sample solution (5  $\mu$ L), BS (5  $\mu$ L). Microplates were incubated for 15 min at 37  $^{\circ}$ C before and after substrate addition. Microplates were read at 405 nm using a microplate reader. The equation given below was used to determine the percentage of pancreatic lipase enzyme inhibition. All samples were run in 3 parallels.

$$\% \text{Pancreatic Lipase Inhibition} = \frac{(A - B) - (C - D)}{(A - B)} \times 100$$

The half maximal inhibitory concentration ( $\text{IC}_{50}$ ) values for enzymatic inhibition of the samples were determined from the equation of the graph obtained using the percentage enzyme inhibition values and the logarithm of the corresponding concentration.

#### *Statistical analysis*

In the activity studies, each sample was studied in triplicate. The results were obtained from graphs plotted using Microsoft Excel. Experimental results were presented as means  $\pm$  standard deviation (SD).

## RESULTS

### *Isolation of major compounds*

According to the results of the isolation studies, four known compounds (two phenolic acids, and two arylnaphtalene lignans) from TOU were purified. Rosmarinic acid (1) (phenolic acid) from TOU-E, danshensu (2) (phenolic acid), globoidnan B (3), and rabdosiin (4) (arylnaphtalene lignans) from TOU-A were isolated. The structures of the purified compounds are presented in Figure 1.

**Compound 1:** ESI-MS (*m/e*) 361.67 [M+H]<sup>+</sup>, ( $\text{C}_{18}\text{H}_{16}\text{O}_8$ ); Proton Nuclear Magnetic Resonance (<sup>1</sup>H-NMR) (400 MHz,  $\text{CD}_3\text{OD}$ ):  $\delta$  7.57 (*d*,  $J=15.9$  Hz, 1H, H-7), 7.07 (*d*,  $J=2.1$  Hz, 1H, H-2), 6.97 (*dd*,  $J=8.2$  Hz,  $J=2.1$  Hz, 1H, H-6), 6.80 (*d*,  $J=8.2$  Hz, 1H, H-5), 6.78 (*d*,  $J=2.0$  Hz, 1H, H-2'), 6.72 (*d*,  $J=8.0$  Hz, 1H, H-5'), 6.64 (*dd*,  $J=8.1$  Hz,  $J=2.1$  Hz, 1H, H-6'), 6.29 (*d*,  $J=15.9$  Hz, 1H, H-8), 5.21 (*dd*,  $J=8.3$  Hz,  $J=4.3$  Hz, 1H, H-8'), 3.12 (*dd*,  $J=14.3$  Hz,  $J=4.4$  Hz, 1H, H-7'a), 3.03 (*dd*,  $J=14.3$  Hz,  $J=8.3$  Hz, 1H, H-7'b); Carbon Nuclear Magnetic Resonance (<sup>13</sup>C-NMR) (100 MHz,  $\text{CD}_3\text{OD}$ ):  $\delta$  173.7 (C-9'), 168.6 (C-9), 149.8 (C-4), 147.9 (C-3), 146.9 (C-7), 146.3 (C-3'), 145.4 (C-4'), 129.4 (C-1'), 127.8 (C-1), 123.3 (C-6), 121.9 (C-6'), 117.7 (C-2'), 116.6 (C-5), 116.4 (C-5'), 115.4 (C-2), 114.5 (C-8), 74.8 (C-8'), 38.0 (C-7'). <sup>1</sup>H-NMR and <sup>13</sup>C-NMR data are in agreement with the previously published data for Rosmarinic acid.<sup>25,26</sup> NMR and MS spectra of Rosmarinic acid are presented in Figures S1-S3.

**Compound 2:** ESI-MS (*m/e*) 199.91 [M+H]<sup>+</sup>, ( $\text{C}_9\text{H}_{10}\text{O}_5$ ); <sup>1</sup>H-NMR (400 MHz,  $\text{CD}_3\text{OD}$ ):  $\delta$  6.63 (*d*,  $J=1.5$  Hz, 1H, H-2), 6.58 (*d*,  $J=8.0$  Hz, 1H, H-5), 6.49 (*dd*,  $J=8.0$  Hz,  $J=2.0$  Hz, 1H, H-6), 4.14 (*dd*,  $J=7.6$  Hz,  $J=4.1$  Hz, 1H, H-2'), 2.86 (*dd*,  $J=14.0$  Hz,  $J=3.8$  Hz, 1H, H-3'a), 2.65 (*dd*,  $J=13.9$  Hz,  $J=7.9$  Hz, 1H, H-3'b); <sup>13</sup>C NMR (100 MHz,  $\text{CD}_3\text{OD}$ ):  $\delta$  178.3 (C-1'), 146.1 (C-3), 145.1 (C-4), 130.7 (C-1), 122.1 (C-6), 117.8 (C-2), 116.3 (C-5), 73.5 (C-2'), 41.3 (C-3'). <sup>1</sup>H-NMR, <sup>13</sup>C-NMR, Correlation Spectroscopy, Heteronuclear Single Quantum Coherence (HSQC), Heteronuclear Multiple Bond Correlation (HMBC), and MS data are agreement with the data given in the literature for Danshensu.<sup>27</sup> NMR and MS spectra of Danshensu are presented in Figures S4-S9.

**Compound 3:** ESI-MS (*m/e*) 536.65 [M-H]<sup>-</sup>, ( $\text{C}_{27}\text{H}_{22}\text{O}_{12}$ ); <sup>1</sup>H-NMR (400 MHz,  $\text{CD}_3\text{OD}$ ):  $\delta$  7.49 (*s*, 1H, H-4), 6.71 (*s*, 1H, H-5), 6.66

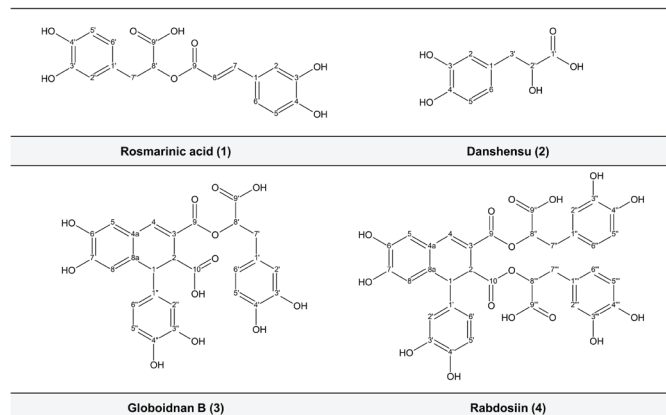


Figure 1. Chemical structures of the isolated compounds

(*d*, *J*=1.5 Hz, 1H, H-2'), 6.57-6.48 (*m*, 3H, H-8, H-5', H-5''), 6.45 (*s*, 1H, H-6'), 6.39 (*d*, *J*=1.8 Hz, 1H, H-2''), 6.31 (*dd*, *J*=8.2 Hz, *J*=1.9 Hz, 1H, H-6''), 4.94 (*s*, 1H, H-8'), 4.32 (*s*, 1H, H-1), 3.74 (*s*, 1H, H-2), 2.97-2.84 (*m*, 2H, H-7'); <sup>13</sup>C-NMR (100 MHz, CD<sub>3</sub>OD): δ 177.5 (C-10), 177.3 (C-9'), 169.2 (C-9), 147.5 (C-6), 144.9 (C-3'), 144.9 (C-3''), 144.2 (C-4''), 143.8 (C-7), 143.4 (C-4'), 138.9 (C-4), 138.1 (C-1''), 132.2 (C-8a), 131.2 (C-1'), 125.6 (C-4a), 125.3 (C-3), 122.2 (C-6'), 119.9 (C-6''), 118.0 (C-2'), 117.3 (C-8), 117.2 (C-5), 116.5 (C-5'), 116.5 (C-5''), 115.9 (C-2''), 77.5 (C-8'), 51.0 (C-2), 47.1 (C-1), 38.2 (C-7'). <sup>1</sup>H-NMR, <sup>13</sup>C-NMR, HSQC, and HMBC data are consistent with the published data for Globoidnan B.<sup>28,29</sup> NMR and MS spectra of Globoidnan B are presented in Figures S10-S15.

**Compound 4:** ESI-MS (*m/e*) 717.16 [M-H]<sup>-</sup>, (C<sub>36</sub>H<sub>30</sub>O<sub>16</sub>); <sup>1</sup>H-NMR (400 MHz, CD<sub>3</sub>OD): δ 7.52 (*s*, 1H, H-4), 6.71 (*s*, 1H, H-5), 6.63-6.59 (*m*, 3H, H-5'', H-2''', H-5'''), 6.57 (*d*, *J*=8.1 Hz, 1H, H-5'), 6.52 (*s*, 1H, H-2''), 6.50 (*s*, 1H, H-2'), 6.45 (*d*, *J*=8.0 Hz, 2H, H-6'', H-6'''), 6.28 (*t*, *J*=8.6 Hz, 2H, H-8, H-6'), 4.98 (*t*, *J*=5.8 Hz, 1H, H-8'), 4.04 (*s*, 1H, H-1), 3.84 (*d*, *J*=2.0 Hz, 1H, H-2), 2.92-2.74 (*m*, 4H, H-7'', H-7'''), H-8'''' (overlapped the solvent peak); <sup>13</sup>C-NMR (100 MHz, CD<sub>3</sub>OD): δ 173.7 (C-9'''), 173.6 (C-9''), 173.6 (C-10), 168.1 (C-9), 149.2 (C-7), 146.3 (C-3''), 146.2 (C-3'''), 146.0 (C-4'), 145.6 (C-4'''), 145.3 (C-3'), 145.2 (C-6), 145.0 (C-4''), 141.3 (C-4), 136.7 (C-1'), 131.5 (C-1'''), 129.6 (C-1''), 129.4 (C-8a), 124.9 (C-4a), 122.2 (C-3), 122.2 (C-6'''), 121.7 (C-6''), 120.1 (C-6'), 117.9 (C-5), 117.6 (C-8), 117.5 (C-5'''), 117.4 (C-2''), 117.4 (C-2'), 116.6 (C-2'''), 116.4 (C-5''), 115.9 (C-5'), 75.8 (C-8''), 75.4 (C-8'''), 50.0 (C-2), 46.7 (C-1), 38.0 (C-7''), 38.0 (C-7'''). <sup>1</sup>H-NMR, <sup>13</sup>C-NMR, HSQC, and HMBC data are consistent with the previous data for Rabdosiin.<sup>29,30</sup> NMR and MS spectra of Rabdosiin are presented in Figures S16-S21.

### Antioxidant activity

To define the antioxidant activities of the extracts and isolated compounds of TOU, FRAP, and CUPRAC assays were performed, and the results are presented in Table 1. It was determined that the isolated compounds had better antioxidant activity than the extracts. Rosmarinic acid showed the highest activity (FRAP: 1260.273 ± 4.499, CUPRAC: 608.250 ± 1.195 μM TE/g, respectively). TOU-E exhibited higher activity than the other extracts in both tests (FRAP: 794.818 ± 8.999, CUPRAC: 583.06 ± 5.882 μM TE/g, respectively).

### Lipase inhibition

The IC<sub>50</sub> values for lipase inhibitory activities of the extracts and isolated compounds are presented in Table 2. It was observed that the extracts and isolated compounds had weaker lipase inhibitory activities than the standard (orlistat). In addition, TOU-A and TOU-E exhibited higher activity (IC<sub>50</sub> = 38.131 ± 0.720, 38.841 ± 1.359 μg/mL, respectively) than the other extracts and isolated compounds. Rosmarinic acid demonstrated the highest activity (IC<sub>50</sub> = 49.421 ± 1.448 μg/mL) among the compounds.

## DISCUSSION

Obesity is a serious public health problem, which is defined as the epidemic of the 21<sup>st</sup> century by the World Health Organization and affects both developed and developing countries.<sup>5,6</sup> Inhibiting the digestion and absorption of nutrients is one of the most important treatment strategies for preventing obesity. Therefore, inhibition of pancreatic lipase, which plays a key role in the digestion of triglycerides, is an interesting therapeutic approach.<sup>31</sup> Herbal products are under investigation for the discovery of effective and safe new pancreatic lipase inhibitor compounds. Natural products, such as saponins, polyphenols, flavonoids, and terpenes, obtained from plants have been reported to be effective.<sup>32</sup>

**Table 1. Antioxidant activities of the extracts and isolated compounds**

Samples	CUPRAC <sup>a</sup>	FRAP <sup>b</sup>
TOU-M	442.972 ± 7.378	677.545 ± 1.285
TOU-C	65.472 ± 4.317	52.394 ± 5.143
TOU-E	583.06 ± 5.882	794.818 ± 8.999
TOU-A	354.083 ± 6.191	770.273 ± 3.857
Rosmarinic acid	608.250 ± 1.195	1260.273 ± 4.499
Danshensu	221.306 ± 0.851	919.364 ± 7.071
Globoidnan B	478.389 ± 1.264	813.909 ± 2.571
Rabdosiin	483.667 ± 1.534	1041.182 ± 8.357

<sup>a</sup>The CUPRAC value is the copper reducing antioxidant power (μM Trolox equivalent/gram), <sup>b</sup>the FRAP value indicates the iron reducing antioxidant power (μM Trolox equivalent/gram).

TOU-M: The methanol extract of the underground parts of *Trachystemon orientalis*, TOU-C: The chloroform subextract of the underground parts of *T. orientalis*, TOU-E: The ethyl acetate subextract of the underground parts of *T. orientalis*, TOU-A: The remaining aqueous subextract of the underground parts of *T. orientalis*, CUPRAC<sup>c</sup>: Cu(II) ion reducing antioxidant capacity, FRAP: Ferric reducing antioxidant power

**Table 2. Lipase inhibitory activities of the extracts and isolated compounds**

Samples	IC <sub>50</sub> (μg/mL) ± SD <sup>a</sup>
TOU-M	54.370 ± 0.937
TOU-C	ND <sup>b</sup>
TOU-E	38.841 ± 1.359
TOU-A	38.131 ± 0.720
Rosmarinic acid	49.421 ± 1.448
Danshensu	65.160 ± 4.443
Globoidnan B	79.881 ± 3.435
Rabdosiin	56.801 ± 2.052
Orlistat	17.581 ± 0.714

<sup>a</sup>Standard deviation, <sup>b</sup>ND: Not determined, TOU-M: The methanol extract of the underground parts of *Trachystemon orientalis*, TOU-C: The chloroform subextract of the underground parts of *T. orientalis*, TOU-E: The ethyl acetate subextract of the underground parts of *T. orientalis*, TOU-A: The remaining aqueous subextract of the underground parts of *T. orientalis*, IC<sub>50</sub><sup>c</sup>: Half maximal inhibitory concentration, SD: Standard deviation

In this study, isolation studies were performed on subextracts prepared from TOU-M. As a result of the isolation studies, rosmarinic acid was isolated from TOU-E, danshensu, globoidnan B, and rabdosiin were isolated from TOU-A. These compounds were purified from the underground parts of the plant for the first time. According to the literature, no previous isolation studies on *T. orientalis* have been reported. Rosmarinic acid was determined in the roots of the plants using high-performance liquid chromatography.<sup>33</sup>

Rosmarinic acid is a polyphenolic compound formed by the esterification of caffeic acid and danshensu.<sup>34</sup> It is commonly found in plants of the Boraginaceae family.<sup>35</sup> In the Boraginaceae family, globoidnan B, and rabdosiin were isolated from the roots of *Symphytum officinale* L. and danshensu from leaves of *Cordia americana* (L.) Gottschling & J.S.Mill.<sup>36,37</sup> Danshensu, globoidnan B, and rabdosiin have been found in Boraginaceae plants (the aerial parts and the roots of *S. officinale*; the leaves and the roots of *S. ibericum* Steven).<sup>38,39</sup>

In this study, the pancreatic lipase inhibitory and antioxidant activities of the extracts and isolated compounds of TOU were evaluated. According to the results of the pancreatic lipase inhibition experiment, the extracts and compounds were less active than orlistat, and TOU-A showed the highest lipase inhibitory activity. TOU-E had an  $IC_{50}$  value similar to that of TOU-A. It was observed that the activity of rosmarinic acid was similar to that of the extracts. It is thought that the activity of the extracts is higher due to the synergistic effects of the isolated phenolic compounds. In an *in vitro* study evaluating the pancreatic lipase inhibition of *Rosmarinus officinalis* L. extract and its phenolic compounds, including rosmarinic acid, the  $IC_{50}$  value of the extract was found to be 13.8  $\mu\text{g}/\text{mL}$ , whereas that of rosmarinic acid was 125.2  $\mu\text{g}/\text{mL}$ . It has been suggested that the effect of the extract may be due to the synergistic effect of rosmarinic acid and other phenolic acids.<sup>7</sup> In another study, it was determined that rosmarinic acid showed high lipase inhibitory activity ( $IC_{50} = 62.8 \pm 2.7 \mu\text{M}$ ) and this result supports our findings.<sup>40</sup> Only a few studies are showing that rosmarinic acid plays a role in different obesity-related mechanisms apart from pancreatic lipase inhibition. A previous study found that it suppresses adipogenesis, lipolysis, and inflammation.<sup>41</sup> In another study, its effects on adipogenesis and lipid metabolism were investigated, and it was reported that it inhibits inflammation and excessive lipid accumulation in human adipocytes.<sup>42</sup>

Obesity causes a decrease in antioxidant capacity by increasing oxidative stress and decreasing the activity of antioxidant enzymes.<sup>1</sup> In this study, according to the antioxidant activity results, TOU-E showed the highest activity among the extracts. In terms of antioxidant activity, the activities of the isolated compounds were better than those of the extracts. It was observed that the activity of rosmarinic acid was the best among the isolated compounds. The isolated compounds are believed to be responsible for the activity of the extracts. In a study, the authors attributed the high antioxidant activity

of the extracts prepared from the aerial parts and roots of *T. orientalis* to rosmarinic acid in its content.<sup>33</sup> It has been shown that rosmarinic acid has free radical-scavenging properties and is effective against oxidative reactive oxygen species.<sup>43</sup> In this study, TOU-A had an antioxidant activity similar to that of TOU-E. Compounds from this subextract may be responsible for the activity. In a study, it was shown that danshensu has higher scavenging activity for free hydroxyl radicals, superoxide anion radicals, 2,2-diphenyl-1-picrylhydrazyl (DPPH), and 2,2'-azino-bis(3-ethylbenzothiazoline-6-sulfonic acid (ABTS) radicals compared with vitamin C.<sup>44</sup> It has been reported that the root extracts of *S. officinale* rich in compounds such as rosmarinic acid, globoidnan B, and rabdosiin, as well as extracts prepared from the aerial parts of *S. anatolicum*, show high antioxidant activity owing to their phenolic acids.<sup>39,45</sup> It has been determined that the antioxidant activity (using the DPPH and ABTS assays) of rabdosiin is higher than that of globoidnan B and rosmarinic acid.<sup>37</sup> Phenolic compounds show radical scavenging, metal chelation, and hydrogen donor properties.<sup>32</sup> *T. orientalis* exhibits high antioxidant and antilipase activity *via* its phenolic compounds, and therefore, it may be a promising therapeutic agent for the treatment of obesity.

#### Study limitations

Further *in vivo*, clinical studies and toxicological analyses are needed to comprehensively reveal the effect of *T. orientalis* on obesity.

## CONCLUSION

This study revealed that TOU-E and TOU-A prepared from TOU and the isolated compounds from these extracts have high antioxidant and pancreatic lipase inhibitory activities. The current study is the first to evaluate the effects of *T. orientalis* on obesity *via* lipase inhibition. It is thought that the compounds (1-4) isolated from the plant for the first time and responsible for high antioxidant and antilipase activities. From the perspective of these results, *T. orientalis* is an important natural source that can be evaluated for the treatment of obesity.

#### Ethics

**Ethics Committee Approval:** Not required.

**Informed Consent:** Not required.

#### Authorship Contributions

Surgical and Medical Practices: A.N.K., T.S., M.B., Ş.K., Concept: A.N.K., M.B., Ş.K., U.Ö., S.Ö.Ş., Design: A.N.K., T.S., U.Ö., Data Collection or Processing: A.N.K., T.S., M.B., Ş.K., U.Ö., Analysis or Interpretation: A.N.K., T.S., M.B., Ş.K., U.Ö., A.D., İ.Ç., Literature Search: A.N.K., T.S., M.B., Ş.K., Writing: A.N.K., T.S., M.B., Ş.K.

**Conflict of Interest:** The authors have no conflicts of interest to declare.

**Financial Disclosure:** This study was supported by the Scientific Research Projects Coordination Unit of Karadeniz Technical University (project number: THD-2023-10793).

## REFERENCES

- Vangoori Y, Dakshinamoorthi A, Kavimani S. Prominent pancreatic lipase inhibition and free radical scavenging activity of a myristica fragrans ethanolic extract *in vitro*. Potential Role in Obesity Treatment. *Maedica (Bucur)*. 2019;14:254-259.
- Rakhra V, Galappaththy SL, Bulchandani S, Cabandugama PK. Obesity and the Western diet: How we got here? *Mo Med*. 2020;117:536-538.
- Huang R, Zhang Y, Shen S, Zhi Z, Cheng H, Chen S, Ye X. Antioxidant and pancreatic lipase inhibitory effects of flavonoids from different citrus peel extracts: An *in vitro* study. *Food Chem*. 2020;326:126785.
- Liu TT, Liu XT, Chen QX, Shi Y. Lipase Inhibitors for obesity: a review. *Biomed Pharmacother*. 2020;128:110314.
- Hou XD, Qin XY, Hou J, Tang H, Ge GB. The potential of natural sources for pancreatic lipase inhibitors: a solution to the obesity crisis? *Expert Opin Drug Discov*. 2022;17:1295-1298.
- de la Garza AL, Milagro FI, Boque N, Campión J, Martínez JA. Natural inhibitors of pancreatic lipase as new players in obesity treatment. *Planta Med*. 2011;77:773-785.
- Bustanji Y, Issa A, Mohammad M, Hudaib M. Inhibition of hormone-sensitive lipase and pancreatic lipase by *Rosmarinus officinalis* extract and selected phenolic constituents. *J Med Plant Res*. 2010;4:2235-2242.
- Yıldırım S. The chorology of the Turkish species of Boraginaceae family. *The Herb Journal of Systematic Botany*. 2000;7:257-272.
- Baytop T. Hodan (Herba Boraginis). In: *Türkiye'de bitkiler ile tedavi (geçmişte ve bugün)* (1<sup>st</sup> ed). İstanbul: İstanbul University Press, No. 3255, 1984:256.
- Sacan O. Antioxidant activity, total phenol, and total flavonoid contents of *Trachystemon orientalis* (L.) G. Don. *Eur J Biol*. 2018;77:70-75.
- Koca AD, Yıldırım S. Ethnobotanical properties of Akçakoca district in Düzce (Türkiye), *HJBC*. 2010;38:63-69.
- Yılar M, Onaran A, Yanar Y, Belguzar S, Kadioglu I. Herbicidal and antifungal potential of *Trachystemon orientalis* (L.) G. Don (Kaldırık). *Iğdır Univ J Inst Sci*. 2014;4:19-27.
- Gul V, Seckin Dinler B. Some medical and aromatic plants growing naturally in the Kumru region (Ordu). *ISUBÜ ZFD*. 2016;11:146-156.
- Yeşilada E, Sezik E, Honda G, Takaishi Y, Takeda Y, Tanaka T. Traditional medicine in Türkiye IX: folk medicine in north-west Anatolia. *J Ethnopharmacol*. 1999;64:195-210.
- Uzun E, Sariyar G, Adsersen A, Akkol EK, Aslan S, Yılmaz F, Kocabas M. Traditional medicine in Sakarya province (Türkiye) and antimicrobial activities of selected species. *J Ethnopharmacol*. 2004;95:287-296.
- Sagiroglu M, Arslanturk A, Akdemir Z, Turna M. An ethnobotanical survey from Hayrat (Trabzon) and Kalkandere (Rize/Türkiye). *Biodicon*. 2012;5:31-42.
- Dimcheva V, Kaloyanov N, Karsheva M. The polyphenol composition of *Cistus incanus* L., *Trachystemon orientalis* L. and *Melissa officinalis* L. infusions by HPLC-DAD method. *Open J Anal Bioanal Chem*. 2019;3:31-38.
- Demir E. Profile of fatty acids, vitamins, phytosterols and phenolic acids in *Trachystemon orientalis* plant and evaluation of its antioxidant activity. *EJOSAT*. 2022;33:112-118.
- Ozen T. Antioxidant activity of wild edible plants in the Black Sea Region of Türkiye. *Grasas Y Aceites*. 2010;61:86-94.
- Boğa M, Hacıbekiroğlu I, Kolak U. Antioxidant and anticholinesterase activities of eleven edible plants. *Pharm Biol*. 2011;49:290-295.
- Erguven M, Ozsoy N, Aktas E, Bitis L, Taskin T, Bilir A. *Trachystemon orientalis* has anticancer activity which is highly induced by rhizomes on endometrial cancer *in vitro*. *Anti-Cancer Drugs*. 2015;26:e12.
- Benzie IF, Strain JJ. Ferric reducing/antioxidant power assay: direct measure of total antioxidant activity of biological fluids and modified version for simultaneous measurement of total antioxidant power and ascorbic acid concentration. *Methods Enzymol*. 1999;299:15-27.
- Apak R, Guclu K, Demirata B, Ozyurek M, Celik SE, Bektaşoğlu B. Comparative evaluation of various total antioxidant capacity assays applied to phenolic compounds with the CUPRAC assay. *Molecules*. 2007;12:1496-1547.
- Bustanji Y, Al-Masri IM, Mohammad M, Hudaib M, Taha M, Najib N. Pancreatic lipase inhibition activity of trilactone terpenes of *Ginkgo biloba*. *J Enzyme Inhib Med Chem*. 2011;26:453-459.
- Ferlinahayati F, Gultom RPJ, Herlina H, Eliza E. Steroid compounds from *Gynura pseudochina* (Lour) DC. *Molekul*. 2017;12:8-13.
- Badem M, Sener SO, Kanbolat S, Kucuk T, Uludağ A, Yılmaz S, Arslan M. Evaluation of biological activities of *Barbarea integrifolia* and isolation of a new glucosinolate derived compound. *Z Naturforsch C J Biosci*. 2021;76:375-382.
- Sidoryk K, Filip K, Cmoch P, Laszcz M, Cybulski M. Efficient synthesis and physicochemical characterization of natural danshensu, its S isomer and intermediates thereof. *J Mol Struct*. 2018;1153:135-148.
- Basli A, Delaunay JC, Pedrot E, Riche C, Nicolas L, Gueguen Y, Toutain B, Boudier A. New cyclolignans from *Origanum glandulosum* active against  $\beta$ -amyloid aggregation. *Rec Nat Prod*. 2014;8:208-216.
- D'Urso G, Masullo M, Seigner J, Rezzonico E, Dal Toso R, Brighenti V, Bresciani A, Delcarlo M, Pezzoni D, Bonati M, Montalto G. LC-ESI-FT-MS<sup>n</sup> metabolite profiling of *Symphytum officinale* L. roots leads to isolation of comfrey n, an unusual aryl-naphthalene lignan. *Int J Mol Sci*. 2020;21:4671.
- Flegkas A, Milosević Ifantis T, Barda C, Samara P, Tsitsilonis O, Skaltsa H. Antiproliferative activity of (-)-rabdosin isolated from *Ocimum sanctum* L. medicines (Basel). 2019;6:37.
- Buchholz T, Melzig MF. Polyphenolic compounds as pancreatic lipase inhibitors. *Planta Med*. 2015;81:771-783.
- Hadrich F, Cher S, Gargouri YT, Adel S. Antioxidant and lipase inhibitory activities and essential oil composition of pomegranate peel extracts. *J Oleo Sci*. 2014;63:515-525.
- Bıyık B, Yılmaz Sarıaltın S, Gökbulut A, Çoban T, Çoşkun M. *Trachystemon orientalis* (L.) G. Don as a valuable source of rosmarinic acid: biological activities and HPLC profiles. *Turk J Pharm Sci*. 2023;20:141-148.
- Habtemariam S. Molecular pharmacology of rosmarinic and salvianolic acids: potential seeds for Alzheimer's and vascular dementia drugs. *Int J Mol Sci*. 2018;19:458.
- Petersen M, Simmonds MS. Rosmarinic acid. *Phytochemistry*. 2003;62:121-125.
- Geller F, Schmidt C, Göttert M, Schröder J, Schübler R, Losch P, Schunk L, Weber T. Identification of rosmarinic acid as the major active constituent in *Cordia americana*. *J Ethnopharmacol*. 2010;128:561-566.
- Trifan A, Skalicka-Woźniak K, Granica S, Trifan G, Sinan KI, Zengin G, Tomczyk M, Góra J, Kwiatkowska B. *Symphytum officinale* L.: Liquid-liquid chromatography isolation of caffeic acid oligomers and evaluation

- of their influence on pro-inflammatory cytokine release in LPS-stimulated neutrophils. *J Ethnopharmacol.* 2020;262:113169.
38. Trifan A, Zengin G, Sinan KI, Wolfram E, Skalicka-Woźniak K, Luca SV. LC-HRMS/MS phytochemical profiling of *Symphytum officinale* L. and *Anchusa ochroleuca* M. Bieb. (Boraginaceae): Unveiling their multi-biological potential *via* an integrated approach. *J Pharm Biomed Anal.* 2021;204:114283.
39. Trifan A, Zengin G, Sinan KI, Skalicka-Woźniak K, Minceva M, Luca SV. *Symphytum ibericum* Steven: LC-HRMS/MS-based phytochemical profile, *in vitro* antioxidant and enzyme inhibitory potential. *Chem Biol Technol Agric.* 2022;42:9
40. Lee IC, Bae JS, Kim T, Kwon OJ, Kim TH. Polyphenolic constituents from the aerial parts of *Thymus quinquecostatus* var. *japonica* collected on ulleung island. *J Korean Soc Appl Biol Chem.* 2011;54:811-816.
41. Rui Y, Tong L, Cheng J, Wang G, Qin L, Wan Z. Rosmarinic acid suppresses adipogenesis, lipolysis in 3T3-L1 adipocytes, lipopolysaccharide-stimulated tumor necrosis factor- $\alpha$  secretion in macrophages, and inflammatory mediators in 3T3-L1 adipocytes. *Food Nutr Res.* 2017;61:1330096.
42. Vasileva LV, Savova MS, Tews D, Wabitsch M, Georgiev MI. Rosmarinic acid attenuates obesity and obesity-related inflammation in human adipocytes. *Food Chem Toxicol.* 2021;149:112002.
43. Alagawany M, Abd El-Hack ME, Farag MR, Taha AE, Elnesr SS, Saadeldin IM, Swelum AA, Abdel-Latif MA, El-Saadony MT. Rosmarinic acid: modes of action, medicinal values and health benefits. *Anim Health Res Rev.* 2017;18:167-176.
44. Zhao GR, Zhang HM, Ye TX, Liu H, Liu M, Zhang Y. Characterization of the radical scavenging and antioxidant activities of danshensu and salvianolic acid B. *Food Chem Toxicol.* 2008;46:73-81.
45. Trifan A, Czerwińska ME, Zengin G, Sinan KI, Wolfram E, Skalicka-Woźniak K, Luca SV. Influence of pyrrolizidine alkaloids depletion upon the biological activity of *Symphytum officinale* L. extracts. *J Ethnopharmacol.* 2023;303:116010.

---

Click the link to access Supplementary Figure 1: <https://t24.im/5Rd>



# Influence of Formulation Composition on the Characteristic Properties of 5-fluorouracil-loaded Liposomes

Tahir Emre YALÇIN\*, Ceren YETGIN

Gazi University Faculty of Pharmacy, Department of Pharmaceutical Technology, Ankara, Türkiye

## ABSTRACT

**Objectives:** Variations in the types and quantities of excipients used to prepare liposomes can affect the physicochemical properties of liposome formulations. This study aimed to provide information about the design and fabrication of 5-fluorouracil (5-FU)-loaded liposome formulations using different lipid and cholesterol (CHOL) derivatives.

**Materials and Methods:** Passive loading *via* a small-volume incubation method was used to prepare liposomes. The particle size, polydispersity index, zeta potential, and encapsulation efficiency (EE%) of the formulations were determined. The release studies of the formulations were conducted using a Franz diffusion cell at 37 °C. In this study, a high-pressure liquid chromatography device was used to measure the amount of 5-FU.

**Results:** The mean particle sizes of all formulations were between 134 and 166 nm, and they had a negative charge on their surface. Increasing the cholesteryl hemisuccinate content reduced the size of the liposomes. Additionally, all formulations exhibited a low polydispersity index (0.3). The EE% of all formulations exceeded 30%. The *in vitro* release of 5-FU from liposome formulations followed the Korsmeyer-Peppas model.

**Conclusion:** Modifying the lipid and CHOL content in the formulations, as indicated by the experimental results, can change the characteristic properties of liposomes. The use of soybean phosphatidylcholine and cholesteryl hemisuccinate appears to be a promising combination for the preparation of hydrophilic drug-loaded liposome formulations.

**Keywords:** 5-fluorouracil, liposomes, cholesteryl hemisuccinate, small-volume incubation method, drug release data modeling

## INTRODUCTION

Cancer is a global public health issue and ranks second in deaths caused by diseases.<sup>1</sup> Despite the advancement of novel therapeutic approaches for cancer, chemotherapy continues to be a primary treatment strategy. Nevertheless, the clinical use of chemotherapeutic agents faces limitations due to their toxicity and insufficient specificity. 5-Fluorouracil (5-FU) is a type of chemotherapy drug that is used to treat various solid tumors, such as colon, breast, and liver cancers. While 5-FU is commonly employed in treating cancer, its short half-life (~10-20 min)<sup>2</sup> and minimal affinity to tumor cells constrain the therapeutic potency of the drug.<sup>3</sup> Because of these limitations,

a significant amount of 5-FU is needed to boost therapeutic efficiency, thereby increasing drug toxicity.<sup>4</sup> Thus, to address these issues, new technologies, such as nanocarrier drug delivery systems, have been introduced.

Nanocarriers are highly advantageous in cancer treatment owing to passive targeting because they exhibit minimal side effects. The term "nanocarrier" includes nanosized drug carrier systems such as nanoparticles, nanoemulsions, nanosuspensions, liposomes, niosomes, dendrimers, transferosomes, and polymeric micelles.<sup>5-7</sup> Based on the number of studies conducted and the number of commercial products available, liposomes are important nanocarrier systems.<sup>8,9</sup>

\*Correspondence: tahiremreyalcin@gmail.com, ORCID-ID: orcid.org/0000-0001-5834-2335

Received: 17.10.2023 , Accepted: 04.03.2024



Liposomes are spherical vesicles consisting of a lipid bilayer structure that can encapsulate various drugs and molecules.<sup>10</sup> These drug delivery systems are biocompatible, biodegradable, and flexible, and their nano-size enables passive targeted drug delivery for cancer treatment. Some commercial liposomal products used for cancer treatment are Marqibo®, Mepact®, DepoCyt®, and Doxil®.<sup>11</sup>

Lipid and cholesterol (CHOL) derivatives can significantly influence the characteristic properties of liposomes. These components can affect the particle size (PS), zeta potential (ZP), encapsulation efficiency (EE%), drug release profiles, and other attributes of formulations. This study aimed to characterize liposome formulations prepared with different types of lipid and CHOL, loaded with 5-FU, and to evaluate the impact of excipients on the characteristic properties of the formulations.

## MATERIALS AND METHODS

### Materials

5-FU, 1,2-dioleoyl-sn-glycero-3-phosphoethanolamine (DOPE), dialysis membrane (MW: 12,000-14,000 Da), and CHOL were acquired from Sigma-Aldrich (USA). Soybean L- $\alpha$ -phosphatidylcholine (SPC, 95%) and cholesteryl hemisuccinate (CHEMS) from Avanti Polar Lipid Inc. (USA). All other reagents and solvents were of analytical grade.

### Methods

#### Preparation of phosphate buffer solution (PBS) (pH 7.4)

PBS (pH 7.4) was prepared according to the methods described in the U.S. Pharmacopeia (the second supplement, USP 35-NF 30). The steps for preparing PBS are as follows: Transferred  $\text{KH}_2\text{PO}_4$  solution (0.2 M, 250 mL) into a 1 L volumetric flask, NaOH solution (0.2 M, 195.5 mL) was added, the volume was diluted to 1 L with purified water, and the mixture was mixed well.

#### Preparation of 5-FU-loaded liposomes

Fourier transform infrared analyses from previous studies have indicated the compatibility of the excipients used in this research with each other and with the active substance, 5-FU.<sup>12-14</sup> Therefore, these excipients were selected as suitable candidates for the preparation of a 5-FU-loaded liposome formulation. The passive loading with small volume incubation (SVI) method was used to prepare liposomes.<sup>15</sup> In this method, empty liposomal pellets devoid of active substances are initially obtained using the thin-film hydration technique. The thin-film hydration technique, also known as the Bangham method, is the most common fabrication technology for liposomes. The SVI method is a passive drug-loading approach that relies on drug diffusion from a solution, creating a substantial concentration gradient across the liposomal membrane to facilitate efficient drug influx into the liposomes.<sup>16</sup> In this method, the derivatives of phospholipid and CHOL are first solubilized in chloroform in a round bottom flask at the amounts shown in Table 1 and then shaken. The organic solvent in the mixture was removed using an evaporator (Rotavapor® R-3, Büchi, Switzerland) at 60 °C,

resulting in the formation of a thin film layer on the flask's wall. The obtained films were slowly hydrated with blank PBS under a magnetic stirrer at 60 °C for 1 h. The liposomes were subjected to sonication using an ultrasonic bath sonicator (Bandelin Sonorex Digitec, Bandelin electronic GmbH & Co, Germany). Furthermore, to reduce PS and improve homogeneity, all formulations were gradually extruded through 400- and 200-nm polycarbonate membranes (10 times each). To obtain empty liposomal pellets, the liposomal suspensions were centrifuged at 70,000 rpm for 1 h using a centrifuge (Hitachi CS 150 GXL, Tokyo, Japan). Subsequently, 5-FU solutions (5 mg 5-FU in 0.5 mL PBS) were added to the empty liposomal pellets and mixed thoroughly by gentle pipetting up and down several times. The resuspended formulations were transferred in 2 mL Eppendorf tubes and incubated at 60 °C for 1 h under magnetic stirring using a 5 mm x 2 mm magnetic stir bar. The resulting 5-FU-loaded liposomes were then centrifuged at 70,000 rpm for 1 h to remove any unencapsulated 5-FU.<sup>17</sup>

#### Lyophilization procedure

The acquired liposomal pellets were resuspended in purified water containing trehalose as a cryoprotectant. After freezing the samples at 80 °C, they were rapidly transferred to a freeze dryer (Christ Alpha 1-2 LD plus, Germany). The samples were freeze-dried inside the device at 55 °C for 40 h.<sup>18</sup> The lyophilized powder was collected and stored at  $5 \pm 3$  °C for further experiments.

#### Characterization of 5-FU-loaded liposomes

##### PS, polydispersity index (PDI), and ZP

The PS, PDI, and ZP values of the formulations were measured using a Zetasizer Nano ZS (Malvern Instruments, UK).<sup>19,20</sup> Before each measurement, the lyophilized formulations were redispersed in purified water (n = 3).

##### EE%

Drug EE% was determined using the direct method.<sup>21,22</sup> A certain amount of lyophilized liposomes were ruptured by adding chloroform. Then, 10 mL of PBS was added to the mixture to extract 5-FU into the aqueous phase. The organic phase was mixed with the aqueous phase. The PBS solution was analyzed using an Agilent 1220 LC high-pressure liquid chromatography (HPLC) system (Germany) to determine 5-FU in the samples. Chromatographic separation was performed using a Waters Xselect reverse phase C18 column (5  $\mu\text{m}$ , 250 mm x 4.6 mm *i.d.*),

**Table 1. Content and codes of formulations**

Formulation code	SPC (mg)	DOPE (mg)	CHOL (mg)	CHEMS (mg)
F1	140	-	45	15
F2	140	-	15	45
F3	133	7	60	-
F4	112	28	60	-

SPC: Soybean L- $\alpha$ -phosphatidylcholine, DOPE: 1,2-dioleoyl-sn-glycero-3-phosphoethanolamine, CHOL: Cholesterol, CHEMS: Cholesteryl hemisuccinate

isocratic conditions (90% acetonitrile and 10% purified water) with 1 mL/min flow rate and detected at 265 nm.<sup>23</sup> The EE% was then calculated using the following Equation (1):

$$EE\% = \frac{(\text{Amount of the drug in liposomes})}{(\text{Amount of the drug added to liposomes})} \times 100 \quad (1)$$

#### *In vitro* release study

To determine the *in vitro* release rate of 5-FU from the formulations, Franz diffusion cells were used. Franz diffusion cells were purchased from Çalışkan Cam (Ankara, Türkiye). Prior to the release experiment, the diffusion membrane was soaked in PBS. The study was carried out under sink conditions, in which the release media (PBS) were able to dissolve at least three times the amount of 5-FU in the samples. A volume of 1 mL of the liposome suspension in PBS was added to the donor chamber, whereas a volume of 2.5 mL of PBS was added to the receptor chamber as the release media. The diffusion cell was then placed in a thermostatic bath maintained at 37 °C. At predefined intervals, all release media in the receptor chamber were withdrawn and an equal volume of PBS was added. Throughout the experiment, a magnetic bar was used to stir the contents of each cell. The samples were then analyzed using the HPLC method, as previously described, with all measurements performed three times.

#### *Drug release data modeling*

Drug release data were assessed using kinetic models, which included zero-order, first-order, Higuchi, Hixson-Crowell, and Korsmeyer-Peppas, using the DDSolver add-in in Excel. The model with the highest adjusted coefficient of determination ( $R^2$  adjusted) was chosen as the most appropriate model for describing the release kinetics. In the context of data modeling, all data were used, except for the Korsmeyer-Peppas model. The release exponent "n" was determined using the initial 60% drug release within the Korsmeyer-Peppas model.<sup>24</sup>

#### *Statistical analysis*

The data were expressed as mean values with standard deviations. Statistical analysis was performed using a One-Way analysis of variance followed by Tukey's posthoc test, using the GraphPad Prism 5.0 software (GraphPad Software, Inc.). Significance was established at  $p \leq 0.05$ .

## RESULTS

#### *PS, PDI, and ZP*

Liposomes prepared using different lipids (SPC and DOPE) and CHOL derivatives (CHOL and CHEMS) were evaluated in terms of PS, PDI, and ZP (Table 2). The mean PSs of the F1 (CHOL 45 mg: CHEMS 15 mg) and F2 (CHOL 15 mg: CHEMS 45 mg) formulations were 138 and 134 nm, respectively. The ZP values of the F1 and F2 formulations were 27.3 and 32.4 mV, respectively. Furthermore, no statistically significant difference was observed in terms of mean PS in formulations containing DOPE (F3 formulation: 166 nm and F4 formulation: 162 nm) ( $p > 0.05$ ).

#### *EE%*

The 5-FU encapsulation efficiencies ranged between 30.8% and 35.8% for the formulations, as shown in Table 2. There is no significant difference was observed between F3 and F4 formulations containing DOPE according to EE% ( $p > 0.05$ ).

#### *In vitro* release studies

The *in vitro* drug release profiles of all formulations are depicted in Figure 1. The way in which 5-FU was released from formulations was observed to have consisted of two distinct stages: an initial rapid release of approximately 50% of the drug within the first 2 h, followed by a gradual and slower release for all formulations.

#### *Drug release data modeling*

Various models were used to determine the kinetics of the formulations. Based on the values of the  $R^2$  adjusted, the model that best describes 5-FU release from liposomes was the Korsmeyer-Peppas model (highest  $R^2$  adjusted) for all formulations (Table 3).

## DISCUSSION

Pre-formulation studies conducted in this study and previous studies in the literature indicate that the lyophilization process generally increases the PS of liposomes due to the fusion/aggregation of vesicles.<sup>25</sup> To enhance the stability of liposomes,<sup>26</sup> all formulations prepared in this study were

**Table 2. PS, PDI, ZP, and EE% of liposomal formulations (n= 3)**

Formulation code	PS (nm)	PDI	ZP (mV)	EE%
F1	138 ± 2	0.130 ± 0.025	-27.3 ± 1.2	32.9 ± 0.7
F2	134 ± 4	0.194 ± 0.010	-32.4 ± 2.1	35.8 ± 1.8
F3	166 ± 2	0.197 ± 0.009	-31.5 ± 0.9	30.8 ± 0.6
F4	162 ± 4	0.247 ± 0.010	-21.0 ± 0.2	32.3 ± 1.8

PS: Particle size, PDI: Dispersity Polydispersity index, ZP: Zeta potential, EE: Encapsulation efficiency

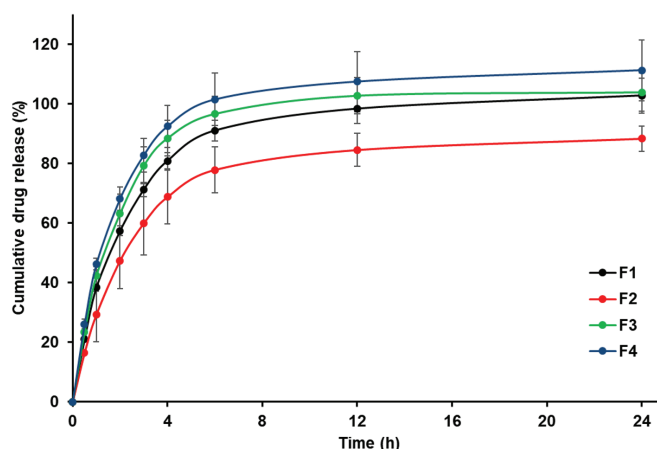


**Figure 1. *In vitro* release profile of 5-FU from formulations**

**Table 3. Results of model fitting of the formulations**

Model	Parameter	F1	F2	F3	F4
Zero-order	R <sup>2</sup> adjusted	-0.4365	-0.3180	-0.6475	-0.6658
First-order	R <sup>2</sup> adjusted	0.9822	0.8055	0.9971	0.9829
Higuchi	R <sup>2</sup> adjusted	0.6867	0.7210	0.5921	0.5968
Hixson-Crowell	R <sup>2</sup> adjusted	0.6692	0.6543	0.5986	0.5738
Korsmeyer-Peppas	R <sup>2</sup> adjusted	0.9913	0.9954	1	1
	n	0.724	0.724	0.857	0.824

lyophilized and characterized. The results indicate that an increase in the amount of CHEMS within the formulation leads to a slight reduction in PS. Similar results were reported by Kulig et al.<sup>27</sup> An increase in the CHEMS content may have resulted in an increase in net negative ZP, which could have led to the production of smaller particles. CHEMS has a negative charge due to the carboxylic acid structure in its composition,<sup>28</sup> which increases the net negative ZP value of the formulations. An increase in ZP may have prevented the formulation from aggregation.<sup>29</sup> The narrow PS distribution in colloidal dispersions indicates their suitability and quality. For this purpose, the PDI must be less than 0.5.<sup>30</sup> All formulations exhibited low PDI (< 0.3) and the PDI values indicate that all formulations have a homogeneous PS distribution.

EE% mainly depended on the compound solubility in the lipids or CHOL materials. The EE% findings are higher than those of some previously published 5-FU-loaded liposome formulations,<sup>31</sup> whereas the results are similar to or lower than those of other formulations.<sup>32</sup> As evident from this comparison, the EE% value of 5-FU in the formulations varied depending on the quantity and type of lipids and CHOL present in the liposome. Higher EE% was achieved using higher CHEMS (F2). This phenomenon is probably due to the presence of CHEMS on the surface of the liposomes. CHEMS has a relatively higher water solubility than CHOL,<sup>27</sup> and this property may make it a suitable candidate for binding highly water-soluble active substances such as 5-FU.

Because 5-FU is a hydrophilic drug (saturation solubility in distilled water and pH 7.4 PBS has been reported as 13.56 mg/mL and 16.76 mg/mL, respectively)<sup>33</sup>, it can rapidly permeate the lipid membrane, potentially leading to the initial release of the drug. The continuous release of the drug could potentially affect the degradation rate of the liposome's structure.<sup>34</sup> The formulations containing DOPE (F3 and F4) were observed to have a higher *in vitro* release percentage at all time points than the formulations without DOPE (F1 and F2). This phenomenon may have been caused by the conical shape of DOPE and its disruption of the bilayer structure upon incorporation into the formulation.<sup>35</sup> In the F2 formulation with a higher amount of CHEMS (45 mg), the 5-FU release occurred more slowly than in the F1 formulation with a lower amount of CHEMS (15 mg). This

could be attributed to the fact that CHEMS enhances membrane stability more effectively than CHOL.<sup>36</sup>

The Korsmeyer-Peppas model was the best model for explaining the release of 5-FU from all formulations. Previous publications on 5-FU-loaded different nanocarriers have also reported that the Korsmeyer-Peppas model best describes the release of 5-FU from these carriers.<sup>37,38</sup> The value of n could be used as an approximation to describe the mechanism of drug release. If n is less than 0.5, drug diffusion occurs within the polymer matrix following Fickian diffusion. If n lies within the range of 0.5 to 1, it indicates a non-Fickian diffusion mechanism, suggesting a combination of both diffusion and matrix erosion. If n > 1, the drug-release mechanism follows supercase II diffusion.<sup>39</sup> In the present study, n values were obtained in the range of 0.724-0.857, indicating a non-Fickian diffusion process. This drug-release mechanism is commonly observed in most drug delivery systems that incorporate liposomes.<sup>40</sup>

## CONCLUSION

The SVI method was effective in preparing liposomes containing 5-FU with liposomes having a PS in the nanometer range, displaying a negative ZP and high drug EE% of > 30%. The experiments revealed that liposome properties, such as PS, EE%, and drug release, were influenced by the amounts of DOPE and CHEMS used in the formulations. The mathematical models used to analyze drug release kinetics indicated that the n values were within the range of 0.5-1. This strongly suggests that the drug-release mechanism follows a non-Fickian diffusion process. Using SPC, DOPE, CHOL, and CHEMS together in the formulation may be useful for obtaining the optimal PS, ZP, EE%, *in vitro* release profile, and stability, although further studies are needed to evaluate the anticancer activity.

### Acknowledgments

The authors would like to thank the Gazi University Academic Writing Application and Research Center for proofreading the article.

### Ethics

**Ethics Committee Approval:** Not required.

**Informed Consent:** Not required.

### Authorship Contributions

Concept: T.E.Y., Design: T.E.Y., Data Collection or Processing: T.E.Y., C.Y., Analysis or Interpretation: T.E.Y., C.Y., Literature Search: T.E.Y., C.Y., Writing: T.E.Y., C.Y.

**Conflict of Interest:** The authors have no conflicts of interest to declare.

**Financial Disclosure:** This study was supported by the Gazi University, Projects of Scientific Investigation (BAP) Council (project Number: 02/2019-02).

## REFERENCES

- Gavas S, Quazi S, Karpiński TM. Nanoparticles for cancer therapy: current progress and challenges. *Nanoscale Res Lett.* 2021;16:173.
- Entezar-Almahdi E, Mohammadi-Samani S, Tayebi L, Farjadian F. Recent advances in designing 5-Fluorouracil delivery systems: a stepping stone in the safe treatment of colorectal cancer. *Int J Nanomedicine.* 2020;15:5445-5458.
- Khaledi S, Jafari S, Hamidi S, Molavi O, Davaran S. Preparation and characterization of PLGA-PEG-PLGA polymeric nanoparticles for co-delivery of 5-Fluorouracil and Chrysin. *J Biomater Sci Polym Ed.* 2020;31:1107-1126.
- Valencia-Lazcano AA, Hassan D, Pourmadadi M, Shamsabadipour A, Behzadmehr R, Rahdar A, Medina DI, Diez-Pascual AM. 5-Fluorouracil nano-delivery systems as a cutting-edge for cancer therapy. *Eur J Med Chem.* 2023;246:114995.
- Aminu N, Bello I, Umar NM, Tanko N, Aminu A, Audu MM. The influence of nanoparticulate drug delivery systems in drug therapy. *J Drug Deliv Sci Technol.* 2020;60:101961.
- Zhang C, Vora LK, Tekko IA, Dowling MB, O'Rourke S, McGinty S, Duffy C, Gorman SP, McCrudden MT, Donnelly RF. Development of dissolving microneedles for intradermal delivery of the long-acting antiretroviral drug bictegravir. *Int J Pharm.* 2023;642:123108.
- Ramadan D, McCrudden MTC, Courtenay AJ, Donnelly RF. Enhancement strategies for transdermal drug delivery systems: current trends and applications. *Drug Deliv Transl Res.* 2022;12:758-791.
- Hasanbegloo K, Banihashem S, Faraji Dizaji B, Ghaffari K, Haghirsadat F, Jafari M, Mahdavi M, Keshavarz M, Sadeghi S, Fathi-Azar S, Ghasemian A. Paclitaxel-loaded liposome-incorporated chitosan (core)/poly( $\epsilon$ -caprolactone)/chitosan (shell) nanofibers for the treatment of breast cancer. *Int J Biol Macromol.* 2023;230:123380.
- Xie Y, Ren Z, Chen H, Zhang X, Guo W, Li Z, Zhang H, Liu J, Zhao Y. A novel estrogen-targeted PEGylated liposome co-delivery oxaliplatin and paclitaxel for the treatment of ovarian cancer. *Biomed Pharmacother.* 2023;160:114304.
- Lombardo D, Kiselev MA. Methods of liposome preparation: formation and control factors of versatile nanocarriers for biomedical and nanomedicine application. *Pharmaceutics.* 2022;14:543.
- Fulton MD, Najahi-Missaoui W. Liposomes in cancer therapy: How did we start and where are we now? *Int J Mol Sci.* 2023;24:6615.
- Udofot O, Affram K, Israel B, Agyare E. Cytotoxicity of 5-fluorouracil-loaded pH-sensitive liposomal nanoparticles in colorectal cancer cell lines. *Integr Cancer Sci Ther.* 2015;2:245-252.
- Khodarahmi M, Abbasi H, Kouchak M, Mahdavinia M, Handali S, Rahbar N. Nanoencapsulation of aptamer-functionalized 5-Fluorouracil liposomes using alginate/chitosan complex as a novel targeting strategy for colon-specific drug delivery. *J Drug Deliv Sci Technol.* 2022;71:103299.
- Shah H, Madni A, Khan MM, Zaheer I, Ali K, Khan N, Arshad M, Malik A. pH-responsive liposomes of dioleoyl phosphatidylethanolamine and cholesteryl hemisuccinate for the enhanced anticancer efficacy of cisplatin. *Pharmaceutics.* 2022;14:129.
- Xu H, Paxton J, Lim J, Li J, Zeng C, Long J, Cheng H. Development of high-content gemcitabine PEGylated liposomes and their cytotoxicity on drug-resistant pancreatic tumor cells. *Pharm Res.* 2014;31:2583-2592.
- Tang M, Svirskis D, Leung E, Kanamala M, Wang H, Wu Z. Can intracellular drug delivery using hyaluronic acid functionalized pH-sensitive liposomes overcome gemcitabine resistance in pancreatic cancer? *J Control Release.* 2019;305:89-100.
- Emre Yalçın T, Yetgin C, Yilmaz A. Development of 5-fluorouracil-loaded nano-sized liposomal formulation by two methods: Strategies to enhance encapsulation efficiency of hydrophilic drugs. *J Res Pharm.* 2021;25:371-378.
- Chaudhury A, Das S, Lee RFS, Rahman MA, Agarwal S, Padhy S, Mishra AK, Subramanian K. Lyophilization of cholesterol-free PEGylated liposomes and its impact on drug loading by passive equilibration. *Int J Pharm.* 2012;430:167-175.
- Demirbolat GM, Altintas L, Yilmaz S, Arsoy T, Sözmen M, Degim IT. Nanodesigning of multifunctional quantum dots and nanoparticles for the treatment of fibrosarcoma. *J Microencapsul.* 2022;39:210-225.
- Yalcin TE, Tuncel E, Yucel C, Tirnaksiz F. Nanoemulsions containing megestrol acetate: development, characterization, and stability evaluation. *AAPS PharmSciTech.* 2022;23:142.
- Bapolisi AM, Nkanga CI, Walker RB, Krause RWM. Simultaneous liposomal encapsulation of antibiotics and proteins: Co-loading and characterization of rifampicin and Human Serum Albumin in soy-liposomes. *J Drug Deliv Sci Technol.* 2020;58:101751.
- Yalcin TE, Ilbasnis-Tamer S, Ibisoglu B, Özdemir A, Ark M, Takka S. Gemcitabine hydrochloride-loaded liposomes and nanoparticles: comparison of encapsulation efficiency, drug release, particle size, and cytotoxicity. *Pharm Dev Technol.* 2018;23:76-86.
- Amasya G, Badilli U, Aksu B, Tarimci N. Quality by design case study 1: Design of 5-fluorouracil loaded lipid nanoparticles by the W/O/W double emulsion - Solvent evaporation method. *Eur J Pharm Sci.* 2016;84:92-102.
- Wu IY, Bala S, Škalko-Basnet N, di Cagno MP. Interpreting non-linear drug diffusion data: Utilizing the Korsmeyer-Peppas model to study drug release from liposomes. *Eur J Pharm Sci.* 2019;138:105026.
- Porfire A, Muntean DM, Rus L, Sylvester B, Tomuță I. A quality-by-design approach for the development of lyophilized liposomes with simvastatin. *Saudi Pharm J.* 2017;25:981-992.
- Yu JY, Chuesiang P, Shin GH, Park HJ. Post-processing techniques for the improvement of liposome stability. *Pharmaceutics.* 2021;13:1023.
- Kulig W, Jurkiewicz P, Olżyńska A, Rog T, Cwiklik L, Katsaras J, Treuner-Lange A, Marrink SJ, Hof M. Experimental determination and computational interpretation of biophysical properties of lipid bilayers enriched by cholesteryl hemisuccinate. *Biochim Biophys Acta.* 2015;1848:422-432.
- Ding WX, Qi XR, Li P, Maitani Y, Nagai T. Cholesteryl hemisuccinate as a membrane stabilizer in dipalmitoylphosphatidylcholine liposomes containing saikosaponin-d. *Int J Pharm.* 2005;300:38-47.
- Sun D, Kang S, Liu C, Lu Q, Cui L, Hu B. Effect of zeta potential and particle size on the stability of SiO<sub>2</sub> nanospheres as a carrier for ultrasound imaging contrast agents. *Int J Electrochem Sci.* 2016;11:8520-8529.
- Md S, Gan SY, Haw YH, Ho CL, Wong S, Choudhury H. *In vitro* neuroprotective effects of naringenin nanoemulsion against  $\beta$ -amyloid toxicity through the regulation of amyloidogenesis and tau phosphorylation. *Int J Biol Macromol.* 2018;118:1211-1219.
- Glavas-Dodov M, Fredro-Kumbaradzi E, Goracinova K, Simonoska M, Calis S, Trajkovic-Jolevska S, Hincal AA. The effects of lyophilization on the stability of liposomes containing 5-FU. *Int J Pharm.* 2005;291:79-86.

32. Alomrani A, Badran M, Harisa GI, Alshehry M, Alamoudi AJ, Ali R, El-Say KM. The use of chitosan-coated flexible liposomes as a remarkable carrier to enhance the antitumor efficacy of 5-fluorouracil against colorectal cancer. *Saudi Pharm J.* 2019;27:603-611.
33. Mutalik S, Shetty PK, Kumar A, Kalra R, Parekh HS. Enhancement in deposition and permeation of 5-fluorouracil through human epidermis assisted by peptide dendrimers. *Drug Deliv.* 2014;21:44-54.
34. Chang M, Lu S, Zhang F, Hu W, Li J, Zhang J, Du L. RGD-modified pH-sensitive liposomes for docetaxel tumor targeting. *Colloids Surf B Biointerfaces.* 2015;129:175-182.
35. Alrbyawi H, Poudel I, Annaji M, AlQahtani FA, Jaradat Y, Alqahtani S, Zafar A, Alshehri S. pH-sensitive liposomes for enhanced cellular uptake and cytotoxicity of daunorubicin in melanoma (B16-BL6) cell lines. *Pharmaceutics.* 2022;14:1128.
36. Xu H, Zhang L, Li L, Wang H, Huang J, Zhao Y, Wu J. Membrane-loaded doxorubicin liposomes based on ion-pairing technology with high drug loading and pH-responsive property. *AAPS PharmSciTech.* 2017;18:2120-2130.
37. Seyedahmadi M, Saeidifar M, Javadpour J, Rezaei HR. Preparation and characterization of 5-fluorouracil loaded cellulose and exosome nanocarriers: sustained release behavior and cytotoxicity studies. *ChemistrySelect.* 2023;8:e202300967.
38. Bayat F, Pourmadadi M, Eshaghi MM, Yazdian F, Rashedi H. Improving release profile and anticancer activity of 5-fluorouracil for breast cancer therapy using a double drug delivery system: chitosan/agarose/ $\gamma$ -alumina nanocomposite@double emulsion. *J Clust Sci.* 2023;34:2565-2577.
39. Martín-Camacho UJ, Rodríguez-Barajas N, Sánchez-Burgos JA, Pérez-Larios A. Weibull  $\beta$  value for the discernment of drug release mechanism of PLGA particles. *Int J Pharm.* 2023;640:123017.
40. Ayachandran P, Ilango S, Suseela V, Sampath M, Thangam R, Vivek R, Ranganathan B, Sundar D. Green synthesized silver nanoparticle-loaded liposome-based nano architectonics for cancer management: *in vitro* drug release analysis. *Biomedicines.* 2023;11(1):217.



# Preparation and Characterization of the Release Behavior of PVA: Na-Alg Microsphere Containing Fampridine

© Serenay AKYOL ÖZDEMİR\*, © Fatoş YÜKSEL GÜVENİLİR

Istanbul Technical University Faculty of Chemical-Metallurgical Engineering, Department of Chemical Engineering, İstanbul, Türkiye

## ABSTRACT

**Objectives:** This study focuses on both the formulation of bio-based microspheres containing fampridine for the treatment of multiple sclerosis and provides an alternative to the commercially available product (Fampyra 10 mg, Biogen).

**Materials and Methods:** The encapsulation of fampridine was achieved using polyvinyl alcohol (PVA) and sodium alginate (Na-Alg) polymers. Glutaraldehyde (GA) and hydrochloric acid (HCl) were used as crosslinking agents. The polymer ratio (PVA: Na-Alg), drug: polymer (*d:p*) ratio, cross-linking agent ratio, and cross-linking time were evaluated for fampridine release. Release studies were analyzed using an ultraviolet spectrophotometer. The microspheres were characterized using scanning electron microscopy, differential scanning calorimetry, and Fourier transform-infrared transform infrared spectroscopy (FT-IR). The particle sizes of the fampridine-loaded microspheres were determined using a laser light scattering device.

**Results:** The study revealed that the optimal conditions for achieving the highest fampridine release involved microspheres formulated with a polymer ratio of PVA:Na-Alg (*w:w*) at 1:1, a drug-to-polymer (*d:p*) ratio of 1:2 (*w:w*), cross-linking agent concentrations of 2.5% (*w:w*) GA and 3% (*w:w*) HCl, and a cross-linking time of 5 minutes. The particle size analysis showed that all microspheres were within the 300-800  $\mu\text{m}$  range, and an increase in the *d:p* ratio correlated with larger particle sizes.

**Conclusion:** The findings demonstrate that bio-based microspheres containing fampridine can be successfully formulated using PVA and sodium alginate polymers, providing a promising alternative to the commercially available product..

**Keywords:** Drug release, fampridine, microsphere, PVA: Na-Alg.

## INTRODUCTION

Multiple sclerosis (MS) is a persistent condition characterized by inflammation and myelin loss, which affects the myelinated nerve fibers within the central nervous system. The components employed in the treatment of MS are glatiramer acetate, dimethyl fumarate, fingolimod, teriflunomide, natalizumab, alemtuzumab, mitoxantrone, fampridine, ocrelizumab.<sup>1-5</sup> Fampridine's performance-based assessments have demonstrated its ability to enhance walking speed, motor control, and balance in approximately 40% of patients who receive treatment.<sup>6,7</sup> In the treatment of MS, even though many molecules are used in various segments, the extended-release 10 mg fampridine tablet, taken twice daily, is the only approved

pharmacological drug for improving walking ability in adults with MS.<sup>8</sup> Injectable hydrogels, direct implantation, crosslinked micelles, and injectable suspensions have been used in drug delivery systems.<sup>9-12</sup> Biodegradable polymers and crosslinking agents may offer advantages.<sup>13-15</sup>

Due to sodium alginate's (Na-Alg) biologically degraded, strong gel-forming characteristics, and cost-effectiveness, Na-Alg has been extensively used in drug delivery systems.<sup>16</sup> All polyvinyl alcohol (PVA): Na-Alg hydrogels are pH sensitive, and using a lower cross-linking agent leads to a higher swelling ratio.<sup>17</sup> The commonly used crosslinking agent combination for PVA: Na-Alg hydrogels is glutaraldehyde (GA) and hydrochloric acid (HCl).<sup>18,19</sup>

\*Correspondence: akyol18@itu.edu.tr, ORCID-ID: orcid.org/0009-0005-0261-7893

Received: 25.11.2023, Accepted: 21.03.2024



Copyright© 2024 The Author. Published by Galenos Publishing House on behalf of Turkish Pharmacists' Association. This is an open access article under the Creative Commons Attribution-NonCommercial-NoDerivatives 4.0 (CC BY-NC-ND) International License.

Na-Alg also improved the encapsulation efficiency (EE) and particle size effect of microspheres, and the single-step polymerization process resulted in a narrow particle size distribution.<sup>20-22</sup>

The results revealed that the applied extraction model increased the initial burst effect and reduced the EE.<sup>23</sup>

Indeed, in microspheres, particle size is directly associated with EE and drug release. Studies have reported that as the polymer ratio, cross-linking ratio, and cross-linking time increase, the particle size tends to increase.<sup>24</sup>

In this study, the effects of various processing parameters on fampridine release from PVA: Na-Alg microspheres were examined for the treatment of MS.

## MATERIALS AND METHODS

### Materials

#### Chemicals

Fampridine (Enaltec, India), PVA ( $M_n = 72,000$  g/mole) (Merck, Germany), Na-Alg ( $M_n = 8,000-12,000$  g/mole) (Merck, Germany), GA (Merck, Germany), HCl (Merck, Germany),  $Na_2HPO_4$  (Merck, Germany),  $NaH_2PO_4$  (Merck, Germany), Methanol (Merck, Germany), NaOH (Merck, Germany), and Acetic Acid (Merck, Germany).

### Equipments

Peristaltic pump (150 mL/h flow rate) (Lefoo, China), Ultraviolet (UV)2-100 UV/visible spectrophotometer (Unicam, Netherlands), Shaking Water Bath (Mettler Toledo, Switzerland), Magnetic Stirrer (Chiltren, United Kingdom), Incubator (Mettmert, Germany), pH Meter (Mettler Toledo, Switzerland), Analytical Scales (Mettler Toledo, Switzerland). FT-IR (Mattson, ABD), scanning electron microscopy (SEM) (JSM 5600, Japan), differential scanning calorimetry (DSC) (Dupont 2000), Mastersizer 2000 instrument (Malvern Instruments, UK), Filter paper whatman number: 42 (Merck, Germany).

### Methods

#### Preparation of the PVA: Na-Alg microspheres

The formulations of the PVA: Na-Alg and empty microspheres are shown in Tables 1 and 2, respectively. Microspheres were obtained using the liquid maturation method. Fampridine was added to the polymer blends and stirred for approximately 12 hours to form a suspension. Then, these suspensions were passed through a peristaltic pump and dripped as droplets at a flow rate of 150 mL/h from a height of 3 cm into solutions of 50 mL HCl and GA, respectively. The formation of microspheres with different PVA: Na-Alg compositions was conducted at room temperature. The transfer of 20 mL drug-polymer mixture was completed in 8-10 minutes. After the last drop,

**Table 1. Formulation of microspheres**

	PVA: Na-Alg	Cross-linking agent concentration (v:v)	Cross-linking time (min.)	Drug: Polymer ratio
O1	1:1	2.5% GA + 3GA+ 3% HCl	5	1:0.5
O2	1:1	2.5% GA + 3% HCl	5	1:1
O3	1:1	2.5% GA + 3% HCl	5	1:1.25
O4	1:1	2.5% GA + 3% HCl	5	1:1.5
O5	1:1	2.5% GA + 3% HCl	5	1:2
P1	2:1	2.5% GA + 3% HCl	5	1:0.5
P2	2:1	2.5% GA + 3% HCl	5	1:1
P3	2:1	2.5% GA + 3% HCl	5	1:1.25
P4	2:1	2.5% GA + 3% HCl	5	1:1.5
P5	2:1	2.5% GA + 3% HCl	5	1:2
K1	3:1	2.5% GA + 3% HCl	5	1:0.5
K2	3:1	2.5% GA + 3% HCl	5	1:1
K3	3:1	2.5% GA + 3% HCl	5	1:1.25
K4	3:1	2.5% GA + 3% HCl	5	1:1.5
K5	3:1	2.5% GA + 3% HCl	5	1:2
L1	3:1	2.5% GA + 3% HCl	2.5	1:1.25
L2	3:1	2.5% GA + 3% HCl	30	1:1.25
M1	3:1	3% GA + 3% HCl	5	1:1.25
M2	3:1	1.5% GA + 1.5% HCl	5	1:1.25

PVA: Polyvinyl alcohol, Na-Alg: Sodium alginate, GA: Glutaraldehyde, HCl: Hydrochloric acid, min.: Minute

**Table 2. Formulation of empty microspheres**

	PVA: Na-Alg	Cross-linking agent concentration (v:v)	Cross-linking time (min.)
O	1:1	2.5% GA+ 3% HCl	5
P	2:1	2.5% GA+ 3% HCl	5
K	3:1	2.5% GA+ 3% HCl	5

PVA: Polyvinyl alcohol, Na-Alg: Sodium alginate, GA: Glutaraldehyde, HCl: Hydrochloric acid, min.: Minute

the microspheres were matured by stirring in the cross-linking solution (GA + HCl) for 2.5, 5, and 30 min. The microspheres were then washed with distilled water and filtered through a filter paper.

#### Release studies of fampridine from PVA: Na-Alg microspheres

25 mg microsphere samples were placed in 250 mL of buffer solutions within 500 mL bottles and positioned in a shaking water bath. Release studies were conducted at 37 °C in pH 1.2 HCl solution, pH 6.8, and pH 7.4. The microspheres were filtered every two hours, and the next buffer solution was introduced. Four mL samples were collected from the solution, and absorbance values at 262 nm were determined using a UV spectrophotometer. Concentrations were calculated using calibration graph shown in Figure 1 based on standard fampridine solutions. All release studies were conducted with 6 samples (n= 6) and average fampridine release was used as a result.

#### Analytical method

The calibration graph of fampridine is shown in Figure 1. The standard solutions were prepared from 0.1 to 2.5 mmol/L. All absorbance values were read thrice, and the mean value was used.

#### Analytical method validation

The selectivity, linearity, range, system precision, and repeatability of the relevant method have been assessed.<sup>25</sup> All absorbance values were read thrice, and the mean value was used.

#### Selectivity

UV spectra at 262 nm were obtained for all excipients present in the microsphere content (HCl, GA, PVA, Na-Alg). The possibility of interference with fampridine at the same wavelength was evaluated.

#### Linearity and range

The absorbance values were obtained using standard fampridine solutions at five different concentrations (0.5 mmol/L, 0.8 mmol/L, 1.0 mmol/L, 2.0 mmol/L, 2.5 mmol/L). The results were evaluated, and a linearity graph was generated.

#### System precision

The standard fampridine solution was prepared at a concentration of 1 mmol/L and was read 6 times using a UV spectrophotometer, and the standard deviation (SD) was measured.

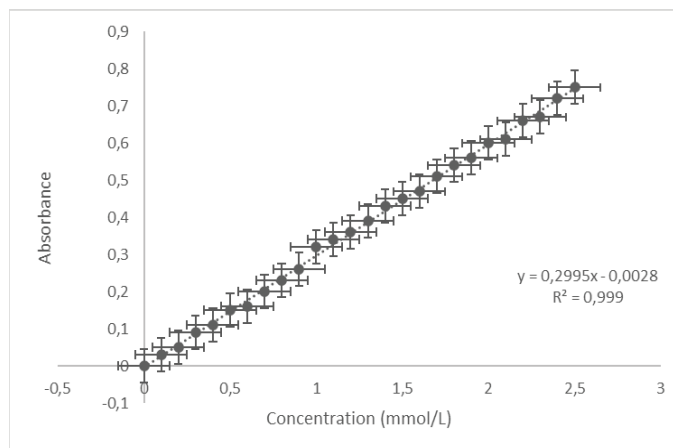


Figure 1. Calibration graph of fampridine

#### Repeatability

Microspheres labeled O5 were prepared six times (n= 6) on two different days, and their absorbance values were recorded at 262 nm. The SD was measured.

#### The water content of microspheres

50 mg microspheres were immersed in 100 mL of distilled water for a 24-hour equilibration period. Equilibrium water content was calculated using Equation 1.

$$\text{The equilibrium water content \%} = \frac{W_f - W_d}{W_d} \times 100 \quad [\text{Eq. 1}]$$

$W_f$  shows the microsphere weight, which includes water, and  $W_d$  shows the dry microsphere weight.

#### Encapsulation Efficiency (EE) of microspheres

50 mg of microspheres containing fampridine were pulverized in an agate mortar and extracted in 50 mL of methanol under cooling for 4 h. The obtained extract was then filtered, and diluted to various concentrations, and the drug content was quantified using UV spectrophotometry. The EE is calculated using Equation 2.

$$\text{EE \%} = \frac{D}{T} \times 100 \quad [\text{Eq. 2}]$$

$D$  shows the actual amount of drug in the microspheres, and  $T$  shows the theoretical amount of drug in the microspheres.

## RESULTS

### Effect of PVA: Na-Alg ratio on fampridine release

O3, P3, and K3 were selected with all other parameters kept constant, solely varying the PVA: Na-Alg ratio. Results are shown in Figure 2. Entering PVA into the formulation leads to an increase in hydrogen bonding interactions between PVA and Na-Alg, and due to the functional group interactions between Na-Alg and fampridine, it was observed that the amount of PVA increased, the release of fampridine decreased, and the diffusion of the solution into the polymeric microsphere more challenging.<sup>26,27</sup>

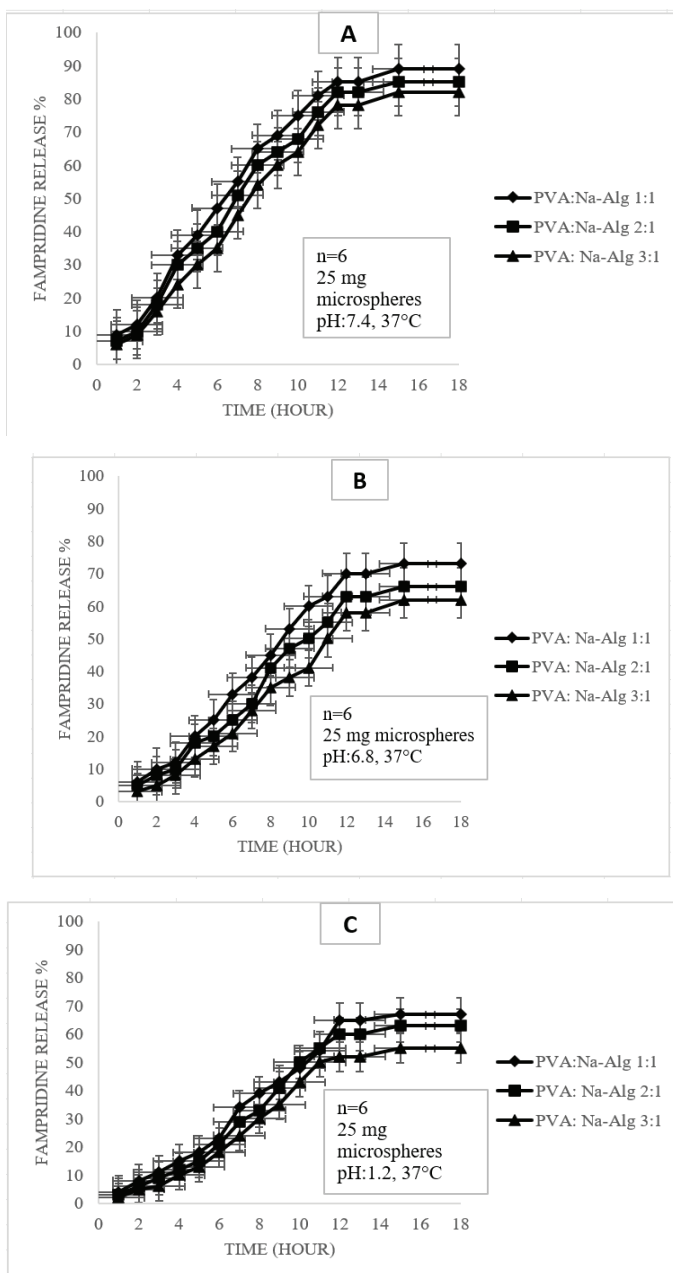


**Figure 2.** Effect of PVA: Na-Alg ratio. A): pH: 7.4, B): pH: 6.8, C): pH: 1.2  
PVA: Polyvinyl alcohol, Na-Alg: Sodium alginate

### Effect of pH on fampridine release

Fampridine release was conducted at pH 1.2, 6.8, and 7.4 for 14 h. The results showed that all microspheres are pH-sensitive.<sup>28</sup> There was maximum release at pH 7.4 (89% after 18 hours), decreasing release at pH 6.8 (73% after 18 hours), and the lowest release occurred at pH 1.2 (67% after 18 hours). This is attributed to the low ionization percentage of fampridine at low pH. Additionally, in controlled release systems containing PVA, the best swelling is observed at high pH, which is consistent with the swelling results obtained from release studies.<sup>28,29</sup> Because the highest release was observed at pH 7.4, subsequent experiments were conducted using a pH 7.4 buffer solution as the medium.

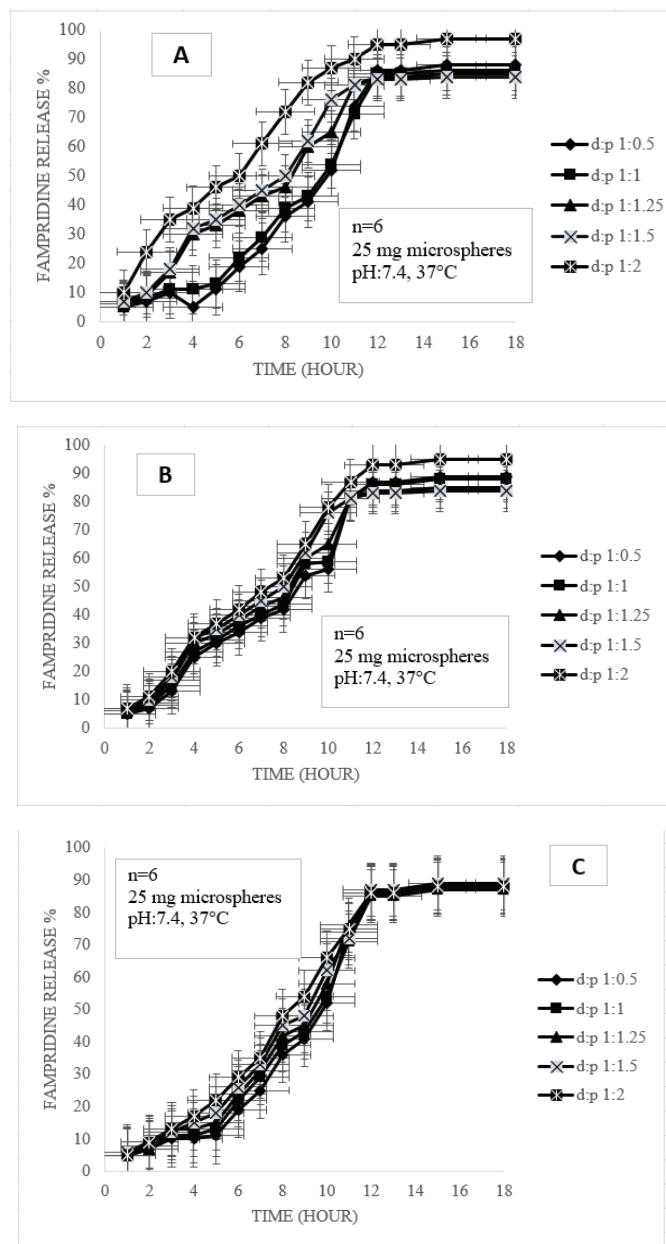


**Figure 3.** Effect of the drug: polymer ratio. A): PVA:Na-Alg (1:1), B): PVA:Na-Alg (2:1), C): PVA:Na-Alg (3:1) PVA: Polyvinyl alcohol, Na-Alg: Sodium alginate

*Effect of the drug: polymer ratio on fampridine release*

O1-K5 was used to evaluate the drug: polymer ratio, and the results are shown in Figure 3. It was observed that the drug: polymer ratio decreased and the release of fampridine increased.

The highest release of fampridine was observed with a drug: polymer ratio of 1:2. These results can be explained by the microspheres adopting a more compact structure as the drug quantity increases, making it more difficult for the solvent to permeate the microsphere matrix. Increasing the drug quantity leads to a deceleration in drug release due to increased interactions between the drug and polymer blends.<sup>30</sup>

*Effect of cross-linking agent concentration on fampridine release*

The microspheres were prepared using three different cross-linking agent concentrations: 3% GA + 3% HCl, 2.5% GA + 3% HCl, 1.5% GA + 1.5% HCl, and K3, M1, and M2 were analyzed. The results are shown in Figure 4. Increasing the concentration of the cross-linking agent in the microspheres leads to less diffusion of the solvent into the microspheres and made more challenging of drug diffusion.<sup>31,32</sup>

*Effect of cross-linking time on fampridine release*

2.5, 5, and 30 min were assessed with K3, L1 and L2. Results are shown in Figure 5. It was observed that the highest fampridine release occurred at a low crosslinking time. But there is not a significant difference between 2.5 and 5 min. It was observed that the cross-linking time increased, leading to a reduction in polymer chain mobility and less solvent diffusion into the microspheres.<sup>32</sup>

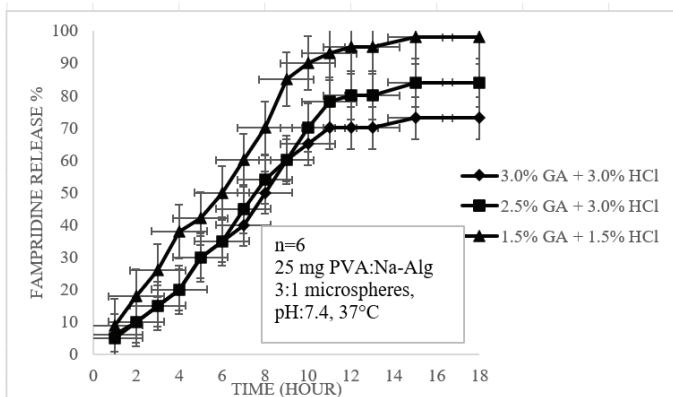


**Figure 4.** Effect of cross-linking agent concentration  
PVA: Polyvinyl alcohol, Na-Alg: Sodium alginate

*The water content of microspheres*

Results are shown in Table 3. It was observed that the highest swelling occurred at pH 7.4. This is due to the low swelling of Na-Alg and PVA in acidic environments in the structure of the microspheres.<sup>28</sup>

*EE and particle size of microspheres*

The encapsulation efficiencies are listed in Table 4. Results showed that the EE increased parallelly with the drug: polymer ratio. At a constant drug: polymer ratio, an increase in the PVA: Na-Alg ratio was observed to increase the EE. This result is attributed to the increased amount of polymer in the structure, leading to the diffusion of more drugs into the polymer.

The particle sizes of the microspheres were between 300 and 800 µm. Increasing amounts of fampridine and PVA led to an increase in particle size because of the decrease in the cross-linking density.<sup>24,33,34</sup>

*Analytical method validation*

*Selectivity*

Because the absorbance values of PVA, GA, and HCl at 262 nm are all zero, it is possible to conclude that the method was selective for fampridine.

*Linearity and range*

Results are shown in Figure 6 and Table 5. The results demonstrate that the proposed method is linear and within the range ( $R^2 = 0.999$ ).

*System precision*

System precision results are shown in Table 6. The results are remarkably close to each other, and the SD value is quite low. It can be concluded that the proposed system provides accurate and precise results.

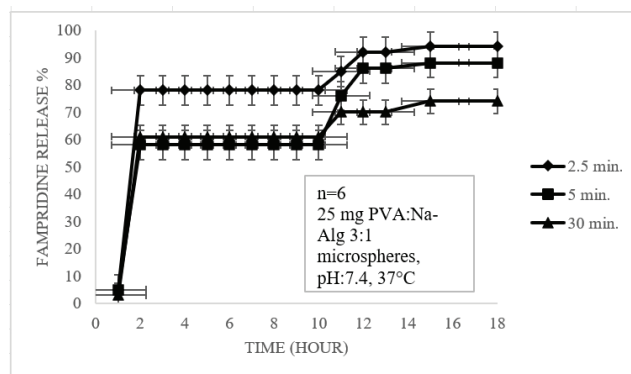


**Figure 5.** Effect of cross-linking agent time  
PVA: Polyvinyl alcohol, Na-Alg: Sodium alginate

**Table 3.** Water content of PVA: Na-Alg microspheres

PVA: Na-Alg	Purified water	pH: 1.2	pH 6.8	pH 7.4
1:1 (O)	70.1% ± 5.6	65.1% ± 3.2	105.1% ± 3.4	109.8% ± 7.9
2:2 (P)	75.6% ± 6.6	88.1% ± 7.6	108.1% ± 6.3	108.7% ± 4.5
3:1 (K)	80.3% ± 4.8	90.1% ± 5.2	110.7% ± 3.8	115.7% ± 6.8

PVA: Polyvinyl alcohol, Na-Alg: Sodium alginate

### Repeatability

Repeatability results are shown in Table 7. O5 results are close to each other, and the SD value is quite low. It can be concluded that the proposed system provides repeatable results.

### Characterization of the microspheres

#### Fourier transform infrared spectroscopy (FT-IR) results

In Figure 7, the FTIR results for PVA, Na-Alg, and the blank microsphere (O) are presented. In Figure 8, the FTIR results for fampridine, the blank microsphere (O), and the fampridine-loaded O5 microsphere are shown. The broad band observed

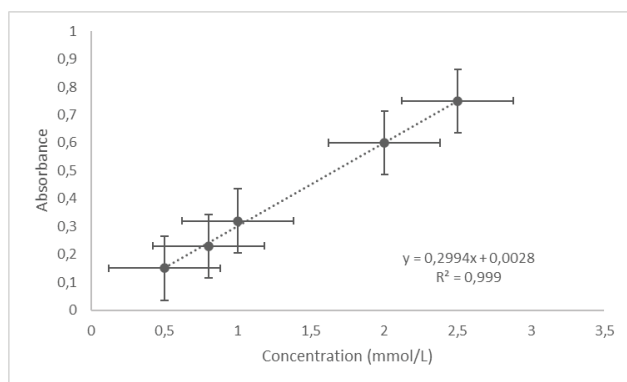


Figure 6. Linearity and range graph of fampridine.

at  $3377\text{ cm}^{-1}$  of PVA is believed to be due to the O-H stretching vibration band. The band observed around  $2921\text{ cm}^{-1}$  is thought to be the aliphatic C-H stretching band. In the Na-Alg FTIR spectrum, the broad band around  $3428\text{ cm}^{-1}$  corresponds to the O-H stretching band, the band at  $2928\text{ cm}^{-1}$  corresponds to the aliphatic C-H band, and the band at  $1618\text{ cm}^{-1}$  corresponds to the ( $\text{C}=\text{O}$ ) group.

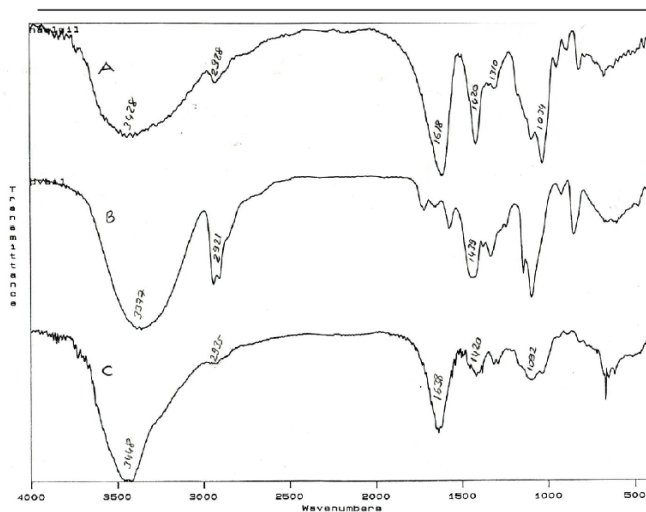


Figure 7. FT-IR results PVA (A), Na-Alg (B), and empty microsphere O (C)

Table 4. EE and particle size of microspheres

	PVA: Na-Alg	d:p	EE%	Mean particle size ( $\mu\text{m}$ )*
O1	1:1	1:0.5	73.5 $\pm$ 6.6	640.6 $\pm$ 1.2
O2	1:1	1:1	72.1 $\pm$ 2.2	535.3 $\pm$ 0.9
O3	1:1	1:1.25	64.7 $\pm$ 1.3	485.4 $\pm$ 1.1
O4	1:1	1:1.5	60.1 $\pm$ 5.6	360.8 $\pm$ 0.6
O5	1:1	1:2	40.4 $\pm$ 0.1	310.4 $\pm$ 0.7
P1	2:1	1:0.5	79.1 $\pm$ 3.8	710.3 $\pm$ 1.6
P2	2:1	1:1	74.5 $\pm$ 6.1	595.6 $\pm$ 1.3
P3	2:1	1:1.25	72.1 $\pm$ 4.3	520.2 $\pm$ 0.9
P4	2:1	1:1.5	60.6 $\pm$ 2.4	390.3 $\pm$ 0.6
P5	2:1	1:2	45.8 $\pm$ 1.8	340.7 $\pm$ 0.7
K1	3:1	1:0.5	87.4 $\pm$ 3.2	780.6 $\pm$ 2.1
K2	3:1	1:1	80.8 $\pm$ 3.9	630.4 $\pm$ 1.8
K3	3:1	1:1.25	75.1 $\pm$ 4.8	580.4 $\pm$ 1.4
K4	3:1	1:1.5	61.3 $\pm$ 2.9	406.8 $\pm$ 1.3
K5	3:1	1:2	55.7 $\pm$ 3.1	380.3 $\pm$ 1.5
L1	3:1	1:1.25	50.4 $\pm$ 6.2	532.3 $\pm$ 0.9
L2	3:1	1:1.25	80.1 $\pm$ 3.6	714.2 $\pm$ 0.6
M1	3:1	1:1.25	80.8 $\pm$ 2.8	695.6 $\pm$ 0.4
M2	3:1	1:1.25	54.6 $\pm$ 4.2	510.8 $\pm$ 0.2

\* $\pm$  SD, n= 3. d:p: Drug: polymer, PVA: Polyvinyl alcohol, Na-Alg: Sodium alginate, EE: Encapsulation efficiency, SD: Standard deviation

It was observed that in the PVA: Na-Alg microspheres, the stretching band of ( $\text{>C} = \text{O}$ ) shifted to  $1638 \text{ cm}^{-1}$  due to its incorporation into the blend structure, and the aliphatic C-H band in the empty microsphere shifted from  $2935 \text{ cm}^{-1}$  to  $2928 \text{ cm}^{-1}$  upon incorporation of the drug into the structure.

**Table 5. Linearity and range results**

Linearity level %	Fampridine concentration (mmol/L)	Absorbance
50%	0.5	0.15
80%	0.8	0.23
100%	1.0	0.32
200%	2.0	0.60
250%	2.5	0.75
Average		0.41
Standard deviation		0.25

**Table 6. System precision results**

Sample (1 mmol/L)	Absorbance
1	0.32
2	0.30
3	0.28
4	0.31
5	0.29
6	0.32
Average	0.30
SD	0.016
RSD%	5.3
Confidence range (n= 6)	$0.30 \pm 0.01$

**Table 7. Repeatability results**

	1 <sup>st</sup> day	2 <sup>nd</sup> day
Sample (O5)	Absorbance	Absorbance
1	0.27	0.26
2	0.28	0.28
3	0.29	0.28
4	0.27	0.27
5	0.28	0.29
6	0.28	0.28
Average	0.28	0.28
SD	0.007	0.01
RSD%	2.7	3.7
Confidence range (n= 6)	$0.28 \pm 0.006$	$0.28 \pm 0.008$

SD: Standard deviation, RSD: Relative standard deviation

### DSC results

DSC diagrams of PVA, Na-Alg, and PVA: Na-Alg 1:1 microspheres (O5) are shown in Figure 9. Results showed that the  $T_g$  value of PVA was  $87^\circ\text{C}$ , the PVA: Na-Alg microsphere is  $95^\circ\text{C}$ , and the Na-Alg is  $102^\circ\text{C}$ . The higher  $T_g$  value of the PVA: Na-Alg microspheres compared to PVA and lower  $T_g$  value compared to Na-Alg indicates the compatibility of these polymers.<sup>35</sup>

### SEM results

SEM analysis was performed with the highest release observed in the O5 and empty microspheres (O). Results are shown in Figure 10. It was observed that after loading the drug into the microspheres, the surface became roughened, and there was a tendency toward shape distortion.

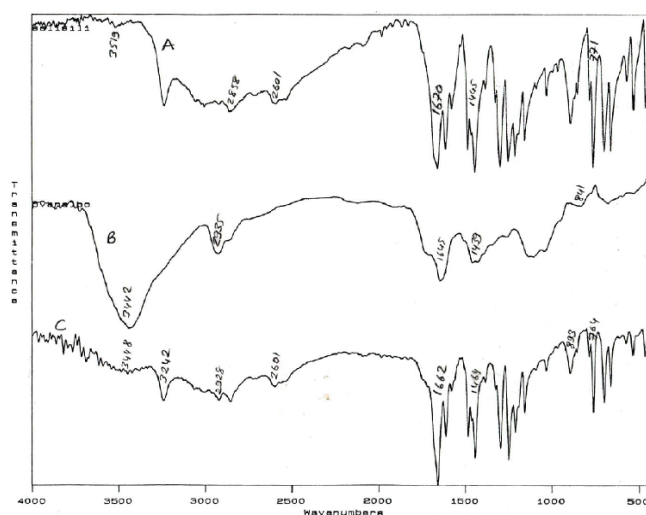


**Figure 8.** Fampridine (A), empty microsphere O (B), and microsphere O5 (C)

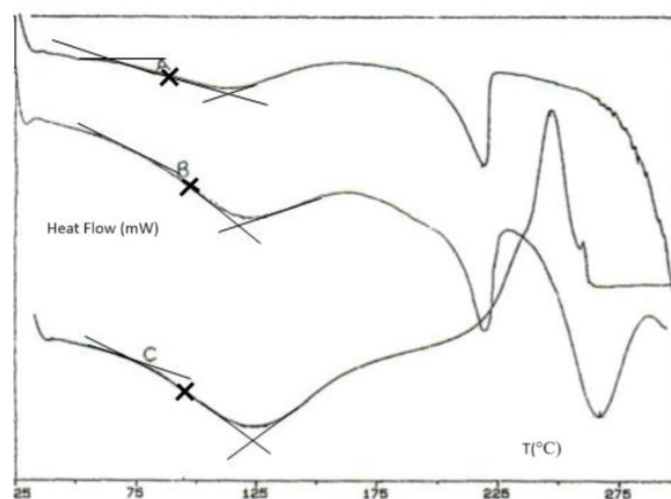


**Figure 9.** DSC results. PVA (A) O5 microspheres, (B) PVA: Na-Alg (C)

DSC: Differential scanning calorimetry, PVA: Polyvinyl alcohol, Na-Alg: Sodium alginate

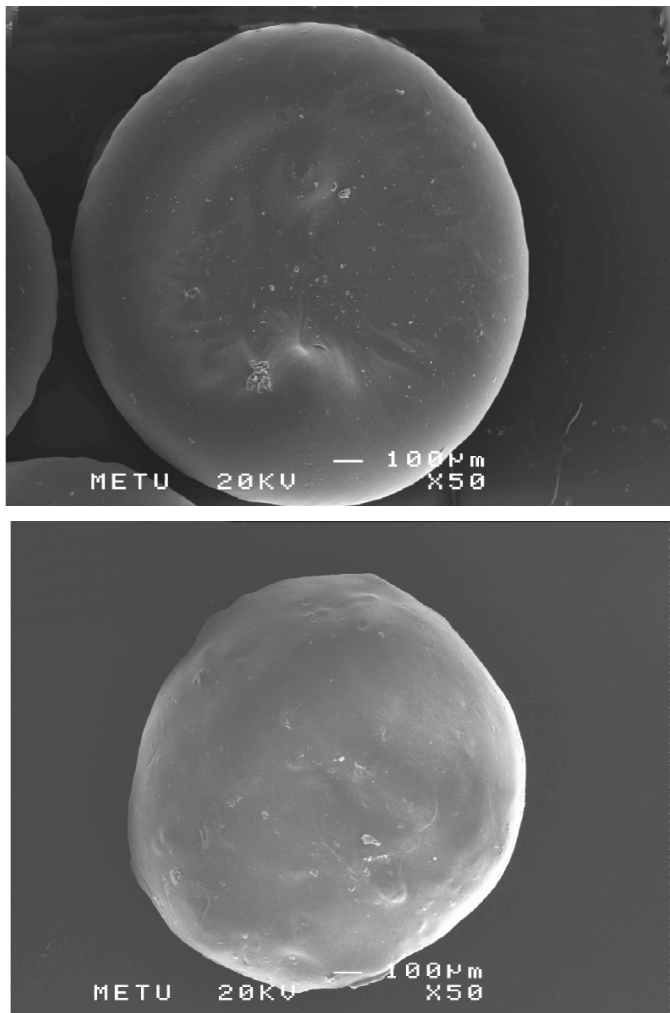


**Figure 10.** SEM results of 0 and 05 microspheres  
SEM: Scanning electron microscopy

## CONCLUSION

It was observed that as the amount of PVA increased in PVA: Na-Alg microspheres, the release decreased and determined that drug release in the microspheres generally increased as the d:p ratio decreased. The optimal d:p (*w:w*) ratio for PVA: Na-Alg microspheres was found to be 1:2. It was observed that an increase in the concentration of the cross-linking agent and the cross-linking time resulted in a decrease in the release rate. It was determined that drug release from the microspheres was affected by the pH of the environment. As the pH value increased, the release of fampridine from PVA: Na-Alg microspheres also increased, with the best release rate observed at pH 7.4. As a result of the studies, it was determined that fampridine release was highest (89%) in microspheres (05) prepared with a PVA: Na-Alg (*w:w*) ratio of 1:1, and d:p ratio of 1:2 (*w:w*), in a cross-linking solution with a concentration of 2.5% GA + 3.0% HCl (*v:v*), and with a cross-linking time of 5 minutes.

## DISCUSSION

The results of this study underscore the effectiveness of using bio-based microspheres for the controlled release of fampridine.

The optimal formulation, achieved with a PVA:Na-Alg ratio of 1:1, a drug-to-polymer ratio of 1:2, and specific cross-linking conditions, demonstrated the highest release rate of fampridine. These findings are consistent with previous research indicating that the balance between polymer types, cross-linking agents, and ratios significantly influences drug release kinetics. The use of PVA and sodium alginate as biocompatible polymers is particularly advantageous as they allow for a controlled and sustained release, which is crucial for the management of conditions like multiple sclerosis, where consistent therapeutic levels of the drug are desired. The observed increase in particle size with a higher d:p ratio suggests that the drug is more effectively encapsulated in larger microspheres, which may provide enhanced stability and release control. While the results are promising, further studies are needed to explore the long-term stability of these microspheres, their *in vivo* behavior, and their comparability to existing treatments, such as Fampyra 10 mg, in clinical settings.

### Ethics

**Ethics Committee Approval:** There is no requirement for ethical approval.

**Informed Consent:** Not required.

### Authorship Contributions

Concept: S.A.Ö., F.Y.G., Design: S.A.Ö., F.Y.G., Data Collection or Processing: S.A.Ö., F.Y.G., Analysis or Interpretation: S.A.Ö., Literature Search: S.A.Ö., Writing: S.A.Ö.

**Conflict of Interest:** The authors have no conflicts of interest to declare.

**Financial Disclosure:** The authors declared that this study received no financial support.

## REFERENCES

- Mamoei S, Hvid LG, Boye Jensen H, Zijdwind I, Stenager E, Dalgas U. Neurophysiological impairments in multiple sclerosis-central and peripheral motor pathways. *Acta Neurol Scand.* 2020;142:401-417.
- Filli L, Werner J, Beyer G, Reuter K, Petersen JA, Weller M, Zörner B, Linnebank M. Predicting responsiveness to fampridine in gait-impaired patients with multiple sclerosis. *Eur J Neurol.* 2019;26:281-289.
- Bakirtzis C, Konstantinopoulou E, Langdon DW, Grigoriadou E, Minti F, Nikolaidis I, Boziki MK, Tatsi T, Ioannidis P, Karapanayiotides T, Afrantou T, Hadjigeorgiou G, Grigoriadis N. Long-term effects of prolonged-release fampridine in cognitive function, fatigue, mood and quality of life of MS patients: The IGNITE study. *J Neurol Sci.* 2018;395:106-112.
- Thorning M, Nielsen HH, Frich LH, Jensen HB, Lambertsen KL, Holsgaard-Larsen A. Gait quality and function after fampridine treatment in patients with multiple sclerosis-a prospective cohort study. *Clin Biomech (Bristol, Avon).* 2022;100:105826.
- Mamoei S, Jensen HB, Pedersen AK, Madsen CG, Plenge T, Nielsen HH, Oturai AB, Illes Z, Sellebjerg F, Frederiksen JL. Clinical, neurophysiological, and MRI markers of fampridine responsiveness in multiple sclerosis-an explorative study. *Front Neurol.* 2021;12:758710.
- Weller D, Lörcincz L, Sutter T, Bohli D, Grob D, Zörner B, Gharabaghi A, Roth F. Fampridine-induced changes in walking kinetics are associated

- with clinical improvements in patients with multiple sclerosis. *J Neurol Sci.* 2020;416:116978.
7. Thorning M, Nielsen HH, Frich LH, Jensen HB, Lambertsen KL, Holsgaard-Larsen A. Gait quality and function after fampridine treatment in patients with multiple sclerosis—a prospective cohort study. *Clin Biomech (Bristol, Avon).* 2022;100:105826.
  8. Castelnovo G, Gerlach O, Freedman MS, Rieckmann P, Schreiber K, Torkildsen Ø, Helland CA, Trojano M, Oreja-Guevara C, Vermersch P, Fuchs T, Stamenković I, Leist TP, Montalban X. Safety, patient-reported well-being, and physician-reported assessment of walking ability in patients with multiple sclerosis for prolonged-release fampridine treatment in routine clinical practice: results of the LIBERATE Study. *CNS Drugs.* 2021;35:1009-1022.
  9. Maghsoudi S, Shahraki BT, Rabiee N, Fatahi Y, Dinarvand R, Bagherzadeh M, Ahmadi S, Rabiee M, Jajarmi V, Saeb MR, Mozafari M. Burgeoning polymer nano blends for improved controlled drug release: a review. *Int J Nanomedicine.* 2020;15:4363-4392.
  10. Iturriz-Rodríguez N, Correa-Duarte MA, Fanarraga ML. Controlled drug delivery systems for cancer based on mesoporous silica nanoparticles. *Int J Nanomedicine.* 2019;14:3389-3401.
  11. Khoe S, Rahimi S. Reversible coreshell crosslinked micelles for controlled release of bioactive agents In: Grumezescu AM, ed. *Nanoarchitectonics Biomed*, 1<sup>st</sup> edition, Romania. 2019;119-167.
  12. Hyland SJ, Deliberato DG, Fada RA, Romanelli MJ, Collins CL, Wasielewski RC. Liposomal bupivacaine versus standard periarticular injection in total knee arthroplasty with regional anesthesia: a prospective randomized controlled trial. *J Arthroplasty.* 2019;34:488-494.
  13. Damiri F, Bachra Y, Bounacir C, Laaraibi A, Berrada M. Synthesis and characterization of lyophilized chitosan-based hydrogels cross-linked with benzaldehyde for controlled drug release. *J Chem.* 2020;10.
  14. Guo B, Qu J, Zhao X, Zhang M. Degradable conductive self-healing hydrogels based on dextran-graft-tetraaniline and N-carboxyethyl chitosan as injectable carriers for myoblast cell therapy and muscle regeneration. *Acta Biomater.* 2019;84:180-193.
  15. Zhang A, Jung K, Li A, Liu J, Boyer C. Recent advances in stimuli-responsive polymer systems for remotely controlled drug release. *Prog Polym Sci.* 2019;99:101164.
  16. Thakur S, Pandey S, Arotiba OA. Development of a sodium alginate-based organic/inorganic superabsorbent composite hydrogel for adsorption of methylene blue. *Carbohydr Polym.* 2016;153:34-46.
  17. Shi Y, Peng L, Yu G. Nanostructured conducting polymer hydrogels for energy storage applications. *Nanoscale.* 2015;7:12796-12806.
  18. Shivakumara LR, Demappa T. Synthesis and swelling behavior of sodium alginate/poly (vinyl alcohol) hydrogels. *Turk J Pharm Sci.* 2019;16:252-260.
  19. Bialik-Wąs K, Królicka E, Malina D. Impact of the type of crosslinking agents on the properties of modified sodium alginate/poly (vinyl alcohol) hydrogels. *Molecules.* 2021;26:2381.
  20. Afshar M, Dini G, Vaezifar S, Mehdikhani M, Movahedi B. Preparation, and characterization of sodium alginate/polyvinyl alcohol hydrogel containing drug-loaded chitosan nanoparticles as a drug delivery system. *J Drug Deliv Sci Technol.* 2021;56:101530.
  21. Lin X, Yang H, Su L, Yang Z, Tang X. Effect of size on the *in vitro/in vivo* drug release and degradation of exenatide-loaded PLGA microspheres. *J Drug Deliv Sci Technol.* 2018;45:346-356.
  22. Caballero Aguilar LM, Duchi S, Onofrillo C, O'Connell CD, Di Bella C, Moulton SE. Formation of alginate microspheres prepared by optimized microfluidics parameters for high encapsulation of bioactive molecules. *J Colloid Interface Sci.* 2021;587:240-251.
  23. Park H. Exploring the effects of process parameters during W/O/W emulsion preparation and supercritical fluid extraction on the protein encapsulation and release properties of PLGA microspheres. *Pharmaceutics.* 2024;16:302.
  24. Rastogi R, Sultana Y, Aqil M, Ali A, Kumar S, Chuttani K, Mishra AK. Alginate microspheres of isoniazid for oral sustained drug delivery. *Int J Pharm.* 2007;334:71-77.
  25. ICH Q2(R2) guideline on validation of analytical procedures-Step 5-Revision 1. Reference Number: EMA/CHMP/ICH/804363/2022 Legal effective date:14/06/2024. <https://www.fda.gov/media/165049/download>
  26. Jin L, Bai R. Mechanisms of lead adsorption chitosan/PVA hydrogel beads. *Langmuir.* 2002;18:9765-9770.
  27. Kumar MK, Yadav I, Kumar SR, Singh NB, Kumar SS, Ray B, Kumar M, Misra N. Polyvinyl alcohol/chitosan lactate composite hydrogel for controlled drug delivery. *Mater Res Express.* 2019;6:115408.
  28. Mulchandani N, Shah N, Mehta T. Synthesis of chitosan-polyvinyl alcohol copolymers for smart drug delivery application. *Polymers.* 2023;15:2028.
  29. Hayes KC. The use of 4-aminopyridine (fampridine) in demyelinating disorders. *CNS Drug Rev.* 2004;10:295-316.
  30. El-Okaily M, EL-Rafei A, Basha M, Shalaby H, Elgindy NA. Efficient drug delivery vehicles of environmentally benign nano-fibers comprising bioactive glass/chitosan/polyvinyl alcohol composites. *Int J Biol Macromol.* 2021;182:1582-1589.
  31. Zhixiang C, Feng Z, Luyin L, Jianhong Z, Zhiping W. Electrospinning, and crosslinking of polyvinyl alcohol/chitosan composite nanofiber for transdermal drug delivery. *ACS Mater.* 2023;13:464-448.
  32. El-Sherbiny I, Lins RJ, Abdal-Bary E, Harding D. Preparation, characterization, swelling and *in vitro* drug release behaviour of poly (Nacryloylglycine-chitosan) interpolymers pH and thermally responsive hydrogels. *Eur Polym J.* 2005;41:2584-2591.
  33. Gritskova IA, Prokopov NI, Ezhova AA, Frolova AY, Khripunov AK. New approaches to the synthesis and stabilization of polymer microspheres with a narrow size distribution. *Polymers.* 2023;15:2464.
  34. Aiedeh K, Gianasi E, Orienti I, Zecchi V. Chitosan microcapsules as controlled release systems for insulin. *J Microencapsul.* 1997;14:567-576.
  35. Zhao L, Mitomo H, Zhai M, Yoshii F, Nagasawa N, Kum T. Synthesis of antibacterial PVA/CM-chitosan blend hydrogels with electron beam irradiation. *Carbohydr Polym.* 2003;53:439-446.



# *In silico* Evaluation of H1-Antihistamine as Potential Inhibitors of SARS-CoV-2 RNA-dependent RNA Polymerase: Repurposing Study of COVID-19 Therapy

✉ Mazin HAMDAN<sup>1</sup>, ✉ Necla KULABAŞ<sup>2</sup>, ✉ İlkey KÜÇÜKGÜZEL<sup>3\*</sup>

<sup>1</sup>Marmara University Institute of Health Sciences, Department of Pharmaceutical Chemistry, İstanbul, Türkiye

<sup>2</sup>Marmara University Faculty of Pharmacy, Department of Pharmaceutical Chemistry, İstanbul, Türkiye

<sup>3</sup>Fenerbahçe University Faculty of Pharmacy, Department of Pharmaceutical Chemistry, İstanbul, Türkiye

## ABSTRACT

**Introduction:** Severe Acute Respiratory Syndrome Coronavirus 2 (SARS-CoV-2), from the family Coronaviridae, is the seventh known coronavirus to infect humans and cause acute respiratory syndrome. Although vaccination efforts have been conducted against this virus, which emerged in Wuhan, China, in December 2019 and has spread rapidly around the world, the lack of an Food and Drug Administration-approved antiviral agent has made drug repurposing an important approach for emergency response during the COVID-19 pandemic. The aim of this study was to investigate the potential of H1-antihistamines as antiviral agents against SARS-CoV-2 RNA-dependent RNA polymerase enzyme.

**Materials and Methods:** Using molecular docking techniques, we explored the interactions between H1-antihistamines and RNA-dependent RNA polymerase (RdRp), a key enzyme involved in viral replication. The three-dimensional structure of 37 H1-antihistamine molecules was drawn and their energies were minimized using Spartan 0.4. Subsequently, we conducted a docking study with Autodock Vina to assess the binding affinity of these molecules to the target site. The docking scores and conformations were then visualized using Discovery Studio.

**Results:** The results examined showed that the docking scores of the H1-antihistamines were between 5.0 and 8.3 kcal/mol. These findings suggested that among all the analyzed drugs, bilastine, fexofenadine, montelukast, zafirlukast, mizolastine, and rupatadine might bind with the best binding energy ( $< -7.0$  kcal/mol) and inhibit RdRp, potentially halting the replication of the virus.

**Conclusion:** This study highlights the potential of H1-antihistamines in combating COVID-19 and underscores the value of computational approaches in rapid drug discovery and repurposing efforts. Finally, experimental studies are required to measure the potency of H1-antihistamines before their clinical use against COVID-19 as RdRp inhibitors.

**Keywords:** SARS-CoV-2, RNA-dependent RNA polymerase, molecular docking, H1-antihistamines, drug repurposing

## INTRODUCTION

Infectious diseases caused by various microorganisms, including viruses, bacteria, fungi, and parasites, continue to be one of the most significant public health issues.<sup>1</sup> Among the most serious infection categories, RNA virus infections significantly contribute to the global index of mortality and morbidity associated with viral infections. Chronic disease caused by

persistent RNA virus infections represents a significant public health concern.<sup>2</sup> The global population continues to combat many infectious diseases caused by these pathogens, some of which have become epidemics or pandemics.<sup>3</sup> The World Health Organization declared the Coronavirus Disease of 2019 (COVID-19), caused by Severe Acute Respiratory Syndrome Coronavirus 2 (SARS-CoV-2), a global public health emergency

\*Correspondence: [ilkay.kucukguzel@fbu.edu.tr](mailto:ilkay.kucukguzel@fbu.edu.tr) ORCID-ID: [orcid.org/0000-0002-7188-1859](https://orcid.org/0000-0002-7188-1859)

Received: 31.05.2024, Accepted: 23.06.2024



Copyright© 2024 The Author. Published by Galenos Publishing House on behalf of Turkish Pharmacists' Association. This is an open access article under the Creative Commons Attribution-NonCommercial-NoDerivatives 4.0 (CC BY-NC-ND) International License.

on March 11, 2020, due to its extensive impact. By early May 2024, more than 7 million deaths and over 775 million infected cases had been reported.<sup>4</sup> The first known case of SARS-CoV-2 was identified in Wuhan, China. The virus is an RNA virus from the Coronaviridae family that rapidly led to a global pandemic because of its high transmissibility.<sup>5-7</sup> The Beta, Gamma, Delta, and Omicron variants arising from SARS-CoV-2 viral mutations have also caused significant damage to the world economy. Repurposed drugs and vaccines developed to combat the pandemic have played a crucial role in mitigating the pandemic's impact and restoring socioeconomic stability.<sup>8</sup>

Reuse can be achieved through high-efficiency *in vitro* analyses, *in vivo* animal investigations, and computer-aided drug discovery. Studies on the reuse of many known drugs, including antivirals, antimalarials, H1-antihistamines, antipsychotics, and anticancer agents, are available in the literature.<sup>9-13</sup> Although known safety profiles of approved drugs have allowed rapid progress in clinical trials, limited success has been achieved in identifying clinically effective small-molecule drugs for COVID-19 treatment.<sup>14-16</sup>

H1-antihistamines are a class of drugs commonly used to treat allergic reactions, such as hay fever, hives, and itching.<sup>17</sup> They work by blocking the action of histamine, a substance in the body that causes allergic symptoms. H1-antihistamines can be divided into two main types; first-generation and second-generation. First-generation H1-antihistamines, such as diphenhydramine and chlorpheniramine, tend to cause more drowsiness and are often used for short-term relief of symptoms. Second-generation H1-antihistamines, such as loratadine and cetirizine, require less sedation and are preferred for long-term use.<sup>18</sup> Traditionally recognized for their role in mitigating allergic responses by antagonizing histamine

receptors, H1-antihistamines have recently attracted attention for their broader pharmacological effects, including potential antiviral properties. This paradigm shift is underpinned by advancements in computational modeling and virtual screening methodologies, which enable us to elucidate the intricate molecular interactions between H1-antihistamines and viral targets.

In a study conducted in 2021, H1-antihistamine agents such as hydroxyzine, azelastine, and diphenhydramine were reported to have *in vitro* antiviral activity against SARS-CoV-2. Moreover, it was reported that hydroxyzine exhibits antiviral activity through the mechanism of angiotensin-converting enzyme 2 inhibition, whereas azelastine and diphenhydramine exert their effects by binding to the sigma-1 receptor.<sup>12</sup> In another study reported by Ghahremanpour et al.,<sup>11</sup> it was found that azelastine has the potential to inhibit the main protease, which is a structural protein of SARS-CoV-2. Additionally, it has been reported in the literature that fexofenadine, another H1-antihistamine, has the potential to inhibit the SARS-CoV-2 helicase enzyme.<sup>10</sup> The interactions of H1-antihistamines with antiviral targets reported in the literature are summarized in Figure 1.

Although the body systems affected, transmission routes, and symptoms are different, there are many studies investigating similarities between the non-structural (NS3) proteins of SARS-CoV-2 and hepatitis-C virus (HCV). These studies indicate that these proteins share structural similarities as well as functional properties. Specifically, NS3 proteins include proteases and helicases that are critical in the replication process of both viruses. These similarities could guide the development of potentially effective antiviral agents against the NS3 proteins of SARS-CoV-2 and HCV. In a groundbreaking study published in 2014, Mingorance et al.<sup>19</sup> revealed compelling evidence of

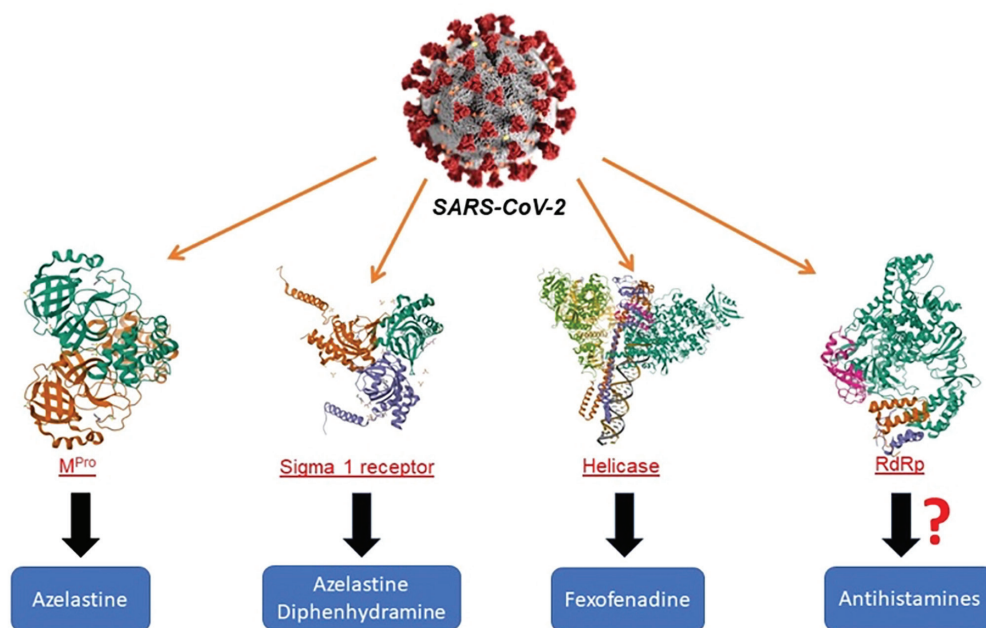


**Figure 1.** Antiviral effects of the known antihistamines against vital enzymes of SARS-CoV-2  
SARS-CoV-2: Severe Acute Respiratory Syndrome Coronavirus 2, RdRp: RNA-dependent RNA polymerase

the selective inhibition of HCV infection by hydroxyzine and benztropine. This study, led by esteemed experts in virology, revealed the remarkable antiviral properties of these two compounds, shedding light on their potential as potent agents against HCV. Through meticulous experimentation and rigorous analysis, the researchers elucidated the mechanism by which hydroxyzine and benztropine exert their inhibitory effects on HCV infection. By selectively targeting key NS3 proteins or host cell factors crucial for viral replication, these compounds demonstrated a remarkable ability to disrupt the viral lifecycle, thereby impeding viral propagation and spread. The findings of this study not only underscore the significance of hydroxyzine and benztropine as possible candidates for antiviral therapy against HCV but also pave the way for further exploration of their therapeutic potential in combating other viral infections.<sup>19</sup> Similarly, a notable study by Zongyi et al.<sup>20</sup> revealed that chlorcyclizine exerts its antiviral effect against HCV by targeting the viral envelope glycoprotein. This finding underscores the potential of chlorcyclizine as a promising antiviral agent against HCV infection.<sup>20</sup>

In the dynamic landscape of drug discovery, the integration of computational techniques has revolutionized pharmaceutical intervention exploration.<sup>21</sup> *In silico* studies, which encompass a spectrum of computational methods, have emerged as invaluable tools for accelerating the identification and evaluation of potential drug candidates. In the approach to repurposing known drugs, the primary objective of computational and experimental techniques has been to identify existing drugs that may be effective against SARS-CoV-2.

In RNA viruses like SARS-CoV-2, the RNA-dependent RNA polymerase (RdRp) enzyme creates the machinery required for RNA synthesis and the organized replication and transcription of genomic RNA.<sup>22</sup> After the virus attacks a host cell, viral genomic RNA is used directly as a template, and the host cell's protein synthesis machinery is utilized to translate RdRp.<sup>23</sup> RdRp is an enzyme crucial for RNA virus replication.<sup>24</sup> It catalyzes the synthesis of RNA from an RNA template, a process essential for the reproduction of RNA viruses like influenza, hepatitis C, and coronaviruses (including SARS-CoV-2). RdRp is a prime target for antiviral drugs aimed at inhibiting viral replication. In the context of the COVID-19 pandemic, drugs like redeliver have gained attention for their ability to inhibit RdRp and potentially

reduce the severity of the disease.<sup>25</sup> The structure of the SARS-CoV-2 RdRp complex comprises a core catalytic unit consisting of a non-structural protein 12 (nsp12) core, an nsp7-nsp8 (nsp8-1) heterodimer, and an additional nsp8 subunit (nsp8-2) (Figure 2). The nsp12-nsp7-nsp8 complex is the minimal core component of viral RNA replication.<sup>26</sup> The 30-kb SARS-CoV-2 genome contains 14 open reading frames (ORF) that encode at least 27 proteins.<sup>27</sup> The ORF 1 ab region at the 5' end consists of a polyprotein that is hydrolyzed to 16 non-structural proteins nsp1-16 to form a replicase/transcriptase complex (RTC). The main RTC is RdRp nsp-12.<sup>28</sup> Nsp-12 has 8 motifs (A to G); Motif C (F753-N767) contains the catalytic motif SDD (Ser759, Asp760, and Asp761), which is required for metal-ion binding,<sup>26</sup> and this site is going to be our main target in this study.

This study lays the groundwork for exploring the rapidly growing field of *in silico* research aimed at uncovering the antiviral potential of H1-antihistamines. By utilizing molecular modeling techniques, we seek to understand the mechanisms behind the potential antiviral effects of SARS-CoV-2 RdRp enzyme inhibition. Moreover, these investigations provide insights into the therapeutic potential of H1-antihistamines against various viral infections, opening new possibilities for drug repurposing and therapeutic development. Although montelukast and zafirlukast are not typically classified as H1-antihistamines, they belong to a class of medications known as leukotriene receptor antagonists. These drugs work by blocking the action of leukotrienes, which are inflammatory substances produced by the body in response to allergens or other triggers. Although they are often used to manage asthma and allergic rhinitis, they do not directly target histamine receptors, as traditional H1-antihistamines do. However, they can help relieve symptoms associated with allergic reactions, such as inflammation and bronchoconstriction.<sup>29</sup> Since the potential of zafirlukast to inhibit the SARS-CoV-2 helicase enzyme has been reported in the literature,<sup>30</sup> an *in silico* investigation of montelukast and zafirlukast was also conducted.

## MATERIALS AND METHODS

### System preparation

### Protein preparation

The recently reported high-resolution X-ray structure of RdRp (2.90 Å) (PDB ID 6M71: <https://www.rcsb.org/3d-view/>)

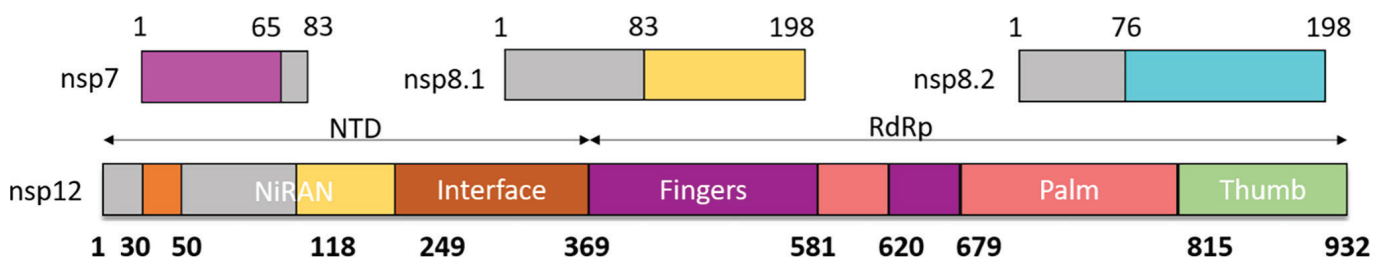


**Figure 2.** Domain organization of SARS-CoV-2 and its (RdRp). Interdomain boundaries are labeled with residue numbers. Here we can see nsp12<sup>22</sup> SARS-CoV-2: Severe Acute Respiratory Syndrome Coronavirus 2, RdRp: RNA-dependent RNA polymerase, NTD: N-Terminal Domain

ngl/6m71)<sup>26</sup> was used in this study. After obtaining the protein crystal structure, all water molecules and ions were initially deleted. The protein was then saved in .pdb format and subsequently converted to .pdbqt format using Autodocktools 1.5.7.<sup>31</sup> Later, the regions of Ser759, Asp760, and Asp761 were determined as the locations of the grid box (114.52, 114.11,122.91) using Discovery Studio 2021 and Autodocktools 1.5.7.

#### Preparation of the ligands

All ligands were drawn using Spartan 4.0, and each molecule's energy was also minimized using Spartan 4.0.<sup>32</sup> The conformations with the lowest energy were saved in .pdb format and then converted to .pdbqt format using Autodocktools 1.5.7. Brompheniramine, levocetirizine, montelukast, and chlorpheniramine were selected as their pharmacologically active (R) stereoisomers. Cetirizine, dexchlorpheniramine, and triprolidine were selected as their pharmacologically active (S) stereoisomers.

#### Molecular docking

The determination of the grid box region (114.52, 114.11,122.91) and dimensions (30,30,30 Å) to include the Ser759, Asp760, and Asp761 regions was performed using AutodockTools 1.5.7. and Discovery Studio 2021. Then, molecular docking was performed using Autodock Vina.<sup>33</sup> Each docking process was repeated at least 3 times to ensure the accuracy of the results. Later, each molecule docking score and confirmation were visualized using Discovery Studio 2021. Each molecule's binding energy is presented in Supplementary Figure 1.

## RESULTS

In this study, the *in silico* binding potentials of 37 drugs, including Food and Drug Administration-approved H1-antihistamines as well as montelukast and zafirlukast, against SARS-CoV-2 RdRp were examined (see Supplementary Figure 1). Table 1-7 present comprehensive visual representations of the three-dimensional (3D) and two-dimensional (2D) interactions of the best potential SARS-CoV-2 RdRp inhibitors, bilastine, fexofenadine, montelukast, zafirlukast, mizolastine, rupatadine, and terfenadine, respectively.

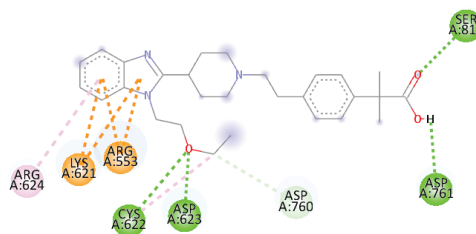
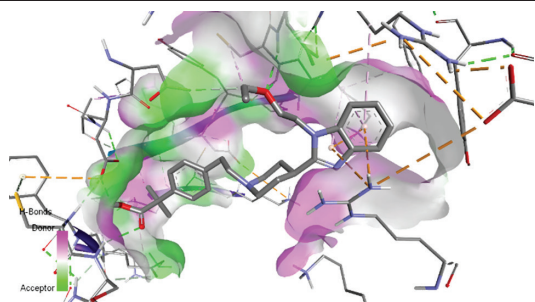
The docking results indicate that bilastine effectively binds to RdRp, primarily through hydrogen bonds and electrostatic interactions (Table 1). The strong binding energy and specific interactions suggest that bilastine inhibits the function of RdRp, potentially blocking viral replication. Bilastine showed significant binding affinity against the SARS-CoV-2 RdRp enzyme at 7.6 kcal/mol. The carboxylic acid group within bilastine forms crucial hydrogen bonds with specific residues of RdRp, highlighting the intricate nature of their molecular interactions. One notable interaction occurred between the carboxylic acid group and Asp761, wherein a hydrogen bond was established with a bond length of 2.26 Å. Additionally, another hydrogen bond was detected between this group and Ser814, further emphasizing the nuanced connectivity between bilastine and RdRp, characterized by a bond length of 2.43 Å. Moreover, the ethoxy group present in bilastine significantly

contributed to its interaction with RdRp. This group forms hydrogen bonds with Asp623 and Cys622, highlighting the multifaceted nature of bilastine's engagement with the receptor. The hydrogen bond lengths between the ethoxy group and Asp623 and Cys622 were measured at 2.25 Å and 2.27 Å, respectively. Beyond hydrogen bonding, electrostatic and cationic interactions also play substantial roles in shaping the binding profile of bilastine with RdRp. The benzimidazole moiety within bilastine demonstrates such interactions with key residues of RdRp, namely Arg553 and Lys621.

These interactions occurred at distances of 4.27 Å and 4.32 Å with Arg553 and at distances of 4.94 Å and 4.78 Å with Lys621, highlighting the diverse array of molecular forces involved in bilastine-RdRp binding. The interactions with critical residues such as Asp761, Ser814, and Arg553 underscore the potential of bilastine as a therapeutic candidate and warrant further investigation.

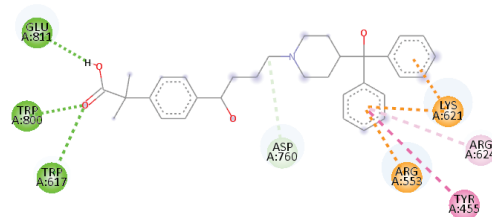
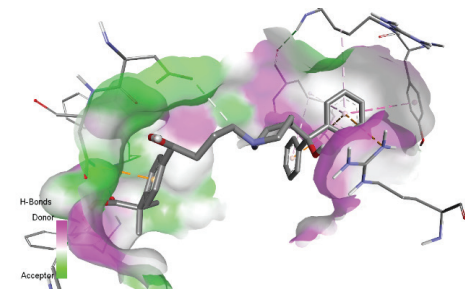
Our docking study identified fexofenadine (Table 2) as a potential inhibitor of SARS-CoV-2 RdRp. The docking results revealed a binding energy of -8.0 kcal/mol, indicating strong binding affinity. In the context of molecular interactions, the carboxylic acid group of fexofenadine plays a crucial role by forming significant hydrogen bonds with specific residues of RdRp. Notably, hydrogen bonds were formed between Trp617 and Trp800 with bond lengths of 2.91 Å and 2.76 Å, respectively. Moreover, a particularly strong hydrogen bond was formed with Glu811, with a bond length of 2.02 Å. Beyond hydrogen bonding, fexofenadine exhibits hydrophobic and pi interactions, further enriching its binding profile with RdRp. The phenyl group of fexofenadine engages in hydrophobic and pi interactions with Tyr455 and Arg553, with distances of 5.57 Å and 4.38 Å, respectively. Additionally, multiple interactions with Lys621 were observed, including electrostatic/pi-cation interactions at distances of 4.62 Å and 5.46 Å. Furthermore, a hydrophobic/pi-alkyl interaction was noted with Arg624, at a distance of 3.09 Å. In summary, a comprehensive analysis of hydrogen bonding, hydrophobic interactions, pi interactions, and additional interactions revealed the intricate molecular landscape governing the interaction between fexofenadine and RdRp, offering valuable insights into its potential therapeutic efficacy against viral infections.

Montelukast, with a binding energy of -7.2 kcal/mol, demonstrated a multifaceted binding profile characterized by hydrogen bonding, hydrophobic interactions, and electrostatic contacts (Table 3). Specifically, the hydrogen bonds formed between montelukast and key residues Lys798, Trp800, and Asp760 underscore the importance of specific molecular recognition patterns in stabilizing the Montelukast-RdRp complex. Moreover, hydrophobic interactions with Tyr455 and electrostatic interactions with Lys621 provided additional stability to the complex, highlighting the diverse array of interactions contributing to the ligand-receptor binding. Three hydrogen bonds are predicted to form between montelukast's carboxylic acid group and residues Lys798, Trp800, and Asp760 of RdRp. These hydrogen bonds significantly contribute to the

**Table 1. Interactions of bilastine with the active site of RdRp**

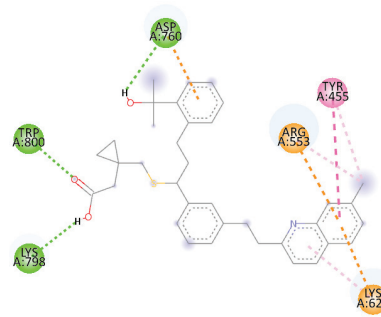
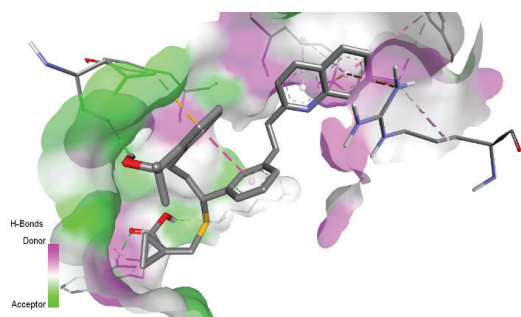
Functional group	Residue	Bond	Distance (Å)
Carboxylic acid	Asp761	H-bond (A-B)	2.26
Carboxylic acid	Ser814	H-bond (D-B)	2.43
Ethoxy	Asp623	H-bond (D-S)	2.25
Ethoxy	Cys622	H-bond (D-S)	2.27
Benzimidazole	Arg553	Electrostatic/pi-cation	4.27
Benzimidazole	Arg553	Electrostatic/pi-cation	4.32
Benzimidazole	Lys621	Electrostatic/pi-cation	4.94
Benzimidazole	Lys621	Electrostatic/pi-cation	4.78
Benzimidazole	Arg624	Hydrophobic/pi-alkyl	5.34
Ethoxy	Asp760	Carbon hydrogen bond	3.49
Ethoxy	Cys622	Hydrophobic/alkyl-alkyl	3.82

For amino acid, A: H-bond acceptor, D: H-bond donor, B: Backbone interaction, S: Sidechain interaction. Light green: Carbon hydrogen bond, Green: H-bond, Orange: Electrostatic interactions, Pink: Hydrophobic interactions, RdRp: RNA-dependent RNA polymerase

**Table 2. Interactions of fexofenadine with the active site of RdRp**

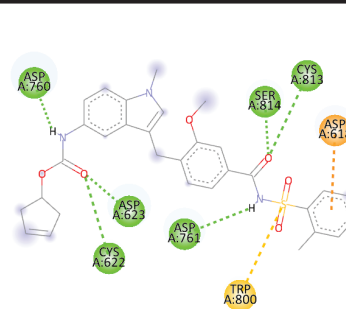
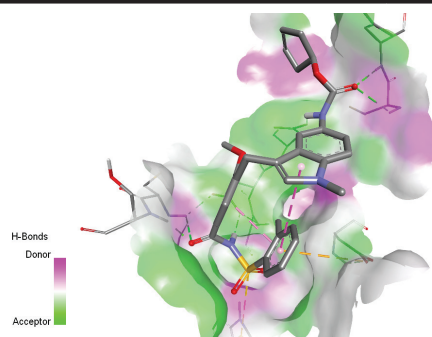
Functional group	Residue	Bond	Distance (Å)
Carboxylic acid	Trp617	H-bond (D-S)	2.91
Carboxylic acid	Trp800	H-bond (D-B)	2.76
Carboxylic acid	Glu811	H-bond (A-B)	2.02
'Phenyl	Tyr455	Hydrophobic/Pi-Pi T-form	5.57
'Phenyl	Arg553	Electrostatic/pi-cation	4.38
'Phenyl	Lys621	Electrostatic/pi-cation	4.62
'Phenyl	Arg624	Hydrophobic/pi-alkyl	3.09
''Phenyl	Lys621	Electrostatic/pi-cation	5.46
Butyl	Asp760	Carbon hydrogen bond	3.59

For amino acid, A: H-bond acceptor, D: H-bond donor, B: Backbone interaction, S: Sidechain interaction. Light green: Carbon hydrogen bond, Green: H-bond, Orange: Electrostatic interactions, Pink: Hydrophobic interactions, RdRp: RNA-dependent RNA polymerase

**Table 3. Interactions of Montelukast with the active site of RdRp**

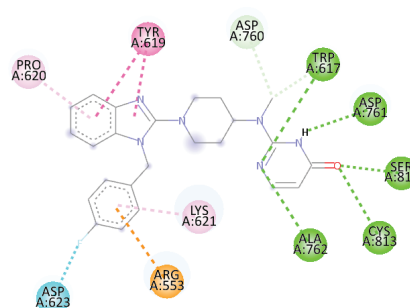
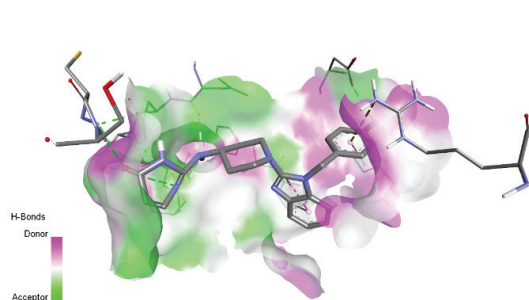
Functional group	Residue	Bond	Distance (Å)
2-Hydroxypropan-2-yl	Asp760	H-bond (A-S)	2.73
Carboxylic acid-COOH	Lys798	H-bond (A-S)	2.20
Carboxylic acid-COOH	Trp800	H-bond (D-B)	2.10
7-Methylquinoline	Tyr455	Hydrophobic/pi-alkyl	4.19
7-Methylquinoline	Tyr455	Hydrophobic/Pi-Pi T-form	5.85
7-Methylquinoline	Arg553	Hydrophobic/alkyl-alkyl	4.39
7-Methylquinoline	Arg553	Electrostatic/pi-cation	4.42
7-Methylquinoline	Lys621	Electrostatic/pi-cation	4.13
7-Methylquinoline	Lys621	Hydrophobic/pi-alkyl	4.50
4-(2-Hydroxypropan-2-yl)phenyl	Asp760	Electrostatic/pi-anion	3.25

For amino acid, A: H-bond acceptor, D: H-bond donor, B: Backbone interaction, S: Sidechain interaction. Light green: Carbon hydrogen bond, Green: H-bond, Orange: Electrostatic interactions, Pink: Hydrophobic interactions, RdRp: RNA-dependent RNA polymerase

**Table 4. Interactions of zafirlukast with the active site of RdRp**

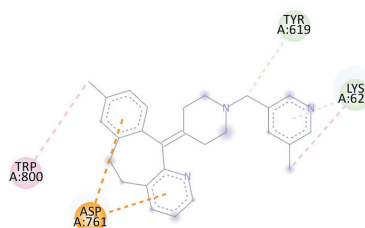
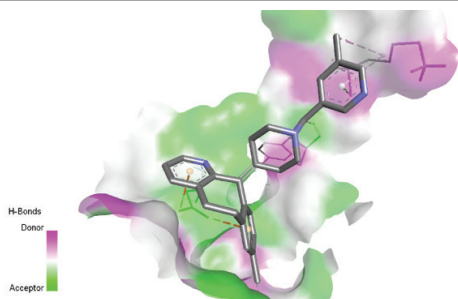
Functional group	Residue	Bond	Distance (Å)
Carbamate-NHCOO-	Cys622	H-bond (D-S)	2.61
Carbamate-NHCOO-	Asp623	H-bond (D-S)	2.24
Carbamate-NHCOO-	Asp760	H-bond (A-B)	2.29
Amide-CONH-	Asp761	H-bond (A-B)	2.06
Amide-CONH-	Cys813	H-bond (D-S)	2.91
Amide-CONH-	Ser814	H-bond (D-S)	1.83
Benzene sulfonyl	Asp618	Electrostatic/pi-anion	4.65
Benzene sulfonyl	Trp800	Pi-sulfur	4.84

For amino acid, A: H-bond acceptor, D: H-bond donor, B: Backbone interaction, S: Sidechain interaction. Light green: Carbon hydrogen bond, Green: H-bond, Orange: Electrostatic interactions, Pink: Hydrophobic interactions, RdRp: RNA-dependent RNA polymerase

**Table 5. Interactions of mizolastine with the active site of RdRp**

Functional group	Residue	Bond	Distance (Å)
1,3-Diazinan-2-yl	Trp617	H-bond (D-S)	3.79
1,3-Diazinan-2-yl	Ala762	H-bond (D-S)	6.58
Carbonyl	Ser814	H-bond (D-S)	2.14
Carbonyl	Gln815	H-bond (D-S)	5.74
N-methyl	Trp617	Carbon hydrogen bond	3.60
N-methyl	Asp760	Carbon hydrogen bond	3.26
Fluorophenyl	Arg553	Electrostatic/pi-cation	4.74
Fluorophenyl	Lys621	Hydrophobic/pi-alkyl	5.04
Fluorophenyl	Asp623	Halogen bond	3.15
Benzimidazole	Pro620	Hydrophobic/pi-alkyl	4.90
Benzimidazole	Tyr619	Hydrophobic/Pi-Pi T-form	4.82
Benzimidazole	Tyr619	Hydrophobic/Pi-Pi T-form	4.86

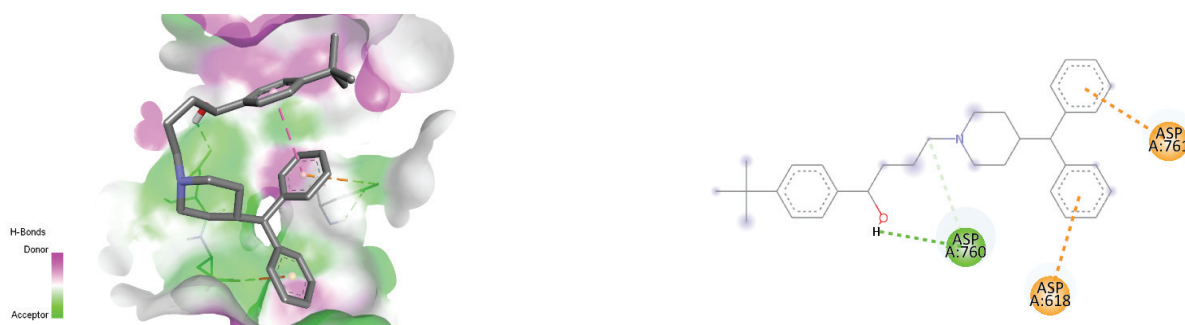
For amino acid, A: H-bond acceptor, D: H-bond donor, B: Backbone interaction, S: Sidechain interaction. Light green: Carbon hydrogen bond, Green: H-bond, Orange: Electrostatic interactions, Pink: Hydrophobic interactions, RdRp: RNA-dependent RNA polymerase

**Table 6. Interactions of rupatadine with the active site of RdRp**

Functional group	Residue	Bond	Distance (Å)
5-MethylPyridine	Lys621	Carbon hydrogen bond	2.89
5-MethylPyridine	Lys621	Hydrophobic/alkyl-alkyl	4.17
(5-MethylPyridin-3-yl)methyl	Tyr619	Carbon hydrogen bond	3.51
8-methyl-BenzocycloheptaPyridine	Asp761	Electrostatic/Pi-anion	3.30
8-methyl-BenzocycloheptaPyridine	Asp761	Electrostatic/Pi-anion	3.95
8-methyl-BenzocycloheptaPyridine	Trp800	Hydrophobic/pi-alkyl	4.33

Light green: Carbon hydrogen bond, Green: H-bond, Orange: Electrostatic interactions, Pink: Hydrophobic interactions, RdRp: RNA-dependent RNA polymerase

Table 7. Interactions of terfenadine with the active site of RdRp



Functional group	Residue	Bond	Distance (Å)
Alcohol	Asp760	H-bond (D-B)	2.17
'Phenyl	Asp618	Electrostatic/Pi-anion	4.62
Butyl	Asp760	Carbon hydrogen bond	3.54
''Phenyl	Asp761	Electrostatic/Pi-anion	3.59

For amino acid, A: H-bond acceptor, D: H-bond donor, B: Backbone interaction, S: Sidechain interaction. Light green: Carbon hydrogen bond, Green: H-bond, Orange: Electrostatic interactions, Pink: Hydrophobic interactions, RdRp: RNA-dependent RNA polymerase

stability of the ligand-receptor complex. The 7-methylquinoline moiety of montelukast participates in many hydrophobic interactions with the Tyr455, Arg553, and Lys621 residues of RdRp, which helps retain the ligand in the binding pocket.

On the other hand, zafirlukast exhibited a higher binding energy of -8.3 kcal/mol, indicating a stronger binding affinity. The binding profile of zafirlukast was characterized by an extensive network of hydrogen bonds involving residues Cys622, Asp623, Asp760, Asp761, Cys813, and Cys814, predominantly mediated by carbamate and amide functional groups (Table 4). This intricate hydrogen bonding network underscores the specific molecular recognition events driving the formation of the zafirlukast-RdRp complex. Zafirlukast utilizes its carbamate group to form hydrogen bonds with both Cys622 and Asp623, potentially anchoring it within the binding pocket. Additionally, hydrogen bonds are formed between the ligand's nitrogens and key residues Asp760 and Asp761, potentially contributing to directional positioning. Furthermore, the participation of Cys813 and Cys814 through hydrogen bonds with the ligand's amide carbonyl group suggests a role in stabilizing the complex. The presence of a pi-anion interaction between the ligand's benzene sulfonyl group and Asp618 suggests an attractive force that could contribute to the overall binding affinity. Moreover, a pi-sulfur interaction between the same sulfonyl group and Trp800 highlights potential aromatic stacking, which further enhances the stability of the complex. The docking analysis suggests that zafirlukast binds favorably to the RdRp receptor through a combination of extensive hydrogen bonding and electrostatic interactions. These findings warrant further *in vitro* and *in vivo* studies to assess the biological significance of this interaction. Mizolastine binds to RdRp with a binding energy of -7.6 kcal/mol, indicating a relatively strong interaction (Table 5). This

interaction involves various types of non-covalent forces, including hydrogen bonds, halogen bonds, and hydrophobic interactions. Hydrogen bond interactions occurred between the 1,3-diazinan-2-yl group and Trp617 and Ala762 residues within distances of 3.79 Å and 6.58 Å, respectively. Additionally, the closest interaction with a bond distance of 2.14 Å was observed between the carbonyl and Ser814 residues. The pi-cation interaction between fluorophenyl and Arg553 was detected at a distance of 4.74 Å. While the fluoro atom was detected at a distance that could form a halogen bond with the Asp623 residue, many hydrophobic interactions were observed with the Tyr619, Pro620, and Lys621 residues.

Rupatadine interacts with RdRp with a binding energy of -7.2 kcal/mol, indicating a relatively strong binding affinity. Significant carbon-hydrogen bonds and hydrophobic and electrostatic interactions were detected between rupatadine with key residues such as Lys619, Lys621, Asp761, and Trp800 (Table 6). Hydrogen bond interactions occurred between the 5-methyl pyridine ring of Rupatadine and the Lys621 residue of RdRp. Rupatadine's 8-methyl-benzocyclohepta pyridine ring exhibited pi-anion interactions with Asp761 on RdRp. Two types of hydrophobic interactions are also observed. One occurs between the (5-methylpyridin-3-yl)methyl group of rupatadine and the Tyr619 residue of RdRp. Another hydrophobic interaction involves the 8-methyl-benzocyclohepta pyridine ring of RdRp and the Trp800 residue of RdRp.

Terfenadine interacts with RdRp with a binding energy of -7.1 kcal/mol, indicating moderate strong interaction. This interaction involves various non-covalent forces, including hydrogen bonds, electrostatic interactions, and carbon-hydrogen bonds (Table 7). An alcohol group on terfenadine forms a hydrogen bond with the Asp760 residue of RdRp at a distance of 2.17



These findings provide valuable insights into the molecular mechanisms underlying the interactions between these ligands and RdRp, offering a foundation for further exploration of their antiviral potential and the development of novel therapeutic strategies targeting RNA viruses.

### Ethics

**Ethics Committee Approval:** Not required.

**Informed Consent:** Not required.

### Authorship Contributions

Concept: İ.K., Design: M.H., N.K., İ.K., Data Collection or Processing: M.H., N.K., Analysis or Interpretation: M.H., N.K., İ.K., Literature Search: M.H., N.K., İ.K., Writing: M.H., N.K., İ.K.

**Conflict of Interest:** The authors have no conflicts of interest to declare.

**Financial Disclosure:** The authors declared that this study received no financial support.

## REFERENCES

- World Health Organization. Infectious diseases. Available at: <https://www.emro.who.int/health-topics/infectious-diseases/index.html> [accessed: May 25, 2024].
- McCarthy MK, Morrison TE. Persistent RNA virus infections: do PAMPS drive chronic disease? *Curr Opin Virol.* 2017;23:8-15.
- Lee M, Kim JW, Jang B. DOVE: An infectious disease outbreak statistics visualization system. *IEEE Access.* 2018;6:47206-47216.
- World Health Organization. Novel coronavirus disease (COVID-19) outbreak.
- Zheng L, Zhang L, Huang J, Nandakumar KS, Liu S, Cheng K. Potential treatment methods targeting 2019-nCoV infection. *Eur J Med Chem.* 2020;205:112687.
- Seliem IA, Panda SS, Girgis AS, Hassaneen HM, Shaldam MA, Ebeid AM. New quinoline-triazole conjugates: Synthesis, and antiviral properties against SARS-CoV-2. *Bioorg Chem.* 2021;114:105117.
- Zhou P, Yang XL, Wang XG, Hu B, Zhang L, Zhang W, Si HR, Zhu Y, Li B, Huang CL, Chen HD, Chen J, Luo Y, Guo HD, Jiang RD, Liu MQ, Chen Y, Shen XR, Wang X, Zheng XS, Zhao K, Chen QJ, Deng F, Liu LL, Yan B, Zhan FX, Wang YY, Xiao GF, Shi ZL. A pneumonia outbreak associated with a new coronavirus of probable bat origin. *Nature.* 2020;579:270-273.
- Krause R, Smolle J. Covid-19 mortality and local burden of infectious diseases: a worldwide country-by-country analysis. *J Infect Public Health.* 2022;15:1370-1375.
- Drayman N, Jones KA, Azizi SA, Froggatt HM, Tan KS, Maltseva NI, Chen SH, Nicastro L, Florez CM, Thompson EA, Julian LD, Taylor GM, Melnyk JE, Guisado DA, Botten JW, Clay MD, Pollard KS, White KM, Schwartz O, Tay S, Vallett L, Moran P, Muramatsu H, Muramatsu T, Wu W, Keng WF, Evans RM, Komatsu T, Tsukamoto H, Gale M, Randall G, Tay SY, Schmid MF, Stevens RC, Young JA, Glenn JS, Tay HK. Drug repurposing screen identifies masitinib as a 3CLpro inhibitor that blocks replication of SARS-CoV-2 in vitro. *bioRxiv [Preprint].* 2020;373:931-936.
- Piplani S, Singh P, Winkler DA, Petrovsky N. Potential COVID-19 therapies from computational repurposing of drugs and natural products against the SARS-CoV-2 helicase. *Int J Mol Sci.* 2022;23:7704.
- Ghahremanpour MM, Tirado-Rives J, Deshmukh M, Ippolito JA, Zhang C, Cho A, Anderson KS, Jorgensen WL. Identification of 14 known drugs as inhibitors of the main protease of SARS-CoV-2. *bioRxiv [Preprint].* 2020:2020.08.28.271957.
- Reznikov LR, Norris MH, Vashisht R, Gabizon R, Lee HR, Jung K, Sham HP, Solis AG, Cohen TS, Gavrilin MA, Tanjore H, Newton JC, Idell S, Yayanos M, Gouda N, Kolls JK, Smith DF, Horowitz JD, Carroll RJ, Banerjee R, Goldberg JB, Ahuja N, Thomas PG, Prokop JW. Identification of antiviral antihistamines for COVID-19 repurposing. *Biochem Biophys Res Commun.* 2021;538:173-179.
- Oh KK, Adnan M, Cho DH. Network pharmacology study to elucidate the key targets of underlying antihistamines against COVID-19. *Curr Issues Mol Biol.* 2022;44:1597-1609.
- Liu J, Cao R, Xu M, Wang X, Zhang H, Hu H, Li Y, Hu Z, Zhong W, Wang M. Hydroxychloroquine, a less toxic derivative of chloroquine, is effective in inhibiting SARS-CoV-2 infection in vitro. *Cell Discov.* 2020;6:16.
- Wang M, Cao R, Zhang L, Yang X, Liu J, Xu M, Shi Z, Hu Z, Zhong W, Xiao G. Remdesivir and chloroquine effectively inhibit the recently emerged novel coronavirus (2019-nCoV) in vitro. *Cell Res.* 2020;30:269-271.
- Dyall J, Gross R, Kindrachuk J, Johnson RF, Olinger GG, Hensley LE, Frieman MB, Jahrling PB, Laidlaw M, Kawaoka Y, Yamada M, Blaney JE, Fenton KA, Holbrook MR. Middle East respiratory syndrome and severe acute respiratory syndrome: current therapeutic options and potential targets for novel therapies. *Drugs.* 2017;77:1935-1966.
- Simons FE. Advances in H1-antihistamines. *N Engl J Med.* 2004;351:2203-2217.
- Church MK. Allergy, histamine and antihistamines. *Handb Exp Pharmacol.* 2017;241:321-331.
- Mingorance L, Friesland M, Coto-Llerena M, Pérez-del-Pulgar S, Boix L, López-Oliva J M, Bruix J, Fornis X, Gastaminza P. Selective inhibition of hepatitis C virus infection by hydroxyzine and benztropine. *Antimicrob Agents Chemother.* 2014;58: 3451-3460.
- Zongyi H, Adam R, Xin H, Xiaolin H, Dalia P, Zhong L, Yuyang G, Andrew WK, Wei J. Chlorcyclizine inhibits viral fusion of hepatitis C virus entry by directly targeting HCV envelope glycoprotein 1. *Cell Chem Biol.* 2020;27:780-792.
- Kitchen DB, Decornez H, Furr JR, Bajorath J. Docking and scoring in virtual screening for drug discovery: methods and applications. *Nat Rev Drug Discov.* 2004;3:935-949.
- Tian L, Qiang T, Liang C, Ren X, Jia M, Yang J, Ren Y, Shen L, Wei J. RNA-dependent RNA polymerase (RdRp) inhibitors: The current landscape and repurposing for the COVID-19 pandemic. *Eur J Med Chem.* 2021;213:113201.
- de Farias ST, Dos Santos Junior AP, Rêgo TG, José MV. Origin and evolution of RNA-dependent RNA polymerase. *Front Genet.* 2017;8:125.
- Kirchdoerfer RN, Ward AB. Structure of the SARS-CoV nsp12 polymerase bound to nsp7 and nsp8 co-factors. *Nat Commun.* 2019;10:2342.
- Elfiky AA. Ribavirin, Remdesivir, Sofosbuvir, Galidesivir, and Tenofovir against SARS-CoV-2 RNA dependent RNA polymerase (RdRp): A molecular docking study. *Life Sci.* 2020;253:117592.
- Gao Y, Yan L, Huang Y, Liu F, Zhao Y, Cao L, Wang T, Sun Q, Ming Z, Zhang L, Ge J, Zheng L, Zhang Y, Wang Q, Rao Z, Lou Z. Structure of the RNA-dependent RNA polymerase from COVID-19 virus. *Science.* 2020;368:779-782.

27. Hillen HS, Kokic G, Farnung L, Dienemann C, Tegunov D, Cramer P. Structure of replicating SARS-CoV-2 polymerase. *Nature*. 2020;584:154-156.
28. Lung J, Lin YS, Yang YH, Chou YL, Shu LH, Cheng YC, Liu HT, Wu CY. The potential chemical structure of anti-SARS-CoV-2 RNA-dependent RNA polymerase. *J Med Virol*. 2020;92:693-697.
29. Choi J, Azmat CE. Leukotriene Receptor Antagonists. 2023 Jun 4. In: StatPearls [Internet]. Treasure Island (FL): StatPearls Publishing; 2024.
30. Al Ghobain M, Rebh F, Saad A, Alhurajji A, Zahrani AM, Alhaddad B. The efficacy of Zafirlukast as a SARS-CoV-2 helicase inhibitor in adult patients with moderate COVID-19 Pneumonia (pilot randomized clinical trial). *J Infect Public Health*. 2022;15:1546-1550.
31. Morris GM, Huey R, Lindstrom W, Sanner MF, Belew RK, Goodsell DS, Olson AJ. Software news and updates gamedit-a graphical user interface for computational chemistry softwares. *J Comput Chem*. 2009;30:174-182.
32. Stewart JJ. Optimization of parameters for semiempirical methods V: modification of NDDO approximations and application to 70 elements. *J Mol Model*. 2007;13:1173-1213.
33. Trott O, Olson AJ. AutoDock Vina: improving the speed and accuracy of docking with a new scoring function, efficient optimization, and multithreading. *J Comput Chem*. 2010;31:455-461.
34. Kulabaş N, Yeşil T, Küçüközel İ. Evaluation of molnupiravir analogues as novel coronavirus (SARS-CoV-2) RNA-dependent RNA polymerase (RdRp) inhibitors-an in silico docking and ADMET simulation study. *J Res Pharm*. 2021;25:967-981.

---

Click the link to access Supplementary Figure 1: <https://l24.im/CjOSE>



# Lactulose Versus Naloxone for Opioid-Induced Constipation in Intensive Care

✉ Mitra RAHIMI<sup>1</sup>, ✉ Maral RAMEZANI<sup>2</sup>, ✉ Shahin SHADNIA<sup>1</sup>, ✉ Babak MOSTAFAZADEH<sup>1</sup>, ✉ Mahnaz Dahdahsti AZANDARYANI<sup>3</sup>,  
✉ Mohammad Hosein ALIJANZADEH<sup>3</sup>, ✉ Latif GACHKAR<sup>4</sup>, ✉ Peyman Erfan Talab EVINI<sup>1\*</sup>

<sup>1</sup>Shahid Beheshti University of Medical Sciences Faculty of Medicine, Toxicological Research Center, Excellence Center and Department of Clinical Toxicology, Tehran, Iran

<sup>2</sup>Arak University of Medical Sciences Faculty of Medicine, Department of Pharmacology, Arak, Iran

<sup>3</sup>Shahid Beheshti University of Medical Sciences, Loghman Hakim Hospital, Clinic of Clinical Toxicology, Tehran, Iran

<sup>4</sup>Shahid Beheshti University of Medical Sciences Faculty of Medicine, Loghman Hakim Hospital, Clinic of Infectious Disease, Tehran, Iran

## ABSTRACT

**Objectives:** Constipation caused by opioid-induced constipation (OIC) is prevalent among critically poisoned patients and can result in complications that prolong hospitalization and, in rare cases, cause bowel perforation. This research aimed to evaluate the safety and efficacy of lactulose and naloxone in the treatment of OIC in the intensive care unit for poisoning.

**Materials and Methods:** This was a randomized, double-blind, clinical trial of patients with opioid poisoning who experienced constipation for 14 months. Patients were divided into two groups: one receiving lactulose (30 cc daily) and the other receiving naloxone (8 mg three times a day). The parameters of age, gender, type of opioid used, Acute Physiology and Chronic Health Evaluation II score, Glasgow Coma Scale score, defecation time, and number of laboratory variables were recorded. All data were collected and analyzed using SPSS software.

**Results:** Of the participants in the lactulose group, 85.37% were male and 14.63% were female. In the naloxone group, 94.9% of patients were male and 5.1% were female. The average age of the lactulose group was  $44 \pm 16.2$  and in the naloxone group was  $48.13 \pm 19.1$  years. The average defecation time was  $30.8 \pm 23.1$  hours in the naloxone group and  $25 \pm 11.5$  hours in the lactulose group. Six patients (15%) in the naloxone group experienced treatment failure. Symptoms of withdrawal syndrome were experienced by 15 patients (39.5%) patients in the naloxone group.

**Conclusion:** The evidence suggests that lactulose is a superior treatment choice because it does not carry the risk of withdrawal syndrome or treatment ineffectiveness.

**Keywords:** Constipation, defecation time, lactulose, naloxone, opioid

## INTRODUCTION

Various factors can lead to constipation, including underlying medical conditions, lifestyle choices, and medications.<sup>1,2</sup> Chronic constipation can lead to serious complications, such as hemorrhage, bowel obstruction, and even death. Additionally, it can cause upper gut problems like gastroesophageal reflux disease.<sup>3,4</sup> Opioid therapy for pain often leads to opioid bowel dysfunction (OBD) because of its impact on the gastrointestinal (GI) tract *via* mu-opioid receptors. The most prevalent type of

OBD is opioid-induced constipation (OIC), which can last for the duration of the treatment.<sup>5-7</sup> The prevalence of OIC is estimated to be between 40% and 95%, with varying degrees of distress and duration of unpleasant symptoms among patients.<sup>2,8</sup>

The primary treatment methods for constipation are oral laxatives and stool softeners. However, in individuals taking chronic opioids, these drugs may directly cause persistent constipation, making laxatives alone insufficient. In addition, OIC does not usually result in tolerance. In 2008, the Food

\*Correspondence: peyman1346erfan@gmail.com, ORCID-ID: orcid.org/0000-0002-0995-4973

Received: 08.11.2023, Accepted: 08.07.2024



and Drug Administration approved methylnaltrexone, an opioid receptor antagonist, for treating OIC.<sup>9-12</sup> The most commonly used approach for treating OIC involves the use of both a stimulant and stool softener. GI stimulants like Senna or bisacodyl work by increasing muscle contractions triggered by an enteric reflex. Stool softeners operate by one of three mechanisms. Surfactants, such as docusate, are emulsifiers that help mix fat and water in feces. Lubricants like mineral oil, slow down the absorption of water from stool in the colon, thus making them softer. Osmotics like lactulose attract water into the colon, thereby hydrating the stools.<sup>2,13</sup>

To prevent oxycodone-induced constipation, a combination of oxycodone and naloxone is consumed orally. When taken orally, naloxone has very low bioavailability (less than 2%) because it is extensively metabolized in the liver. As a result, oral naloxone binds only to peripheral opioid receptors in the GI tract at pharmacologically relevant concentrations. This binding inhibits oxycodone's ability to affect GI function, thereby reducing the risk of OIC.<sup>14,15</sup>

Numerous studies have demonstrated that naloxone is a secure and efficient treatment for OIC in the ICU.<sup>16-19</sup> The purpose of this study was to compare the effectiveness of lactulose and naloxone in the treatment of OIC.

## MATERIALS AND METHODS

In this clinical trial, a randomized, double-blind approach was used to study patients who experienced constipation (3 days without defecation) due to opioid use. The study was conducted in the poisoning intensive care unit of Loghman Hakim Hospital in Tehran between November 2022 and December 2023. Patients were divided into two groups using simple randomization, with one group receiving lactulose and the other receiving naloxone.

The lactulose group received a daily dose of 30 cc, whereas the naloxone group received 8 mg (20 cc) three times a day. The time to first defecation after treatment initiation was recorded for both groups, with patients monitored for 72 hours. Failure

to defecate during this period was considered treatment failure.

Patients were excluded from the study if they concurrently consumed substances that caused constipation, did not provide consent to participate, or had underlying conditions such as intestinal obstruction, rheumatological or neurological disorders, shock, or iron deficiency anemia. The parameters of age, gender, type of opioid used, Acute Physiology and Chronic Health Evaluation II score (APACHE II), Glasgow Coma Scale (GCS) score, drug dose, frequency of drug use, defecation time, and number of laboratory variables were recorded.

This study was approved by the institutional ethics board of Shahid Beheshti University of Medical Sciences (approval number: IR.SBMU.RETECH.REC.1400.1024, date: 02.06.2022). This article was also registered in the Iranian Registry of Clinical Trials with number: IRCT20210720051946N4.

### Statistical analysis

The data were analyzed using IBM SPSS 23 software. The dispersion and descriptive indices of the variables were investigated. The chi-square test was used to compare qualitative variables. The independent *t*-test and Mann-Whitney *U* test were also used to compare groups. Kolmogorov-Smirnov test was used to assess the normality of data distribution. A significance level of  $p \leq 0.05$  was considered.

## RESULTS

The study comprised a total of 80 individuals, with 39 receiving naloxone and 41 receiving lactulose. In the lactulose group, there were 35 (85.37%) males and 6 (14.63%) females, whereas in the naloxone group, there were 37 (94.9%) males and 2 (5.1%) females. The average age of the lactulose group was  $44 \pm 16.2$  and in the naloxone group was  $48.13 \pm 19.1$  years. There were no significant differences between the two groups in age and gender distribution. Table 1 displays the mean values of body temperature, systolic and diastolic blood pressure, heart rate, APACHE II score, GCS score, and weight of patients in the two groups.

**Table 1. Vital and fundamental details regarding patients who underwent intervention**

Variable	Naloxone group, mean $\pm$ SD	Lactulose group, mean $\pm$ SD	<i>p</i> value
Gender male	37 (94.9%)	35 (85.37%)	0.157
Age (year)	48.13 $\pm$ 19.1	44 $\pm$ 16.2	0.301
Temperature ( $^{\circ}$ C)	36.9 $\pm$ 0.34	37.37 $\pm$ 0.4	0.001*
Systolic blood pressure (mmHg)	119.8 $\pm$ 21.1	122.8 $\pm$ 16.1	0.486
Diastolic blood pressure (mmHg)	74.4 $\pm$ 12.2	78.8 $\pm$ 12.9	0.124
Heart rate (pulses/min.)	89 $\pm$ 17.7	88.5 $\pm$ 25.4	0.925
Breathing rate (breaths/min.)	16.9 $\pm$ 3.7	16.7 $\pm$ 1.9	0.785
Body weight (kg)	87.9 $\pm$ 30.3	84.2 $\pm$ 17.3	0.649
APACHE II score	16.1 $\pm$ 6.6	148.1 $\pm$ 5.3	0.132
GCS score	9.7 $\pm$ 4.1	7.8 $\pm$ 3.3	0.026*

\* $p < 0.05$ , SD: Standard deviation, APACHE: Acute Physiology and Chronic Health Evaluation, GCS: Glasgow Coma Scale

None of the patients had a history of abdominal or pelvic surgery within the last month. In the lactulose group, 26 individuals required intubation, whereas in the naloxone group, only 3 individuals required intubation. Fifteen (39.5%) patients who received naloxone experienced symptoms of withdrawal syndrome, and the treatment had to be discontinued after 7 doses in one patient because their vital signs became unstable. The most consumed opioids in both the lactulose and naloxone groups were methadone (53.7% vs. 23.1%) and opium (19.5% vs. 23.1%) (Figure 1).

The results of the Mann-Whitney *U* test showed that there is no significant difference between the two groups in defecation time ( $p= 0.769$ ). However, the mode of data was 16 in the naloxone group and 26 in the lactulose group. The average defecation time was  $30.8 \pm 23.1$  hours in the naloxone group and  $25 \pm 11.5$  hours in the lactulose group. Of the total number of cases, 6 (15%) patients in the naloxone group experienced treatment failure, whereas no treatment failure was observed in the lactulose group.

The effect size was determined using Cohen’s *d*-test. The calculated effect size *d* was 0.32 (medium effect size), which falls within the small range. This suggests that the difference between the means of naloxone and lactulose is small. Based on a *t*-test power calculator, a power (the likelihood of accurately rejecting the null hypothesis) of 0.268 was obtained ( $df = 70$ , non-centrality parameter: 1.357, critical *t*: 1.994).

**DISCUSSION**

Although opioids can effectively manage moderate-to-severe pain, up to 18.9% of patients discontinue opioid therapy due to the side effects associated with the drugs. OIC, which is a common side effect of pain therapy, often results in the discontinuation of opioid therapy due to its significant negative impact on quality of life.<sup>20</sup> In this study, we compared the effectiveness of lactulose and naloxone in the treatment of constipation caused by opioid poisoning. There was no significant difference in the average

defecation time between the two groups. Of the patients who received naloxone, 15 individuals (39.5%) exhibited signs of withdrawal syndrome. Six patients (15%) in the naloxone group experienced treatment failure, whereas there were no cases of treatment failure in the lactulose group.

Lactulose is a disaccharide that cannot be digested and has been utilized in the medical field. Depending on the prescribed amount, oral lactulose can function as a prebiotic, osmotic laxative, or detoxifying agent.<sup>21</sup> There is limited information regarding the use of laxatives for treating OIC, and there is hardly any evidence from studies that involve placebos or comparisons.<sup>22</sup> One instance involves the examination of Senna and lactulose’s impact on cancer patients who are undergoing opioid treatment, but the findings indicated that there was no notable contrast between the two.<sup>23</sup> Freedman et al.<sup>24</sup> compared the effects of lactulose and polyethylene glycol to determine their effects. They discovered that the use of polyethylene glycol/electrolyte solution resulted in the loosest stool consistency, resembling diarrhea. Additionally, polyethylene glycol/electrolyte solution is probably the most economical option. Both experimental groups showed no significant differences in reducing the formation of hard stool.<sup>24</sup>

Previous studies have investigated the dosage of oral naloxone for the treatment of OIC.<sup>25-27</sup> Gibson and Pass<sup>18</sup> conducted a study on patients aged 18 to 89 years admitted to the medical intensive care unit and found that enteral naloxone was safe for the treatment of OIC. They reported that the median duration of bowel movements was 24.4 h. The median number of naloxone doses administered before achieving bowel movement was 3.<sup>18</sup> There were no comparative or placebo-controlled studies. A systematic review and meta-analysis conducted in 2020 showed that only 6 blinded and randomized controlled trials have investigated naloxone for the treatment of OIC.<sup>28</sup> The combination of oxycodone and naloxone was the subject of four studies.<sup>14,15,29,30</sup> A study was conducted on sustained-release naloxone.<sup>31</sup>

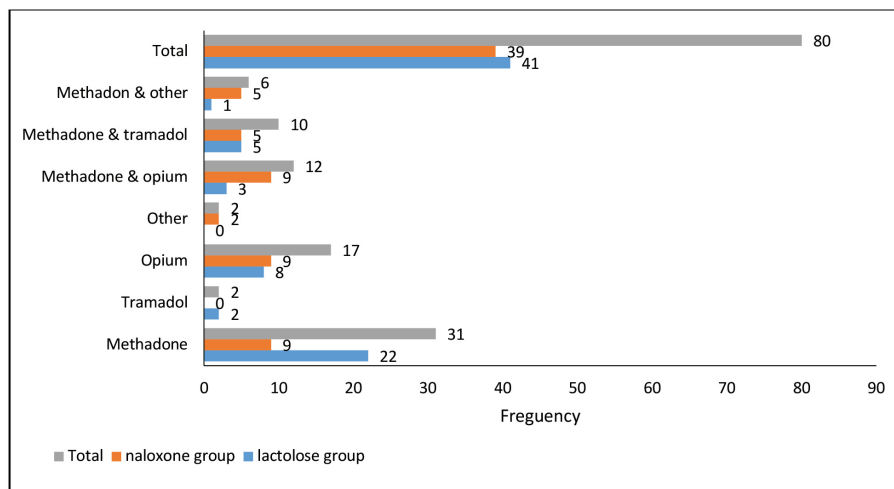


Figure 1. Type of opioids in the lactulose and naloxone groups

Meissner examined 202 individuals suffering from long-term pain who received sustained oral oxycodone for treatment. They were randomly divided into groups and administered 10, 20, or 40 mg/day of naloxone or placebo. The study found that bowel function improved as the naloxone dosage increased. In particular, participants who received 20 and 40 mg of naloxone showed significant improvement in bowel function compared with those who received placebo. However, there was a tendency toward a higher incidence of diarrhea with higher naloxone doses.<sup>32</sup>

Unfortunately, no previous studies have compared the effects of naloxone and lactulose on improving OIC. Moreover, naloxone was not compared with other laxatives. Nevertheless, several recommendations suggest that laxatives should be given to patients with cancer and non-cancer pain as a means of preventing or treating OIC.<sup>33-35</sup>

A significant difference was observed between the patient's body temperature and GCS scores in the two groups. Unfortunately, before starting any treatment, vital signs were recorded, and patients were randomly selected, and then we noticed this difference in the data analysis stage. We do not have any justification for this.

## CONCLUSION

In conclusion, although there was no significant variation in the average defecation time between naloxone and lactulose, lactulose appears to be a better option due to its lack of risk of withdrawal syndrome and treatment failure.

### Acknowledgement

The authors would like to thank the Clinical Research Development Unit (CRDU) of Loghman Hakim Hospital, Shahid Beheshti University of Medical Sciences, Tehran, Iran for their support, cooperation and assistance throughout the period of study.

### Ethics

**Ethics Committee Approval:** This study was approved by the institutional ethics board of Shahid Beheshti University of Medical Sciences (approval number: IR.SBMU.RETECH.REC.1400.1024, date: 02.06.2022). This article was also registered in the Iranian Registry of Clinical Trials with number: IRCT20210720051946N4.

**Informed Consent:** Written consent was obtained from the participants.

### Authorship Contributions

Surgical and Medical Practices: M.R., Concept: M.R., Design: M.R., Data Collection or Processing: M.R., M.D.A., M.H.A., Analysis or Interpretation: L.G., Literature Search: Ma.R., S.S., B.M., Writing: M.R., P.E.T.E.

**Conflict of Interest:** The authors have no conflicts of interest to declare.

**Financial Disclosure:** The authors declared that this study received no financial support.

## REFERENCES

- Bharucha AE, Wald A, editors. Chronic constipation. Mayo Clinic Proceedings; 2019: Elsevier.
- Kumar L, Barker C, Emmanuel A. Opioid-induced constipation: pathophysiology, clinical consequences, and management. *Gastroenterol Res Pract.* 2014;2014:141737.
- Benyamin R, Trescot AM, Datta S, Buenaventura R, Adlaka R, Sehgal N, Glaser SE, Vallejo R. Opioid complications and side effects. *Pain Physician.* 2008;11:S105-S120.
- Holzer P. Opioids and opioid receptors in the enteric nervous system: from a problem in opioid analgesia to a possible new prokinetic therapy in humans. *Neurosci Lett.* 2004;361:192-195.
- Webster LR. Opioid-induced constipation. *Pain Med.* 2015;16 Suppl 1:S16-S21.
- Camilleri M, Drossman DA, Becker G, Webster LR, Davies AN, Mawe GM. Emerging treatments in neurogastroenterology: a multidisciplinary working group consensus statement on opioid-induced constipation. *Neurogastroenterol Motil.* 2014;26:1386-1395.
- Dorn S, Lembo A, Cremonini F. Opioid-induced bowel dysfunction: epidemiology, pathophysiology, diagnosis, and initial therapeutic approach. *Am J Gastroenterol Suppl.* 2014;2:31-37.
- Pappagallo M. Incidence, prevalence, and management of opioid bowel dysfunction. *Am J Surg.* 2001;182:11S-18S.
- Noble M, Treadwell JR, Tregear SJ, Coates VH, Wiffen PJ, Akafomo C, Schoelles KM. Long-term opioid management for chronic noncancer pain. *Cochrane Database Syst Rev.* 2010;2010:CD006605.
- Mehta N, O'Connell K, Giambrone GP, Baqai A, Diwan S. Efficacy of methylnaltrexone for the treatment of opioid-induced constipation: a meta-analysis and systematic review. *Postgrad Med.* 2016;128:282-289.
- Bader S, Jaroslowski K, Blum HE, Becker G. Opioid-induced constipation in advanced illness: safety and efficacy of methylnaltrexone bromide. *Clin Med Insights Oncol.* 2011;5:201-211.
- Michna E, Blonsky ER, Schulman S, Yaffe K, Diamond R. Subcutaneous methylnaltrexone for treatment of opioid-induced constipation in patients with chronic, nonmalignant pain: a randomized controlled study. *J Pain.* 2011;12:554-562.
- Goodheart CR, Leavitt SB. Managing opioid-induced constipation in ambulatory-care patients. *Pain Treat Top.* 2006:1-9.
- Simpson K, Leyendecker P, Hopp M, Klose P, Zimmerman B. Fixed-ratio combination oxycodone/naloxone compared with oxycodone alone for the relief of opioid-induced constipation in moderate-to-severe noncancer pain. *Curr Med Res Opin.* 2008;24:3503-3512.
- Vondrackova D, Leyendecker P, Meissner W, Hopp M, Szombati I, Hermanns K, Ruckes C, Weber S, Grothe B, Fleischer W, Reimer K. Analgesic efficacy and safety of oxycodone in combination with naloxone as prolonged-release tablets in patients with moderate to severe chronic pain. *J Pain.* 2008;9:1144-1154.
- Meissner W, Dohrn B, Reinhart K. Enteral naloxone reduces gastric tube reflux and frequency of pneumonia in critical care patients during opioid analgesia. *Crit Care Med.* 2003;31:776-780.
- Arpino PA, Thompson BT. Safety of enteral naloxone for the reversal of opiate-induced constipation in the intensive care unit. *J Clin Pharm Ther.* 2009;34:171-175.
- Gibson CM, Pass SE. Enteral naloxone for the treatment of opioid-induced constipation in the medical intensive care unit. *J Crit Care.* 2014;29:803-807.

19. Merchan C, Altshuler D, Papadopoulos J. Methylnaltrexone versus naloxone for opioid-induced constipation in the medical intensive care unit. *Ann Pharmacother*. 2017;51:203-208.
20. Lang-Ilievich K, Bornemann-Cimenti H. Opioid-induced constipation: a narrative review of therapeutic options in clinical management. *Korean J Pain*. 2019;32:69-78.
21. Pranami D, Sharma R, Pathak H. Lactulose: a prebiotic, laxative and detoxifying agent. *Drugs & Therapy Perspectives*. 2017;33:228-233.
22. Ruston T, Hunter K, Cummings G, Lazarescu A. Efficacy and side-effect profiles of lactulose, docusate sodium, and sennosides compared to PEG in opioid-induced constipation: a systematic review. *Can Oncol Nurs J*. 2013;23:236-246.
23. Agra Y, Sacristán A, González M, Ferrari M, Portugués A, Calvo MJ. Efficacy of senna versus lactulose in terminal cancer patients treated with opioids. *J Pain Symptom Manage*. 1998;15:1-7.
24. Freedman MD, Schwartz HJ, Roby R, Fleisher S. Tolerance and efficacy of polyethylene glycol 3350/electrolyte solution versus lactulose in relieving opiate-induced constipation: a double-blinded placebo-controlled trial. *J Clin Pharmacol*. 1997;37:904-907.
25. Meissner W, Schmidt U, Hartmann M, Kath R, Reinhart K. Oral naloxone reverses opioid-associated constipation. *Pain*. 2000;84:105-109.
26. Liu M, Wittbrodt E. Low-dose oral naloxone reverses opioid-induced constipation and analgesia. *J Pain Symptom Manage*. 2002;23:48-53.
27. Latasch L, Zimmermann M, Eberhardt B, Jurna I. Aufhebung einer Morphin-induzierten Obstipation durch orales Naloxon [Treatment of morphine-induced constipation with oral naloxone]. *Anaesthesist*. 1997;46:191-194.
28. Vijayvargiya P, Camilleri M, Vijayvargiya P, Erwin P, Murad MH. Systematic review with meta-analysis: efficacy and safety of treatments for opioid-induced constipation. *Aliment Pharmacol Ther*. 2020;52:37-53.
29. Ahmedzai SH, Nauck F, Bar-Sela G, Bosse B, Leyendecker P, Hopp M. A randomized, double-blind, active-controlled, double-dummy, parallel-group study to determine the safety and efficacy of oxycodone/naloxone prolonged-release tablets in patients with moderate/severe, chronic cancer pain. *Palliat Med*. 2012;26:50-60.
30. Löwenstein O, Leyendecker P, Hopp M, Klose P, Zimmermann G, Wulf H. Combined prolonged-release oxycodone and naloxone improves bowel function in patients receiving opioids for moderate-to-severe non-malignant chronic pain: a randomized controlled trial. *Expert Opin Pharmacother*. 2009;10:531-543.
31. Sanders M, Jones S, Löwenstein O, Jansen JP, Miles H, Simpson K. New formulation of sustained release naloxone can reverse opioid-induced constipation without compromising the desired opioid effects. *Pain Med*. 2015;16:1540-1550.
32. Meissner W, Leyendecker P, Mueller-Lissner S, Nadstawek J, Hopp M, Ruckes C, Wirz S, Fleischer W, Reimer K. A randomized controlled trial with prolonged-release oral oxycodone and naloxone to prevent and reverse opioid-induced constipation. *Eur J Pain*. 2009;13:56-64.
33. Caraceni A, Hanks G, Kaasa S, Olesen F, Currow D, Lorenz W, De Conno F, Van Der Rijt W. Use of opioid analgesics in the treatment of cancer pain: evidence-based recommendations from the EAPC. *Lancet Oncol*. 2012;13:e58-e68.
34. Manchikanti L, Abdi S, Atluri S, Balog CC, Benyamin RM, Boswell MV, Brown KR, Bruel BM, Bryce DA, Burks PA, Burton AW, Calodney AK, Caraway DL, Cash KA, Christo PJ, Damron KS, Datta S, Deer TR, Diwan S, Eriator I, Falco FJ, Fellows B, Geffert S, Gharibo CG, Glaser SE, Grider JS, Hameed H, Hameed M, Hansen H, Harned ME, Hayek SM, Helm S, Hirsch JA, Janata JW, Kaye AD, Kaye AM, Kloth DS, Koyalagunta D, Lee M, Malla Y, Manchikanti KN, McManus CD, Pampati V, Parr AT, Pasupuleti R, Patel VB, Sehgal N, Silverman SM, Singh V, Smith HS, Snook LT, Solanki DR, Tracy DH, Vallejo R, Wargo BW; American Society of Interventional Pain Physicians. American Society of Interventional Pain Physicians (ASIPP) guidelines for responsible opioid prescribing in chronic non-cancer pain: Part 2-guidance. *Pain Physician*. 2012;15:S67-S116.
35. Argoff CE, Brennan MJ, Camilleri M, Davies A, Fudin J, Galluzzi KE, Gudin J, Lembo A, Stanos SP, Webster LR. Consensus recommendations on initiating prescription therapies for opioid-induced constipation. *Pain Med*. 2015;16:2324-2337.

## 2024 Referee Index

Arif Tanju Özçelikay  
Ahmet Aydın  
Ahmet Doğan Ergin  
Alankar Shrivastava  
Ali Kemal Ateş  
Amaechi Dennis  
Archana Sidagouda Patil  
Arpan Dey Bhowmik  
Arzu Zeynep Karabay  
Aslinur Albayrak  
Assia Zeghib  
Asuman Yekta Özer  
Ayşe Özdemir  
Ayşe Selen Alp  
Aysegul Karatas  
Aysel Berkkan  
Aysu Selçuk  
Azize Şener  
Benay Can Eke  
Berrin Başaran Küçüktürkmen  
Beyza Ayazgök  
Bhoomendra Bhongade  
Bilge Sözen  
Birsen Tozkoparan Köprücü  
Bondigalla Ramachandra  
Bülent Kıran  
Burak Barut  
Burçin Ergene  
Burcu Doğan Topal  
Burcu Mesut  
Büşra Ertaş  
Büşra Nur Çattık  
Canan Karaalp  
Canan Kuş  
Cansel Köse Özkan  
Cansu Göncüoğlu  
Cengizhan Ceylan  
Cennet Duran  
Çetin Taş  
Ceyda Sibel Kılıç  
Çiğdem Karaaslan Kırmızıoğlu  
Çiğdem Yücel  
Derya Çiçek Polat  
Dilan Konyar  
Dilan Özmen Özgün  
Dilek Ak  
Dilek Bilgiç Alkaya  
Dilek Kul  
Durisehvar Özer Ünal  
Ebru Alimoğulları  
Ebru Arıoğlu İnan  
Ebru Derici Eker  
Eknath Damu Ahire  
Ekrem Murat Gönülalan  
Elif Ertuna  
Elif İnce Ergüç

Elif Nur Barut  
Elif Ulutaş Deniz  
Emel Öykü Çetin Uyanıkgil  
Emrah Özakar  
Emre Durmaz  
Emre Kara  
Eren Aytekin  
Esra Demirtürk  
Esra Tatar  
Esther Del Olmo  
Fatih Göğher  
Gamze Çamlık  
Gizem Rüya Topal  
Gonca Çakmak  
Gözde Elgin Cebe  
Gül Özhan  
Gülbeyaz Yıldız Türkyılmaz  
Gülbin Özçelikay  
Gülengül Duman  
Gülşah Karakaya  
Gülşen Kendir  
Hakan Parlakpınar  
Hala Fouad Kasım  
Hande Sipahi  
Hasan Kırmızıbekmez  
Hasan Şahin  
Herman M. Bolt  
Hüseyin İstanbullu  
I Made Dwi Mertha Adnyana  
İne Suharyani  
İpek Suntar  
Işık Özgüney  
İsmail Tuncer Değim  
İsmail Yener  
John Paul Sese Tosoc  
Kadriye Arzum Erdem Gürsan  
Kailash Sidramappa Chadchan  
Kartik Singhal  
Keriman Özadalı Sarı  
Latha Damle  
Leyla Yurttaş  
Mahendra Kumar Verma  
Mahmoud Abudayyak  
Mahmut Ozan Toksoy  
Margaret O. Ilomuanya  
Mehmet Alp  
Mehmet Barlas Uzun  
Mehmet Emin Önger  
Mehmet Zuhuri Arun  
Melike Sessevmez  
Meltem Çetin  
Meriç Köksal Akkoç  
Mert Can Güzel  
Merve Çelik Tekeli  
Merve Demirbüğen Öz  
Meryem Sedef Erdal

Meryem Şeyda Kaya  
Mesut Sancar  
Miray İlhan  
Mustafa Abdullah Yılmaz  
Mustafa Çelebier  
Nadir Yalçın  
Nazlı Müzeyyen Şencan  
Neda Taner  
Nilay Aksoy  
Nilay Tarhan  
Nuraniye Eruygur  
Nuray Ulusoy Güzeldemirci  
Nursel Sürmelioglu  
Okan Aykaç  
Ongun Mehmet Saka  
Onur Kenan Ulutaş  
Onur Pınarbaşı  
Oya Kerimoğlu  
Özge Gün  
Özgür Eşim  
Özlem Çoban  
Özlem Nazan Erdoğan  
Raghavendra Kumar Gunda  
Rashida Muhammad Umar  
Rukiye Sevinç Özakar  
Şafak Ermertcan  
Samet Özdemir  
Sedef Kır  
Selin Seda Timur  
Sema Arısoy  
Serap Ayaz Seyhan  
Serdar Tort  
Şermin Tetik  
Sevgi Sarıgül Özbek  
Sevinç Şahbaz  
Shailesh Laxman Patwekar  
Shoab Mohammad Sadequ Syed  
Sibel İlbasmış Tamer  
Sirisha L. Vavilala  
Sonali Labhade  
Suchita Gupta  
Tahir Emre Yalçın  
Talha Bin Emran  
Tansel Çomoğlu  
Tantri Liris Nareswari  
Tuğba Erçetin  
Tuğba Gülsün İnal  
Uğur Karagöz  
Vaibhavkumar Baldevbhai Patel  
Yamaç Tekintaş  
Yeşim Aktaş  
Yusuf Karagözoğlu  
Zafer Çalışkan  
Zarife Nigar Kumral Özdemir  
Zeynep Aydoğmuş